Development of Novel Composite Membrane with High Selectivity for Direct Methanol Fuel Cell Applications

A Thesis

Submitted in Partial

Fulfilments of the Requirements for the Degree of

DOCTOR OF PHILOSOPHY

by

Pradip Das
(146107011)

Department of Chemical Engineering
Indian Institute of Technology Guwahati
Guwahati, Assam 781039

November 2020

Dedicated

To

My Parents and My Mentors

Department of Chemical Engineering
Indian Institute of Technology Guwahati
Guwahati, Assam 781039

STATEMENT

I hereby declare that the content embodied in this thesis entitled "**Development of Novel Composite Membrane with High Selectivity for Direct Methanol Fuel Cell Applications**" is the result of investigations carried out by me at the Department of Chemical Engineering, Indian Institute of Technology Guwahati, Guwahati, India, under the guidance of Prof. Bishnupada Mandal and Prof. Sasidhar Gumma. In keeping with the general practice of reporting scientific observations, due acknowledgements have been made wherever the work described is based on the findings of other investigators.

Pradip Das

November, 2020 Pradip Das

Department of Chemical Engineering
Indian Institute of Technology Guwahati
Guwahati, Assam 781039

CERTIFICATE

It is certified that the work described in this thesis, entitled "**Development of Novel Composite Membrane with High Selectivity for Direct Methanol Fuel Cell Applications**", done by **Mr. Pradip Das** (Roll No. 146107011) for the award of degree of Doctor of Philosophy is an authentic record of the results obtained from the research work carried out under our supervision in the Department of Chemical Engineering, Indian Institute of Technology Guwahati, India and this work has not been submitted elsewhere for the award of any other degree or diploma.

This thesis in our opinion, has reached the standard fulfilling the requirements for the award of the degree of Doctor of Philosophy in accordance with the regulations of the institute.

(**Prof. Bishnupada Mandal**)
Professor
Department of Chemical Engineering
Indian Institute of Technology, Guwahati
Assam -781039, India

(**Prof. Sasidhar Gumma**)
Professor
Department of Chemical Engineering
Indian Institute of Technology, Tirupati
Andhra Pradesh- 517506, India

ACKNOWLEDGEMENTS

The journey towards completion of my doctoral thesis is an amalgamation of opportunities, successes, failures, and challenges. The voyage would have been much tougher or even impossible without the help of many wonderful people. I would like to express my sincere gratitude to each and everyone who have been my support system when the "tough gets going and going gets tough".

First and foremost, my sincere gratitude to my supervisor ***Dr. Bishnupada Mandal*** *and* ***Dr. Sasidhar Gumma*** *for their meticulous guidance and support. Enriching scientific discussions, engaging work environment and independency of work provided by them have nourished my professional growth. Their critical analysis of the experimental work and preparing the manuscript, are the ways one needs to adopt to do a perfect research. I consider myself fortunate to work under their supervision throughout this journey. I whole-heartedly thank them for extending moral support as and when required.*

I am thankful to my Doctoral Committee members ***Dr. Animes Kr. Golder****,* ***Dr. Amit Kumar*** *and* ***Dr. Debasis Manna*** *for their help and support in providing reviews, suggestions, and insightful comments, which have led to improvement of my doctoral research. I am fortunate enough to complete my thesis under their supervision.*

The instrumental facilities available at IIT Guwahati specifically, Analytical Lab Facility (Department of Chemical Engineering), Centre of Excellence for Sustainable Polymers (CoE-SusPol), Central Instrument Facility (CIF) and Centre for Nanotechnology are kindly acknowledged.

I am also grateful to all the ***faculty members and staff*** *of Department of Chemical Engineering for helping and providing the necessary facilities.*

A very special thanks to all my friends and colleagues of IIT Guwahati for making my stay enjoyable and memorable. They proved to be my best teachers and I thank them from the core of my heart for creating an amazing and unforgettable working environment. Professional and personal interactions with them have helped me grow as a researcher and a good human being.

Pradip Das

Abstract

Fossil fuels are the primary sources of power and energy to the mankind even today. Cost-effective and environmentally friendly alternate energy sources alleviate problems associated with fossil fuels. Development of a cost-effective fuel cell along with a high performance has been the objective of several research works. Direct Methanol Fuel Cells (DMFCs) are attractive due to their simple working principle, portability, low operation temperatures, convenient fuel storage and high energy density of methanol. This work involves synthesis of novel nanocomposites for proton exchange membranes for direct methanol fuel cell applications (DMFC) and determination of their selectivity. Initially, general strategies were developed to control the surface functional groups namely carboxyl, carbonyl, epoxy and hydroxyl present on the graphite Oxide (GO) by changing the oxidation temperature from 30 to 110 ºC in modified Hummer's method to determine the best synthesis temperature for modification of membranes. The optimized GO was doped with UiO-66 for fabrication of Sulfonated poly (ether ether ketone) (SPEEK) based polymeric composite membrane. Further it was modified with palladium (Pd) to increase the membrane selectivity for DMFC application. The study encompasses the effect of amino acid (L-Tyrosine) on selectivity of developed SPEEK membrane. The functional groups and constituent elements were characterized by Fourier Transform Infrared Spectroscopy (FTIR), X-ray photoelectron spectroscopy (XPS). The surface morphology was analyzed by Scanning Electron Microscopy (SEM), Atomic Force Microscopy (AFM) and Transmission Electron Microscopy (TEM). The crystallinity and thermal stability was studied using X-Ray Diffraction (XRD) and Thermogravimetric analysis (TGA) respectively. The physicochemical properties of the SPEEK and SPEEK composite membranes such as ion exchange capacity (IEC), water uptake, methanol permeability, proton conductivity were measured. The results include significant improvement in blocking of methanol upon modification of base polymer using novel composites while on the other hand the membrane conductivity increased significantly. Both these factors result in higher selectivity of the SPEEK composite membrane for DMFC applications, compared to that of benchmark Nafion-117 membrane.

List of Figures

List of Tables

CHAPTER 1

Introduction, background to the problem and objectives

CHAPTER 1

Introduction, background to the problem and objectives

This chapter delivers an overview with the importance of Direct Methanol Fuel Cell technology and emphasizes on various fuel cell technology presently available. This chapter also highlights the motivation and scope of this fuel cell technology. Based on the gaps and challenges, the research objectives were defined.

1.1 Background

Population boom and immensely rapid industrial development have resulted in an exponential increase in the global demand for energy consumption and a speedy decline in the fossil fuel resources. The current alarming rate of renewable energy depletion is highly detrimental to the environment and puts forward an inevitable risk of energy exhaustion. The present energy techniques also contribute significantly to the increasing pollution levels of the world. Thus, it is important that one comes up with newer alternatives which are cleaner and greener [1]. In the present situation, the dire need of the hour is to find a sustainable alternative source of energy that is cheap, effective, ensures high performance and is environment friendly. This currently forms the focus area of many researchers around the world. Fuel cells have time and again proven to be very promising for energy storage and conversion due to their high efficiency and low degrees of pollution. They have been proposed as a future portable and mobile energy conversion device for their high energy density, easy handling and quiet operation. These environmentally-benign designs have a simple structural design and easy refueling system. Fuel cells are potential replacements for the current energy techniques and their

clean, quiet and efficient nature makes them all the more considerable for the future [2-4]. As quoted by George W. Bush, on February 25, 2002, "We happen to believe that fuel cells are the wave of the future. We need to have a focused effort to bring fuel cells to market, and that's exactly what my administration is dedicated to do" [5].

1.2 History of Fuel Cell Technology

William Robert Grove (1811-1896) is credited for inventing the fuel cell technology in 1839. He was a British barrister and an amateur physicist [6,7]. Following this, Hydrogen Fuel Cells were experimented by Ludwig Mond (1839-1909) and his assistant Carl Langer in 1888. This fuel cell produced 6 amps per square foot at 0.73V. The first alkaline fuel cell was invented by Francis Thomas Bacon in 1932. He also invented a 5 kW fuel cell for practical applications in 1959. The same year, 120 years after the first fuel cell was created, NASA revealed some prospective applications of fuel cells for producing power in space flights. The Proton Exchange Membrane Fuel Cell (PEMFC) was created during that time. These successes proved the mettle of fuel cells and consequently, the industry started recognizing the calibre they possessed by the 1960s [8.9]. But technical problems and the expensive nature of these fuel cells were still acting as the limitations. The commercialization of these fuel cells is a hot topic for several hundred companies around the world. 1993 saw the first fuel cell car developed by Ballard Corporation, Canada [10]. The research and development of the fuel cell technology is largely being supported by the Office of Transportation Technologies at the U.S. Department of Energy since 1984. The reliability, durability, low cost and environmental benefits are key factors that drive the companies today towards commercialization.

1.3 Advantages of Fuel Cells Compared to Conventional Technologies

Fuel cells are different from Carnot cycle (thermal energy based) engines. The direct conversion of fuel to electricity gives fuel cells the advantage of being operated at much higher efficiencies as compared to conventional energy conversion processes. This enables the fuel cells to extract more electricity for the same amount of fuel. Fuel cells also give out lesser emissions. The waste generated is comparatively lower. In case of hydrogen fuel cells, water is the only waste product generated. Fuel cells have no moving parts, which leads to its quiet nature and makes it mechanically ideal [10].

A fuel cell is analogous to a battery in terms of its operation and principle. However, it comes with the advantage of no recharging requirement. A fuel cell only needs continuous supply of fuel and oxidant to run smoothly. A battery is typically an energy storage device, which runs down (becomes dead or discharged) when the reactants it stores are exhausted. However, in fuel cells, the fuel is stored externally and so it can never get internally dead.

In view of the higher thermal efficiencies, lower waste generation, quiet nature and energy prospects make fuel cells better as compared to conventional technologies.

1.4 Type of Fuel Cells

Fuel cells are generally categorized based on the electrolyte material being used. The material that is used between the anode and the cathode is called the electrolyte. It acts as a conductor exclusive to protons and not electrons for ion exchange. The electrolyte plays a key role in the production of the electric current. The prime five kinds of fuel cells that are being subjected to study and research have been tabulated in the **Table 1.1** below. Though, the below mentioned fuel cells are different in many aspects, electrolyte

membrane is a prime characteristic of difference. All types of fuel cells operate on the same basic principle [11-13].

Table 1.1 Types of fuel cell and their operating condition

Type	Alkaline Fuel Cell (AFC)	Molten Carbonate Fuel Cells (MCFC)	Phosphoric Acid Fuel Cells (PAFC)	Solid Oxide Fuel Cells (SOFC)	Proton Exchange Membrane Fuel Cells (PEMFC)
Type of Electrolyte	Typically aqueous KOH solution	Typically, molten Li_2CO_3/K_2CO_3 eutectics	H_3PO_4 solutions	Stabilized ceramic matrix with free oxide ions	Proton exchange membrane
Typical construction	Plastic, metal	High temp metals, porous ceramic	Carbon, porous ceramics	Carbon, porous ceramics	Plastic, metal, or carbon
Primary contaminate sensitivities	CO, CO_2, and Sulfur	Sulfur	CO < 1%, Sulfur	Sulfur	CO, Sulfur, and NH_3
Applications	Military space	Electric utility	Electric utility, transportation	Electric utility	Electric utility, portable power, transportation
Advantages	Cathode reaction faster in alkaline electrolyte therefore high performance	High temperature advantages	Up to 85 % efficiency in co-generation of electricity and heat. Impure H_2 as fuel	Up to 85 % efficiency in co-generation of electricity and heat. Impure H_2 as fuel	Solid electrolyte reduces corrosion & management problems. Low temperature. Quick start-up
Disadvantages	Expensive removal of CO_2 from fuel and air streams required	High temperature enhances corrosion and breakdown of cell components	Pt catalyst. Low current and power. Large size.	High temperature enhances breakdown of cell components	Low temperature requires expensive catalysts. High sensitivity to fuel impurities

1.5 Proton Electrolyte Membrane Fuel Cells (PEMFCs)

The high energy conversion efficiency of PEMFCs at considerable temperatures (<100°C), which leads to a rapid start, makes them highly promising for large practical applications. PEMFCs are the most up-and-coming fuel cells for commercialization in fields such as portable electronics and automobiles among others [14]. The ability of a PEMFC to rapidly change power output is a reason for this. PEMFCs are primarily categorized into H_2-PEMFC and DMFCs because of the solid electrolyte membrane that is used as the electrolyte. An ideal membrane for PEMFCs must be an excellent proton conductor with high affinity to protons and not electrons [15].

An ideal membrane should be equipped with the following properties to ensure high efficiency in the PEMFC:

a) It should be stable chemically and electrochemically under operating conditions.
b) It should be mechanically strong and stable.
c) It should promote high electron transport so that the electrolyte is uniformly spread and no local drying occurs.
d) It should be compatible and should provide good adhesion to the contents of the PEMFC.
e) It should have low permeability to the reactants so as to maximize coulombic efficiency.
f) It should possess excellent proton conductivity to ensure minimum losses due to resistance.
g) The production costs of the fuel cell must be appropriate for the purpose that is planned for.

H_2-PEMFCs and DMFCs differ in the type of fuel that is used in them. Hydrogen is used in H_2-PEMFCs and methanol is used in the latter.

1.6 H_2-PEMFC

While hydrogen fuel cells came into existence in the late 1800s, the H_2-PEMFCs were not developed until the 1960s. General Electric Company developed these H_2-PEMFCs to be used as supplementary power sources in the Gemini space missions. These fuel cells come with the remarkable advantage of zero emission of pollutants. Platinum (Pt) catalyst and hydrogen fuel are used as the cathode and Pt and air/O_2 form the anode. The extreme sensitivity of Pt towards CO poisoning makes it necessary to use extremely pure fuels. This ensures high efficiency. But the storage of hydrogen and issues in transportation are some of the prime limitations here. Thus, other alternatives are being considered [16,17].

1.7 Direct Methanol Fuel Cell

Direct Methanol Fuel Cells (DMFCs) have formed the centre for many research works in the recent past owing to their simple working principle, convenient fuel storage, low working temperature and portable nature. A fuel cell typically consists of a cathode and anode with a proton exchange membrane sandwiched in between. The conversion of electrical energy to chemical energy takes places without any intermediate step which ensures no emissions and thereby, proves as an efficient alternative for power production. The main objective of a fuel cell is the production of electricity and heat without any toxic or pollutant as by-product.

1.7.1 Advantages and comparison of DMFC with respect to H_2-PEMFC

DMFCs are one of the potential alternatives for H_2-PEMFC. The applications of DMFCs have been successfully implemented in cars, mobile phones, etc. DMFCs show promising

applications in the future [18]. The direct fuel feeding system of methanol without the transitional stage of forming hydrogen gives a lot of advantage to DMFCs as compared to H_2-PEMFCs. Hydrogen has storage issues as opposed to methanol, which is easy to store. Methanol possesses high energy density, is non-corrosive, biodegradable and cost effective. It also has several sources of generation such as natural gas and coal.

For the electrodes, catalysts like ruthenium have to be added to platinum to facilitate the cleavage of anodic methanol bonds. A typical temperature range of 50-100°C is optimum for both the fuel cells. Higher temperatures give better efficiencies. Oxidation of methanol takes place at the anode in place of hydrogen, in case of DMFCs. A 1-2 M methanol solution and catalyst mixture are used at the anode and Pt and air/O_2 are used at the cathode. The oxidation reaction of hydrogen is relatively simpler as compared to that of methanol.

1.7.2 Working principle

Fuel cells are fundamentally electrochemical energy devices that convert chemical energy of a fuel (e.g., hydrogen, methanol, etc.) and an oxidant (air or pure oxygen) in the presence of a catalyst directly into electrical energy via chemical reactions. A DMFC typically consists of an anode, electrolyte and a cathode. The anode is a negative electrode. Methanol is separated from a methanol-water mixture at the anode by the action of catalysts. Methanol is broken down into carbon dioxide and hydrogen atoms. The protons from the hydrogen then pass through the membrane to the positive electrode. This transport should be smooth to ensure high efficiency, which is why a highly proton conductive membrane is desired for fuel cell applications [18].

The reactions of the DMFC are mentioned below:

Cathode reaction: $3/2\ O_2 + 6H^+ + 6e^- \rightarrow 3H_2O$ ------ (R1.1)

Anode reaction: $CH_3OH + H_2O \rightarrow CO_2 + 6H^+ + 6e^-$ ------ (R 1.2)

Overall reaction: $CH_3OH + 3/2\ O_2 \rightarrow CO_2 + 2H_2O$ ------ (R 1.3)

1.8 Motivation

Several reviews [14] focusing on different membranes have been made. Sulfonation is an important modification of DMFC membranes that several researchers around the globe have been focusing on. It is a technique that has caused significant improvements in the membranes of DMFCs towards higher efficiencies. Sulfonated membranes have shown better properties than the commercial Nafion membrane in many literature works [14]. Thus, it is important to study the reaction mechanism and the effects of sulfonation. However, it still requires improvement in terms of the proton conductivity and methanol permeability. This parameter can be enhanced by considering novel fillers [14]. In this regard, it is necessary to design a composite membrane alternative to Nafion having higher performance for economical commercial application. Hence, the present work has been formulated in order to study the developments and modification of membranes using various composite in recent times.

1.9 Objectives of the Thesis

Focusing on all background of this work, the objectives have been divided in two ways:

1. Fabrication of a sulfonated polyelectrolyte membrane to be used for direct methanol fuel cell.

2. Further improvement of their mechanical and physical properties with an optimum increase in selectivity for polymer electrolyte membrane fuel cell by incorporation of different nanomaterials and fillers.

The following research works have been undertaken on the basis of the above objectives:

1. Fabrication and characterization of a proton exchange membrane using sulfonated polyether ether ketone.
2. Role of oxidation temperature on the structural and functional characteristics of graphite oxide nanosheets.
3. Development of graphite oxide doped UiO-66 composite for modification of SPEEK membrane.
4. Exploring palladium /graphite oxide /UiO-66 composite to construct an effective methanol blocking mixed matrix membrane.
5. Preparation and performance analysis of amino acid functionalized palladium grafted graphite oxide embedded SPEEK membrane.

1.10 Organisation of the Thesis

On the basis of the above discussion, the thesis work has been divided into nine chapters. A brief overview of each chapter is presented below.

Chapter 1: This chapter focuses on the importance of direct methanol fuel cell technology in the global demand for energy consumption. Also, various technologies available for fuel cell technology and their advantages and disadvantages are discussed. Emphasis was laid on the advantages of direct methanol fuel cell technology. Finally, this chapter listed its major objectives and the research work undertaken.

Chapter 2: This chapter includes the detailed literature survey for the direct methanol fuel cell technology using proton exchange membrane and also their composite membranes and the major existing research work using polyether ether ketone polymer has been elaborated.

Chapter 3: This chapter contains detailed representation and discussion of different experimental methods which has been mainly used to characterize the synthesized materials and fabricated membranes to complete the objectives of this thesis.

Chapter 4: This chapter focused on sulfonation of PEEK polymer and fabrication of a sulfonated membrane using sulfonated PEEK. Successfully fabrication membrane was confirmed based on characterization involving TGA, FTIR, XRD and FESEM followed by selectivity measurement.

Chapter 5: This chapter discussed a very interesting finding on synthesis of graphite oxide using modified Hummers method. For the first time, a general strategy has developed to control the surface functional groups namely carboxyl, carbonyl, epoxy and hydroxyl presents on the graphite oxide by changing the oxidation temperature from 30 to 110 ^{o}C.

Chapter 6: This chapter includes facile synthesis of composites by 2D carbon functionalization of MOFs as an emerging field of research for proton exchange membrane. Accordingly, our study focused on synthesis of graphite oxide decorated UiO-66 MOF (UiO-66/GO) and its performance evaluation in DMFC.

Chapter 7: A novel composite was synthesized in this chapter using UiO-66, GO and palladium (UiO-66/GO-Pd). The use of palladium nanoclusters blocked the methanol

permeability in the hydrophilic channel, thus significantly reducing the methanol crossover while the proton conductivity of the membrane stayed intact.

Chapter 8: This chapter involves synthesis of amino acid grafted palladium graphite oxide based nanocomposites as proton exchange membranes for direct methanol fuel cell applications and determination of their selectivity. Membrane synthesis includes grafting of L-Tyrosine on palladium decorated graphite oxide (Pd-GO-L-Tyr) in a polymeric substrate viz. sulfonated poly(ether ether ketone) (SPEEK) by solution casting.

Chapter 9: This chapter draws appropriate overall conclusions based on the investigation in the present study. This chapter also provides some useful recommendations for future research in the relevant field.

References:

1. S.A. Sherif, F. Barbir, T. Veziroglu, Wind energy and the hydrogen economy—review of the technology, Solar Energy 78(5) (2005) 647-660.
2. J. Divisek, J. Fuhrmann, K. Gärtner, R. Jung, Performance modeling of a direct methanol fuel cell, Journal of the Electrochemical Society 150(6) (2003) A811-A825.
3. W.G. Grot, Perfluorinated ion exchange polymers and their use in research and industry, Macromolecular Symposia, Wiley Online Library, 1994, pp. 161-172.
4. C. Pu, W. Huang, K.L. Ley, E.S. Smotkin, A methanol impermeable proton conducting composite electrolyte system, Journal of the Electrochemical Society 142(7) (1995) L119.
5. President George Bush from the White House Lawn, February 25, 2002.
6. E.H. Wakefield, History of the electric automobile battery-only powered cars, 1993.
7. A.J. Appleby, Fuel Cell Handbook, (1988).
8. R. Glazebrook, Efficiencies of heat engines and fuel cells: the methanol fuel cell as a competitor to otto and diesel engines, Journal of Power Sources 7(3) (1982) 215-256.
9. L. Verma, Studies on methanol fuel cell, Journal of Power Sources 86(1-2) (2000) 464-468.
10. A. Brown, Can fuel cells make the jump to the family garage, Chemical Engineering Progress 98(2) (2002) 12-14.
11. L. Carrette, K.A. Friedrich, U. Stimming, Fuel cells: principles, types, fuels, and applications, ChemPhysChem 1(4) (2000) 162-193.
12. L. Carrette, K. Friedrich, U. Stimming, Fuel cells–fundamentals and applications, Fuel cells 1(1) (2001) 5-39.
13. K.V. Kordesch, G.R. Simader, Environmental impact of fuel cell technology, Chemical Reviews 95(1) (1995) 191-207.

14. H. Luo, Polymer/nano-organic composite proton exchange membranes for direct methanol fuel cell application, University of the Western Cape, 2005.
15. B. Smitha, S. Sridhar, A. Khan, Synthesis and characterization of proton conducting polymer membranes for fuel cells, Journal of Membrane Science 225(1-2) (2003) 63-76.
16. S. Geiger, D. Jollie, Fuel cell market survey: Military Applications, Fuel Cell Today 1 (2004).
17. M. Watanabe, S. Motoo, Electrocatalysis by ad-atoms: Part I. Enhancement of the oxidation of methanol on platinum and palladium by gold ad-atoms, Journal of Electroanalytical Chemistry and Interfacial Electrochemistry 60(3) (1975) 259-266.
18. Z. Połtarzewski, W. Wieczorek, J. Przyłuski, V. Antonucci, Novel proton conducting composite electrolytes for application in methanol fuel cells, Solid State Ionics 119(1-4) (1999) 301-304.

CHAPTER 2

Literature Review

CHAPTER 2

Literature review

This chapter provides a brief survey of scholarly research work on the Direct Methanol Fuel Cell topic. It describes an overview of current knowledge along with some basic importance of modification of polymer, methods and gaps in the existing research.

2.1 Introduction

Direct Methanol Fuel Cells (DMFCs) are an active research topic concerning sustainable energy devices owing to their small size, light weight, low working temperatures, high energy density, convenient fuel cell storage and so on [1]. DMFCs have the potential to play the role as the most ideal power source for vehicles with lower costs at lower temperature and higher energy density, in the long run. This review primarily focuses on separation membrane, with minor supports taken from the other two sections wherever needed. High cost of production, methanol crossover and water balancing issues are some of the common critical limitations that a commercial fuel cell faces. Therefore, substantial study is being conducted on the modification and material selection of these membranes.

The membrane may either act as an electrolyte between anode and cathode facilitating conduction or as a separator for two reactant gases. So, membrane material technology plays a crucial role in the membrane performance as well as the overall fuel cell efficiency. Today, Nafion (manufactured by DuPont), Dow membranes (manufactured by Dow Chemical Company) and perfluorinated ionomers (PFI) are commercially available for DMFCs. However, these have some serious cost and efficiency issues. Dow membranes exhibit a relatively higher performance than Nafion membranes, however

these are extremely efficient in terms of the market value and also have a critical amount of methanol permeation [2]. Nafion, a perfluorosulfonic acid polymer membrane, has excellent chemical and electrochemical stabilities, good mechanical properties and high proton conductivities [3]. Though cost-effective, has a lower efficiency and loses a significant amount of conductivity (almost 10 times) for a small increase in temperature (60℃ to 80℃) [2].

This field of membrane selection has thus, attracted a lot of attention. Membranes have to be developed keeping in mind the interdependence of the "iron triangle" comprising performance, durability and cost [4]. So, it is necessary to understand that it is not easy to achieve all desired properties from a membrane naturally, certain suitable modifications have to be made.

Several methods like preparation of new ionic random and block copolymers, graft copolymerization of ionic polymers on hydrophobic membranes, blending of ionic and non-ionic polymers, synthesis of interpenetrating networks of ionic and non-ionic polymers and composite membranes incorporating a large variety of fillers (silica, zeolites, etc.) are being used for the development of these membranes [5].

2.2 Proton Transfer in Membranes

Proton transfer is one of the first and foremost aspect that is considered while analysing the membranes for fuel cell applications. At a molecular level, the proton conduction in hydrated polymer membranes can be explained by either of the two proposed fundamental mechanisms [4,6]:

I. Proton hopping mechanism or GrÖthous mechanism

II. Diffusion mechanism

The proton hopping mechanism deals with the jumping of a proton from one hydrolyzed ionic site ($SO_3^- H_3O^+$) to another. This proton adheres to a water molecule and forms a provisional hydronium ion from which another proton continues the chain (**Fig. 2.1**). Ionic aggregates are formed in this mechanism and proton transfer occurs. However, the perfluorinated sulfonic acid membranes like Nafion do not have pronounced application of this mechanism [7].

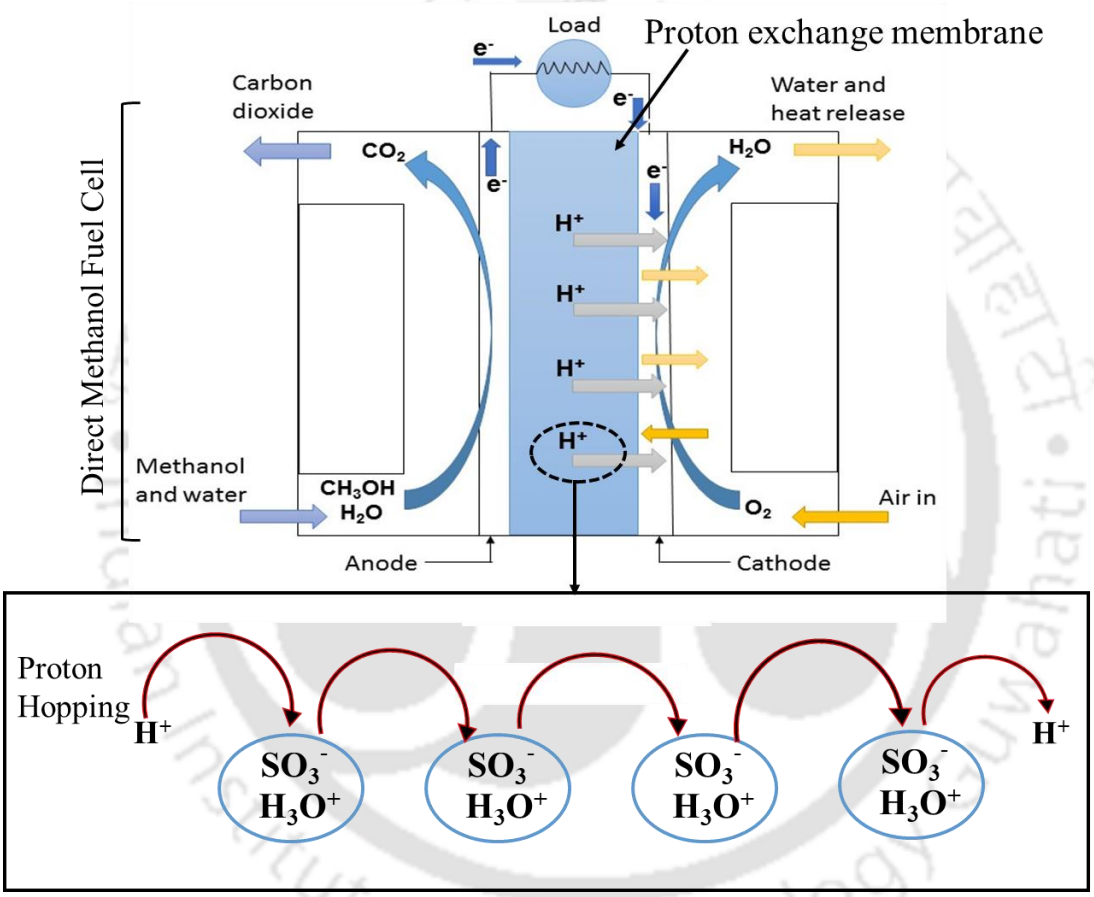

Figure 2.1 Multicomponent molecular transport of proton via proton hopping mechanism in PEM

In the second mechanism which is a diffusion or vehicular mechanism, the proton which is adhered to a water molecule (H_3O^+) diffuses through the aqueous medium (**Fig. 2.2**). The free volumes present within the polymeric chains in proton exchange membranes

facilitate the easy and smooth transport of the water connected protons via the electrochemical difference and electroosmotic drag [5-10].

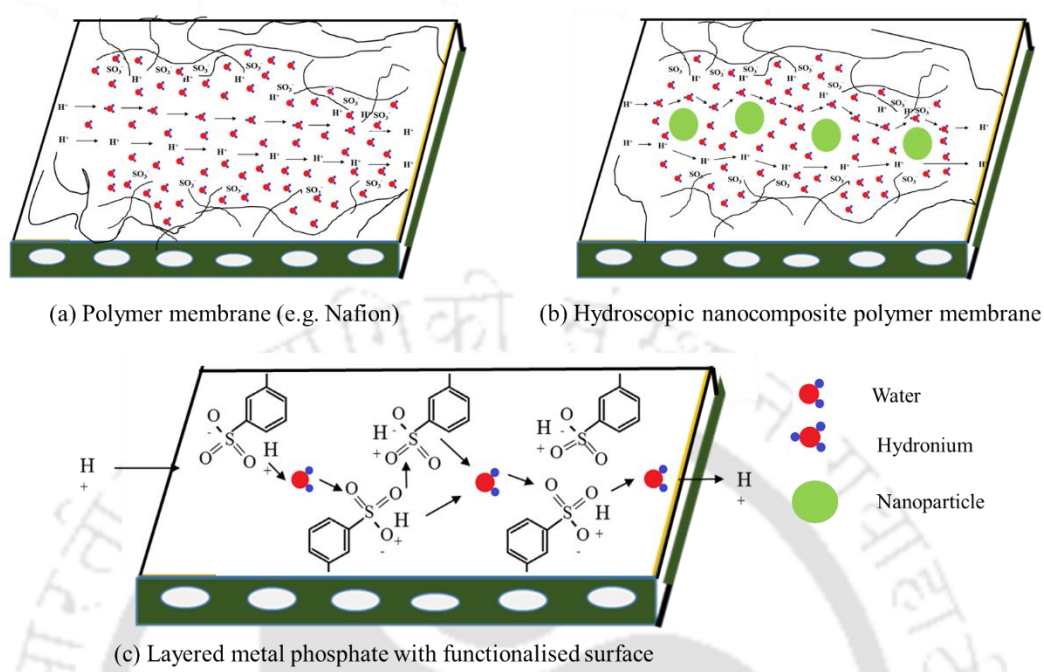

Figure 2.2 Proton transport through membranes [8]

The dominance of one mechanism over the other is dependent on the hydration level of the membrane. However, the transport mechanisms in nanocomposite and hybrid membranes are yet under discussion as the involvement of surface and chemical properties of the inorganic and organic phases make the process sophisticated. Inorganic additives like heteropolyacids act as alternative proton transporters, which implies that their contribution to proton transfer has to be taken into account.

2.2.1 Recent studies concerning the sulfonation of polymer exchange membranes

The sulfonation of polymer membranes, recorded in text, dates back to 1998. A vast amount of research work has been done towards the improvement of membranes through sulfonation. **Fig. 2.3** illustrates the trend in the number of publications from 1998 to 2018. A combination of different keywords was used to identify the publications concerning

this topic from different research work. This search was performed on 7th December, 2018 and a constant increase in the number of publications from 1998-2002 was observed. However, the following year saw a fall in the number only to increase for the next 3 years till 2006 which was at its peak of productivity with a total of 142 papers being published on this topic. The years 2001, 2006 and 2015 saw a significant sudden jump in the numbers as compared to their preceding years. The numbers remained stagnant in 2008 and 2009 following an increase to 130 in 2010. Similarly, the numbers stayed still in 2011 and 2012 but saw an increase in 2018 when 107 papers were published. The interest of researchers globally, in the synthesis of efficient membranes via sulfonation is evident from the given statistics. It is clear that a great amount of work is being done in the concerned field.

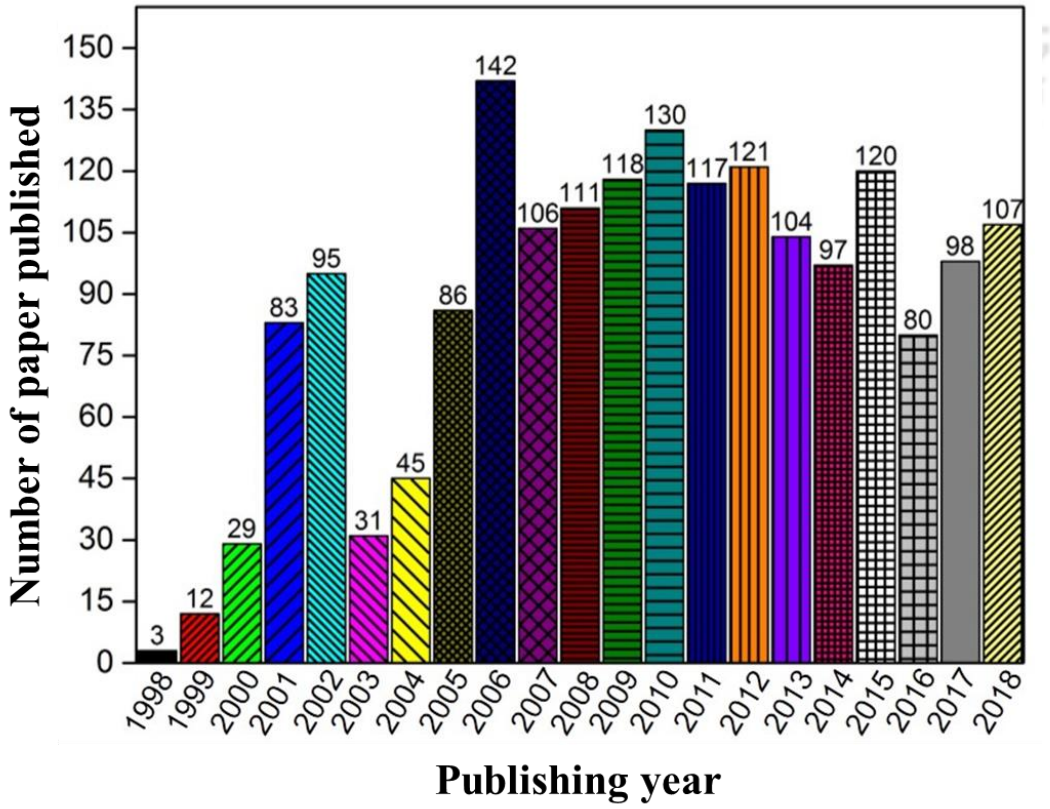

Figure 2.3 Literature on sulfonated polymers in the years 1998-2018

2.2.2 Sulfonated Poly Ether Ether Ketone (SPEEK)

SPEEK membranes have been proven to perform superior to Nafion membranes in terms of thermochemical properties, lower fuel crossover and specifically, lower costs [10]. Sulfonation of the PEEK membrane could be carried out through various approaches, which were strictly classified into the following three classes, as reported earlier [5].

a) Electrophilic sulfonation of PEEK membrane [11].
b) SPEEK and non-functional polymers and/or solids blending [12].
c) SPEEK, heteropoly compounds and polyetherimide doping with inorganic acids [13].

2.2.2.1 Microstructural approach towards the differences between SPEEK and Nafion membranes

The microstructures of membranes play an important role in the determination of the performance of a fuel cell [14,15]. Nafion is a perfluorosulfonic polymer. The hydrophilicity of the membrane is attributed to the perfluorinated backbone while the sulfonic acid groups are responsible for the hydrophilicity of the membrane, thus giving Nafion a blend of both the distinct properties. Polyether ether ketones are thermostable polymers with an aromatic non-sulfonated backbone, in which 1-4-disubstituted phenyl groups are separated by any number of -O- and -CO- group [16]. PEEK which contains a hydrophobic polymer backbone is semi-crystalline in nature. On sulfonation, ionic -SO_3H groups are introduced in the polymer backbone, as a result, the hydrophilic SO_3H groups get preferentially hydrated at the oxygens of the SO_3 groups (**Fig. 2.4**). On the contrary, the hydrophobic groups aid in preventing the dissolution of polymer with water. This helps in gaining thermochemical stability [14].

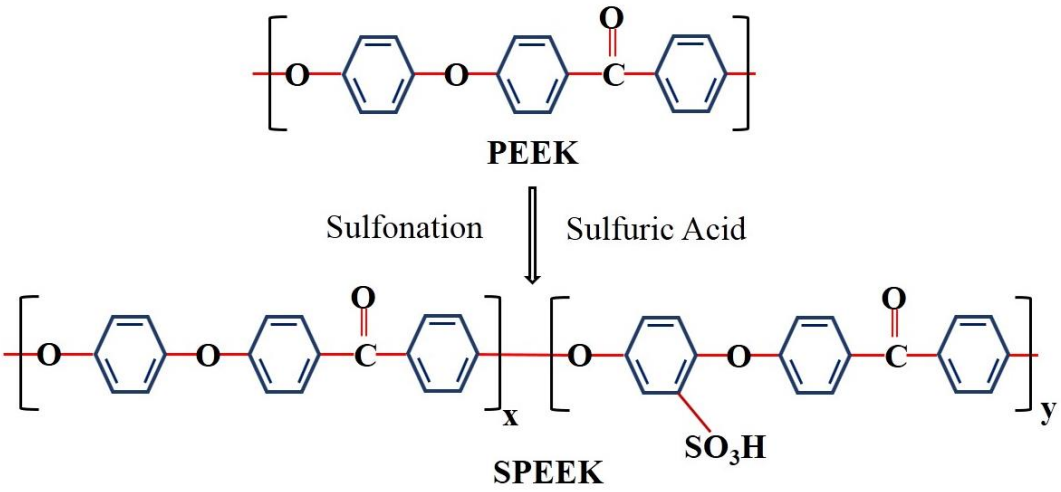

Figure 2.4 The scheme of sulfonated poly(ether ether ketone)

The variation of the proton conductivities of SPEEK membranes with the degree of sulfonation is reported in the literature [17]. As the degree of sulfonation is increased, the ionic group starts forming hydrophilic aggregates, owing to the decrease in distance, which leads to the physical crosslinking of neighboring -SO_3H groups (**Fig. 2.5**). The increase in degree of sulfonation (DS) also leads to a homogeneous distribution of the ionic clusters within the SPEEK membranes, which facilitates the proton conductivity that happens via ion hopping mechanism [13]. When compared to Nafion, the hydrophilic channels are narrower and more branched with increased dead ends in SPEEK [18].

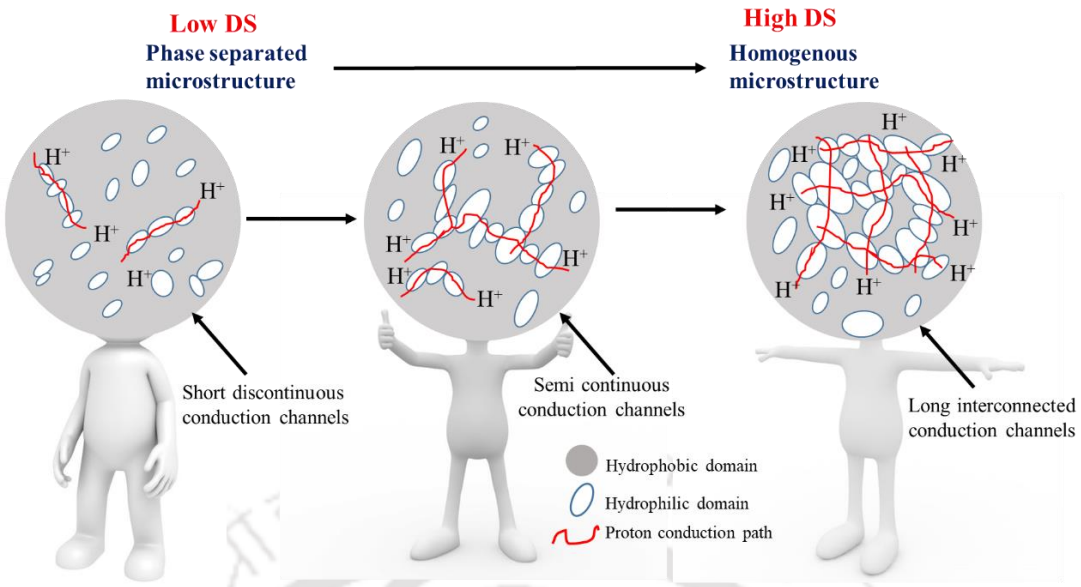

Figure 2.5 Dependency of microstructure formation with degree of sulfonation.

However, very high degrees of sulfonation, the less pronounced hydrophobic/hydrophilic separation regions of SPEEK membranes due to the clustering of the hydrophilic ionic groups, leads to higher swelling and a huge decrease in the proton transfer across the membrane, which is not beneficial for the fuel cell performance. So, an intermediate degree of sulfonation is to be done [14,15].

2.2.2.2 IEC and dependence on DS of SPEEK membranes

The degree of sulfonation affects the Ionic Exchange Capacity of a membrane. IEC is a measure of the density of ionisable hydrophilic groups in the membrane matrix, which are the responsible factors for the ionic conductivity of a membrane. As the degree of sulfonation increases, the hydrophobic groups' concentration increases, thus increasing the water content and loosening the membrane structure, which provides more channels for co-ionic transport. This explains the trends in IEC. It can be inferred from **Table 2.1** that the IEC of the membrane is the best for an intermediate degree of sulfonation. A high

degree of sulfonation leads to a significant decrease in the IEC, which is not desirable for membrane applications in fuel cells.

Table 2.1 Trends in IEC of SPEEK membranes with degree of sulfonation

S. No.	Polymer	DS(%)	IEC(meq./g)	Reference
1	SPEEK	40	0.712	[19]
2	SPEEK	46	1.426	[20]
3	SPEEK	54	1.5	[21]
4	SPEEK	60	1.79	[22]
5	SPEEK	65	1.43	[23]
6	SPEEK	73	2.01	[24]
7	SPEEK	78	2.21	[24]
8	SPEEK	80	1.312	[19]
9	SPEEK	83	2.2	[25]
10	SPEEK	89	2.4	[25]
11	SPEEK	98	2.37	[24]
12	SPEEK	120	1.521	[19]

2.2.2.3 Proton Conductivity of SPEEK membranes

Degree of sulfonation is also a powerful method to increase the proton transfer capacity of SPEEK membrane under identical conditions [26]. This is because the solubility of SPEEKs in organic solvents increases with DS, owing to the increased hydrophilicity which aids in proton transport. So, with increasing DS, apart from the increased number of protonated sites (SO_3H), several water mediated pathways are also formed which help in enhancing the proton transfer, and hence, the proton conductivity.

Apart from dependence on degree of sulfonation, proton conductivity trends also vary with temperature, as can be seen from **Table 2.2.** As the temperature increases, the effect of dehydration keeps on getting pronounced as compared to the negligible effect at low temperature [26,27]. The sulfonated groups, as mentioned earlier, are hydrophilic in nature. Thus, with increasing temperature, the stronger ability to retain water leads to rapid loss in conductivity. This is why, intermediate degrees of sulfonation have been seen to exhibit optimum conductivity. This shows that the water uptake and water retaining capabilities also play a crucial role in determining the conductivity of SPEEK membranes [26-29]. With increasing temperature, the interaction between the polymer chains gradually decreases, which again leads to a decreased conductivity [26,29].

A vast difference in conductivity with different casting solvents can also be observed. This is because, different casting solvents interact differently with the SPEEK polymers. Robertson et al. [30] reported the interaction of SPEEK samples with various casting solvents. DMF or DMAc can react with the left out sulfuric acid, which, if failed to be washed out, can form DMam sulphate and formic or acetic acid. This implies a decrease in the sulfuric acid (hydrophilic groups) concentrations, which suggests lower conductivity. Similarly, NMP and DMAc are aprotic solvents that exhibit almost zero hydrogen bonding in contrast to DMF. Thus there exists discrepancies in the many values of proton conductivity for SPEEK. The hydrogen bonding prevents the protons of SO_3H groups from participating in proton transfer and hence leading to a depletion in proton conductivity [26,31].

Table 2.2 Trends in conductivity of SPEEK membranes with degree of sulfonation

Sl. No.	Polymer	DS(%)	WU(%)	Conductivity at T=25°C (mS/cm)	Conductivity at T=80°C (mS/cm)	Casting Solvent	Ref.
1	S-PEEK	39	-	-	10.8	DMAc	[32]
2	S-PEEK	40	-	24	33	DMAc	[19]
3	S-PEEK	46	41	9.93	-	DMSO	[20]
4	S-PEEK	47	-	-	16.8	DMAc	[32]
5	S-PEEK	54	-	36	49	DMAc	[21]
6	S-PEEK	65	20.01	25.01	33.12	DMAc	[30]
7	S-PEEK	80	-	38	67	DMAc	[19]
8	S-PEEK	83	-	37.37	-	DMAc	[25]
9	S-PEEK	89	-	38.56	-	DMAc	[25]
10	S-PEEK	98	-	3.3	-	DMF	[33]
11	S-PEEK	120	-	70	134	DMAc	[19]
12	S-PEEK	-	-	57	190	NMP	[34]

2.2.2.4 Effects of various methods of sulfonation on the polymer

The sulfonation of PEEK, as mentioned before has been achieved by various approaches.

2.2.2.4.1 PEEK nucleophilic substitution

Nucleophilic substitution is one of the commonly used methods for the sulfonation of PEEK membranes. Early research presented a detailed study on the kinetics taking place in a sulfonated PEEK membrane [35,36]. Post-sulfonation method was used by them for the synthesis of SPEEK membrane. This method, however, degraded the mechanical and thermal stability of the polymer and also made it challenging for controlling the degree

of sulfonation. The direct synthesis method via nucleophilic substitution of monomer has proved to be more advantageous as it allows a better control over the degree of the sulfonation while also giving better thermal and mechanical stability. So, in this particular section, the reasons behind the improved properties due to nucleophilic substitution have been discussed extensively, by taking into account several key factors like methanol permeability, ion exchange capacity, proton conductivity. The work on the synthesis of sulfonated PEEK membranes began as early as 1999 (in accordance with the information extracted from the Science Direct records) [13]. They synthesized SPEEK membranes by carrying out sulfonation via nucleophilic substitution and found the modified membranes to have remarkable thermal stability as well as a high selectivity. Since then, sulfonated PEEK membranes have been largely experimented with.

After fabrication of SPEEK membranes via nucleophilic substitution, the membranes were found to have a superior conductivity than Nafion 115, the commercial membrane [33], even at higher temperatures, i.e. above 80°C. The methanol permeability was also found to be lower than the Nafion 115, giving an overall better performance than the Nafion membrane. The IECs were found to increase with increasing degrees of sulfonation [37]. The methanol diffusion coefficients were found to be in the range of 3×10^{-7} to 5×10^{-8}, depending on the degrees of sulfonation, which were an order lower than the standard Nafion membrane [19]. SPEEK membrane has also been synthesized [38] by carrying out sulfonation via nucleophilic substitution and fabricated membrane shows a remarkable thermal stability as well as a high selectivity. Various other texts have been reported where sulfonation via nucleophilic substitution has shown similar trends, i.e. increased proton conductivity, decreased methanol permeation and an overall good fuel performance.

The microstructure analysis of these SPEEK membranes can be used to explain these trends. The increase in IEC, with an increase in degree of sulfonation, as it has been demonstrated by **Table 2.1**, can be explained by the following theory. As it has been mentioned before, in the SPEEK membranes, after sulfonation, hydrophilic groups (SO_3H groups) are increased in number, these hydrophilic groups cluster together and cause an increased number of channels for co-ionic transport. Thus, these water mediated pathways facilitate smoother ion transport, which explains the increasing trend of IEC. Similarly, the proton conductivity trends can also be attributed to the same reason, that is the sulfonate groups form hydrophilic aggregates that provide hydrated pathways, which support proton conductivity, aided by water dynamics.

2.2.2.4.2 Composite/blend SPEEK membranes with heteropolyacids and polyetherimides

SPEEK, as it has been well-established in the previous paragraphs, has an excellent potential for application in fuel cells. However, due to poor separation between hydrophilic/hydrophobic regions and narrow passages of poorly connected water channels, proton conductivities after a certain extent of degree of sulfonation. So, several attempts at maintaining the equilibrium balance between hydrophilic and hydrophobic regions are being carried out. Methods like covalent or physical crosslinking, preparation of composite membranes with inorganic fillers dispersed in organic filler network have been adopted for overcoming these limitations [35-37]. Crosslinking via ionomeric polymers blending proves fruitful as the positive characteristics from each of the blends are taken into advantage. Electrochemical performances are seen to improve, as this technique lowers the average separation between the acidic groups [26]. This increased affinity between the acidic groups will assist a non-vehicular proton transport

mechanism. This particular section gives a detailed analysis on the synthesis and characterization of various composite membranes, blends, inorganic-organic filler membranes, that have been put forward in recent literature. The performance analysis of different modified SPEEK membranes has been given below. Since each modification results in different interactions, specific care has been taken towards elucidating the trends of crucial factors that affect the performance of a fuel cell, for each blend being considered.

The first recorded work on blend membranes of SPEEK dates back to 2000 and the investigation was done using polysulfone-SPEEK based composite membranes [39]. These membranes were found to have a remarkable combination of permeability, rejection properties and low adhesion character. Since then, a substantial amount of work has been done on the improvement of the performance of SPEEK membranes via various approaches, as will be seen further in this section.

A new kind of hybrid polymer was prepared [26] where the Si atoms were bound to a SPEEK backbone. These membranes were found to have a good thermal stability, better water uptake and resulted in good electrical characteristics, because of the formation of covalently bound inorganic clusters which help in increasing the water uptake without resulting in excessive swelling. These membranes were found to have a better solubility and a suitable potential for applications as conducting membranes. In yet another study, composite membranes were formed by SPEEK and sulfonated/silylated polyphenylsulfone (SPPSU) [40]. These SPEEK and SiPPSU membranes, although had sulfonic acid groups and silanol groups which were weak points since the thermal decomposition started at these points, showed superior mechanical properties and much lower water uptake coefficients as compared to pristine SPEEK. This could be attributed

to the bulky phenyl silanol groups which act as a hindrance to chain motion under an applied tensile strength. It has been reported a composite membrane based on SPEEK and PEEK-BI [36]. These membranes were found to have reduced water uptake and swelling ratio as compared to pristine SPEEK. Although, these composite membranes showed lower proton conductivity than the pristine SPEEK membrane, they also showed exceptionally low methanol permeabilities. The reduced proton conductivity could be attributed to the fact that the water uptake is reduced due to the interactions between benzimidazole and sulfonic groups which make a part of protons in sulfonic acid groups useless for proton conduction. This reduced water uptake restricts the formation of the water mediated pathways which act as proton transferring channels. This same reason could be attributed to the significant reduction in methanol permeability as well. Some research group worked on the synthesis of a crosslinked sulfonated polyether ether ketone poly ethylene glycol/silica organic inorganic nanocomposite membrane for fuel cell applications [40]. Crosslinking via ionomeric polymer blends proves fruitful as the positive characteristics from each of the blends are taken into advantage. Electrochemical performances are seen to improve, as this technique lowers the separation between acidic groups [26] which helps in proton transfer via a non-vehicular transport. For instance, a highly ionic crosslinked sulfonated PEEK has been fabricated for fuel cell [41]. It has been previously noticed that crosslinked membranes were found to lose their conductivity. In this particular study, alkyl-chain attached ionic crosslinks were used to demonstrate the conductivity and swelling.

2.3 Graphene Oxide as Composite in DMFC

The specific application potential of graphite-based materials is mostly dependent on their structural and surface properties and thus to their synthetic conditions. Among the

graphite family, graphite oxide (GO) nanosheets have demonstrated their uses in the fields of ionic conductor, sensor and nano-electronic structural support (**Fig. 2.6**). Graphene has rapid charge carrier features which facilitate easy transport of charges without any scattering. The extensive conjugated sp^2 carbon network of graphene promotes higher electrical conductivity. The excellent electrochemical properties of graphene like high conductivity, stability at high temperatures, electronic capabilities were considered and hence, was chosen as a suitable membrane for DMFC [42].

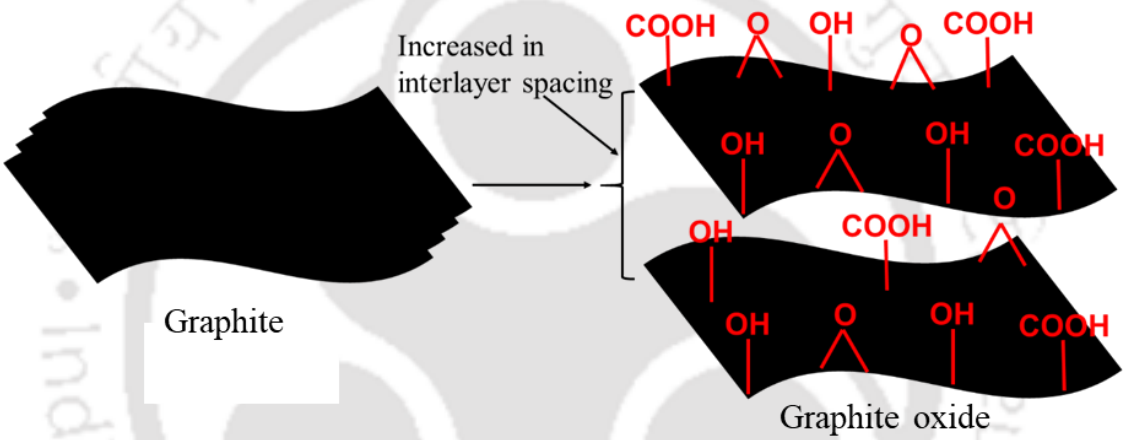

Figure 2.6. Microstructure of graphite and graphite oxide

Graphene oxide (GO) paper itself works as a membrane for DMFCs [43]. GO papers are synthesized by a flow directed assembly of a colloidal graphite oxide solution prepared by Hummers' method. It is worth noting that the GO papers offer proton conductivity in the range of 4.1×10^{-2} S cm^{-1} to 8.2×10^{-2} S cm^{-1}. The hydrolysis of GO papers gives way to the presumptions that proton conduction takes place in both the vehicular and non-vehicular mechanisms. The proton forms an ion adduct with the carrier molecule in the vehicular model and the protons hop from one site to another without any carrier molecule in the non-vehicular model. The water molecules are presumed to be connected in between the GO sheets forming hydrogen bonds and the scanning tunneling

microscopy (STM) shows oxygen to be arranged in a rectangular lattice. These interesting conduction properties make GO a potential candidate for DMFCs. However, it is seen that GO papers have an undesired high permeability which reduces the selectivity of the membrane. Graphite oxide papers get easily hydrated which lead to significant methanol crossover. This degrades the performance of the DMFC. It is observed that the GO DMFC gave a peak power density of 8 mW/cm^2 at a current density of 5 mA/cm^2 whereas the Nafion 115 gave a power density of 62 mW/cm^2 at a current density of 97 mA/cm^2. The membrane's high conductivity, activation energy statistics with temperature, the transport mechanism due to the intramolecular hydrogen bonding in rectangular lattice along with the arrangement of the oxygen atoms in epoxy linkage facilitate easy proton conduction. However, the fuel cell performance is still poor. But, the conductivity properties and the experimental outcomes show that GO papers, with some appropriate modifications can prove to be a good membrane for DMFCs.

The preparation of a cost-effective non-noble metal supported on copper/polypyrrole graphene oxide (Cu_2O/PPy-GO) as an anode catalyst for methanol oxidation in DMFCs has also been reported [44]. In this study, borohydride reduction method was used to prepare the Cu_2O nanoparticles supported PPy-GO matrices. The FTIR results showed the formation of intermolecular hydrogen bonding between the carboxyl groups of GO sheets and -NH groups of PPy. The SEM results of Cu_2O/GO composites showed spherical metals dispersed in the expanded GO sheets. The Cu_2O nanoparticles were found to be uniformly dispersed in the matrices. The TEM analysis of the membranes showed that there were no agglomerations and the nanoparticles were homogeneously incorporated in the matrices. It was observed that the Cu_2O nanoparticles on the PPy-GO support were of the smallest size. This was attributed to the active functional groups on the GO surfaces which properly entrap the nanoparticles and prevent their

agglomerations. The Cu_2O/PPy-GO catalyst system produced the highest forward peak current density which was because of the stability of the system as compared to Cu_2O/GO and Cu_2O/PPy catalyst systems. It was concluded that, among the membranes used, Cu_2O nanoparticles supported on PPy-GO material offered the highest activity due to its better electrical properties, effective deposition and dispersion in the matrix. A maximum current density of 155 mA/cm^2 and a maximum power density of 31 mW/cm^2 was observed in the said Cu_2O/PPy-GO catalyst system which proved to be more stable than the commercial Pt-Ru/C system. Thus, establishing that these membranes could prove as a suitable alternative for Direct Methanol Fuel Cell applications. However, the impedance value of the Cu_2O/PPy-GO was found to be lower than Cu_2O/Ppy or Cu_2O/ GO.

Sulfonated poly (ether ether ketone) grafted graphene oxide-based composites also proves to be a promising membrane for proton exchange [45]. Esterification was carried out between graphene oxide (GO) and hydroxylatedsulfonated poly (ether ether ketone) (SPEEK-OH) for the synthesis of sulfonated graphene oxide (SGO). This was then incorporated into sulfonated polyarylene ether nitrile (SPEN) to study the effect on proton exchange membranes. The FTIR analysis showed successful hydroxylation of SPEEK-OH membranes. Sulfonic acids, benzenes and carbonyl groups were introduced as a result of the oxidation of SPEEK-OH. The TGA curves showed a two-step degradation behavior of the membrane which was assumed to be because of the breaking off of the derivative groups and the second step was considered to be due to the degradation of the main chain. The SEM results showed that the composite SPEN/SGO membranes showed a rougher cross-section when compared to the pristine membrane. The SPEN/SGO-2 (2 wt%) was found to have better interfacial compatibility and connectivity than the other compositions. The Ion exchange capacity of SPEN/SGO-2 was found to increase with the increase in the SGO content while the water uptake was found to decrease with it.

Also, the SPEN/SGO-2 membrane showed the lowest swelling ratio which was attributed to the stronger interfacial interaction of the membrane. These properties are favorable for long-time operation of a DMFC. As can be predicted by the low water uptake, the SPEN/SGO-2 membrane showed excellent proton conductivity. It was concluded that these composite SPEN/SGO membranes were better than the pristine SPEN as indicated clearly by the enhanced proton conductivity, the decreased water uptake and swelling ratio.

Synthesis of nanohybrids GO also reported for applications in proton exchange membrane fuel cells where GO was chemically bonded with Nafion [46]. Atom Transfer Radical addition was carried out between the C-F groups of Nafion and C=C groups of Graphene oxide for bonding GO into Nafion membranes. The FTIR studies indicated the presence of $-CF_2$ groups, $-SO_3H$ groups and C=O groups. These functional groups indicated the proper bonding between Nafion and GO matrix. The Raman spectroscopy showed a moderately high value of the I_D/I_G which indicated better performance of the addition reaction between Nafion chains and C=C groups of GO. The GO-Nafion membrane was seen to undergo a significant increase in the thickness after the chemical bonding due to the Nafion side chains entrapped on the GO surface. The TEM analysis indicated relatively dark spots which showed the presence of heavy sulfur atoms. The proton conductivity was found to be 40.8 mS/cm at 25℃ and 82.3 mS/cm at 95℃ which is significantly higher than pristine recast Nafion membrane. The ionic clusters formed on the Nafion-GO nanosheets due to Nafion chain aggregations assist in enhancing the proton conductivity by acting as the channels for proton transfer. The membranes gave a highest power density of 586 $mWcm^{-2}$ and a maximum current density of 826 $mAcm^{-2}$ which is 40% higher than that of recast Nafion membrane. The hydrophilic nature and the water absorption ability of GO-Nafion membrane facilitated in the increase of the

water uptake with the increase in the filler content. The NM/GO membranes were seen to have high water retention capacities which indicated their comfortable operation at low humidities and high temperatures. It was concluded that since these GO-Nafion nanocomposite membranes had enhanced interfacial compatibilities and higher proton conductivities and performance when compared to the recast Nafion membrane, this technology can prospectively be used for proton exchange membrane fuel cells. However, the membrane was found to possess decreased stability.

Sulfonated graphene oxide (SGO) was also used as a composite for membrane preparation [47]. The membranes with low SGO content showed better dispersion in the Nafion matrix. XPS test was carried out to check the sulfonation of GO in the Nafion matrix. The test showed the presence of C-C, C-O, C=O and also $–PhSO_3^-$ groups which indicated proper dispersion of GO. The TEM analysis showed that SGO was homogeneously distributed in the Nafion matrix. The XRD peak saw a downfall as the wt% of SGO loading was increased. The water uptake of the composite membranes was found to be 6% less than that of Nafion membrane. However, when the wt% was increased above 0.5%, the increase in the SGO aggregation led to increase in water uptake. A maximum proton conductivity of 0.0367 S/cm was observed for 0.5 wt % SGO-Nafion membrane. This also showed higher selectivity (4.11×10^5 S s cm^{-3}) and hence better fuel performance than the Nafion membrane. However, the proton conductivity was seen to decrease with increase in the content of SGO loading. The lowest permeability was exhibited by 0.05 wt% SGO-Nafion membrane which corresponded to 0.0884×10^{-6} cm^2s^{-1}.

A vacuum filtration method has also been reported for synthesis of Nafion 115 membrane laminated with highly ordered graphene oxide with parallel orientation [48]. SEM analysis of pure graphite powder showed a rough clustered structure while the oxidized

GO sheets showed smooth surface. The FTIR spectrum of GO sheets indicated the presence of many oxygen functional groups which implied proper oxidation of graphite. The XRD peak of GO sheet was seen at 11° from 26.5° of graphite which was because of the disturbance caused to the layers of graphite due to the oxidation which led to a decrease in the interplanar distance between the sheets and the matrix. The SEM analysis of the GO-laminated Nafion membrane showed enhanced interfacial bonding between the Nafion matrix and the GO paper. The permeability of the membrane was found to be 0.928×10^{-6} cm^2s^{-1} and the selectivity was 40% higher than that of Nafion 115. Also, the GO-laminated Nafion membrane showed 38% higher peak power density than the pristine Nafion membrane thus, proving their capability to be used in DMFC. However, the proton conductivity (2.35×10^{-2} S/cm) of GO-laminated Nafion membrane was found to be slightly lower than that of the Nafion membrane (2.82×10^{-2} S/cm). A summarized table of proton conductivity discussed in this section has given below.

Table 2.3 Summary of the proton conductivity of GO based membrane

Membrane	**GO (wt%)**	**Proton Conductivity ($S\ cm^{-1}\times 10^{-2}$)**	**Ref.**
Graphene oxide paper	-	8.2	43
Sulfonated polyarylene ether nitrile/Sulfonated graphene oxide	1 %	4.87	44
Sulfonated polyarylene ether nitrile/Sulfonated graphene oxide	2%	5.89	44
Sulfonated polyarylene ether nitrile/Sulfonated graphene oxide	3 %	5.57	44
Nafion based nanocomposite membrane/Graphene oxide	0.05	3.67	45
Nafion based nanocomposite membrane/Graphene oxide	0.10	4.08	45
Nafion based nanocomposite membrane/Graphene oxide	0.15	2.23	45
Graphene oxide /Nafion	2	2.35	47

2.4 Metal Organic Framework as a Composite in DMFC

Metal Organic Frameworks (MOFs) are excellent examples of crystalline porous materials that have been applied in diverse fields such as catalysis, gas separation etc. [49,50], owing to their high surface area and regular structure. In addition, the crystalline nature of the MOFs makes it easier to study the proton conduction mechanism, as opposed to the ionic polymers, where their amorphous hinders the study of the proton transfer pathways. Also known as porous coordination polymers (PCPs), the MOFs are extremely customizable in nature. MOFs, as the name suggests, are created using metal and organic linkers (**Fig. 2.7**). Various organic units can be integrated at the molecular level to obtain the suitable framework.

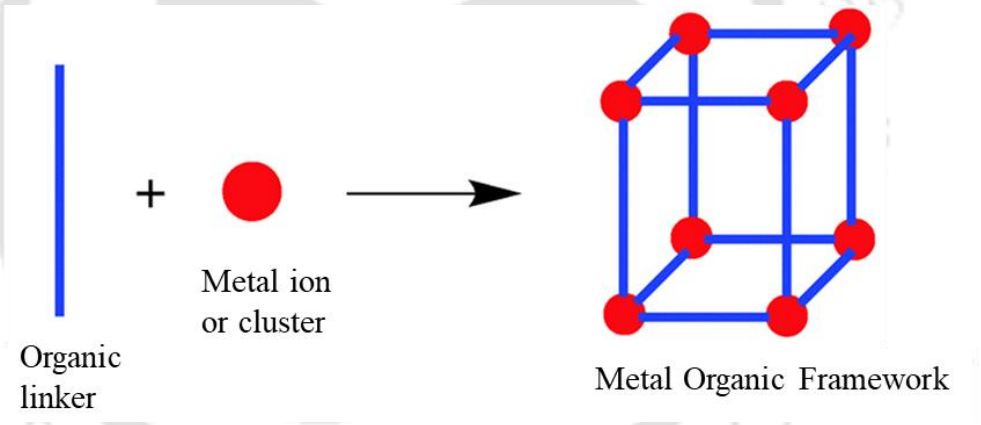

Figure 2.7 Formation of Metal Organic Framework

In recent times, these MOFs have also shown promising behavior for applications as proton conductors. As mentioned, their proton conductivity has only recently been experimented with. The first known study in literature studying the proton conductivity and the mechanism of proton transfer on the MOF-integrated membranes was recorded by Wu et al. [51]. It was found that the MOFs prepared showed high proton conductivity at a temperature of 90°C. Hybridization of the polymer and the hydrogen bonding in the

MOFs were mainly given as the reasons for the obtained trends in proton conduction. The vehicle mechanism and Grotthus mechanism were proposed as the plausible methods of proton transfer. The MOF polymer composite membranes synthesized by Liang et al. [52] showed enhanced proton conductivity and good functionality at low humidity. Similarly, a recent publication by Mukhopadhyay et al. [53] demonstrated the synthesis of a MOF-based proton conductor by integrating amine and sulfonic groups onto the surface of H_2N-MIL-53-AL. A Cu(II) MOF was prepared by incorporating amine and sulfonate groups which are anticipated to promote proton conductivity [54].

Despite high proton conductivities, MOFs come with several limitations such as limited chemical stability and extreme sensitivity to water and acidic solutions. And it is still a challenge to make these MOFs efficient enough for commercial use. Moreover, most of the studies concerning proton-conducting MOFs involved pellets or single crystals. These cannot be used in real applications as the mobility of the proton carriers decreases in bulk phase because of the loss of distant conductivity across boundaries. Consequently, MOFs in the pellet form or bulk phase result in extremely low values of proton conductivity.

To overcome this drawback, this study formulates the MOFs as membranes, which is ideal for usage in fuel cells. However, MOF alone cannot handle a fuel cell functionalization. One of the major drawbacks of the MOFs is its low chemical stability. Hence, the study aimed at bridging this gap by creating mixed matrix membranes (MMMs) of the MOF with stronger membranes that can provide chemical stability. In this regard, PVDF was used as the polymeric membrane matrix since it has excellent mechanical strength and remarkable chemical and thermal stability. However, its hydrophobic nature poses a serious threat to the PEM. So, a PVP-PVDF mixture was used so that the hydrophilicity of the PVP can tackle the hydrophobicity of the PVDF.

The synthesis of the MOF was one-pot in a round bottom flask. A moderate temperature was maintained. Cu-SAT $\{[CU_2(\mu_2\text{-}OH)_2(NDS)(t\$A)_2.2DMF\}_n$ crystals were synthesized and the nanoparticles of this MOF were blended with PVP-PVDF mixture . The membranes were prepared via simple casting with varying percentages of the MOFs. It was found that these composite membranes exhibited higher proton conductivities than the pristine MOFs and thus proving to be of promising nature for fuel cell applications.

Nafion based MOF-GO composite membrane has proved them as a promising candidate for proton conduction [55], stability and moderate performance in mild conditions. Graphene oxide has been found to enhance the proton conductivity of PEMs because of their dual abilities of proton donation as well as proton transfer. Hence, these advantages of MOF and GO were taken into account and a Metal Organic Framework-GO membrane was prepared by in-situ growth method. A ZIF-8 ($Zn(MeIM)_2$ MeIM=2-methylimidazole) framework was taken owing to its good chemical stability. The oxygen containing groups of GO facilitated an in-situ growth of ZIF-8 on the GO sheet as these oxygen containing groups act as binders for the Zn^{2+} ions, thereby acting as sites of nucleation. The so-formed ZIF@GO was then integrated into the Nafion matrix. The hydrogen bonding interactions between ZIF-8 and GO greatly improved the water retention. The performance was found to be greatly enhanced due to the speedy proton transfer carried out by the monolayer structure of the ZIF-8@GO. The proton conductivity of these membranes was found to be 55 times more than that of pristine Nafion. A reduced methanol permeation was also noted. Thus, these MOF@GO/Nafion membranes showed promising behavior for use in fuel cells to yield high performance. However, it rapidly loses its proton conductivity and suffers water loss at high temperature. So, further studies aim on modifying these Nafion membranes in order to achieve more desirable membrane characteristics.

As mentioned earlier, MOFs exhibit extreme sensitivity to water and acidic solutions. So, to conquer this limitation, a researcher group has synthesized a MOF that exhibited strong coordination bonds facilitating the MOF to behave better in water and acidic solutions, without compromising the proton conductivity [56]. Phosphate and phosphonate esters were considered for the ligand groups since they are known to form strong bonds with metal ions. Alleviating the cause of the phosphate and phosphonate esters for use, recent reports have demonstrated excellent usage of these esters in proton conduction. Phytic acid was chosen as the organic ligand owing to the presence of a significant amount of phosphoric groups and its green, bioavailable nature. A hexasphoric MOF named JUC-200 ($Zn_{10}(C_6H_8P_6O_{24})_2(-H_2O)_{14}.x(H_2O)$] was synthesized and membranes were formed by a simple casting method. The resultant membrane exhibited high opposition to water and acidic media. Thus, stable, conductive modified MOF membranes were formed.

The anisotropic conductivity of novel CFA-17 MOF ($[Fe(C_6N_6O_2)(H_2O)_4]$ MOF helped in the analysis of the influence of the network of the pores on the transfer of protons [57]. This MOF, based on alternating bistriazole-p-benzoquinone anions exhibited high proton conductivity values comparable to some of the best known water-mediated MOFs. The study provided a better outlook towards theorizing the conduction mechanisms in MOFs which can prove to be useful in tailoring the MOFs accordingly in order to obtain favorable outcomes.

The sub-micrometer sized crystalline particles of MOF named MOF-801 [$(Zr_6O_4(OH)_4(fumarate)_6\text{-}(DMF)_{1.9}(H_2O)_{22}$] were incorporated into PVP-PVDF matrix to form MOF-801@PP-X composite membranes [58] (X denotes the mass percentage of the MOF-801). As mentioned earlier, the PVP-PVDF membranes were used taking into consideration their excellent chemical, mechanical, thermal stability, their ease of

formation of membranes and the ability of PVP to counterbalance the unfavorable hydrophobicity of PVDF. These membranes exhibited good proton conductivities and ultra-resistance against water and acidic media.

A novel bifunctional MOF was synthesized named MNS (MIL-101-NH_2-SO_3H). Varying amounts of MNS were added into a dimethylacetamide solution of SNF-PAEK to form SNF-PAEK-XX membranes where XX stood for the weight % of MNS. A Nafion membrane was used for comparison purposes. It was found that MNS acted as an cross-linking agent and thus greatly enhanced the mechanical strength and stability of the organic-inorganic hybrid membranes. The MNS@SNF-SPAEK-3% membrane exhibited moderate cell performance thus showing potentials for use in PEMFCs [59].

In spite of this enormous amount of researches being conducted, MOFs based membranes are unable to meet the demands of the energy-environment sector in terms of proton exchange capacity. Thus, studies on improving the properties of MOFs is an area of present concern. In this regard, the proton conductivities in MOFs are generally aggravated using two methods. The first method is to induce guest molecules such as imidazole, triazole, hydronium ions etc., and then entrap them within the pores of the molecules [60]. The second method is to modify the organic ligand by functionalization as proton conduction is promoted by these functional groups.

As an example, UiO-66-NH_2 and UiO-66-SO_3H MOFs were chosen over pure MOF owing to their better stabilities and slightly larger pore size. -SO_3H and -NH_2 groups were chosen because of their tendency to favor proton conduction [60]. Various membranes were then prepared by first individually doping the MOFs on Nafion membrane to form UiO-66-NH_2/Nafion and UiO-66-SO_3H/Nafion membranes and then codoping the Nafion membrane with both the MOFs to form UiO-66-NH_2+UiO-66-SO_3H/Nafion

membrane. It was found that this PEM prepared by codoping both the different functionalized MOFs showed the high conductivity. This was attributed to the synergistic promotion caused by the MOFs that led to the formation of more hydration channels. The high stabilities of the MOFs also provide high proton conductive stability to the codoped PEM. The methanol permeability was also found to be reduced owing to the pores of the MOF which have the tendency to trap methanol. The study also demonstrates how synergistic promotions can be used with different materials to achieve high PEMFC performance.

Electrospinning technique was also used to synthesize a novel MOF-anchored-nanofibre network (UiO-66-NH_2@NFs) on sulfonated poly (ether sulfone) (SPES) membrane matrix [61]. 3D organic or inorganic nanofibers modified with acid or base have been found to result in high performance PEMs. Electrospun nanofibers proved to be highly effective owing to interconnections in their structure and high surface area. Better proton transfer pathways are formed due to proton transport taking place through both the membrane matrix as well as the nanofiber networks. Hence, this particular study aims at forming a PEM that is a combination of functional MOFs and electrospun nanofibers. The nanofibers will also help in a better dispersion of the MOF. UiO-66-NH_2 MOF was used for anchoring. Thus, UiO-66-NH_2@NFs membranes were prepared. It was found that the interconnected networks of the nanofibers along with the outstanding hydrophilic nature of the -SO_3H and -NH_2 groups helped in the formation of continuous hydration channels that promote proton transfer. The -SO_3H and -NH_2 groups provided continuous hydrogen bonded networks that greatly facilitated proton hopping mechanism while also helping in blocking methanol permeation.

A PEM with interconnected UiO-66-NH_2 which bound onto GO was integrated onto a Nafion membrane matrix [62]. This study aimed at facilitating proton conduction at both high humidity and low humidity. The proton transfer takes place in a membrane mostly by two mechanisms, namely the Vehicle mechanism and the GrÖthous mechanism. The vehicle mechanism occurs predominantly in high humidity conditions, wherein the protons diffuse in the form of H_3O^+ and $H_5O_2^+$, and high water retention capacity is required, while the GrÖthous Mechanism occurs in low humidity conditions where the proton transfer takes place through hopping mechanism. The current study has GO@UiO-66-NH_2 incorporated into a Nafion matrix which shows high performance. The tethering effect of the GO and the MOF give rise to well interconnected proton transfer pathways and also decreases the conducting barriers of conduction in both the mechanisms. Thus, proton conductivity is enhanced. The UiO-66-NH_2 has a high water retention capacity which facilitates proton transfer through vehicle type mechanism even at high humidity. The GO@UiO-66-NH_2 also provides moderate water stability and thermal stability to these composite membranes. The decrease in the conduction barriers led to a significant reduction in the methanol permeability. Thus, this study achieved good performance PEMs that can be used in PEMFCs.

Table 2.4 Summay of the proton conductivity of MOF based membrane

Membrane	**MOF (wt%)**	**Proton Conductivity (S cm^{-1}× 10^{-2})**	**Ref.**
Hexaphosphate ester-based MOF, JUC200 / poly(vinyl alcohol)	5	0.014	55
Hexaphosphate ester-based MOF, JUC200 / poly(vinyl alcohol)	10	0.0331	55
Iron(II)-MOF	2%	0.21	56
MOF-801@ PVP and Poly(vinylidene fluoride)	20	0.03013	57

MOF-801@ PVP and Poly(vinylidene fluoride)	40	0.0243	57
MOF-801@ PVP and Poly(vinylidene fluoride)	60	0.0184	57
MIL-101-NH_2-SO_3H@SNF-Poly(arylene ether ketone)	1	5.5	58
MIL-101-NH_2-SO_3H@SNF-Poly(arylene ether ketone)	2	6	58
MIL-101-NH_2-SO_3H@SNF-Poly(arylene ether ketone)	3	6.6	58
MIL-101-NH_2-SO_3H@SNF-Poly(arylene ether ketone)	4	8.0	58
MIL-101-NH_2-SO_3H@SNF-Poly(arylene ether ketone)	5	7.5	58
UiO-66-SO_3H/Nafion-0.6	-	10.4	59
UiO-66-NH_2/Nafion-0.6	-	7.7	59
UiO-66-NH_2 + UiO-66-SO_3H/Nafion-0.6	-	13.4	59
UiO-66-NH_2 nanofiber/ Nafion	2	7.3	60
UiO-66-NH_2 nanofiber/ Nafion	6	9.4	60
UiO-66-NH_2 nanofiber/ Nafion	8	11.5	60
UiO-66-NH_2 nanofiber/ Nafion	10	9.7	60

2.5 Research Gap

Among the polymeric membranes used for DMFC applications, PEEK is a widely researched polymer due to their structural properties. PEEK membrane was subjected to sulfonation to enhance its hydrophilicity and proton conductivity. This was performed by using concentrated sulfuric acid, which resulted in introduction of –SO_3H groups into the polymer chains of PEEK, making them ion-exchangeable. However, the chemical and thermal stability decreases due to incorporation of –SO_3H groups. Moreover, when degree of sulfonation exceeds a threshold limit, the membrane is accompanied with changes in the hydrophilicity/hydrophobicity ratio and reduction in water channels, hence

lowering the proton conductivity. In order to overcome the aforementioned limitation, various organic and inorganic materials such as clays, zeolites, MOFs, etc. have been added to SPEEK matrix membranes. The current literature survey concludes that MOFs acts as a medium of proton conduction. However, they pose certain road gaps due to their particle boundaries and bulk phase. In this regard, GO can be used as a suitable dopant. The structure of GO possesses hydrophilic functional groups such as, hydroxyl, carboxyl and epoxy which assists in formation of proton conduction channels via hydrogen bonding. Thus, it enhances the proton conduction via hopping mechanism and improved water retention. However, due to hydrophilic functional groups on the surface of GO, it cannot restrict the passage of methanol to the desired extent. This calls in for doping of a third suitable material, which can a) reduce the methanol permeability, keeping the proton conductivity unaltered or b) increase the conductivity without affecting the methanol permeability.

2.6 Conclusions

This chapter encompasses published research works relating to fabrication, characterization, and performance of various composites and membranes in terms of methanol permeability, conductivity, and selectivity for DMFC applications. A clear, conclusive, definite approach has been made towards adopting composite membrane based process as an economic and robust option. The conversion of electrical energy to chemical energy takes places without any intermediate phase which ensures no emissions and thereby, proves as an efficient alternative for power production. The main objective of a fuel cell is the production of electricity and heat without any toxic or pollutant as by-product. However, the expensive nature and the unsatisfactory outcome of the fuel cells hinder them from being commercialized. Thus, developing a cost-effective fuel cell along

with a high performance is the pivotal objective of many research works. However, despite a substantial amount of research being done on DMFCs, several limitations pose as hindrance which obstruct them from being commercialized. A membrane is of utmost importance in a fuel cell since they affect the designs of the other components of a fuel cell. The longevity of the fuel cell also depends on the membrane. The major drawbacks of the membranes developed so far are regarding their proton conductivity, ability to resist methanol crossover. Hence, suitable membranes must be developed which can overcome these limitations.

References:

1. M. Wang, M. Chen, Z. Yang, Y. Wang, Y. Wang, G. Liu, J.K. Lee, X. Wang, A study on fuel additive of methanol for room temperature direct methanol fuel cells, Energy Conversion and Management 168 (2018) 270-275.
2. L. Carrette, K. Friedrich, U. Stimming, Fuel cells-fundamentals and applications, Fuel Cells 1(1) (2001) 5-39.
3. T. Yang, Z. Li, H. Lyu, J. Zheng, J. Liu, F. Liu, Z. Zhang, H. Rao, A graphene oxide polymer brush based cross-linked nanocomposite proton exchange membrane for direct methanol fuel cells, RSC Advances 8(28) (2018) 15740-15753.
4. L. Gong, Z. Yang, K. Li, W. Xing, C. Liu, J. Ge, Recent development of methanol electrooxidation catalysts for direct methanol fuel cell, Journal of Energy Chemistry 27(6) (2018) 1618-1628.
5. A. Iulianelli, A. Basile, Sulfonated PEEK-based polymers in PEMFC and DMFC applications: A review, International Journal of Hydrogen Energy 37(20) (2012) 15241-15255.
6. K.-D. Kreuer, S.J. Paddison, E. Spohr, M. Schuster, Transport in proton conductors for fuel-cell applications: simulations, elementary reactions, and phenomenology, Chemical Reviews 104(10) (2004) 4637-4678.
7. B. Smitha, S. Sridhar, A. Khan, Solid polymer electrolyte membranes for fuel cell applications—a review, Journal of membrane science 259(1-2) (2005) 10-26.
8. D. Gupta, V. Choudhary, Studies on novel heat treated sulfonated poly (ether ether ketone) [SPEEK]/diol membranes for fuel cell applications, International Journal of Hydrogen Energy 36(14) (2011) 8525-8535.

9. N.W. Deluca, Y.A. Elabd, Polymer electrolyte membranes for the direct methanol fuel cell: a review, Journal of Polymer Science Part B: Polymer Physics 44(16) (2006) 2201-2225.
10. X. Liu, Y. Zhang, S. Deng, C. Li, J. Dong, J. Wang, Z. Yang, D. Wang, H. Cheng, Semi-interpenetrating polymer networks toward sulfonated poly (ether ether ketone) membranes for high concentration direct methanol fuel cell, Chinese Chemical Letters 30(2) (2019) 299-304.
11. S. Ren, C. Li, X. Zhao, Z. Wu, S. Wang, G. Sun, Q. Xin, X. Yang, Surface modification of sulfonated poly (ether ether ketone) membranes using Nafion solution for direct methanol fuel cells, Journal of Membrane Science 247(1-2) (2005) 59-63.
12. E. Şengül, H. Erdener, R.G. Akay, H. Yücel, N. Baç, İ. Eroğlu, Effects of sulfonated polyether-etherketone (SPEEK) and composite membranes on the proton exchange membrane fuel cell (PEMFC) performance, International Journal of Hydrogen Energy 34(10) (2009) 4645-4652.
13. F. Wang, J. Li, T. Chen, J. Xu, Synthesis of poly (ether ether ketone) with high content of sodium sulfonate groups and its membrane characteristics, Polymer 40(3) (1999) 795-799.
14. K. Kreuer, On the development of proton conducting materials for technological applications, Solid State Ionics 97(1-4) (1997) 1-15.
15. M. Ise, Polymer-Elektrolyt-Membranen: Untersuchungen zur Mikrostruktur und zu den Transporteigenschaften für Protonen und Wasser, (2000).
16. B. Bauer, D. Jones, J. Roziere, L. Tchicaya, G. Alberti, M. Casciola, L. Massinelli, A. Peraio, S. Besse, E. Ramunni, Electrochemical characterisation of sulfonated

polyetherketone membranes, Journal of New Materials for Electrochemical Systems 3(2) (2000) 93-98.

17. X. Li, Z. Wang, H. Lu, C. Zhao, H. Na, C. Zhao, Electrochemical properties of sulfonated PEEK used for ion exchange membranes, Journal of Membrane Science 254(1-2) (2005) 147-155.
18. B. Yang, A. Manthiram, Multilayered membranes with suppressed fuel crossover for direct methanol fuel cells, Electrochemistry Communications 6(3) (2004) 231-236.
19. M. Gil, X. Ji, X. Li, H. Na, J.E. Hampsey, Y. Lu, Direct synthesis of sulfonated aromatic poly (ether ether ketone) proton exchange membranes for fuel cell applications, Journal of Membrane Science 234(1-2) (2004) 75-81.
20. M.M. Ali, A. Azam, S. Rizvi, Synthesis and characterization of sulfonated poly ether ether ketone (SPEEK)/CNTs composite proton exchange membrane for application in fuel cells, Materials Today: Proceedings 5(9) (2018) 17901-17905.
21. S. Sasikala, S. Meenakshi, S. Bhat, A. Sahu, Functionalized Bentonite clay-sPEEK based composite membranes for direct methanol fuel cells, Electrochimica Acta 135 (2014) 232-241.
22. E. Sgreccia, M. Di Vona, P. Knauth, Hybrid composite membranes based on SPEEK and functionalized PPSU for PEM fuel cells, International Journal of Hydrogen Energy 36(13) (2011) 8063-8069.
23. K. Kreuer, On the development of proton conducting polymer membranes for hydrogen and methanol fuel cells, Journal of Membrane Science 185(1) (2001) 29-39.

24. S. Xue, G. Yin, Methanol permeability in sulfonated poly (etheretherketone) membranes: a comparison with Nafion membranes, European Polymer Journal 42(4) (2006) 776-785.

25. M.J. Parnian, S. Rowshanzamir, F. Gashoul, Comprehensive investigation of physicochemical and electrochemical properties of sulfonated poly (ether ether ketone) membranes with different degrees of sulfonation for proton exchange membrane fuel cell applications, Energy 125 (2017) 614-628.

26. S. Banerjee, K.K. Kar, Impact of degree of sulfonation on microstructure, thermal, thermomechanical and physicochemical properties of sulfonated poly ether ether ketone, Polymer 109 (2017) 176-186.X. Jin, M.T. Bishop, T.S. Ellis, F.E. Karasz, A sulphonated poly (aryl ether ketone), British Polymer Journal 17(1) (1985) 4-10.

27. S. Zaidi, S.D. Mikhailenko, G. Robertson, M. Guiver, S. Kaliaguine, Proton conducting composite membranes from polyether ether ketone and heteropolyacids for fuel cell applications, Journal of Membrane Science 173(1) (2000) 17-34.

28. G. Alberti, M. Casciola, L. Massinelli, B. Bauer, Polymeric proton conducting membranes for medium temperature fuel cells (110–160 C), Journal of Membrane Science 185(1) (2001) 73-81.

29. G.P. Robertson, S.D. Mikhailenko, K. Wang, P. Xing, M.D. Guiver, S. Kaliaguine, Casting solvent interactions with sulfonated poly (ether ether ketone) during proton exchange membrane fabrication, Journal of Membrane Science 219(1-2) (2003) 113-121.

30. D. Daoust, P. Godard, J. Devaux, R. Legras, C. Strazielle, Chemical modification of poly (ether ether ketone) for size exclusion chromatography at room temperature: 1. Absolute molecular-mass determination for sulfonated PEEK, Polymer 35(25) (1994) 5491-5497.

31. D. Shukla, Y.S. Negi, J.S. Uppadhyaya, V. Kumar, Synthesis and modification of poly (ether ether ketone) and their properties: a review, Polymer Reviews 52(2) (2012) 189-228.
32. N. Asano, M. Aoki, S. Suzuki, K. Miyatake, H. Uchida, M. Watanabe, Aliphatic/aromatic polyimide ionomers as a proton conductive membrane for fuel cell applications, Journal of the American Chemical Society 128(5) (2006) 1762-1769.
33. M.J. Parnian, S. Rowshanzamir, A.K. Prasad, S.G. Advani, Effect of ceria loading on performance and durability of sulfonated poly (ether ether ketone) nanocomposite membranes for proton exchange membrane fuel cell applications, Journal of Membrane Science 565 (2018) 342-357.
34. S. Kaliaguine, S. Mikhailenko, K. Wang, P. Xing, G. Robertson, M. Guiver, Properties of SPEEK based PEMs for fuel cell application, Catalysis Today 82(1-4) (2003) 213-222.
35. J. Han, Y. Wu, J. Pan, Y. Peng, Y. Wang, C. Chen, Q. Pan, B. Xie, N. Zhao, Y. Wang, Highly conductive and stable hybrid ionic cross-linked sulfonated PEEK for fuel cell, Electrochimica Acta 291 (2018) 353-361.
36. X. Li, Z. Wang, H. Lu, C. Zhao, H. Na, C. Zhao, Electrochemical properties of sulfonated PEEK used for ion exchange membranes, Journal of Membrane Science 254(1-2) (2005) 147-155.
37. F. Wang, T. Chen, J. Xu, Sodium sulfonate-functionalized poly (ether ether ketone) s, Macromolecular Chemistry and Physics 199(7) (1998) 1421-1426.
38. W.R. Bowen, T.A. Doneva, H. Yin, Polysulfone -sulfonated poly (ether ether) ketone blend membranes: systematic synthesis and characterisation, Journal of Membrane Science 181(2) (2001) 253-263.

39. D. Gupta, V. Choudhary, Non-fluorinated hybrid composite membranes based on polyethylene glycol functionalized polyhedral oligomeric silsesquioxane [PPOSS] and sulfonated poly (ether ether ketone)[SPEEK] for fuel cell applications, Reactive and Functional Polymers 73(9) (2013) 1268-1280.
40. M. Kumari, H. Sodaye, R. Bindal, Cross-linked sulfonated poly (ether ether ketone)-poly ethylene glycol/silica organic–inorganic nanocomposite membrane for fuel cell application, Journal of Power Sources 398 (2018) 137-148.
41. H.-J. Choi, S.-M. Jung, J.-M. Seo, D.W. Chang, L. Dai, J.-B. Baek, Graphene for energy conversion and storage in fuel cells and supercapacitors, Nano Energy 1(4) (2012) 534-551.
42. R. Kumar, M. Mamlouk, K. Scott, A graphite oxide paper polymer electrolyte for direct methanol fuel cells, International Journal of Electrochemistry 2011 (2011).
43. P. Pattanayak, N. Pramanik, P. Kumar, P.P. Kundu, Fabrication of cost-effective non-noble metal supported on conducting polymer composite such as copper/polypyrrole graphene oxide (Cu2O/PPy–GO) as an anode catalyst for methanol oxidation in DMFC, International Journal of Hydrogen Energy 43(25) (2018) 11505-11519.
44. M. Feng, Y. Huang, Y. Cheng, J. Liu, X. Liu, Rational design of sulfonated poly (ether ether ketone) grafted graphene oxide-based composites for proton exchange membranes with enhanced performance, Polymer 144 (2018) 7-17.
45. K.-J. Peng, J.-Y. Lai, Y.-L. Liu, Nanohybrids of graphene oxide chemically-bonded with Nafion: Preparation and application for proton exchange membrane fuel cells, Journal of Membrane Science 514 (2016) 86-94.
46. H.-C. Chien, L.-D. Tsai, C.-P. Huang, C.-y. Kang, J.-N. Lin, F.-C. Chang, Sulfonated graphene oxide/Nafion composite membranes for high-performance

direct methanol fuel cells, International Journal of Hydrogen Energy 38(31) (2013) 13792-13801.

47. C. Lin, Y. Lu, Highly ordered graphene oxide paper laminated with a Nafion membrane for direct methanol fuel cells, Journal of Power Sources 237 (2013) 187-194.
48. Q.-L. Zhu, Q. Xu, Metal–organic framework composites, Chemical Society Reviews 43(16) (2014) 5468-5512.
49. A. Huang, Q. Liu, N. Wang, J. Caro, Highly hydrogen permselective ZIF-8 membranes supported on polydopamine functionalized macroporous stainless-steel-nets, Journal of Materials Chemistry A 2(22) (2014) 8246-8251.
50. B. Wu, X. Lin, L. Ge, L. Wu, T. Xu, A novel route for preparing highly proton conductive membrane materials with metal-organic frameworks, Chemical Communications 49(2) (2013) 143-145.
51. X. Liang, F. Zhang, W. Feng, X. Zou, C. Zhao, H. Na, C. Liu, F. Sun, G. Zhu, From metal–organic framework (MOF) to MOF–polymer composite membrane: enhancement of low-humidity proton conductivity, Chemical Science 4(3) (2013) 983-992.
52. S. Mukhopadhyay, J. Debgupta, C. Singh, R. Sarkar, O. Basu, S.K. Das, Designing UiO-66-Based Superprotonic Conductor with the Highest Metal–Organic Framework Based Proton Conductivity, ACS Applied Materials & Interfaces 11(14) (2019) 13423-13432.
53. R. Moi, A. Ghorai, S. Banerjee, K. Biradha, Amino-and Sulfonate-Functionalized Metal–Organic Framework for Fabrication of Proton Exchange Membranes with Improved Proton Conductivity, Crystal Growth & Design 20(8) (2020) 5557-5563.

54. L. Dong, M. Chen, J. Li, D. Shi, W. Dong, X. Li, Y. Bai, Metal-organic framework-graphene oxide composites: A facile method to highly improve the CO2 separation performance of mixed matrix membranes, Journal of Membrane Science 520 (2016) 801-811.

55. K. Cai, F. Sun, X. Liang, C. Liu, N. Zhao, X. Zou, G. Zhu, An acid-stable hexaphosphate ester based metal–organic framework and its polymer composite as proton exchange membrane, Journal of Materials Chemistry A 5(25) (2017) 12943-12950.

56. H. Bunzen, A. Javed, D. Klawinski, A. Lamp, M. Grzywa, A. Kalytta-Mewes, M. Tiemann, H.-A.K. von Nidda, T. Wagner, D. Volkmer, Anisotropic water-mediated proton conductivity in large iron (II) metal–organic framework single crystals for proton-exchange membrane fuel cells, ACS Applied Nano Materials 2(1) (2018) 291-298.

57. J. Zhang, H.-J. Bai, Q. Ren, H.-B. Luo, X.-M. Ren, Z.-F. Tian, S. Lu, Extra water- and acid-stable MOF-801 with high proton conductivity and its composite membrane for proton-exchange membrane, ACS applied materials & interfaces 10(34) (2018) 28656-28663.

58. C. Ru, Z. Li, C. Zhao, Y. Duan, Z. Zhuang, F. Bu, H. Na, Enhanced proton conductivity of sulfonated hybrid poly (arylene ether ketone) membranes by incorporating an amino-sulfo bifunctionalized metal–organic framework for direct methanol fuel cells, ACS applied materials & interfaces 10(9) (2018) 7963-7973.

59. Z. Rao, B. Tang, P. Wu, Proton conductivity of proton exchange membrane synergistically promoted by different functionalized metal–organic frameworks, ACS Applied Materials & Interfaces 9(27) (2017) 22597-22603.

60. L. Wang, N. Deng, Y. Liang, J. Ju, B. Cheng, W. Kang, Metal-organic framework anchored sulfonated poly (ether sulfone) nanofibers as highly conductive channels for hybrid proton exchange membranes, Journal of Power Sources 450 (2020) 227592.

61. Z. Rao, K. Feng, B. Tang, P. Wu, Construction of well interconnected metal-organic framework structure for effectively promoting proton conductivity of proton exchange membrane, Journal of Membrane Science 533 (2017) 160-170.

CHAPTER 3

Characterization Techniques and Experimental protocols

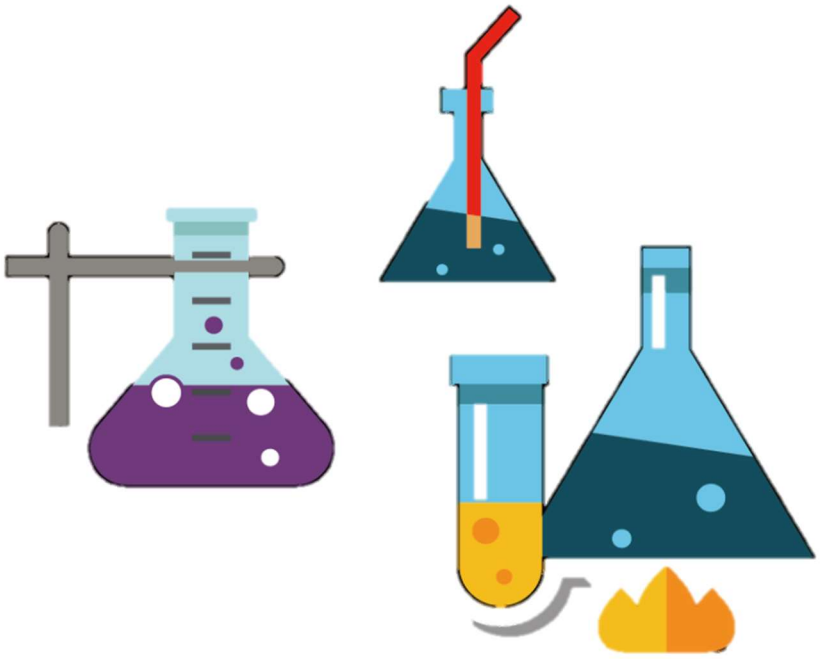

CHAPTER 3

Characterization techniques and experimental protocols

This chapter outlines the different methods which have been mainly used to characterize the synthesized materials and fabricated membranes. Brief descriptions on the experimental protocols for measurement of water uptake, ion exchange capacity, methanol permeability and ion conductivity of fabricated membranes are also presented. Experimental protocols for material synthesis and membrane fabrication are included in the related chapters.

3.1 Field-Emission Transmission Electron Microscope (FETEM)

Transmission electron microscopy (TEM) is used for detailed analysis of structure and morphology of particles. Selected area electron diffraction (SAED) attached to it provides information about amorphous crystalline nature of the sample.. An objective aperture is placed in the back focal plane, behind objective lens. By adjusting position of objective aperture on specific positions in the back focal plane, two types of images are generated. Bright-field (BF) image is formed when only transmitted electrons are allowed by the aperture to pass through it. In the dark field (DF), only diffracted electrons pass through the aperture. SAED analysis involves magnification of transmitted or diffracted signal from the sample by a system of electromagnetic lenses which is ultimately visible as an image on the fluorescent screen. Except spatial imaging and diffraction, the high-energy electrons produced as a result of inelastic scattering excite the atoms of the sample under investigation. Also, chemical composition of the specimen can be obtained using energy dispersive X-ray spectra (EDS) attached to the TEM setup [1].

All the TEM analyses in this dissertation were done using TEM (Jeol, JEM 2100) in the bright field mode with an accelerating voltage of 200 kV. The samples were homogenously dispersed in ethanol and drop casted on 300 mesh copper grid followed by vacuum drying before mounting.

3.2 Field Emission Scanning Electron Microscopy (FESEM)

The structure, surface texture and morphology are analyzed by field emission scanning electron microscope (FESEM). The tungsten field emitter generates electron beam which hits the sample and collides with the electrons generated by it. This elastic scattering generates highly energetic (>50 eV) back scattered electrons (BSE) which are reflected in back scattered mode. Secondary electrons (SE) having lower energy (2-50 eV) are formed due to inelastic collisions. After detection and amplification of the signals, they are transferred to a computer, where image is generated with resolution upto 1 nm [2]. Sample is coated with either carbon, gold or palladium to enhance the surface conductivity via sputtering. The atomic number of the element constituting the sample determines the brightness of the image formed by BSE. Low molecular weight elements give rise to darker images whereas heavier elements form bright images. Narrow probing beams at low as well as high electron energy results in improved resolution [1].

FESEM (Zeiss, Sigma) was used in the present work to obtain the images of synthesized materials. Sample dispersed in ethanol was drop casted on glass slide, dried under vacuum overnight and then coated with carbon or gold.

3.3 Atomic Force Microscopy (AFM)

Atomic force microscopy is a type of scanning probe microscopy (SPM) with a higher resolution scanning microscope. AFM is used to analyze different type of surface properties such as size, surface roughness, texture along with three-dimensional topography. For this experiment carbon tape is generally used to place the sample for analysis. The high resolution topographical images were recorded using AFM (Oxford, Cypher) at a scan rate of 0.7 Hz in tapping mode. AFM images were further processed using flatten filter in Windows-Scanning-x-Microscope (WSxM) software [3].

3.4 X-Ray Diffraction Analysis (XRD)

X-ray diffraction (XRD) technique is an important characterization technique for determining the chemical composition, structure, crystallinity, phase of the samples. Atoms in crystalline materials are considered as sets of parallel crystallographic planes which are characterized by Miller indices (h k l). According to Bragg's law, diffraction maxima occur when the crystallographic planes fulfill the conditions for constructive interference [4].

$$n\lambda = 2dsin\theta \qquad (3.1)$$

where θ is the angle between the crystallographic plane and incident beam, d is the distance between two successive planes, λ is the wavelength of radiation, and n is an integer. The sample, X-ray tube, and the detector are located on the focusing circle. The X-ray tube is kept fixed, while the detector rotates along the goniometer maintaining a specific angular speed. The detector is always kept at angle 2θ whereas, the sample surface is always at angle θ with respect to the incident beam during the XRD analysis. The detector records the angle and the relative intensity of diffracted radiation [5]. In this

dissertation, all the analyses were performed using XRD (Bruker, D8 Advance) operating at 40 kV and 40 mA. Measurements were taken from 2θ= 3 to 80°. Monochromatic Cu-Kα (λ= 1.5417 Å) was used as source of radiation.

3.5 Fourier Transform Infrared Spectroscopy (FTIR)

FTIR (IRAffinity-1, M/s Shimadzu) spectroscopy was used to analyze the chemical structure of the synthesized composite and fabricated membranes. A Perkin Elmer Paragon 1000 FTIR Spectrophotometer was used for the purpose. Before analysis samples were dried in an oven at 110 °C overnight. KBr background was used for testing. Absorbance spectra was recorded for both the samples [6].

3.6 X-ray Photoelectron Spectroscopy (XPS)

X-ray Photoelectron Spectroscopy (ESCALAB Xi+, Thermo-Scientific) spectrometer is widely used as a surface analysis technique to determine the chemical state information with a valuable quantitative data. In XPS technique the average depth of analysis is 5nm. For emission of photoelectrons from sample to surface, the mono-energetic Al kα x-rays is used to excite the samples and the energy of the emitted photoelectrons is measured by an electron energy analyzer. Elemental composition, chemical state and quantitative analysis can be estimated from the binding energy values [7].

3.7 Raman Spectroscopy

Raman spectroscopy is a form of vibrational spectroscopy similar to infrared (IR) spectroscopy which measures the samples vibrational energy modes. Due to the change in the polarizability of the molecules, Raman bands arise and then it can be identified by plotting the transition energy when it’s plotted as a spectrum. Its help us to provide both chemical and structural information which is applicable to many different chemical

species [8]. Raman spectroscopy (Horiba Jobin Vyon, LabRam HR) has used to get the detailed information regarding the chemical structure, crystallinity and phase has been analyzed using this spectroscopy.

3.8 Thermogravimetric Analysis (TGA)

Thermogravimetric analysis (TGA) is a method for analyzing the thermal stability of a sample. Here, changes in properties of materials are measured as a function of increasing temperature (maintaining constant heating rate), or as a function of time (with constant temperature and/or constant mass loss). TGA plot can interpret any physical change occurring in a material with change of temperature, such as vaporization, sublimation, absorption, adsorption, and desorption. TGA plot can also explain about chemical reactions like chemisorption, decomposition, dehydration and solid-gas reactions (e.g., oxidation or reduction). It can predict degradation mechanisms [9], determine organic and inorganic content in a sample.

TGA (TGA-50, Shimadzu) analysis helps us to analyze the stability of the materials, degradation mechanisms and temperature needed for calcinations [10].

3.9 Specific Surface Area

Specific surface area of any material is calculated from the nitrogen adsorption/desorption isotherm data using different models. The most common is the Brunauer-Emmett-Teller (BET) method which is based on the following equation:

$$\frac{1}{\left(\frac{P}{P_0}-1\right)n} = \frac{1}{Cn_m} + \frac{(C-1)}{Cn_m}\frac{P}{P_0} \qquad (3.2)$$

where amount of nitrogen n is adsorbed at pressure P, nm is the amount of nitrogen

forming a monolayer, and constant C is related to the adsorption energy in the first adsorbed monolayer (C usually ranges between 50 and 250). Plot of $\frac{1}{\left(\frac{P}{P_0}-1\right)n}$ versus $\frac{P}{P_0}$ yields a straight line with a slope of $\frac{(C-1)}{Cn_m}$ and intercept $\frac{1}{Cn_m}$. From these values, n_m can be calculated from which surface area S is found following the equation

$$S = \frac{n_m}{M_r} N_A \sigma \qquad (3.3)$$

Where, Mr represents molecular weight of nitrogen, N_A is the Avogadro number, and σ is the cross-sectional area of one molecule of nitrogen [11].

In this work, the BET surface area (Tristar II , Micromeritics, U.S.A.) for all the samples was analyzed using Autosorb iQ where the relative pressure (P/P_0) range was kept between 0.05 and 0.3.

3.10 Water Uptake Behavior

The water uptake of fabricated membrane was observed by recording the weight of the dry membrane (W_{dry}) and the weight of the wet membrane (W_{wet}). The membrane was cut into a specific shape. Then, the membrane was immersed in water solution for 24h. Afterwards, the weight of the wet membranes was measured by rapidly taking out the membranes using a forcep and then wiping the excess water with tissue paper. The water uptake percentage was calculated, using the formula [12]:

$$\text{Uptake (\%)} = \frac{W_{wet} - W_{dry}}{W_{dry}} \times 100\% \qquad (3.4)$$

3.11 Ion Exchange Capacity

IEC is a measure of number of counter-ions exchangeable in membranes. It is defined as the presence of H^+ ion in polymer matrix. In order to determine the IEC, the membrane

was cut and dipped in 1M HCl for 24h solution to protonize the membrane. Then, the membrane was kept in 2M NaCl solution for 24h again. The membrane was removed from the NaCl solution and it was back titrated using 0.1M NaOH solution using phenolphthalein as an indicator. IEC was measured using the formula [12]:

$$\text{IEC} = \frac{C_{NaOH} \times V_{NaOH}}{W_d} \qquad (3.5)$$

Where C_{NaOH} is the concentration of NaOH solution, V_{NaOH} is the volume of NaOH used in the titration and W_d is the weight of the dry membrane.

3.12 Methanol Permeability

The resistance offered against the permeation of methanol through the membranes was analyzed by evaluating the methanol permeability (*P*) of the membranes. A glass cell setup (**Fig. 3.1**) was fabricated in our laboratory, which consisted of two identical glass chambers. The membrane was placed in between the compartments and securely clenched with clamps. The two compartments in the glass setup were the 'feed' section and the 'permeate' section. 5M methanol was poured as the feed whereas distilled water was kept in the permeate section. The chambers were magnetically stirred at a fixed rpm. This permeation experiment was carried out under room temperature. Samples from the permeate section were collected and recorded on an hourly basis. The samples were then analyzed under the High Performance Liquid Chromatography (HPLC) setup [12].

$$\text{Permeability} = \frac{\kappa \times V \times L}{A \times C} \qquad (3.6)$$

Where, $\boldsymbol{\kappa}$ is the slope of the curve between concentration of methanol on the water side and corresponding methanol permeation time, V indicates the initial volume of the

deionized water, L is the thickness of the membrane, A is the area of the membrane and C is the initial concentration of methanol.

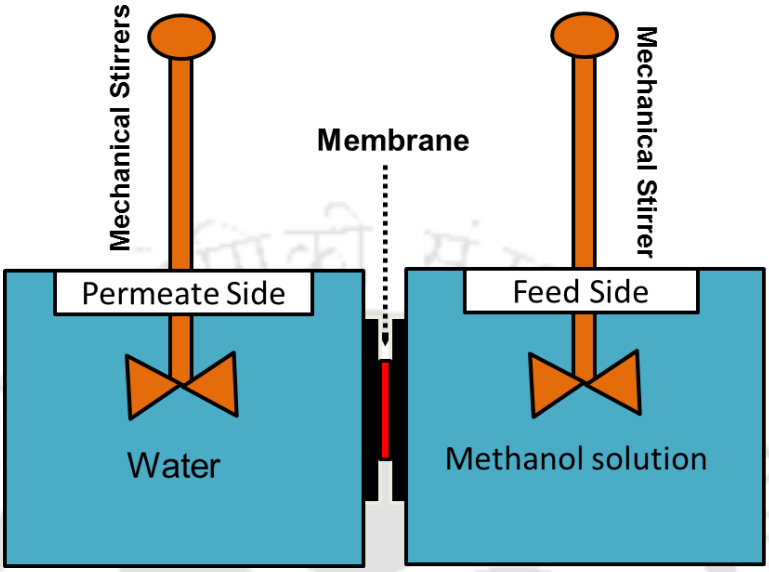

Figure 3.1 Schematic of methanol permeability setup

3.13 Proton Conductivity

The impedance spectroscopy for measuring the ionic conductivity (σ) of the PEM was done using the Autolab PGSTAT204 system. The membranes were immersed in 1M H_2SO_4 solution for 24 h to allow the protonation to take place. Deionized water was then used to wash them three times. The ion conductivity measurement was done using a single cell system which has been purchased from Sainergy Fuel Cell India Private Limited. The dimension is 2.5cm × 2.5cm. The membrane of 5 cm^2, which was kept in water for 24 h, was placed between the Cu electrodes of the single cell system. A frequency over the range of 1 Hz to 1 MHz was set for the impedance measurement, which was carried out at room temperature.

$$\text{Ionic Conductivity} = \frac{L}{R \times A}\ S/cm \qquad (3.7)$$

Where R is the resistance obtained from the high frequency intercept of the impedance with the real axis (Z'), A indicates the area of the membranes and L is the thickness of the membranes [12].

3.14 Membrane Selectivity

The selectivity of a membrane for DMFC application is calculated using the ratio of their ionic conductivity (σ) and methanol permeability (P). Higher selectivity of a membrane indicates more suitability for DMFC application.

$$S = \sigma / P \qquad (3.8)$$

References

1. G.R. Chalmers, R.M. Bustin, I.M. Power, Characterization of gas shale pore systems by porosimetry, pycnometry, surface area, and field emission scanning electron microscopy/transmission electron microscopy image analyses: Examples from the Barnett, Woodford, Haynesville, Marcellus, and Doig units Characterization of Gas Shale Pore Systems, AAPG bulletin 96(6) (2012) 1099-1119.
2. L. Reimer, Scanning electron microscopy: physics of image formation and microanalysis, IOP Publishing, 2000.
3. H.H. Fang, K.-Y. Chan, L.-C. Xu, Quantification of bacterial adhesion forces using atomic force microscopy (AFM), Journal of microbiological methods 40(1) (2000) 89-97.
4. A. Monshi, M.R. Foroughi, M.R. Monshi, Modified Scherrer equation to estimate more accurately nano-crystallite size using XRD, World journal of nano science and engineering 2(3) (2012) 154-160.
5. F.H. Chung, Quantitative interpretation of X-ray diffraction patterns of mixtures. II. Adiabatic principle of X-ray diffraction analysis of mixtures, Journal of Applied Crystallography 7(6) (1974) 526-531.
6. D.M. Byler, H. Susi, Examination of the secondary structure of proteins by deconvolved FTIR spectra, Biopolymers: Original Research on Biomolecules 25(3) (1986) 469-487.
7. M. Chen, X. Wang, Y. Yu, Z. Pei, X. Bai, C. Sun, R. Huang, L. Wen, X-ray photoelectron spectroscopy and auger electron spectroscopy studies of Al-doped ZnO films, Applied Surface Science 158(1-2) (2000) 134-140.
8. D.A. Long, D. Long, Raman spectroscopy, McGraw-Hill New York1977.

9. B.D. Noble, M. Satyanarayanan, D. Narayanan, J.E. Tilton, J. Flinn, K.R. Walker, Agile application-aware adaptation for mobility, ACM SIGOPS Operating Systems Review 31(5) (1997) 276-287.
10. A. Coats, J. Redfern, Thermogravimetric analysis. A review, Analyst 88(1053) (1963) 906-924.
11. D. Dollimore, P. Spooner, A. Turner, The BET method of analysis of gas adsorption data and its relevance to the calculation of surface areas, Surface Technology 4(2) (1976) 121-160.
12. S.S. Gaur, P. Dhar, A. Sonowal, A. Sharma, A. Kumar, V. Katiyar, Thermo-mechanically stable sustainable polymer based solid electrolyte membranes for direct methanol fuel cell applications, Journal of Membrane Science 526 (2017) 348-354.

CHAPTER 4

Fabrication and characterization of a sulfonated proton exchange membrane (SPEEK)

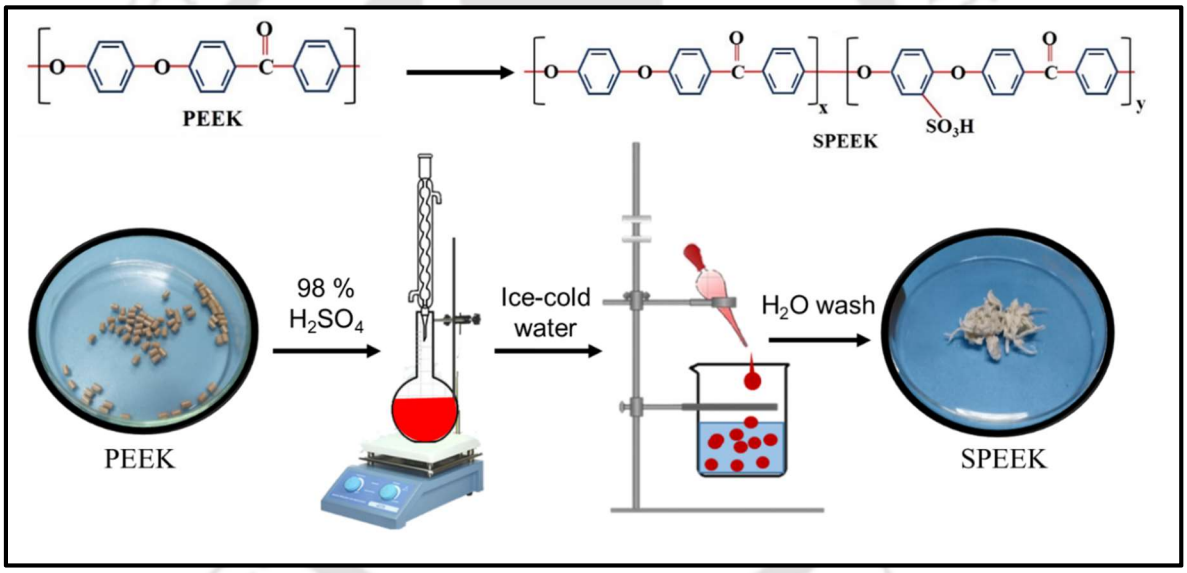

Graphical abstract of sulfonation process of PEEK polymer

CHAPTER 4

Fabrication and characterization of a sulfonated proton exchange membrane (SPEEK)

This chapter deals with the synthesis of sulfonated membrane, for which SPEEK polymer was prepared and investigated. The reaction time was controlled for preparing SPEEK using concentrated H_2SO_4. For confirmation of sulfonation, various characterization details have been furnished by instrumental analyses like FESEM, EDS, XPS, FTIR, TGA and XRD. Water uptake capacity, methanol permeability and conductivity of the membrane were also measured.

4.1 Introduction

The proton exchange accounts for a very crucial component of a fuel cell system. A membrane has to hold out against the extremely harsh chemical and physical environments in a fuel cell. Thus, high stability is a very important quality that a proton exchange membrane must fulfil and must possess excellent resistance against the extreme conditions of a fuel cell like methanol, chemically active noble metal catalysts, chemically energetic fuels, etc. to name a few. As of the current trends, perfluorinated polymers such as Nafion® are the most widely used polymer membranes in DMFCs. These membranes were found to exhibit excellent results in terms of chemical stability and performance, thus accounting to their substantial usage. However, these membranes are highly expensive and come with toxic and environmentally harmful intermediates in the production process. High methanol permeability which severely damages the DMFC performance is another important limitation that needs to be accounted for. It, therefore, becomes the need of the hour to develop efficient alternatives to these perfluorinated ionomers and this forms the area of concern to many researches across the globe. Various

arylene main chain polymers have been in development in the last decade. This can be attributed to the outstanding chemical and mechanical stability of these membranes which is only second to that of the perfluorinated ionomers clan. These membranes have been further sulfonated to bring out proton conducting nature. Polysulfones [1,2], polyimides [3], and polyetheretherketones (PEEK) [4] form the family of arylenes that have been sulfonated. There is a variety of literature supporting the promising nature of SPEEK membranes, taking into account its desirable properties such as good thermal, mechanical and chemical stability, less expensive nature and sufficient conductivity. This chapter deals with the synthesis of sulfonated membrane for which SPEEK polymers were prepared and investigated.

4.2 Experimental Section

4.2.1 Material and methods

Poly(ether ether ketone) (PEEK) was supplied by Polyscience Lab. The analytical grade sulphuric acid (H_2SO_4, 98 wt% Merck), and dimethylacetamide (DMAc) also were purchased commercially from market. Without any further purification all chemicals were used. Throughout the whole experiments Milipore® water (Merck) was used.

4.2.2 Sulfonation of PEEK

The PEEK polymer was sulfonated by adding 5g of PEEK gradually in 98% concentrated H_2SO_4 solution (100 mL) and it was stirred for 5 h using a magnetic stirrer at 323K. The precipitated polymer was then taken and put in ice-cold water and was left to settle overnight (**Fig. 4.1**). The precipitated SPEEK formed white noodle-like strands. Several filtrations and washing were performed with deionized water to bring the pH to neutral. This was then dried in a vacuum oven for one week at 60 °C [5].

4.2.3 Fabrication of SPEEK membrane

A 10 wt% solution was prepared by 1.0 g of SPEEK in N, N-dime-thylacetamide (DMAc) for the synthesis of the membranes. The resulting SPEEK solution were filtered after proper dissolution was ensured, following which a thin film of the polymer solution was casted onto a flat glass plate using a casting knife (Digital II Microm, GARDCO, USA). The casted membrane was dried in a vacuum oven at 60 °C for 48 hours, followed by 120 °C for 24 hours, allowing the DMAc solvent to evaporate (**Fig. 4.1**). The resultant membrane was peeled off from the glass using deionized water after the solvent had evaporated [5]. The thickness of the fabricated membrane is 129 µm.

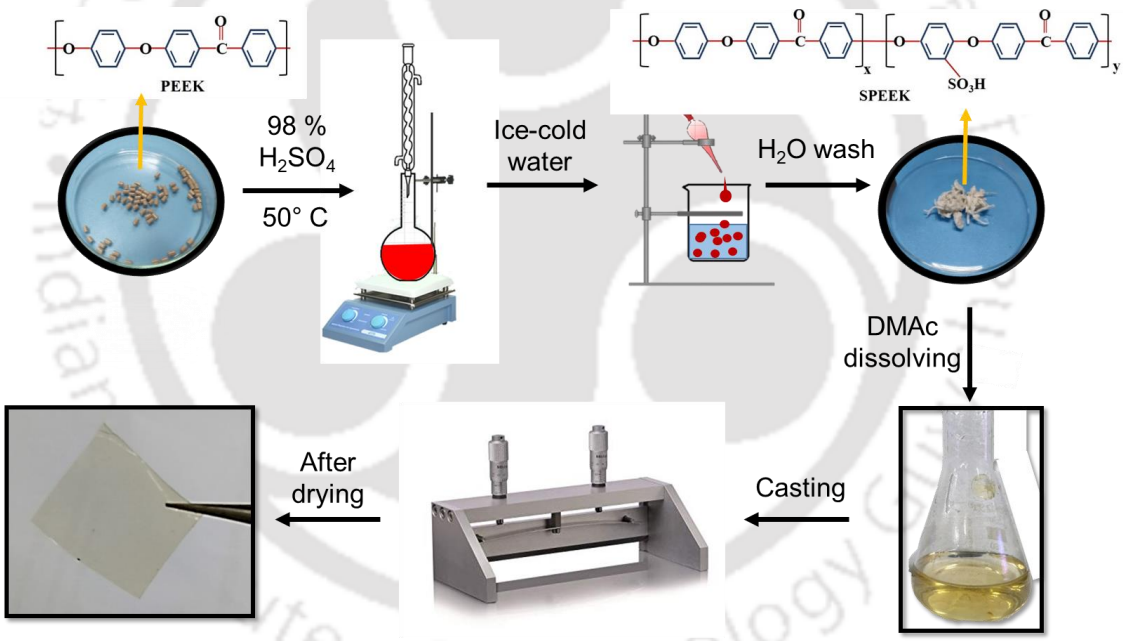

Figure 4.1 Schematic representation of sulfonation of PEEK and fabrication of SPEEK membrane

4.2.4 Membrane characterization

In this section X-ray diffractometer, Field emission scanning electron microscope, X-ray photo electron spectroscopy, Fourier transform infrared spectroscopy,

Thermogravimetric analysis has been used for characterization of fabricated membrane and the weight differences between the full-hydrated membranes and the dried membranes along with their water uptake, methanol permeability and proton conductivity of the membranes (refer to Chapter 3).

4.3 Results and Discussion

The abbreviation PEEK stands for the polymer poly (oxy-1,4-phenylene-oxy-1,4-phenylene-carbonyl-1, 4-phenylene). Various literatures suggest excellent thermal, chemical, electrical and mechanical properties of this semi crystalline polymer. The chemical structure of PEEK is depicted in **Fig. 4.1**. From earlier research, it has been noted that the DMAc, DMF solvent provide a better interaction with the SO^3H groups in SPEEK membrane in compression with NMP and DMSO [6]. That why in DMAc solvent it readily dissolves in strong acids because of protonation and various chemical modifications in the likes of sulfonation.

4.3.1 FESEM and EDX analysis

From FESEM analysis, the image of the top surface (**Fig. 4.2a**) at 1 kX magnification of SPEEK membrane displays a smooth surface, which proposes the good membrane-forming ability. **Fig. 4.2b** shows the cross-sectional view of SPEEK membrane. Top surface of membrane shows symmetrically smothered the polymer surface as well as surface irregularities became small ripple. We have performed EDX mapping analysis (**Fig. 4.2c**) also where we found the presence of sulfur group. Homogeneous distribution of all element on the whole surface confirms the functionalization of PEEK polymer. These topographical and element mapping analyses suggest uniform sulfonation sites

throughout the membrane and suggest this SPEEK membrane made for this study as suitable polymer for proton exchange membrane.

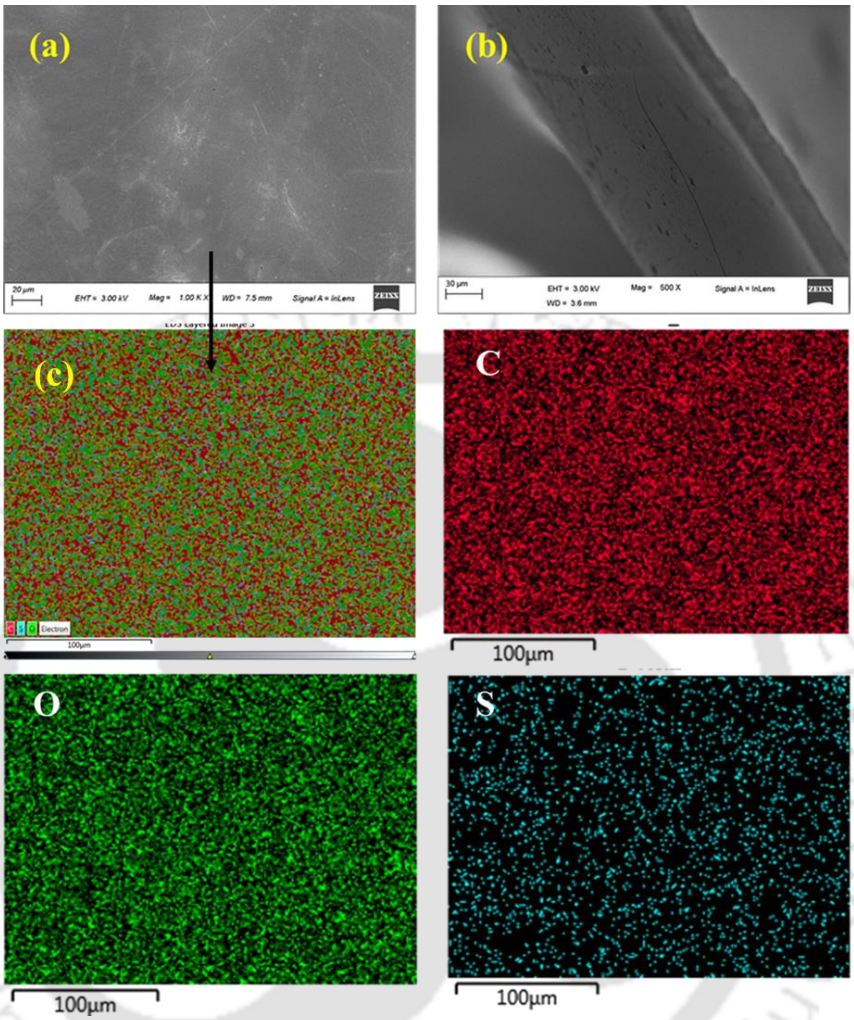

Figure 4.2 FESEM and EDX mapping of fabricated SPEEK membrane

4.3.2 FTIR analysis

The functional groups in a material can be remarkably characterized with Fourier Transform InfraRed Spectroscopy. The FTIR spectra of SPEEK is indicates the chemical structure of the SPEEK membranes (**Fig. 4.3**). The O-H vibration from sulfonic acid groups interacting with molecular water can be seen from the broad spectrum at 3454 cm^{-1}. The substitution upon sulfonation causes the aromatic C-C band to split at 1480 cm^{-1}.

The sulphur-oxygen symmetric vibration O=S=O causes the new absorption band at 1017 cm^{-1} and 1080 cm^{-1} because of the sulfonic acid groups in SPEEK [7]. The intensity of the absorption band at 1080 cm^{-1} is attributed due to mono substituted benzene ring after sulfonation while the absorption band at 1017 cm^{-1} is assigned to para substituted benzene ring and the S-O stretching vibration. This confirms that the PEEK polymer is sandwiched between the ether groups at one position of the phenylene ring. The spectral information demonstrates that only the para position of the terminal phenoxy group is sulfonated.

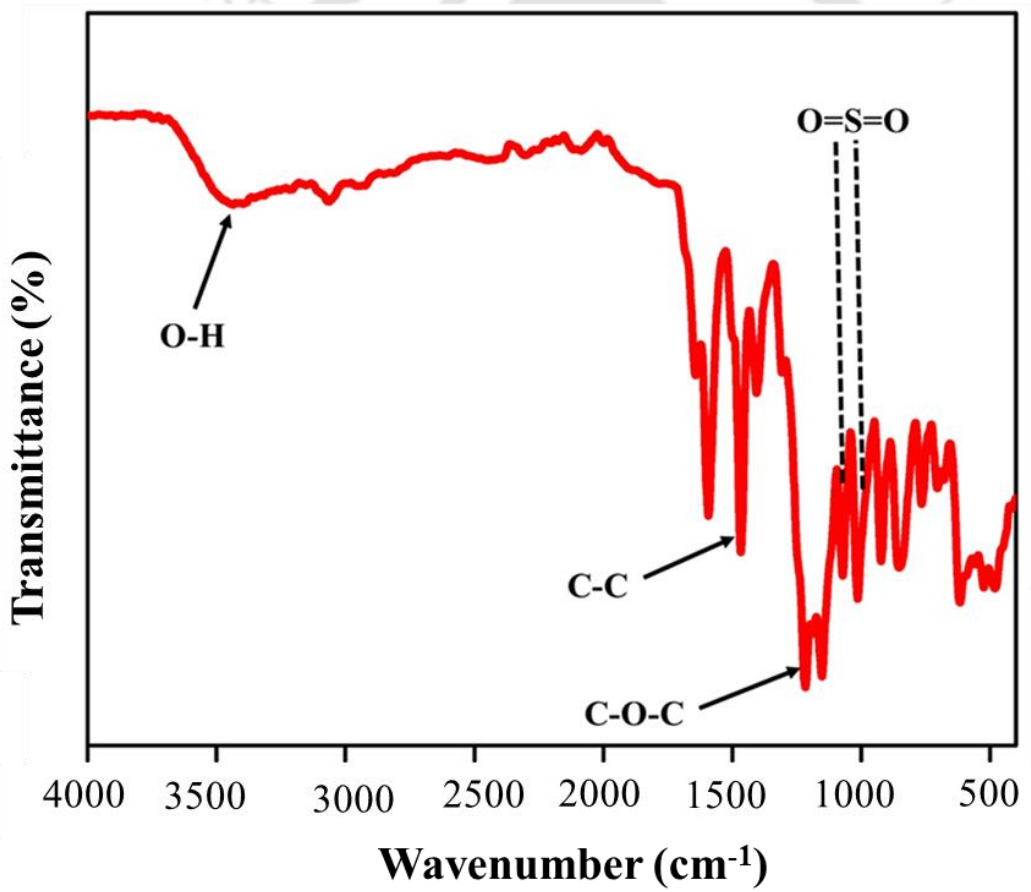

Figure 4.3 FTIR analysis of fabricated SPEEK membrane

4.3.3 XPS analysis

Further to verify the inducement effect of sulfonation with quantitative analysis, XPS was performed in the range of 0-700 eV (**Fig. 4.4**). From the survey scan of SPEEK membrane, three significant spectra perceived were C1s, O1s and s2p. C1s and O1s peaks arise (**Fig. 4.4a**). The peak attributed in the range of 165 eV to 170 eV (**Fig. 4.4b**) is due to the s2p orbital from sulfur in $–SO_3H$ groups group [8]. After deconvolution of C 1s spectrum, three major peaks at the binding energies of 284.8 eV, 286.7 eV and 289.2 eV has arisen which is corresponds to C atoms with sp2 hybridization, C-O from ether groups and carbon atom in the carbonyl group. There are also two different oxygen environments which are C=O (532.7 eV) and C-OH (533.9 eV). We found the elemental composition of sulfur in the membrane SPEEK is 1.79%.

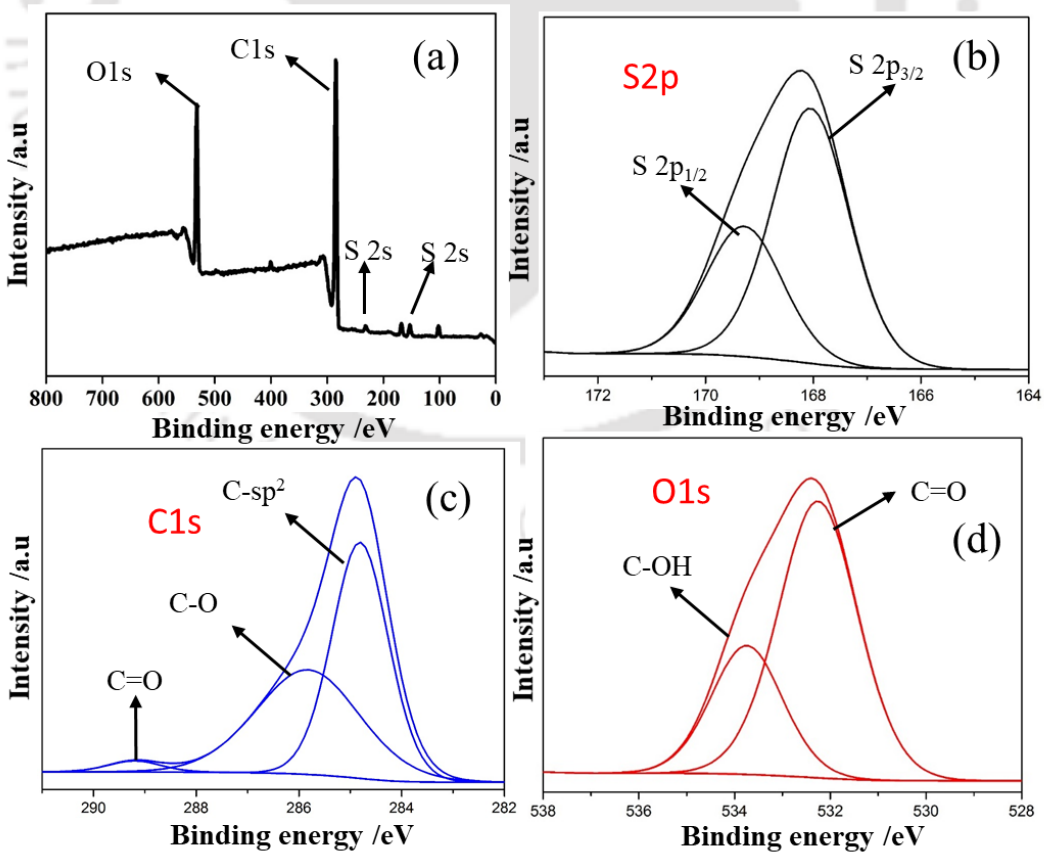

Figure 4.4. XPS analysis of fabricated SPEEK membrane

4.3.4 TGA analysis

The thermal stability of the SPEEK and pristine PEEK powder were characterized by the analysis of TGA. SPEEK shows thermal degradation in three different weight loss (**Fig. 4.5**). Initially, the water that is physically absorbed in the sample gets desorbed. The splitting up of sulfonic acid groups in the temperature range of 300-400°C forms the second step. At temperatures above 500°C, the decomposition of the main chain of SPEEK takes place thus completing the third step. SO_3H causes decomposition of polymer chain, which is why SPEEK starts decomposing at a lower temperature than PEEK. The literature supporting the use of TGA analysis for the determination of the DS of SPEEK is authored by Zaidi et al. [9]. The said study also mentions that SO_3 release mainly influences the second weight loss step.

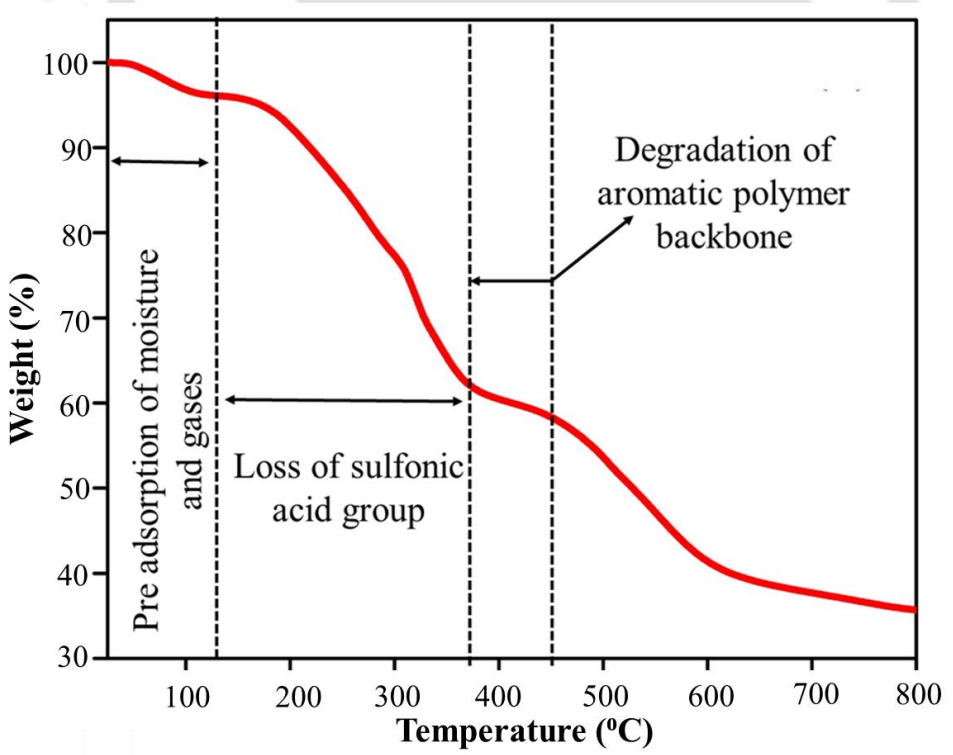

Figure 4.5 TGA of fabricated SPEEK membrane

4.3.5 XRD analysis

The XRD spectra of SPEEK was studied. Bruker D8 advance system for 2θ angles in 5°-45° range with Cu-K alpha electron source was used for the crystallography studies. X-Ray Diffraction was carried out on the membrane to analyze the crystal structure and atomic spacing in the membranes (**Fig. 4.6**). XRD pattern of fabricated membrane shows a broad peak at 2θ = 20º, which disclosed the amorphous nature of the membrane [10].

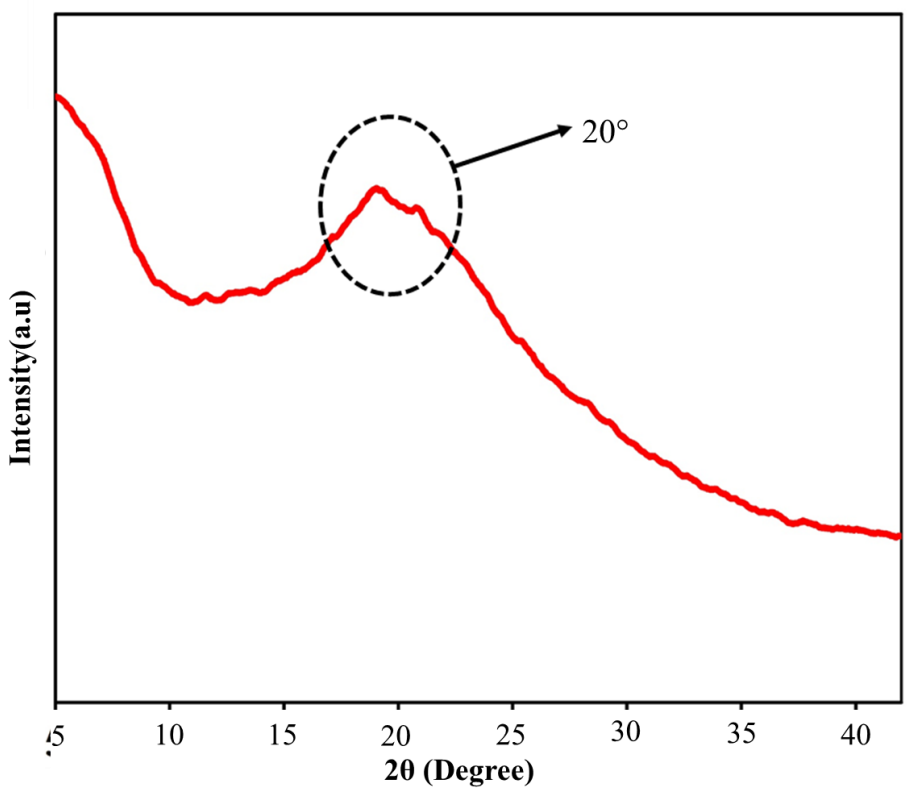

Figure 4.6 XRD spectra of fabricated SPEEK membrane

4.3.6 Water uptake measurement

Weight differences between the hydrated membranes and the dried membranes were calculated for determining the water uptake of the membranes. The membrane was immersed in deionized water at room temperature for one day prior to measurement. This was done until the membranes were saturated which was indicated by no weight gain.

Following this, tissue paper was used to wipe off the liquid water on the surface of these membranes. They were then immediately weighed so as to obtain the wet mass of these swollen fully-hydrated membranes. The water uptake was found to be 45.3 wt %. Water ensures easy and convenient proton transfer as well as increases the conductivity. These are both very desirable properties for an efficient membrane. Sulfonation of PEEK increases the acidity and hydrophilicity, thus positively affecting the membrane's conductivity properties. The number of acid groups available for interaction and the dissociation capability in water affect the proton conductivity of monomeric membranes. It is important to take the water uptake into serious consideration when studying proton exchange membranes as water molecules help in facilitating proton transport. So, water uptake is a very vital parameter that needs to be taken into account.

4.3.7 Methanol permeability, conductivity and selectivity measurement

The methanol permeability of PEM membranes is a major limitation for their commercialization. Methanol permeability of the SPEEK membranes at room temperatures has been plotted in **Fig. 4.7a**. It is to be noted that the membranes were immersed in water, prior to the methanol permeability measurement, for hydration. The methanol permeability of SPEEK membrane was found to be 2.3×10^{-6} cm^2/s. However, the methanol permeability of the prepared SPEEK membranes were found to be slightly lower than that of standard Nafion-117 membrane. Fully hydrated SPEEK membrane was used for the measurement of the conductivity. The conductivity was found as 1.04×10^{-3} S/cm. SPEEK membrane becomes more hydrophilic after sulfonation, thus increasing the water transport. Sulfonation increases water mediated pathways for proton and also increases the number of protonated sites (SO^3H). Both of these attributes help in increasing the conductivity of the membrane.

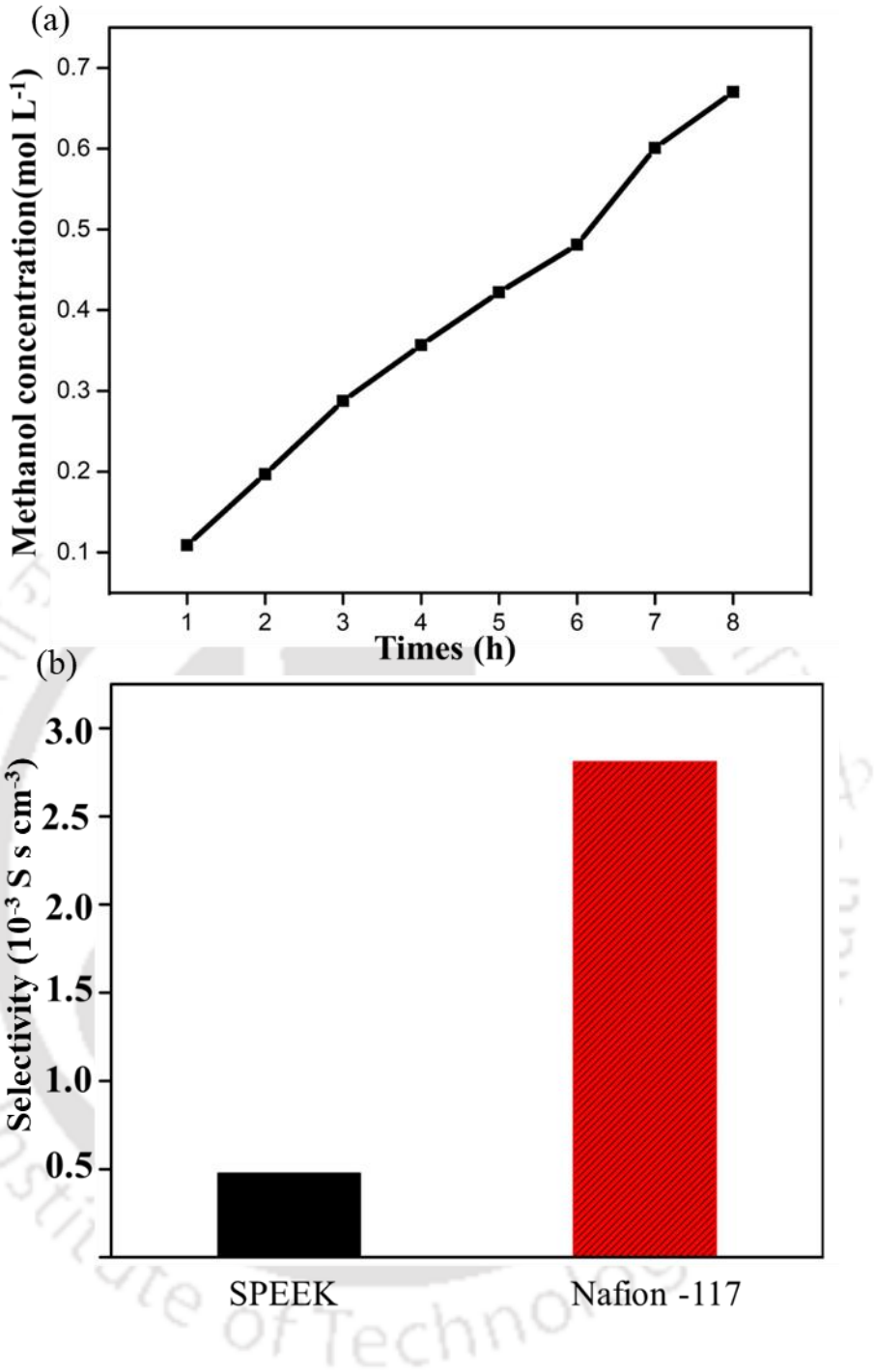

Figure 4.7 (a) Methanol concentration profile and (b) selectivity of SPEEK membrane

4.3 Conclusions

This study had been formulated keeping in mind the objective of fabrication of SPEEK membrane. The sulfonation of PEEK in sulfuric acid only takes place at the para position

of the terminal phenoxy group which is found from the FTIR spectral data. This is consistent with the existing literature. The water uptake was found as 43.5 wt%. Conductivity value was found to be 1.04×10^{-3} S/cm at room temperature whereas Nafion 117 have 6.46 $\times10^{-3}$ S/cm. The selectivity value of fabricated SPEEK was found as 4.7×10^{2} S s cm^{-3} which is ca. 6 times lesser than Nafion 117. So, the properties of the SPEEK membrane could be improved by incorporation of suitable fillers for better selectivity for DMFC application.

References

1. B. Lafitte, L.E. Karlsson, P. Jannasch, Sulfophenylation of polysulfones for proton-conducting fuel cell membranes, Macromolecular Rapid Communications 23(15) (2002) 896-900.
2. M. Ulbricht, M. Riedel, U. Marx, Novel photochemical surface functionalization of polysulfone ultrafiltration membranes for covalent immobilization of biomolecules, Journal of Membrane Science 120(2) (1996) 239-259.
3. J. Fang, X. Guo, S. Harada, T. Watari, K. Tanaka, H. Kita, K.-i. Okamoto, Novel sulfonated polyimides as polyelectrolytes for fuel cell application. 1. Synthesis, proton conductivity, and water stability of polyimides from 4, 4 '-diaminodiphenyl ether-2, 2 '-disulfonic acid, Macromolecules 35(24) (2002) 9022-9028.
4. B. Bonnet, D. Jones, J. Roziere, L. Tchicaya, G. Alberti, M. Casciola, L. Massinelli, B. Bauer, A. Peraio, E. Ramunni, Hybrid organic-inorganic membranes for a medium temperature fuel cell, Journal of New Materials for Electrochemical Systems 3(2) (2000) 87-92.
5. W. Dai, Y. Shen, Z. Li, L. Yu, J. Xi, X. Qiu, SPEEK/Graphene oxide nanocomposite membranes with superior cyclability for highly efficient vanadium redox flow battery, Journal of Materials Chemistry A 2(31) (2014) 12423-12432.
6. M.-S. Jun, Y.-W. Choi, J.-D. Kim, Solvent casting effects of sulfonated poly (ether ether ketone) for Polymer electrolyte membrane fuel cell, Journal of Membrane Science 396 (2012) 32-37.
7. D. Daoust, J. Devaux, P. Godard, Mechanism and kinetics of poly (ether ether ketone)(PEEK) sulfonation in concentrated sulfuric acid at room temperaturePart 1. Qualitative comparison between polymer and monomer model compound sulfonation, Polymer International 50(8) (2001) 917-924.

8. S. He, Y. Lin, H. Ma, H. Jia, X. Liu, J. Lin, Preparation of sulfonated poly (ether ether ketone)(SPEEK) membrane using ethanol/water mixed solvent, Materials Letters 169 (2016) 69-72.
9. S. Zaidi, S.D. Mikhailenko, G. Robertson, M. Guiver, S. Kaliaguine, Proton conducting composite membranes from polyether ether ketone and heteropolyacids for fuel cell applications, Journal of Membrane Science 173(1) (2000) 17-34.
10. M. Song, X. Lu, Z. Li, G. Liu, X. Yin, Y. Wang, Compatible ionic crosslinking composite membranes based on SPEEK and PBI for high temperature proton exchange membranes, International Journal of Hydrogen Energy 41(28) (2016)

CHAPTER 5

Role of oxidation temperature on the structural and functional characteristics of graphite oxide nanosheets

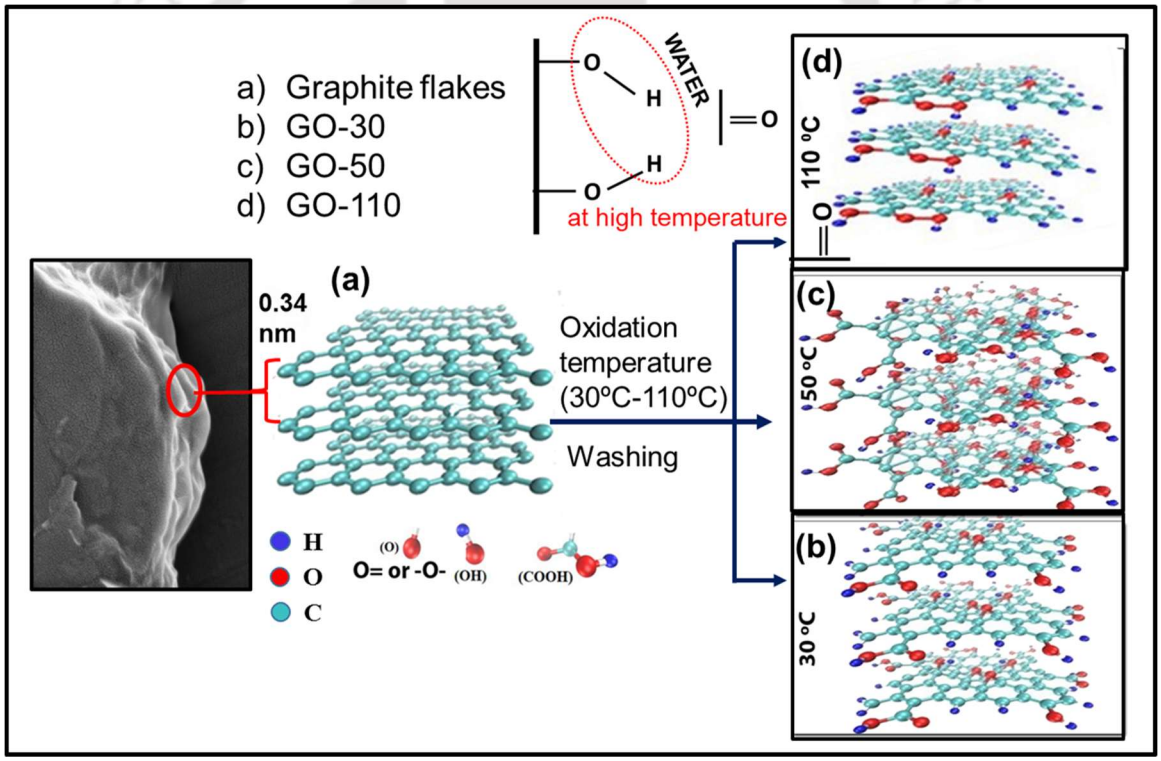

Graphical abstract of proposed mechanism of GO synthesis with different degrees of oxidation

CHAPTER 5

Role of oxidation temperature on the structural and functional characteristics of graphite oxide nanosheets

*This study opens up a new approach to tune the structural and surface functional properties of graphite oxide nanosheets for various applications. As per our objective we have planned to prepare a graphite oxide mixed composite which will increase the PEM selectivity for DMFC application. Herein, we have reported a modified approach towards synthesis of GO nanosheets by varying the temperature in the range of 30-110 ºC. Analytical investigations suggested that the best condition for synthesizing GO was about 50 ºC based on the crystallinity and its single sheet nature. This work has been scientifically acknowledged in "**Applied Surface Science**".*

5.1 Introduction

Over the last decade, graphite-based materials such as graphene oxide, reduced graphene oxide and graphene have emerged as promising candidates for applications in energy storage, support formation for nano structures, polymer composites, supercapacitors, biomedical applications, etc. due to their excellent electrical, mechanical and thermal properties [1–6]. Among the graphite family, graphite oxide (GO) is an intermediate product during the synthesis of graphene oxide. GO is usually synthesized by the well-known wet chemical Hummer's method based on the oxidation of graphite [7]. There are ample reports available on the synthesis and formation of GO sheets (especially in acidic conditions) [8-14]. GO demonstrates considerable variation of physical properties depending on the synthesis method, particle sizes, reaction temperature, residence time and degree of oxidation, while maintaining its two-dimensional planar carbon network

[9–11]. During the formation of GO sheets from graphite, significant amount of graphitic C-sp^2 is oxidized into C-sp^3 bonding with oxygen atom [6, 15]. Notably, the GO sheets possess various oxygenated functionalities such as hydroxyl, carboxyl, carbonyl and epoxy groups on the basal planes and on the edge sites [15]. The excellent electrochemical properties of graphene like high conductivity, stability at high temperatures and electronic capabilities were considered and hence, was chosen as a suitable membrane for DMFC.

The engineering of the structural and surface functional properties of GO nanosheets by varying temperature, which is one of the significant reaction conditions has not been explored yet in any literature. The temperature dependent tunability in the structural as well as functional properties of GO is explained based on the modulation in the functional groups present on their surface. This is vital for tailoring the properties of GO nanosheets and can help in the development of sustainable carbon materials.

5.2 Experimental Section

5.2.1 Materials

The analytical grade sulphuric acid (H_2SO_4, 98 wt%, Merck), orthophosphoric acid (H_3PO_4, 88 wt%, Merck), potassium permanganate ($KMnO_4$, Merck), hydrogen peroxide (H_2O_2, 30 wt%, Merck) and hydrochloric acid (HCl, 37 wt%, Merck) were purchased and used without further purification. Graphite powder (Sigma-Aldrich) was used as a carbon source for the synthesis of GO. Millipore® (Merck) purified water was used during the synthesis procedure.

5.2.2. Synthesis of GO

GO was synthesized by oxidation of graphite following modified Hummers method [16]. Graphite powder (0.5gm) was dispersed in a mixture of H_2SO_4/H_3PO_4 (63:7 mL) and stirred for 30 minutes at room temperature. Subsequently, $KMnO_4$ (3.0 g) was added to the solution slowly in an ice bath (ensuring that the temperature change is less than 5 ^oC) and the solution is stirred for an hour. Further, the reaction (oxidation) temperature was increased to 30 °C and stirred for additional 12 h. Next, water (150 mL) was added to the solution followed by the addition of H_2O_2 (4 mL). The resulting greenish solution is shown in **Fig. 5.1** The mixture was centrifuged at 500 rpm to remove the unreacted graphite. Further, supernatant liquid was centrifuged at 15000 rpm to separate the synthesized GO. The resulting gel was washed (3 times) with 1 M HCl solution. Finally, it was washed with water (about 8 times) such that the pH of the supernatant is about 7. The gel thus obtained was dried under vacuum and resulting GO was denoted as GO-30. The samples were also synthesized at other oxidation temperatures according to the above procedure by varying the oxidation temperature (50 °C, 75 °C, 90 °C and 110 °C). They were accordingly labelled GO-50, GO-75, GO-90, and GO-110, respectively. The pictures of the resulting GO solutions after reaction are also shown in **Fig. 5.1**.

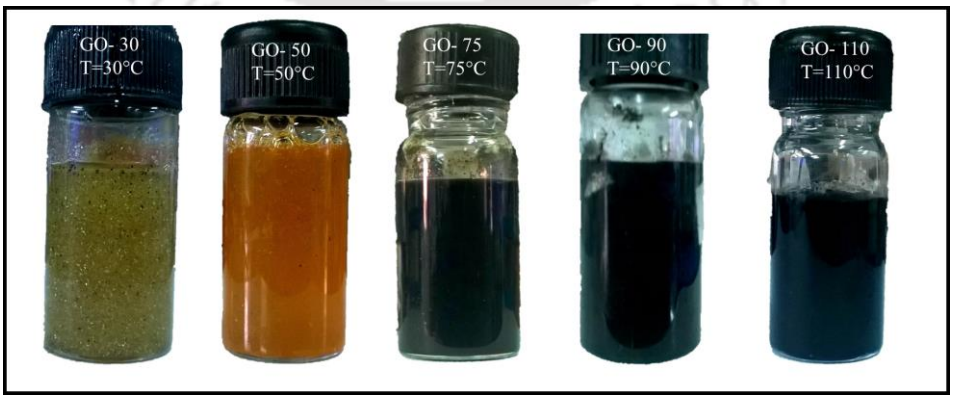

Figure 5.1 As-synthesized GO solutions after the oxidation at different synthesis temperature from 30 °C to 110 °C.

5.2.3. Material characterization

In this section X-ray diffractometer, Field emission scanning electron microscope, X-ray photo electron spectroscopy, Fourier transform infrared spectroscopy, Thermogravimetric analysis, BET surface area analyser, UV Visible spectrophotometer, Raman spectroscopy has been used for characterization (refer to Chapter 3).

5.3. Results and Discussion

5.3.1 XRD analysis

The XRD pattern of temperature dependent synthesis of GO nanosheets is depicted in **Fig. 5.2**. Generally, the graphite powder shows a strong diffraction peak at a 2θ=26.5º which is due to the (002) reflection plane, with inter-planar spacing of 0.335 nm [18]. However, the peak corresponding to 2θ=26.5º of pristine graphite completely disappeared and new peak appears at 2θ=8.03º when graphite oxidizes at 30 ºC. This clearly indicates the conversion from graphite to GO and the successful formation of GO. The sharp peak corresponding to 2θ=8.03º is due to the (001) plane of GO, with inter-planar spacing of 1.1 nm (calculated using *Bragg's law*) and this result matches well with the earlier work [19]. The appearance of peak at 2θ=8.03º is due to the introduction of oxygen functionalities in the graphite. After increasing the temperature from 30 to 110 ºC, the peak corresponding to 2θ=8.03º shifted towards the higher 2θ values. Additionally, XRD peak intensity gradually decreased with increase in oxidation temperature above 75 ºC. This may be due to the reduction of intercalated oxygen functionalities [19]. After reaching the synthesis temperature of 90 ºC, the peak corresponding to (001) plane nearly disappeared and a new and broad peak appeared

corresponding to 2θ=25.83º. This may be due to the formation of reduced graphene oxide (rGO) [20]. The structural disorder can also be explained in terms of crystallite size [9].

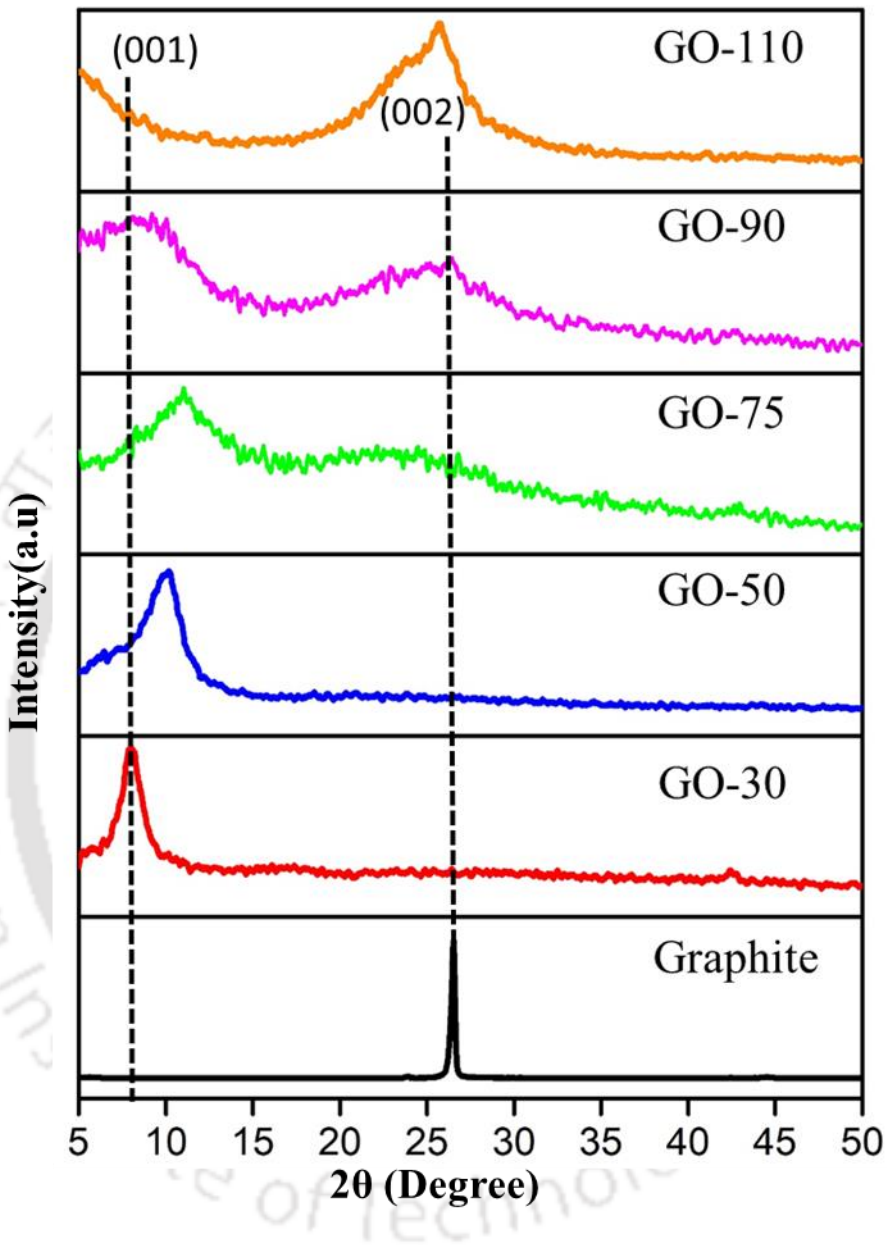

Figure 5.2 XRD spectra of GO samples.

The calculated crystallite size is reported in **Table 5.1**. Pure graphite has a crystallite size ~42 nm after oxidation it reduces 4.2 nm in GO-50 which indicates the structural disorder to the in-plane sp^2 domain of the graphite because of the high influence of oxidation

process [9]. With further increase in temperature up to 110ºC the crystallite size becomes lesser (~1.4 nm) which indicates the formation of rGO. [21].

Table 5.1 Physical properties of synthesized GO.

Sample name	From XRD		From RAMA N
	Peak position (2θ)	Crystallite size (nm)	I_D/I_G
GO-30°C	8.2	5.1	0.92
GO-50°C	9.19	6.5	0.98
GO-75°C	11.02	2.4	0.88
GO-90°C	25.83	1.9	0.82
GO-110°C	25.83	1.4	0.53

5.3.2 FETEM analysis

TEM images of GO synthesized at five different temperatures are shown in **Fig. 5.3** As a result of oxidation, the exfoliation of graphite is also visible from TEM analysis. The wrinkled morphology suggests the presence of large number of functional groups such as hydroxyl, carboxyl on the edge, and carboxyl and epoxide groups in the inner part of synthesized GO [18,22]. Significantly, selected area electron diffraction (SAED) pattern of GO was used to understand the successful oxidation at different temperatures. In case of GO-30, a diffused diffraction ring pattern with disordered structure was observed in **Fig. 5.3(a)**. This demonstrates that the chemical oxidation as well as exfoliation of graphite layer does not occur completely at room temperature and consists in layers [23]. With further increase in temperature up to 50 ºC, a diffused diffraction ring pattern of GO displayed the set of six-fold symmetric diffraction point of a typical hexagonal ring. Further increasing the synthesis temperature to 110 ºC **Fig. 5.3(e)** led to complete

disappearance of a diffused diffraction ring pattern of GO. This illustrates that the GO became disordered in nature and lost its crystallinity which is presumably due to the oxidation reaction.

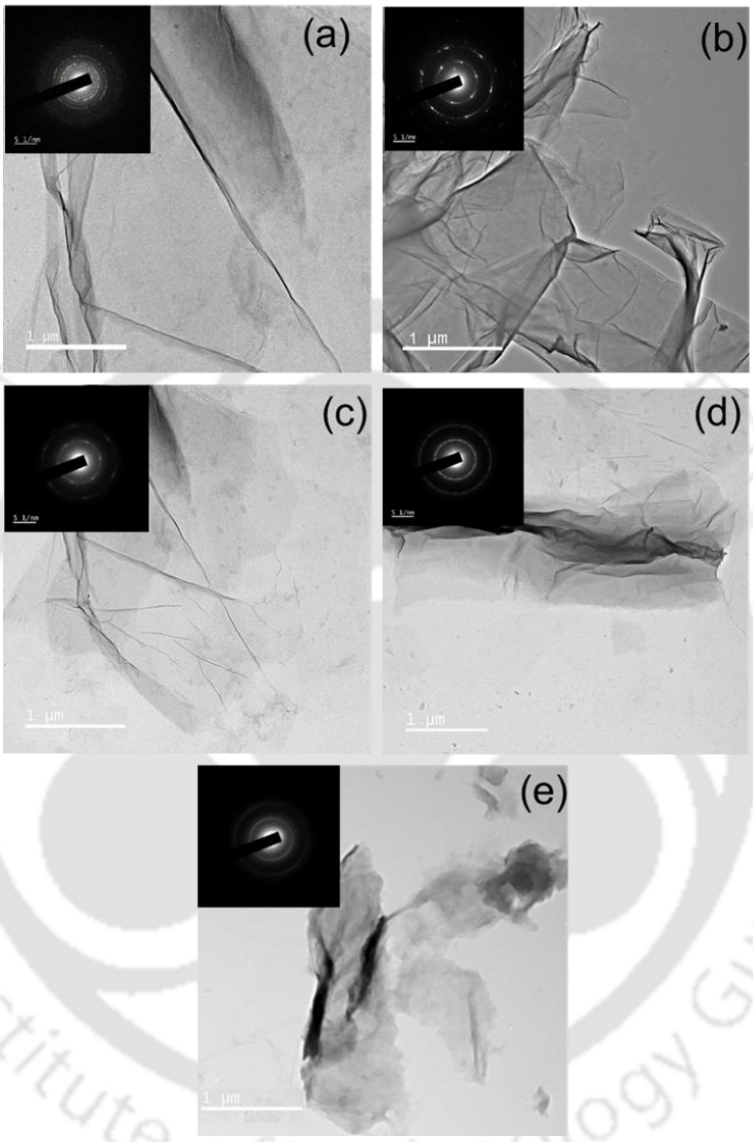

Figure 5.3 TEM micrograph of (a) GO-30 (b) GO-50 (c) GO-75 (d) GO-90 and (e) GO-110 samples and its corresponding SAED pattern.

5.3.3 TGA analysis

The effect of the synthesis temperature on the thermal stability of the GO was investigated by TGA analysis. The TGA curves of the synthesized GO are shown in **Fig.**

5.4. The TGA curve of GO exhibited three distinct stages of weight loss with increase in temperature. The initial weight loss between 30 to 100 ºC is mainly for the adsorbed moisture and the gases. With further increase in temperature up to 300 ºC, a sharp weight loss is observed. This is associated with the removal of C–OH, C–O–OH, C=O and C–O–C groups present in GO [24]. The weight loss between 100 to 300 ºC is mainly due to the lower bond energy C–OH and C–O–C groups. In the last stage (up to 800 ºC), the weight loss is related to the pyrolysis of carbon skeleton present in the GO [23]. In comparison in between 100 ºC – 300 ºC, it is observed that the change in weight loss follows the order GO-110 (10.2 wt %) < GO-90 (10.5 wt %) < GO-75 (31.5 wt %) < GO-30 (39.4 wt %) < GO-50 (42.5 wt %). This suggests that the oxygen containing functional groups concentration is maximum for GO-50 [25].

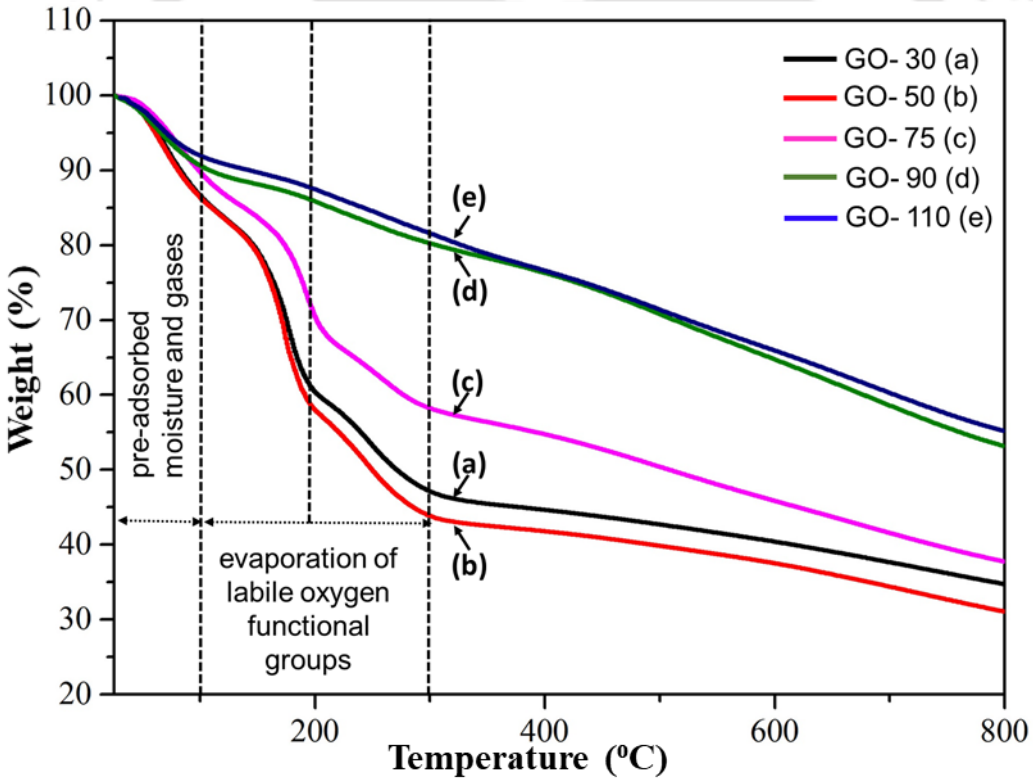

Figure 5.4 TGA spectra of GO-30, GO-50, GO-75, GO-90 and GO-110 samples.

5.3.4 Raman spectroscopic analysis

Raman spectroscopic analysis is a non-destructive technique used to analyse carbon based materials. The Raman spectra of graphite and the synthesized GO's are shown in **Fig. 5.5**. The peaks corresponding to 1580 cm^{-1}, 2730 cm^{-1} and 3250 cm^{-1} are characteristic for the graphite [26, 27]. The peak at ~ 1580 cm^{-1} corresponds to the planer stretching of C-sp^2 bond [27]. After oxidation of graphite, new peaks appeared at ~1360 cm^{-1} and indicate the change in the electronic structure of graphite during oxidation process. This is associated with the C-sp^3 bond vibration [27]. On the other hand, the peak at 1580 cm^{-1} shifted to slightly higher wave number ~ 1585 cm^{-1}. These changes are characteristic of the Raman spectrum of GO [18, 27]. These changes are prominent in GO synthesized at 30 and 50 ^oC, but their intensity decreases at higher synthesis temperatures; in fact at 110 ^oC, these peaks completely disappear. The *D*-peak represents the defects and disordered carbon in the GO layer while the G-peak is mainly from the two dimensional hexagonal lattice [23, 28]. The *2D* band at ~2700 cm^{-1} is originated due to the crystalline nature of graphitic materials and the *D+G* band at 2950 cm^{-1} suggests the disorder of graphite [29].

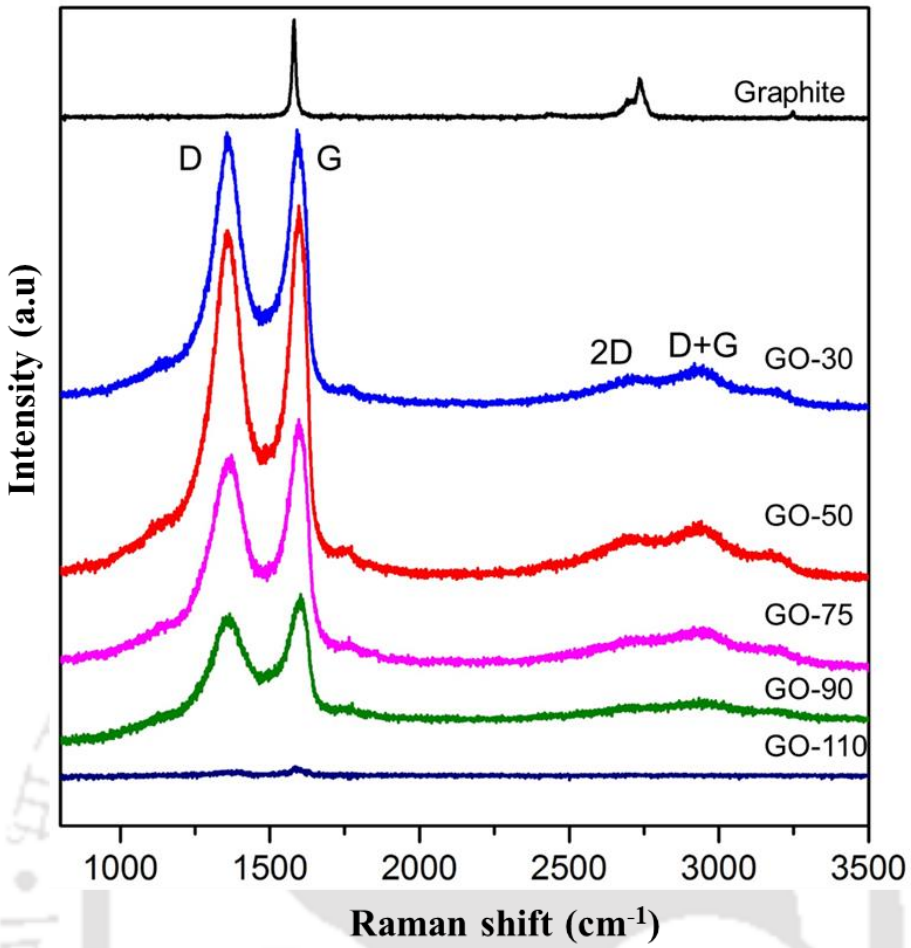

Figure 5.5 RAMAN spectra of GO samples.

The intensity ratio of *D* band and *G* band (I_D/I_G) was used to investigate the phenomenon of the temperature dependent changes in the properties of GO nanosheets. The (I_D/I_G) ratio increases with increase in temperature from 30 to 50 ºC during synthesis of GO nanosheets as shown in **Table 5.1** (discussed in section **5.3.1**) and decreases thereafter at higher synthesis temperatures. The increment in (I_D/I_G) ratio may be attributed to the enhancement in the defects in GO [26]. The (I_D/I_G) ratio of GO-30 (0.93) is slightly lower than the GO-50 (0.98), indicating that the GO-50 has more defects in its structure. However, with further increase in the oxidation temperature, (I_D/I_G) ratios decreased up to 0.53 (GO-110), which indicates the formation of disordered graphitic layer.

5.3.5 Nitrogen adsorption/desorption

For nitrogen adsorption/desorption GO was used as form of powder without any further treatment. The porous structural parameter which has been calculated from the isotherm and pore size distribution are reported in **Table 5.2**. Low BET surface area signifies partial oxidation of non-porous graphite. Defects are incorporated into the carbon layers with increase in the oxidation as found from Raman spectra (**Fig. 5.5**) resulting in increased porosity [30]. Thus, here we found that GO-50, which has the highest oxidation degree, shows more surface area (42.35 m^2/g) with a significant range of pore micropore volume (0.018 cm^3/g) compared to others GO sample. This type of enhancement nature indicates the formation of more pores or cracks on the interface between graphite layers.

Table 5.2 Calculated structural parameters from nitrogen adsorption.

Sample	BET Surface Area (m^2/g)	t-Plot micropore volume (cm^3/g) $\times 10^3$
GO-30°C	9.93	3.0
GO-50°C	42.35	18.0
GO-75°C	13.24	2.0
GO-90°C	4.92	0.26
GO-110°C	1.07	0.12

5.3.6 FTIR analysis

FTIR spectra of all the GO scanned between 2000 - 500 cm^{-1} are shown in **Fig. 5.6**. The peak at ~ 1630 cm^{-1} of pristine graphite corresponds to C=C carbon backbone vibration of aromatic groups [31]. In GO, the peaks corresponding to 1050 cm^{-1} and 1155 cm^{-1} represent the C–O-C and C-O stretching vibration of alkoxy and epoxy groups [18]. The

weak –OH bending vibration at 1410 cm^{-1} is observed in all the synthesized GO [18]. The presence of C=O group is confirmed by the corresponding peak at ~1750 cm^{-1} [18, 31]. It is observed that the peak intensity corresponding to 1050 cm^{-1}, 1155 cm^{-1} and 1720 cm^{-1} are maximum for GO-50 and further decreased with increase in temperature.

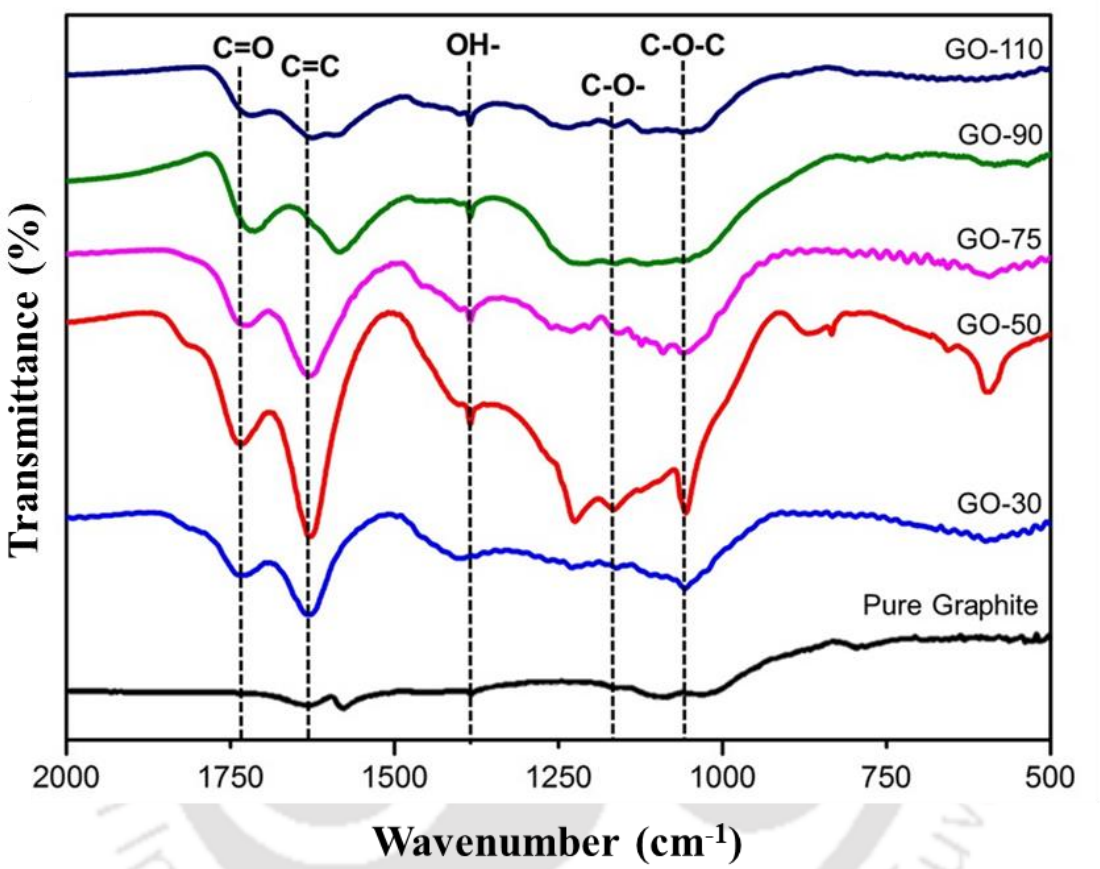

Figure 5.6 FTIR spectra of graphite, GO-30, GO-50, GO-75, GO-90, GO-110 samples.

5.3.7 XPS analysis

X-ray photoelectron spectroscopy measurement of synthesized GO samples (GO-30, GO-50 and GO-110) was also performed to confirm the presence of functional groups. The high resolution core level characteristic peaks in the region of C1s is shown in **Fig. 5.7**. After deconvolution (**Fig. 5.8**) in C1s region, four prominent peaks were found at 284.7, 286.7, 287.8 and 289.1 eV which corresponds to the graphitic or sp^2 carbon, the

C-O in hydroxyl or epoxy, the C=O in the carbonyl group and the O-C=O in the carboxyl group, respectively [32, 33]. On other hand four major peak around 530.9, 532.0, 533.2 and 534.5 eV which are assigned to C=O, COOH, C-OH and C-O-C, respectively, have also been observed after deconvolution of O1s spectra [34]. In post oxidation process, there has been a considerable formation of functional groups of GO-30 which marks a notable improvement over that of pristine graphite [35]. The formation of functional groups increases with increase in temperature up to 50 °C; beyond a synthesis temperature of ~ 50 °C temperature, a decrease in the number of functional groups and their intensity is observed. Presence of oxygen moieties was quantified by C/O atomic ratio (**Fig. 5.7**). The C/O atomic ratio was found to be only 1.6 for GO-50 which indicates that it is more hydrophilic in nature than GO-30 and GO-110 [36]. The degree of oxygenation of sp^2 carbon fraction in graphite to sp^3 moieties in GO was calculated by division of area under sp^2 peak and C1s peak (**Table 5.3**). We found that sp^2 hybridized zone for GO-50 is 42.5 % which is much less than that of GO-30 and GO-110 [44]. Thus 50 ºC seems to be an optimum temperature for retention of maximum possible functional groups.

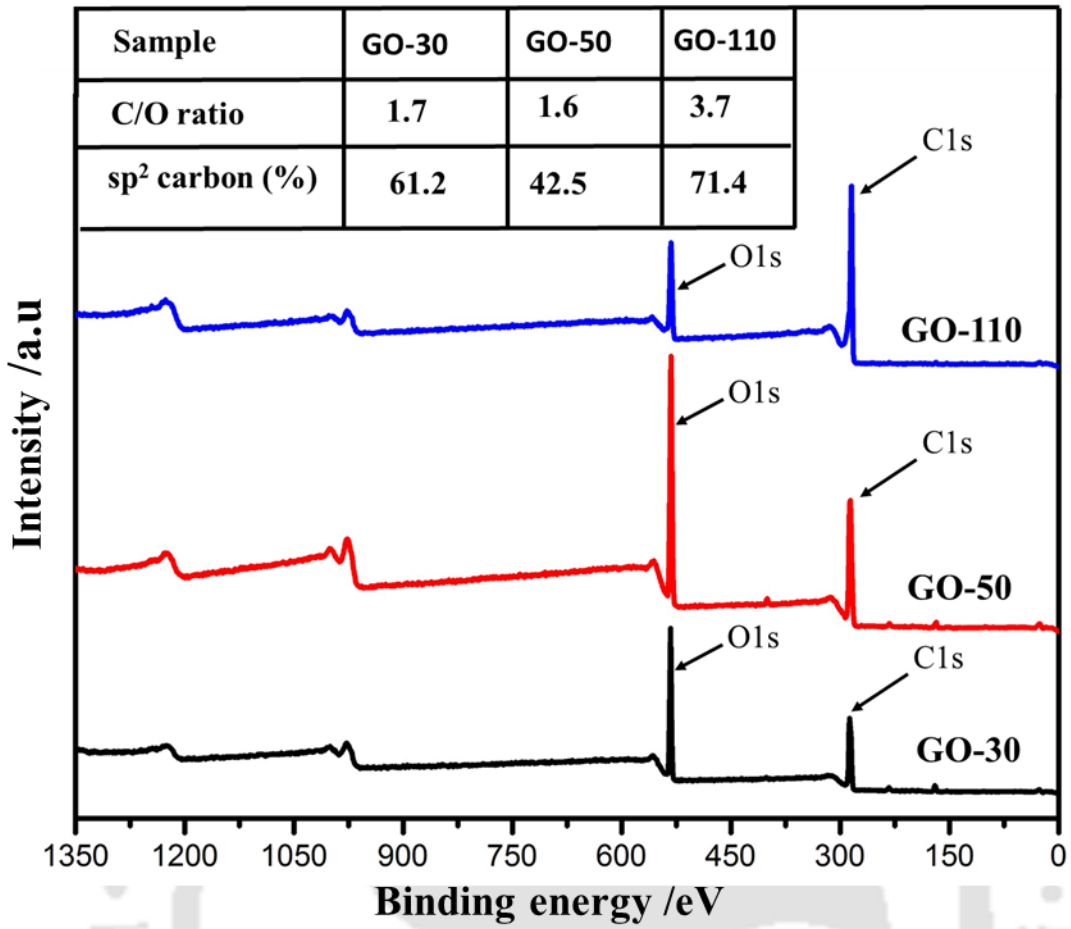

Figure 5.7 XPS survey spectra of synthesized graphene oxides.

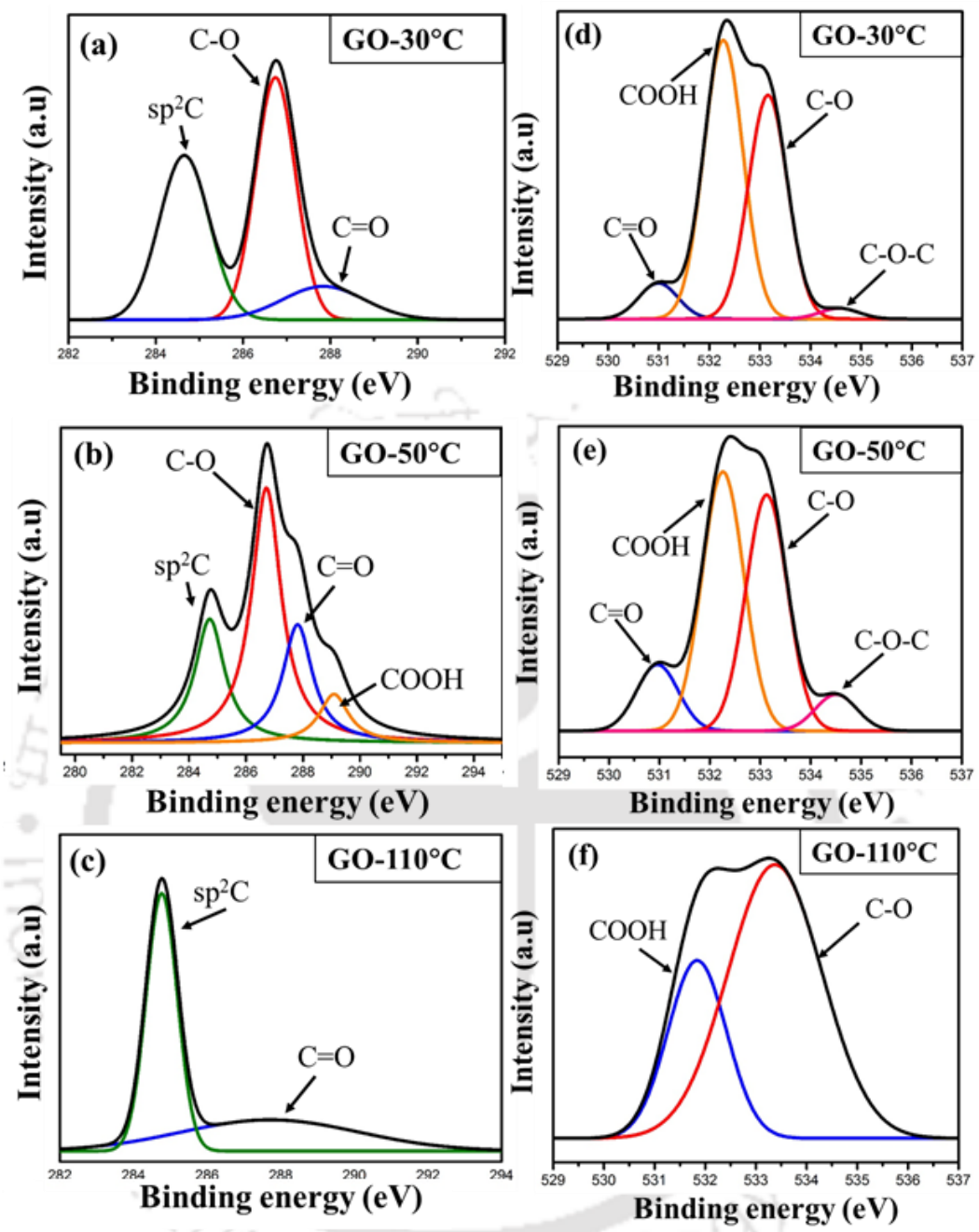

Figure 5.8 High-resolution C1s (a-c) and O1s (d-f) XPS spectra: deconvoluted peaks of synthesized graphene oxides.

Table 5.3 XPS compositional analysis

Sample	C atomic (%)	O atomic (%)	sp^2-C (%)
GO-30	63.45	36.55	56.0
GO-50	62.77	37.23	42.5
GO-110	79.02	20.98	71.4

5.3.8 UV-Vis absorption

The light absorption and emission of synthesized GO samples vary with change in oxidation temperature as represented by their UV-visible spectra (**Fig. 5.9**). GO-50 shows strong absorption peak at 230 nm which arises due to conjugative effect of π-π* electronic transitions of the sp^2 moieties and chromophore units i.e. carboxyl and carbonyl groups [18]. The n-π* transitions of these groups result in a peak at 303 nm [18]. The band gap (an energy difference between the conduction band and valance band) is linearly proportional to the extent of functionalization of the graphitic carbon which determines its oxygen content [37]. The intensity and position of both the peaks vary due to change in the amount of oxygen incorporated as found from the XPS analysis (**Fig. 5.7**). Incomplete oxidation of graphite at 30 °C cause deviation of the peak position to 226 nm. On further increasing the temperature beyond 50 °C, a red shift along with reduction in the peak intensity was noticed due to decrease in concentration of functional groups as explained in previous sections. The band gap as calculated from Tauc's plot in **Fig. 5.9** (GO-50) considering GO as a direct band semiconductor shows increasing trend with increase in oxygen to carbon ratio [37]. The band gap was found to vary from 3.1 eV to 4.4 eV, which is higher than most of the reported values [38]. GO showed high band gap of 4.4 eV by oxidation of graphite at a moderate temperature and this opens up the possibility of utilizing GO as a standalone photocatalyst for application in

environmentally benign and energy saving sectors like water treatment, water splitting and CO_2 reduction to fuels.

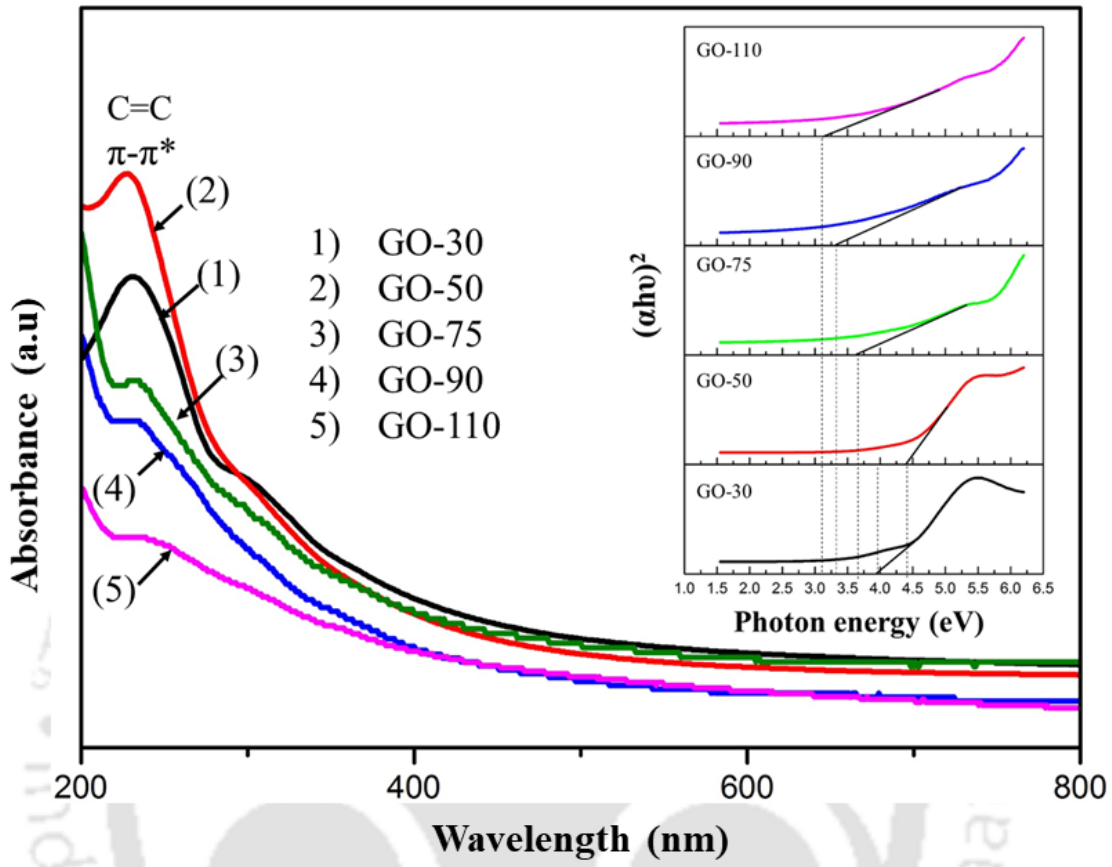

Figure 5.9 Plot of UV-Vis absorption spectra and $(\alpha h\nu)^2$ vs photon energy (inside image) of synthesized graphite oxides.

5.3.9 Zeta potentials

The resulting zeta potentials (ζ) of GO samples are shown in **Fig. 5.10** (GO, 50 mg and Millipore water, 25 mL). Zeta potential (ζ) is the most important parameter to evaluate the degree of oxidation as well as functional groups [39]. The concentration of the surface functional groups present on GO surface gets altered after oxidation at 30 ºC. It can be seen that the pristine graphite has lower ζ (–12 mV) value. The ζ of graphite is nearly zero, since very few functional groups are present on the graphite surface [39]. As the oxidation temperature for GO increases to 50 ºC, the ζ value goes to 49 mV (GO-50).

Similar value of ζ (50 – 52 mV between 6 – 8 pH) was also observed by Chen et al. [40]. With further increase in the oxidation temperature the ζ value became lower and it reaches -25 mV at 110 °C.

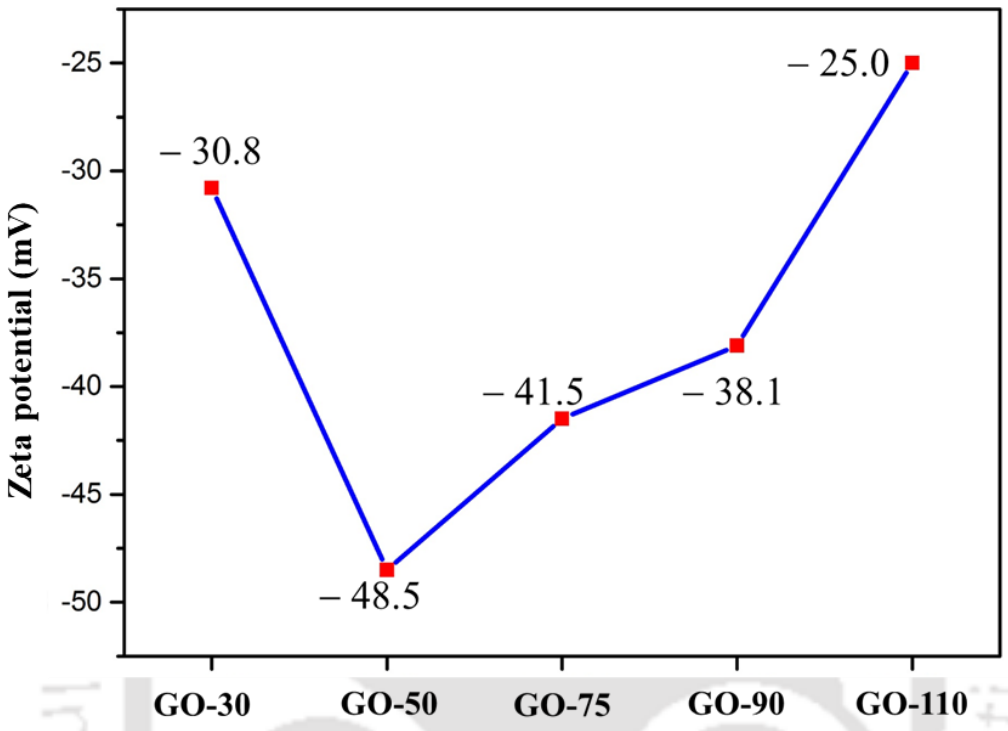

Figure 5.10 Zeta potential of synthesized GO (GO, 50 mg and Millipore water, 25 mL).

The proposed mechanism for the synthesis of tailored surface charge of GO is described in **Fig. 5.11**. Natural graphite flake is the most common source of carbon for synthesis of GO and it contains wide variety of mineral as a heteroatom. The graphite stacks are arranged with the van der Waal attraction in graphitic domains. After oxidation, epoxy (C-O-C), hydroxyl (C-OH), carboxyl (C-O-OH) and carbonyl (C=O) groups are formed on the GO surface. In stage 1, the natural flakes of graphite are dispersed in a mixture of H_3PO_4 and H_2SO_4 to exfoliate the graphite layers which increases the inter layer distance between the stacks [41]. Before the oxidation (stage 2) of graphite, potassium permanganate ($KMnO_4$) and concentrated H_2SO_4 react with each other and formed the red dimanganeseheptoxide (Mn_2O_7) which can be represented as follows: $2KMnO_4$+

$H_2SO_4 \rightarrow Mn_2O_7 + 2KHSO_4 + H_2O$ [42]. Trömel and Russ demonstrated [42] that the ability of oxidation performance of di-metallic Mn_2O_7 is higher over mono metallic $KMnO_4$. They observed that the di-metallic Mn_2O_7 more selectively oxidized the unsaturated double bond over $KMnO_4$ during the oxidation. The heteroatoms present in graphite creates the localized defects and it serves as a seed point for oxidation and formation of the C-OH, C-O-OH, C=O and C-O-C groups on the surface. During oxidation, nearly 33.3 % of carbon with sp^3 bond is converted into sp^2 bond [43-45]. On the other hand, sulphates ions present in the solution covalently attached with carbon skeleton during reaction. During washing, sulfate ions detached from GO and generates two –OH groups per sulfate ions as illustrated elsewhere [44].

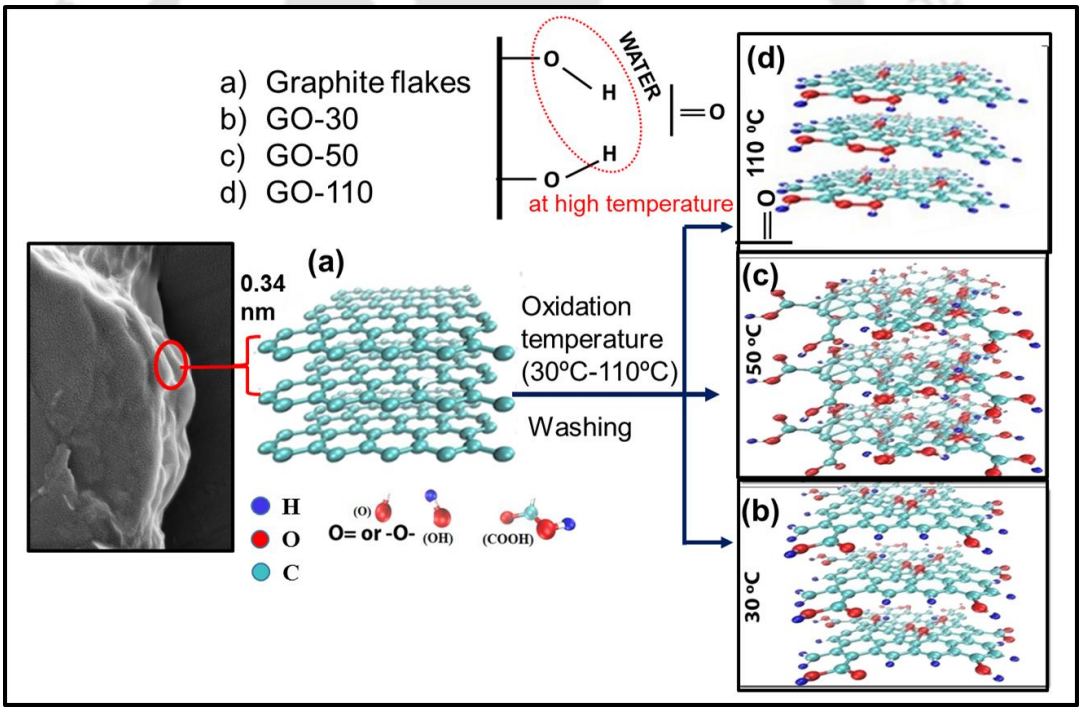

Figure 5.11 Proposed mechanism of GO synthesis with different degrees of oxidation.

The exfoliation of graphite and the rate of Mn_2O_7 diffusion in between layers is directly proportional to the synthesis temperature and is lowest for room temperature (30 ºC). The resulting phenomena shows the lower functional groups formation for GO-30. Further increase in temperature increases the degree of oxidation and rate of Mn_2O_7

diffusion in the graphitic layers. Along with this higher temperature also promotes the deoxygenation of functional groups from the surface. These functional groups, C–OH (~ 3.73 eV), C–O–C (~ 3.82 eV) and C=O (7.67 eV), have different bond energies [45]. The large number of oxygen moieties (~ 88 %) is for the C–OH and C–O–C present on basal plane. However, the isolated C=O with high bond energy is likely to be rare. Now, as the epoxide and C-OH bond are very close to one another, at moderate temperature (90 to 110 ºC) they form the aromatic diol (phenol) and additionally the layers of GO terminate the C–OH and COOH groups as illustrated by Martín Rodríguez [46]. Furthermore, two hydroxyl groups react with each other via condensation reaction and reduced the oxygen based functional groups on the GO surface. Hereafter, rate of oxidation and Mn_2O_7 diffusion is more prominent up to 50 ºC and show the maximum concentration of functional groups in the GO-50. Further increase in temperature (above 50 ºC) leads to more prominent rate of condensation reaction and deoxygenation, and shows the gradual decrease in the functional groups with temperature up to 110 ºC.

5.4 Conclusions

In conclusion, the control over the oxidation temperature in the range of 30-110 ºC in modified Hummers method for the synthesis of GO nanosheets resulted in the modulation of their structural and surface functional properties. Analytical investigations suggested that the concentration of functional groups on the surface of GO nanosheets increases with increase in oxidation temperature up to 50 ºC and decreases with further increase in temperature as the condensation reaction between epoxy and hydroxyl groups proceed. Importantly, an oxidation temperature of ~50 ºC was found to be the best for the synthesis of the GO nanosheets with better crystallinity and single sheet nature. The temperature dependent structural as well as surface functional properties changes of GO are explained

based on the chemical condensation and modulation of the functional groups present on their surface. This study is vital for tailoring the properties of GO nanosheets and thus towards the progress of sustainable carbon materials as well as designing the charged based electronic materials.

According to the proton transport mechanism, the incorporation of hydrophilic fillers like GO enhanced the water absorbing property of the composite membrane. Water is an important factor for GrÖthous and Vehicle mechanisms which are mechanisms of proton transport. Hence, GO-50 has been chosen for further study and synthesis of composite for SPEEK membrane.

References

1. V. Georgakilas, J.N. Tiwari, K.C. Kemp, J.A. Perman, A.B. Bourlinos, K.S. Kim, R. Zboril, Noncovalent functionalization of graphene and graphene oxide for energy materials, biosensing, catalytic, and biomedical applications, Chemical Reviews 116(9) (2016) 5464-5519.

2. M.P. Down, S.J. Rowley-Neale, G.C. Smith, C.E. Banks, Fabrication of graphene oxide supercapacitor devices, ACS Applied Energy Materials 1(2) (2018) 707-714.

3. S. Kumar, A.K. Singh, A.K. Dasmahapatra, T.K. Mandal, D. Bandyopadhyay, Graphene based multifunctional superbots, Carbon 89 (2015) 31-40.

4. P. Zhu, B.G. Sumpter, V. Meunier, Electronic, thermal, and structural properties of graphene oxide frameworks, The Journal of Physical Chemistry C 117(16) (2013) 8276-8281.

5. P. Kumar, F. Shahzad, S. Yu, S.M. Hong, Y.-H. Kim, C.M. Koo, Large-area reduced graphene oxide thin film with excellent thermal conductivity and electromagnetic interference shielding effectiveness, Carbon 94 (2015) 494-500.

6. X. Li, G. Zhang, X. Bai, X. Sun, X. Wang, E. Wang, H. Dai, Highly conducting graphene sheets and Langmuir–Blodgett films, Nature Nanotechnology 3(9) (2008) 538.

7. W.S. Hummers Jr, R.E. Offeman, Preparation of graphitic oxide, Journal of the American Chemical Society 80(6) (1958) 1339-1339.

8. T. Nakajima, A. Mabuchi, R. Hagiwara, A new structure model of graphite oxide, Carbon 26(3) (1988) 357-361.

9. J. Guerrero-Contreras, F. Caballero-Briones, Graphene oxide powders with different oxidation degree, prepared by synthesis variations of the Hummers method, Materials Chemistry and Physics 153 (2015) 209-220.

10. A.V. Talyzin, G. Mercier, A. Klechikov, M. Hedenström, D. Johnels, D. Wei, D. Cotton, A. Opitz, E. Moons, Brodie vs Hummers graphite oxides for preparation of multi-layered materials, Carbon 115 (2017) 430-440.

11. E.M. Deemer, P.K. Paul, F.S. Manciu, C.E. Botez, D.R. Hodges, Z. Landis, T. Akter, E. Castro, R.R. Chianelli, Consequence of oxidation method on graphene oxide produced with different size graphite precursors, Materials Science and Engineering: B 224 (2017) 150-157.

12. C. Botas, P. Álvarez, C. Blanco, R. Santamaría, M. Granda, P. Ares, F. Rodríguez-Reinoso, R. Menéndez, The effect of the parent graphite on the structure of graphene oxide, Carbon 50(1) (2012) 275-282.

13. S. You, S.M. Luzan, T. Szabo, A.V. Talyzin, Effect of synthesis method on solvation and exfoliation of graphite oxide, Carbon 52 (2013) 171-180.

14. A. Bannov, A. Manakhov, A. Shibaev, A. Ukhina, J. Polčák, E. Maksimovskii, Synthesis dynamics of graphite oxide, Thermochimica Acta 663 (2018) 165-175.

15. H. He, J. Klinowski, M. Forster, A. Lerf, A new structural model for graphite oxide, Chemical Physics Letters 287(1-2) (1998) 53-56.

16. N. Zaaba, K. Foo, U. Hashim, S. Tan, W.-W. Liu, C. Voon, Synthesis of graphene oxide using modified hummers method: solvent influence, Procedia Engineering 184 (2017) 469-477.

17. R.K. Sonker, S. Sabhajeet, B. Yadav, TiO 2–PANI nanocomposite thin film prepared by spin coating technique working as room temperature CO 2 gas sensing, Journal of Materials Science: Materials in Electronics 27(11) (2016) 11726-11732.

18. A. Kaniyoor, T.T. Baby, T. Arockiadoss, N. Rajalakshmi, S. Ramaprabhu, Wrinkled graphenes: a study on the effects of synthesis parameters on exfoliation-reduction of graphite oxide, The Journal of Physical Chemistry C 115(36) (2011) 17660-17669.

19. N. Morimoto, T. Kubo, Y. Nishina, Tailoring the oxygen content of graphite and reduced graphene oxide for specific applications, Scientific Reports 6 (2016) 21715.

20. G. Wang, X. Sun, C. Liu, J. Lian, Tailoring oxidation degrees of graphene oxide by simple chemical reactions, Applied Physics Letters 99(5) (2011) 053114.

21. L. Stobinski, B. Lesiak, A. Malolepszy, M. Mazurkiewicz, B. Mierzwa, J. Zemek, P. Jiricek, I. Bieloshapka, Graphene oxide and reduced graphene oxide studied by the XRD, TEM and electron spectroscopy methods, Journal of Electron Spectroscopy and Related Phenomena 195 (2014) 145-154.

22. Y. Gong, D. Li, Q. Fu, C. Pan, Influence of graphene microstructures on electrochemical performance for supercapacitors, Progress in Natural Science: Materials International 25(5) (2015) 379-385.

23. A. Ghosh, S. Shukla, G.S. Khosla, B. Lochab, S. Mitra, Sustainable sulfur-rich copolymer/graphene composite as lithium-sulfur battery cathode with excellent electrochemical performance, Scientific Reports 6 (2016) 25207.

24. J. Paredes, S. Villar-Rodil, A. Martínez-Alonso, J. Tascon, Graphene oxide dispersions in organic solvents, Langmuir 24(19) (2008) 10560-10564.

25. X. Li, X. Xu, F. Xia, L. Bu, H. Qiu, M. Chen, L. Zhang, J. Gao, Electrochemically active MnO2/RGO nanocomposites using Mn powder as the reducing agent of GO and the MnO2 precursor, Electrochimica Acta 130 (2014) 305-313.

26. A.C. Ferrari, J. Robertson, Interpretation of Raman spectra of disordered and amorphous carbon, Physical Review B 61(20) (2000) 14095.

27. M.R. Karim, M.S. Islam, K. Hatakeyama, M. Nakamura, R. Ohtani, M. Koinuma, S. Hayami, Effect of interlayer distance and oxygen content on proton conductivity of graphite oxide, The Journal of Physical Chemistry C 120(38) (2016) 21976-21982

28. V. Zólyomi, J. Koltai, J. Kürti, Resonance Raman spectroscopy of graphite and graphene, Physica Status Solidi (b) 248(11) (2011) 2435-2444.

29. A. Ganguly, S. Sharma, P. Papakonstantinou, J. Hamilton, Probing the thermal deoxygenation of graphene oxide using high-resolution in situ X-ray-based spectroscopies, The Journal of Physical Chemistry C 115(34) (2011) 17009-17019.

30. M. Seredych, C. Petit, A.V. Tamashausky, T.J. Bandosz, Role of graphite precursor in the performance of graphite oxides as ammonia adsorbents, Carbon 47(2) (2009) 445-456.

31. S.N. Alam, N. Sharma, L. Kumar, Synthesis of graphene oxide (GO) by modified hummers method and its thermal reduction to obtain reduced graphene oxide (rGO), Graphene 6(01) (2017) 1-18.

32. K. Muthoosamy, R.G. Bai, I.B. Abubakar, S.M. Sudheer, H.N. Lim, H.-S. Loh, N.M. Huang, C.H. Chia, S. Manickam, Exceedingly biocompatible and thin-layered reduced graphene oxide nanosheets using an eco-friendly mushroom extract strategy, International Journal of Nanomedicine 10 (2015) 1505.

33. K. Haubner, J. Murawski, P. Olk, L.M. Eng, C. Ziegler, B. Adolphi, E. Jaehne, The route to functional graphene oxide, ChemPhysChem 11(10) (2010) 2131-2139.

34. Y.C.G. Kwan, G.M. Ng, C.H.A. Huan, Identification of functional groups and determination of carboxyl formation temperature in graphene oxide using the XPS O 1s spectrum, Thin Solid Films 590 (2015) 40-48.

35. H. Al-Kandari, A. Abdullah, S. Al-Kandari, A. Mohamed, Effect of the graphene oxide reduction method on the photocatalytic and electrocatalytic activities of reduced graphene oxide/TiO 2 composite, RSC Advances 5(88) (2015) 71988-71998.

36. R. Al-Gaashani, A. Najjar, Y. Zakaria, S. Mansour, M. Atieh, XPS and structural studies of high quality graphene oxide and reduced graphene oxide prepared by different chemical oxidation methods, Ceramics International 45(11) (2019) 14439-14448.

37. M. Acik, Y.J. Chabal, A review on reducing graphene oxide for band gap engineering, J. Mater. Sci. Res 2(1) (2012) 5539.

38. H. Jeong, M. Jin, K. So, S. Lim, Y. Lee, Tailoring the characteristics of graphite oxides by different oxidation times, Journal of Physics D: Applied Physics 42(6) (2009) 065418.

39. B. Zhang, F. Li, T. Wu, D. Sun, Y. Li, Adsorption of p-nitrophenol from aqueous solutions using nanographite oxide, Colloids and Surfaces A: Physicochemical and Engineering Aspects 464 (2015) 78-88.

40. J.-T. Chen, Y.-J. Fu, Q.-F. An, S.-C. Lo, S.-H. Huang, W.-S. Hung, C.-C. Hu, K.-R. Lee, J.-Y. Lai, Tuning nanostructure of graphene oxide/polyelectrolyte LbL

assemblies by controlling pH of GO suspension to fabricate transparent and super gas barrier films, Nanoscale 5(19) (2013) 9081-9088.

41. R.L. Whitby, Chemical control of graphene architecture: tailoring shape and properties, ACS Nano 8(10) (2014) 9733-9754.

42. M. Trömel, M. Russ, Dimanganese heptoxide for the selective oxidation of organic substrates, Angewandte Chemie International Edition in English 26(10) (1987) 1007-1009.

43. D. Lee, J. Seo, sp^2/sp^3 carbon ratio in graphite oxide with different preparation times, The Journal of Physical Chemistry C 115(6) (2011) 2705-2708.

44. A.M. Dimiev, J.M. Tour, Mechanism of graphene oxide formation, ACS Nano 8(3) (2014) 3060-3068.

45. D.E. Lobo, J. Fu, T. Gengenbach, M. Majumder, Localized deoxygenation and direct patterning of graphene oxide films by focused ion beams, Langmuir 28(41) (2012) 14815-14821.

46. Rodriguez A. M. and Jimenez P. S. V., Some new aspects of graphite oxidation at 0°c in a liquid medium. A mechanism proposal for oxidation to graphite oxide, Carbon, 1986, 24, 163-167.

CHAPTER 6

Construction of Graphite Oxide Doped Metal Organic Framework (UiO-66) Composite Membrane

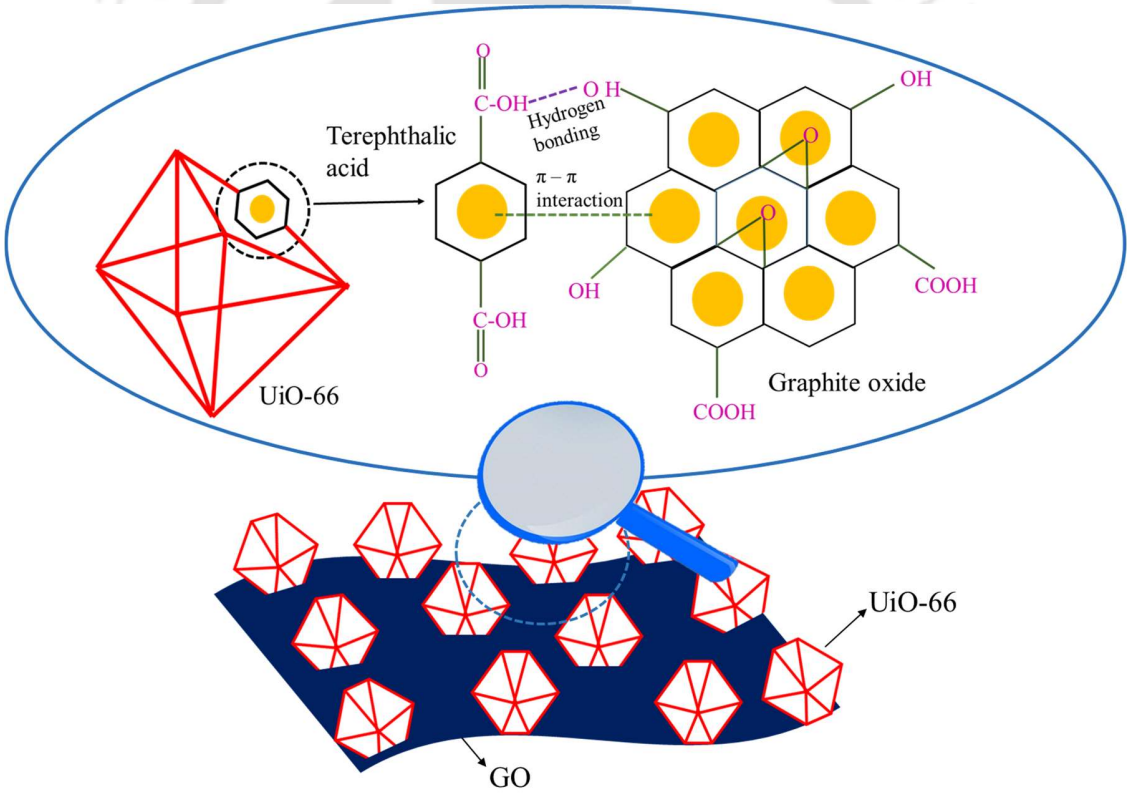

Graphical abstract of possible interaction between UiO-66 and Graphite oxide

CHAPTER 6

Construction of Graphite Oxide Doped Metal Organic Framework (UiO-66) Composite Membrane

This chapter deals with facile synthesis of composites by 2D carbon functionalization of MOFs and its performance evaluation as proton exchange membrane. Extensive characterization of the composite including its crystallinity, chemical composition, surface morphology- and porosity have been discussed. After fabrication of membrane water uptake capacity and conductivity have also been measured.

6.1 Introduction

The proton conductivity also depends greatly on the charge carriers such as protons and their mobility that is mainly ensured by water molecules and their clusters. After sulfonation, the hydrophilic pathways become narrower, ensuring better travel of protons but along with that the methanol permeability also increased. Polymeric phase hosting functional inorganic particle mixed matrix membrane also shows a promising candidate for addressing traditional proton exchange membrane [1]. This inorganic filler helps to increase the membrane flexibility, thermal-mechanical stability, conductivity as well as methanol crossover. Some recent reviews discussed about the functionalization of inorganic materials because all inorganic materials do not act as a proton conductor. Recently, the scientific community is drawn towards an emerging group of inorganic (metal core)–organic (linker) hybrid, crystalline compounds i.e. metal-organic frameworks (MOFs) for fuel cell application due to their high porosity, high surface area, tunable structure and chemistry [2,3]. They are used as photocatalysts, adsorbents, sensor, proton conduction, drug delivery, etc. The recent study reviewed details on the

utilizations and applications of MOFs in electrochemical systems for clean energy applications which includes solar cell, fuel cell, lithium ion batteries, and super capacitors [4]. This chapter deals with the synthesis of composites using graphite oxide and MOF for proton exchange.

6.2. Experimental Section

6.2.1 Materials

The precursors for composite formation i.e. graphite flakes, zirconium chloride octahydrate ($ZrCl_4 \geq 99.5\%$ metals basis) and terephthalic acid (BDC, 98%) were purchased from Sigma Aldrich, USA. N'N-Dimethyl formamide (DMF), sulphuric acid (98%), hydrochloric acid (HCl, 35 wt%), hydrogen peroxide (25%), potassium permanganate and ethanol (99.9%) were supplied by Merck, India. Dimethylacetamide (DMAc) was obtained from Spectrochem Private Limited. Ultrapure Millipore® water was used in all the experiments. All the reagents were of analytical grade and were used without further purification.

6.2.2 Synthesis of UiO-66

In a typical synthesis, BDC (0.983 g) and $ZrCl_4$ (1.00 g) were dissolved in DMF acidified by HCl. The solution was then transferred to a Teflon lined stainless steel autoclave and kept in oven at 80°C for 24 h. The solution was then centrifuged at 12000 rpm. The precipitate was washed with DMF and ethanol to remove any unreacted linker. The sample was then dried at 80°C.

6.2.2 Synthesis of UiO-66/GO

Graphite oxide was synthesized by oxidation of graphite at 50 °C following modified Hummer's method [5]. For preparing the composite via in-situ solvothermal method, GO was dispersed in DMF by sonication to obtain a homogenous, stable slurry. The amount of GO was varied in such a way that the expected amount of GO introduced in the UiO-66 framework was 1 wt%, 2.5 wt% and 5 wt% of UiO-66. $ZrCl_4$ was added to the GO dispersion and sonicated for 2 h. It was then acidified by HCl followed by BDC addition and similar protocol as for UiO-66 synthesis followed. The as-synthesized powder was named as UiO-66/GO-n, where n=1, 2.5, 5 based on the amount of GO doped in the MOF (**Fig. 6.1a**).

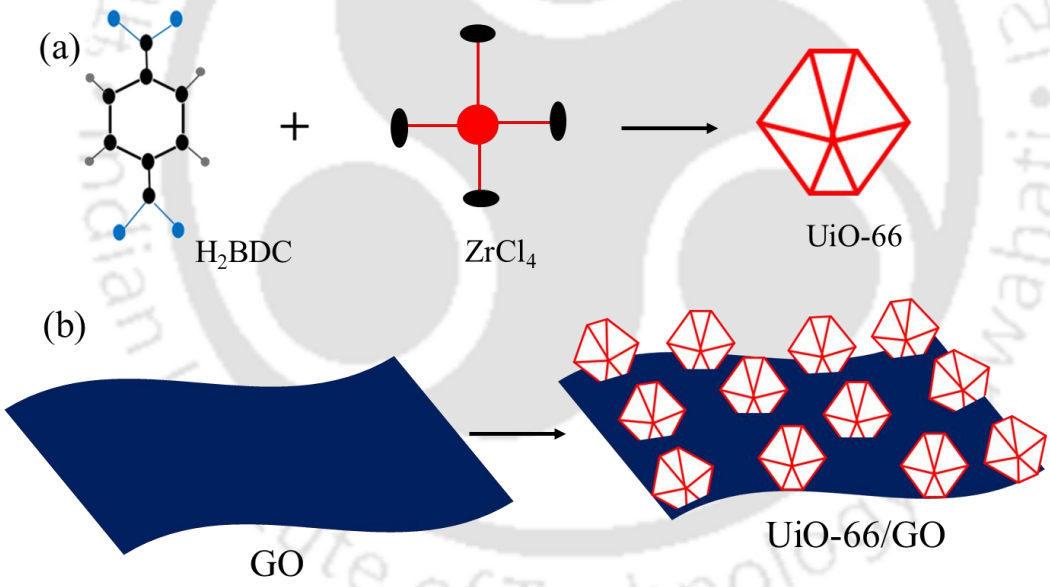

Figure 6.1 Synthesis of UiO-66 and UiO-66/GO composite

6.2.4 Fabrication of UiO-66 and UiO-66/GO composite membrane

Initially, UiO-66 was added to 9g of dimethylacetamide by varying the ratio in the range of 1- 4 wt% with respect to the polymeric content and sonicated upto 1hr to form a

uniform mixture. 1 gm of SPEEK was then added into the solution which, after 12h of stirring, was degassed for removal of bubbles. This solution was then carefully coated on a glass plate. The cast membrane was dried in a vacuum oven at 60 °C for 48 hours, followed by 120 °C for 24 hours, allowing the DMAc solvent to evaporate. The resultant membrane was peeled off from the glass using deionized water after the solvent had evaporated.

GO at a varying concentration (1 – 5 wt %) was added to the membrane casting solution containing optimized UiO-66/SPEEK (3 wt %). Similar protocol was followed for the preparation of the membrane as mentioned previously.

6.2.5 Material characterization

In this section X-ray diffractometer, field emission scanning electron microscope, X-ray photo electron spectroscopy, Fourier transform infrared spectra, Thermogravimetric analysis, Transmission Electron Microscope , BET surface area analyzer has been used for characterization of fabricated membrane and the weight differences between the full-hydrated membranes and the dried membranes along with their water uptake, methanol permeability and proton conductivity of the membranes (refer to Chapter 3).

6.3 Results and Discussion

6.3.1 Characterization of UiO-66 and UiO-66/GO composite

6.3.1.1 FESEM analysis

FESEM images in **Fig. 6.2** shows the change in morphology of the composite formed compared to GO and MOF. GO sheets are stacked forming a lamellar structure. Crystals of UiO-66 are present in an agglomerated form. UiO-66/GO composites show different

surface texture. The cross-sectional view of the composite shows layered sandwich-like structure suggesting GO sheets act as dividers between the MOF particles which is similar to previous findings [7]. The surface image show that UiO-66 are well embedded on the GO sheets in the composites. Although only 2.5 wt% GO was incorporated in the MOF, it was found to have significant effect upon the morphology as reported by Petit and Bandosz [7]. The coordination between oxygen functionalized groups in GO with ligand and Zr^{+4} metallic centres of MOF favors composite formation [8].

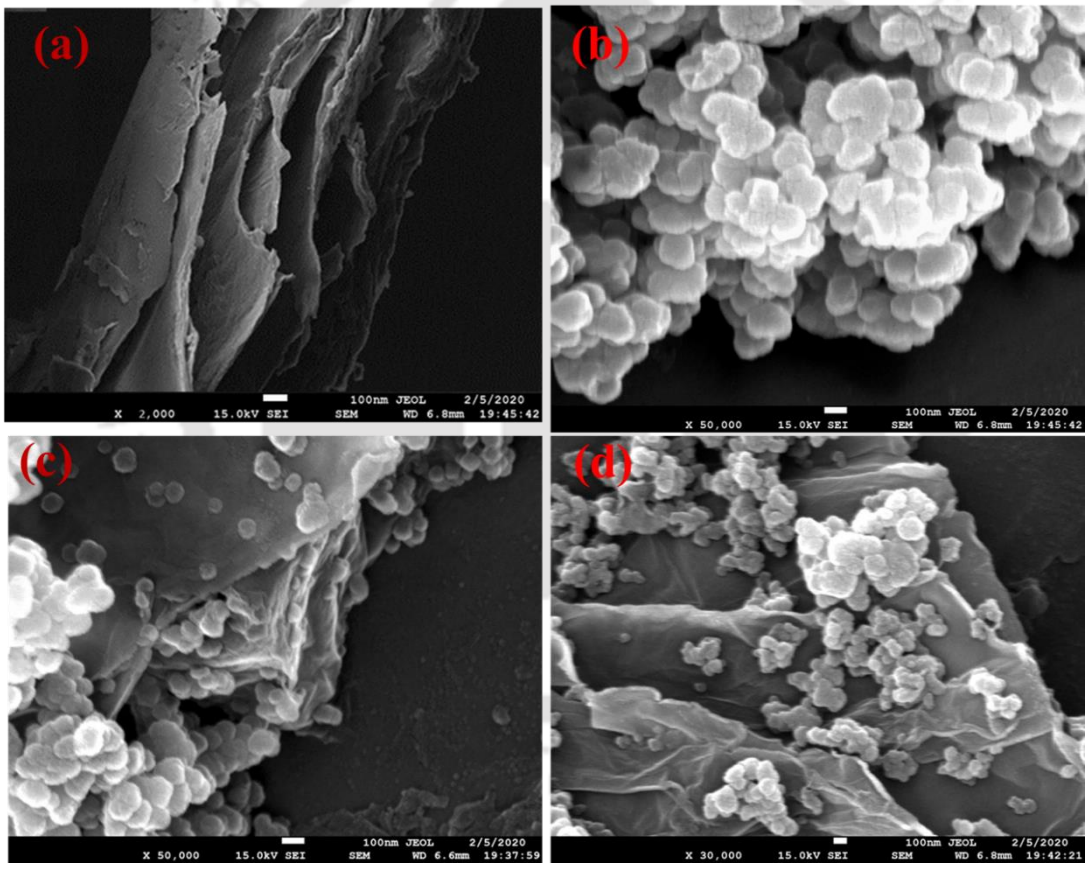

Figure 6.2 FESEM of (a) GO; (b) UiO-66; (c) cross-section and (d) surface of UiO-66/GO composite

6.3.1.2 FETEM analysis

Similar observations are found from the FETEM bright field images of composites (**Fig. 6.3**) which show uniform dispersion of spherical UiO-66 particles on the wrinkled layer like structures which are the GO sheets. The aggregation of the MOF decreased upon incorporation of GO due to their controlled nucleation and growth [8]. Upon doping GO beyond 2.5 wt%, the particles become irregular and aggregated.

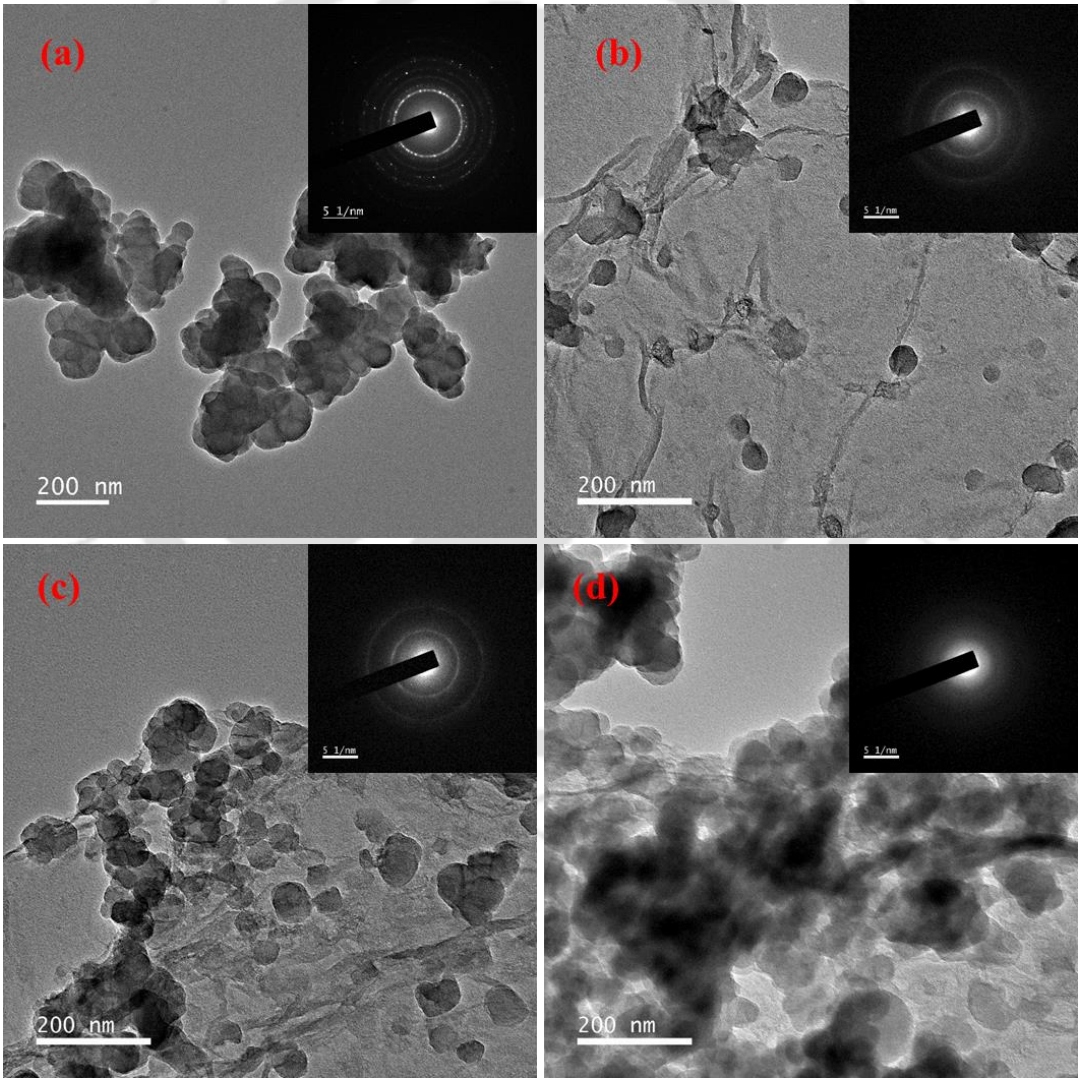

Figure 6.3 FETEM of (a) UiO-66, (b) UiO-66/GO-1, (c) UiO-66/GO-2.5 and (d) UiO-66/GO-5 composite.

6.3.1.3 EDX analysis

The elemental composition of the synthesized UiO-66 was also determined by EDX analysis which is shown in **Fig. 6.4**. The elemental mapping analysis was done in a randomly selected area to reveal the presence of C, O and Zr elements.

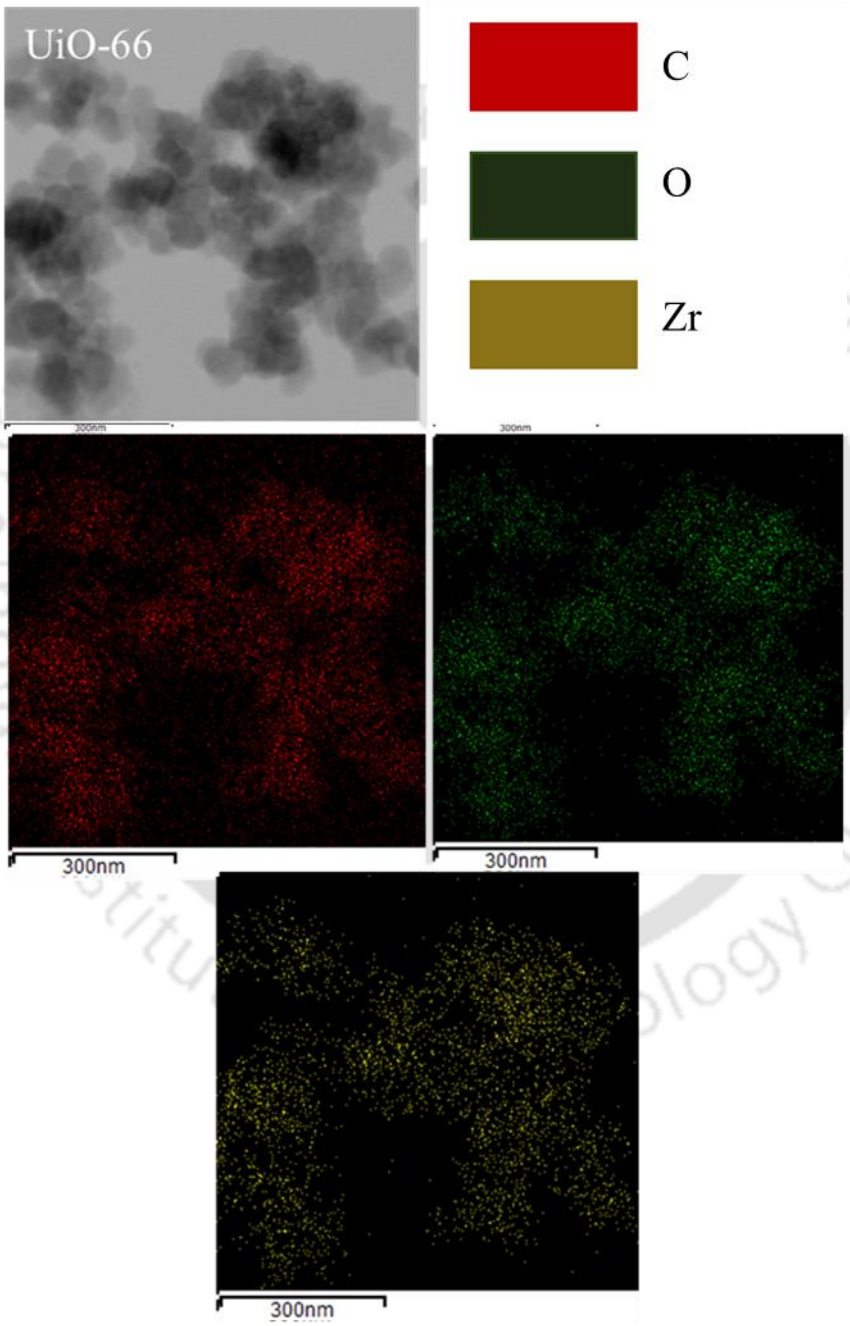

Figure 6.4 EDX mapping analysis of synthesized UiO-66

6.3.1.4 XRD analysis

The crystallographic structure of UiO-66 and their composites with GO as estimated from XRD is shown in **Fig. 6.5**. The sharp characteristic peaks at 2θ = 7.4° and 8.5° (d = 11.91 Å and 10.33 Å respectively) in UiO-66 represent its crystalline nature and are in agreement with previously reported studies [9]. UiO-66/GO composites had similar XRD patterns, indicating predominant presence of UiO-66, which is about 95 wt% of the composites. Moreover, it concludes that GO was highly dispersed in the polar solvent used i.e. DMF and incorporation of GO did not disrupt the bonding between Zr^{+4} and linker BDC hence, no distortion of the UiO-66 crystal framework [8]. Slight reduction in peak intensity can be observed in UiO-66/GO-5 on increasing GO doping which is similar to previous findings [10, 11].

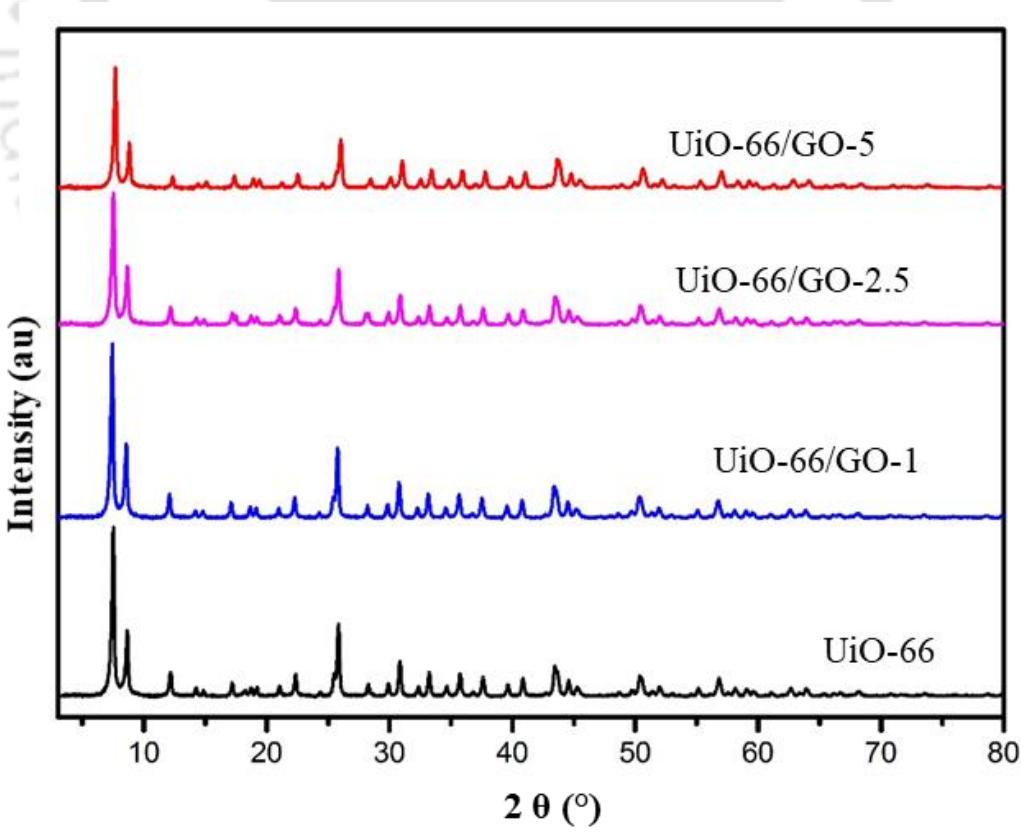

Figure 6.5 XRD of synthesized composites

6.3.1.5 FTIR analysis

FTIR spectra of UiO-66 as shown in **Fig. 6.6** is generated due to vibration and stretching of different functional groups present in the organic linker BDC. Weak peak arises at 1658 cm^{-1} due to stretching vibration of C=O bond of carboxylic acid group [12]. Strong transmission peak at 1581cm^{-1} can be assigned to asymmetric stretching of O-C-O group. Vibration of unsaturated carbon (C=C) in benzene rings of BDC ligand results in weak peak at 1505 cm^{-1} whereas symmetric stretching of C=O of carboxylic acid causes intense peak at 1398 cm^{-1} [13]. The small peaks present at 813 cm^{-1} and 753 cm^{-1} are due to stretching vibration of C-H bond whereas O-H bending in BDC ligand is linked to the peak at 664 cm^{-1} [14]. In UiO-66/GO composites, the FTIR spectra is similar to UiO-66 concluding that the structure of UiO-66 is preserved upon GO addition. The small peak at 1658 cm^{-1} disappears in UiO-66/GO-5.

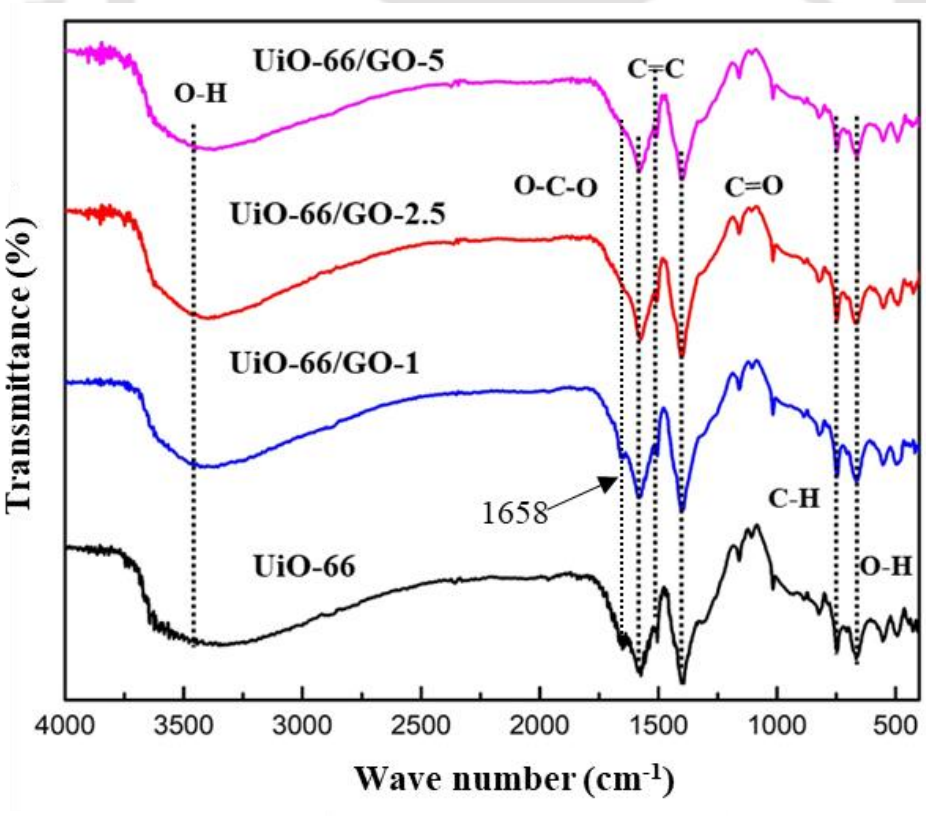

Figure 6.6 FTIR of synthesized UiO-66 and UiO-66 composites

6.3.1.6 Nitrogen adsorption/desorption

The nitrogen adsorption-desorption isotherms of UiO-66 and UiO-66/GO composites (**Fig. 6.7**) represent typical Type-I adsorption isotherms indicating microporous nature of the samples. The porous parameters as calculated from the isotherms is given in **Table 6.1**.

Table 6.1 Parameters obtained from Nitrogen adsorption-desorption isotherm

Sample	BET surface area (m^2/g)	Total pore volume (cm^3/g)	Micropore volume (cm^3/g)	Mesopore volume (cm^3/g)
UiO-66	1460	0.78	0.53	0.25
UiO-66/GO-1	1283	0.71	0.45	0.26
UiO-66/GO-2.5	1165	0.70	0.42	0.28
UiO-66/GO-5	42	0.67	0.38	0.29

The specific surface area of UiO-66 was 1460 m^2/g, which is consistent with previously reported results [15]. However, it is noteworthy that the mesopore volume (2 - 50 nm) of the sample increases with increase in the GO doping. Similar trend in change of surface area and pore volume was reported by Petit and Bandsoz [7].

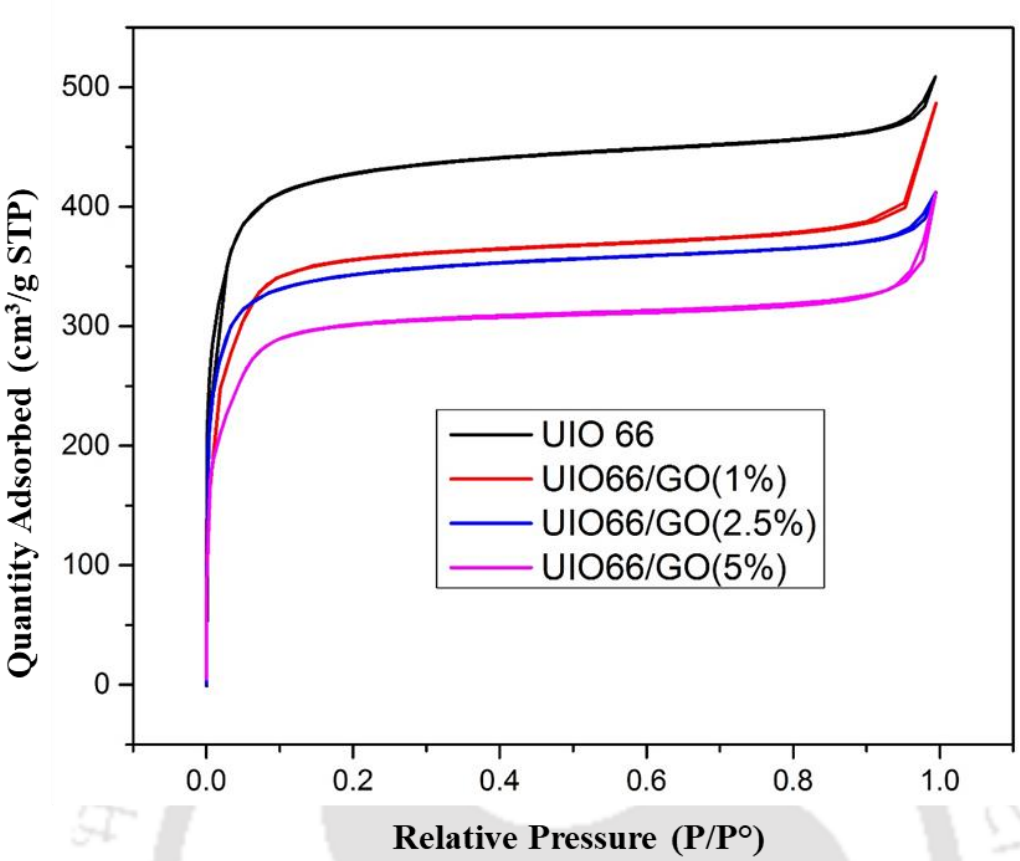

Figure 6.7 Nitrogen adsorption-desorption isotherms of synthesized composites

6.3.1.7 XPS analysis

XPS analysis was done to understand the presence of chemical states of synthesized pure UiO-66 and UiO-66/GO-2.5 composite. As indicated in **Fig. 6.8a**, the XPS spectra confirms the existence of Zr, C and O in the hybrids. Zr 3d core level XPS spectra for UiO-66 shows peaks for Zr $3d_{3/2}$ and Zr $3d_{5/2}$ at 184.67 and 182.31 eV respectively (**Fig. 6.8b)**. These results match with earlier literature [16, 17]. On the other hand, these peaks appear at 184.55 eV and 182.18 eV for the UiO/GO composite (**Fig. 6.8c)**. The spectra for O1s region shows three major peaks at 531.80 eV (O-C=O), 530.20 eV (Zr-O-C) and 528.85 eV (Zr-O-Zr) for UiO-66 [17]; and at 531.75 eV, 530.25 eV and 528.87 eV, respectively after incorporation of GO in UiO-66 framework (**Fig. 6.8d)**.

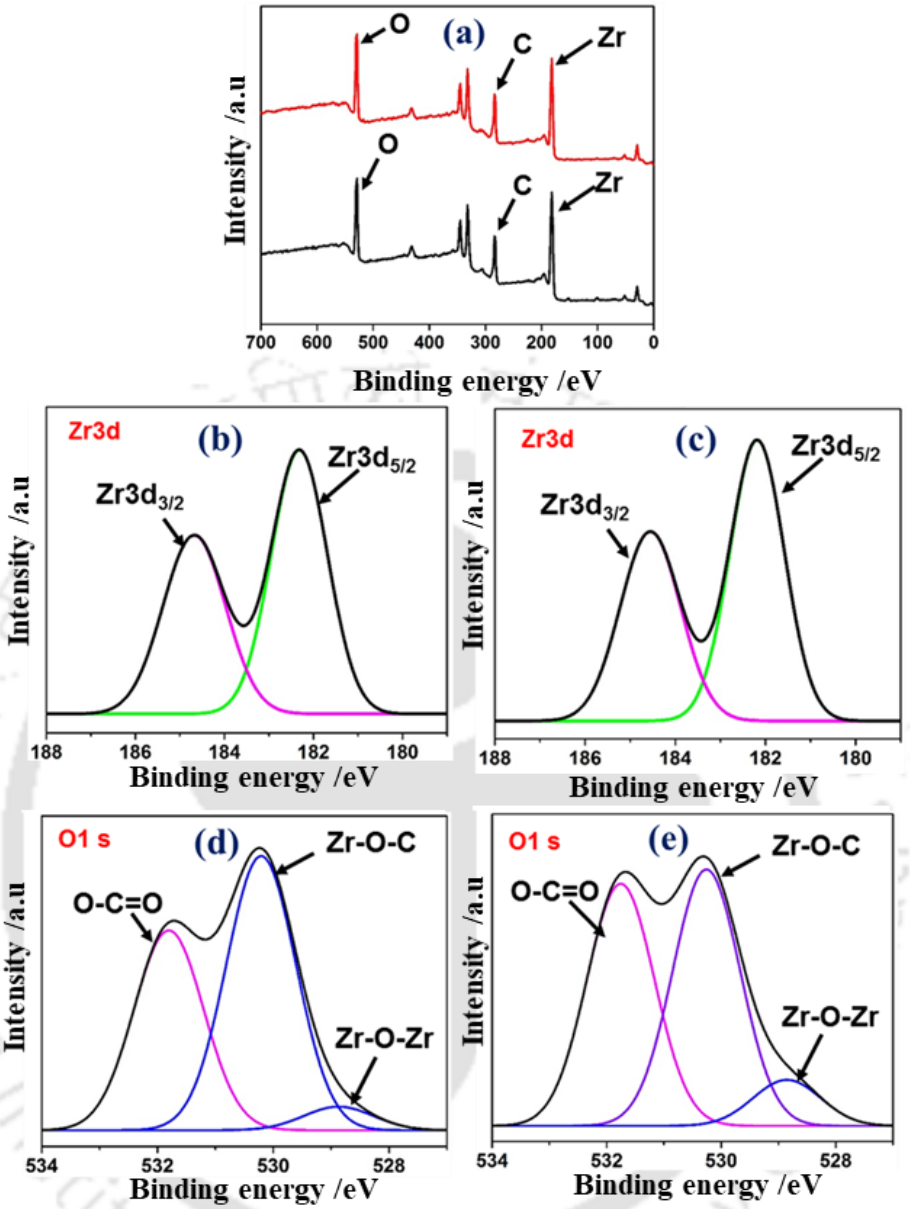

Figure 6.8. XPS of synthesized composites

A negligible variation in peak area percentage and binding energy of core level functional groups has been found from area analysis of the peaks and reported in **Table 6.2**. This similarity in peak position and peak area concludes that thecoordination number of Zr remains unchanged upon GO incorporation to the MOF.

Table 6.2 Peak analysis from XPS scan

Region	Peak	Peak position / BE (eV)		Peak area percent (%)	
		UiO-66	**UiO-66/GO**	**UiO-66**	**UiO-66/GO**
Zr 3d	Zr $3d_{3/2}$	184.67	182.18	42.92	42.54
	Zr $3d_{5/2}$	182.31	184.55	57.08	57.46
O1s	O-C=O	531.80	531.75	42.48	44.46
	Zr-O-C	530.20	530.25	52.51	47.08
	Zr-O-Zr	528.87	528.85	5.01	8.46

6.3.1.8 TGA analysis

The TGA curves of the pristine UiO-66 and UiO-66/GO have been depicted in **Fig. 6.9**. UiO-66 undergoes a weight loss of about 15 wt% at the initial stage upto a temperature of 110 °C, which is due to removal of adsorbed water molecules and residual solvent molecules in the MOF framework. UiO-66/GO shows a relatively lesser weight loss (~7 wt%) in this region [18]. A gradual weight loss was found upto 520 °C for both the materials due to the decomposition of organic linker in the structures . In contrast, the UiO-66 and UiO-66/GO underwent weight loss of 42% and 30% respectively as a result of only 80 °C spike in temperature.

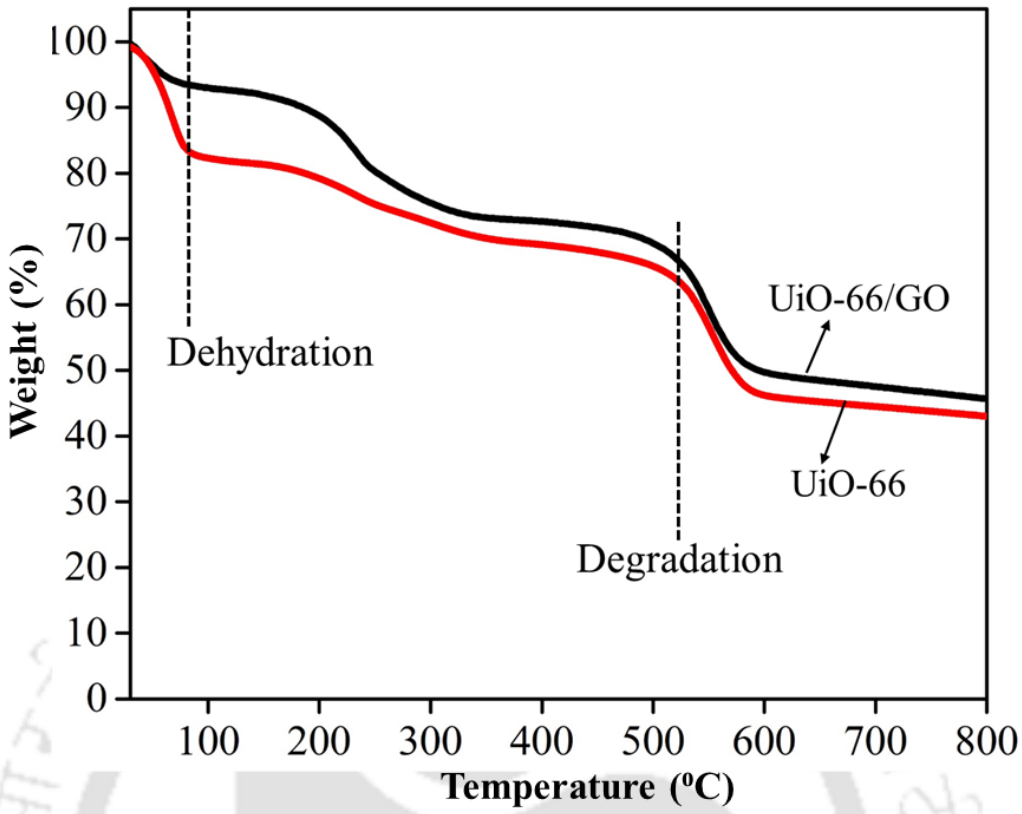

Figure 6.9 TGA analysis of UiO-66 and UiO-66/GO composites

6.3.1.9 Leaching test of GO from the composite

A small experiment has done to make sure that GO does not leach out from UiO-66 (**Fig. 10**). The UiO-66/GO composite was immersed in methanol solution (5 M) for 24 h followed by UV- visible spectroscopic analysis of the solution to analyze leaching of GO from the composite. UV-visible spectra of GO and graphene are shown in **Fig. 10a.** There are two characteristic absorption bands in the UV-visible spectra of GO. The absorption band centred at 231.6 nm is attributed to π-π transitions of aromatic C-C bonds. The shoulder centred at 298.8 nm is corresponding to n-π transitions of C=O bonds. However, in case of the composite, no such peak is found. This confirms negligible leaching of GO from the composite in our working solution methanol.

FTIR of the aforementioned solutions was also performed (**Fig. 10b**) and compared with that of pure methanol as shown in the figure. The spectra of both the samples were similar, speculating absence of GO in the solution, even after immersing for 24 h. The peaks at 3328 ,1636, 1016, and 585 cm^{-1} can be assigned to various functional groups of methanol (ref). This further confirms the stability of the synthesized composite.

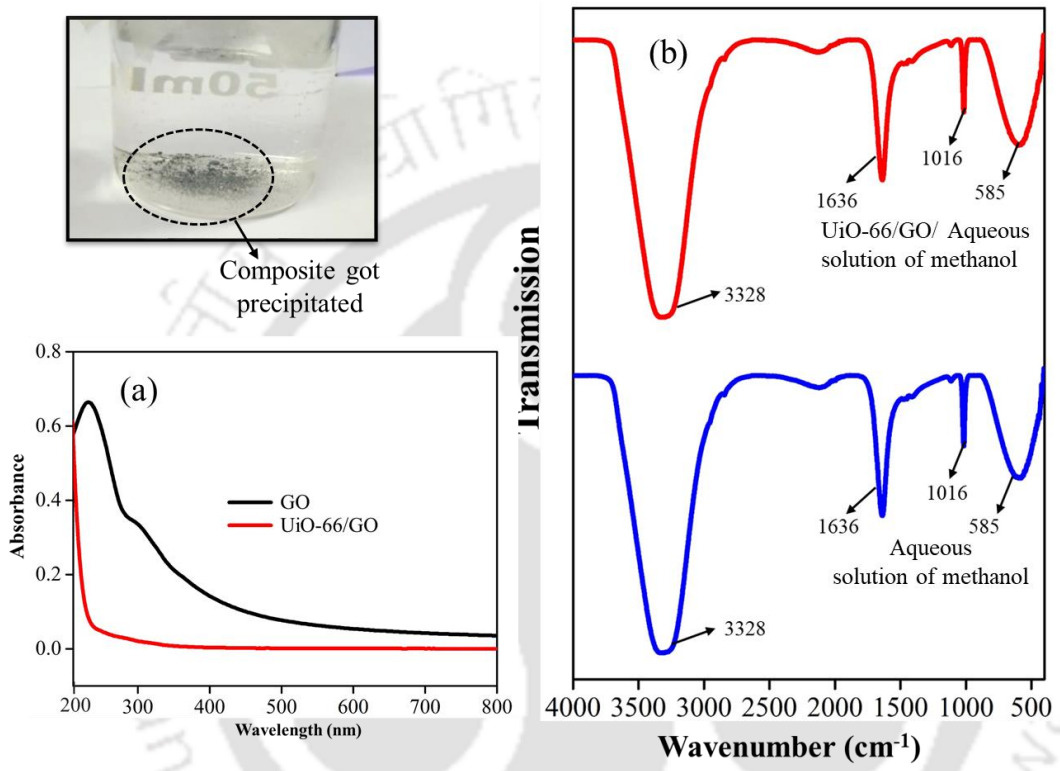

Figure 6.10 UV spectroscopy and FTIR analysis of pure aqueous methanol and UiO-66/GO in aqueous methanol

6.3.2 Characterization of UiO-66 and UiO-66/GO composite membrane

6.3.2.1 FESEM and EDX analysis

The FESEM images for the internal structures of the membranes are shown in **Fig. 6.11.** The newly synthesized UiO-66/GO mixed SPEEK membrane showed the presence of UiO-66/GO on the surface of SPEEK. However, the surface of the SPEEK/UiO-66/GO (**Fig. 6.11b**) was found to be rougher. The mutual interactions between the SPEEK and

UiO-66/GO nanosheets may be a possible reason for this roughness. The hydrophobic nature and the strong interparticle interactions of the MOF particles makes it particularly difficult to achieve a uniform dispersion [19]. However, a uniform dispersion was seen in the case of UiO-66/GO particles induced in SPEEK membranes because of the unique hybrid structure of the sheets. The FESEM images were found to be in agreement with a good affinity between the SPEEK membranes and the UiO-66/GO, owing to the mutual interactions between them. EDX analysis also supports this statement. There might be a strong hydrogen bonding between the -SO_3H groups of the SPEEK and the UiO-66/GO which can be attributed to these mutual interactions. This might also be a probable effect of the $\pi - \pi$ interactions between the unsaturated C-C bonds in graphite oxide and benzene rings in SPEEK [23].

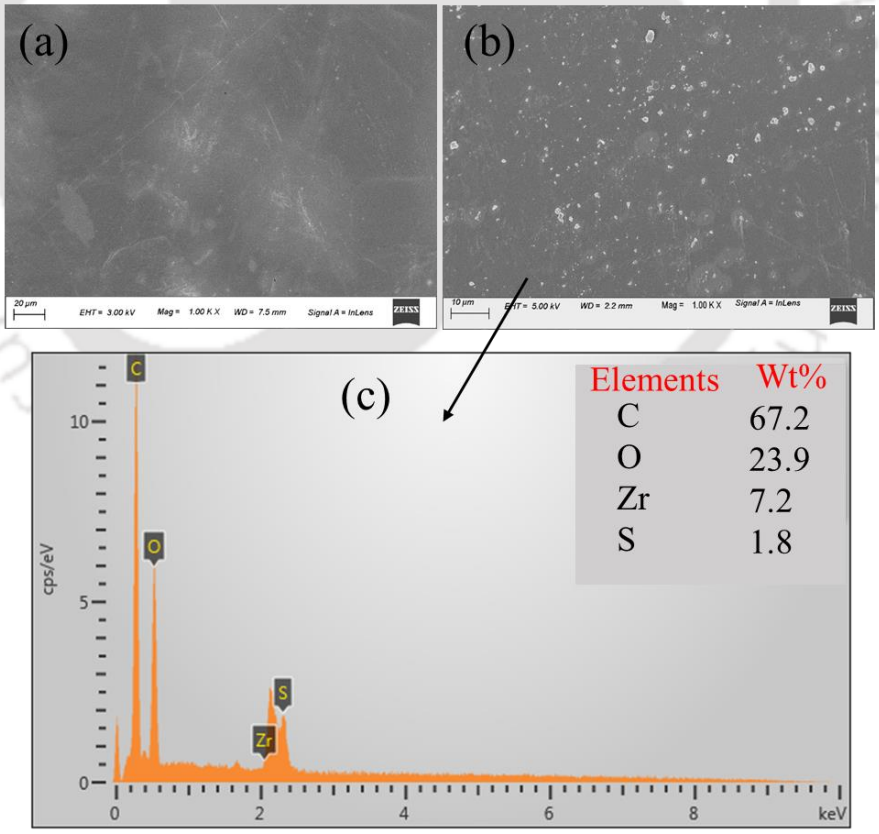

Figure 6.11 FESEM and EDX analysis of SPEEK and of SPEEK/UiO-66/GO composites membrane

6.3.2.2 XRD analysis

Fig. 6.12 represents the XRD analysis of SPEEK and SPEEK/UiO-66/GO composite membrane. It is can be seen from the figure that UiO-66/GO composite membrane shows a strong peak at 5 º and 6.8 º which correspond to the (111) and (002) characteristic peaks from UiO-66. Pure SPEEK membrane exhibited a broad peak on 20º which is shifted to the high value of 2θ (21.2º) after the addition of UiO-66/GO composite. This behaviour of mixed membrane indicates a strong filler-polymer interaction and also a well dispersion capability of MOF-GO composite with higher specific area [20].

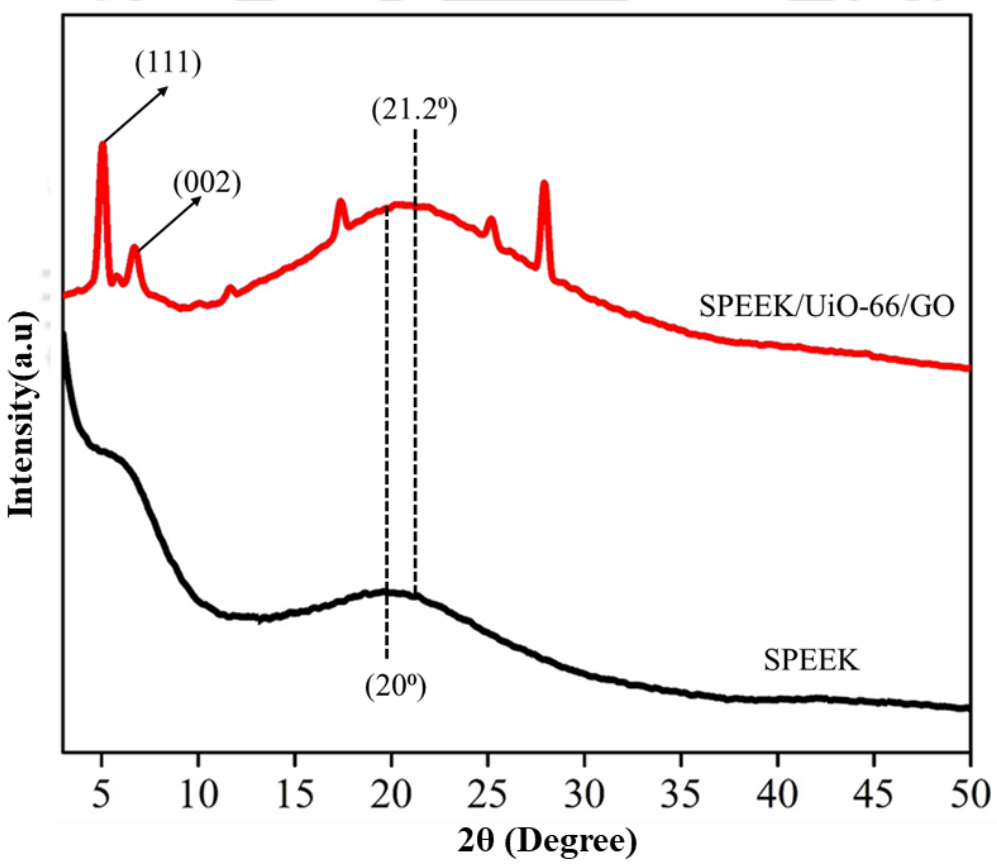

Figure 6.12 XRD analysis of SPEEK and of SPEEK/UiO-66/GO composites membrane

6.3.2.3 TGA analysis

TGA analysis for the SPEEK, SPEEK-UIO-66, and SPEEK- UiO-66/GO composite membranes was performed to predict the thermal stability of the fabricated membrane and explore the scope of application in methanol fuel cells (**Fig. 6.13**). Initial weight loss at temperature 100 °C occurs due to loss of adsorbed water molecules. The membranes remain stable, showing negligible weight loss upto 280 °C. Decomposition of sulfonic acid groups of SPEEK membrane matrix results in sharp weight loss upto 380 °C [21]. Above this temperature, breakage of cross-linked –CO–O– bonds, which resulted from the de-sulfonation of sulfonic acid group occurs. As seen from the figure, the weight loss of the filler incorporated membranes i.e., SPEEK-UIO-66 and SPEEK- UiO-66/GO are lower compared to pristine SPEEK membrane, concluding their increased thermal stability and potential candidates for DMFC applications.

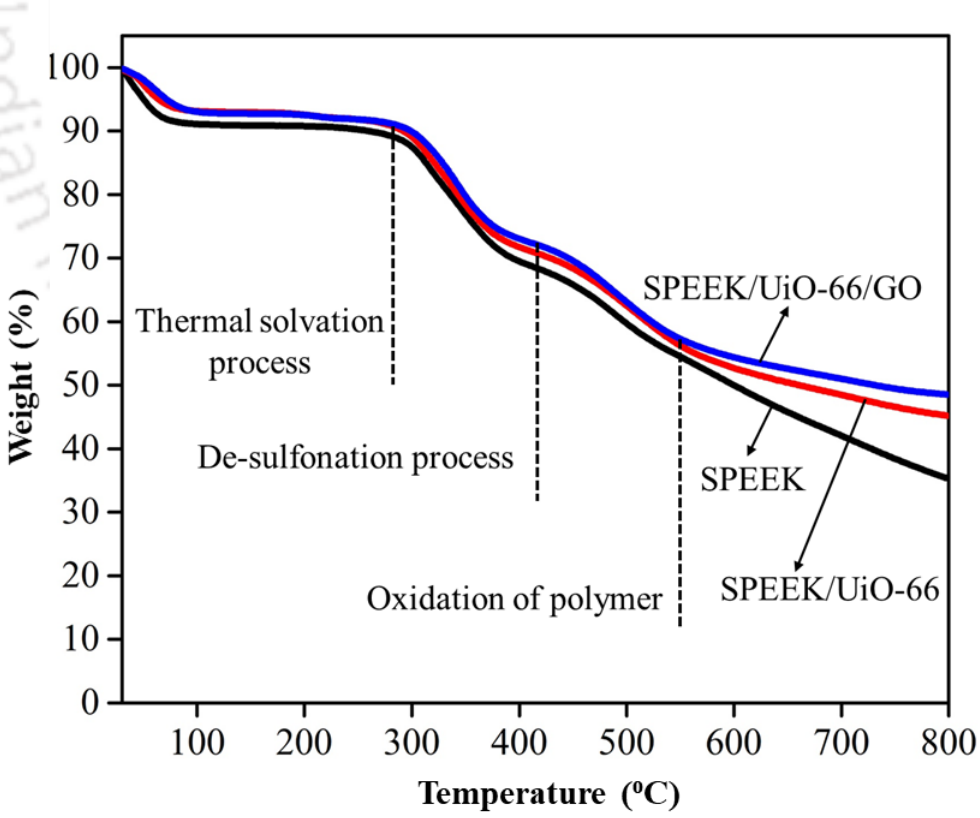

Figure 6.13 TGA analysis of SPEEK and SPEEK/UiO-66/GO composites membrane

6.3.2.4 Water uptake and IEC measurement

Fig. 6.14 shows the water uptake and ion exchange of SPEEK and SPEEK/ UIO-66/GO composite membranes as a function of GO content at room temperature. As the GO content increases, the water uptake is found to increase. Water ensures easy and convenient proton transfer as well increases the conductivity [22]. These are both very desirable properties for an efficient membrane. UiO-66/GO, treatment of the membrane prior to measurement, state of hydration at ambient conditions all play a very important role in determining the proton conductivity of SPEEK. Functional groups of GO available for interaction and the dissociation capability in water affect the proton conductivity of monomeric membranes. It is important to take the water uptake and ion exchange capacity into serious consideration when studying proton exchange membranes as water molecules help in facilitating proton transport. It is important to maintain an optimum water uptake as excessive water uptake may lead to dimensional changes resulting in mechanical failures and solubility in water.

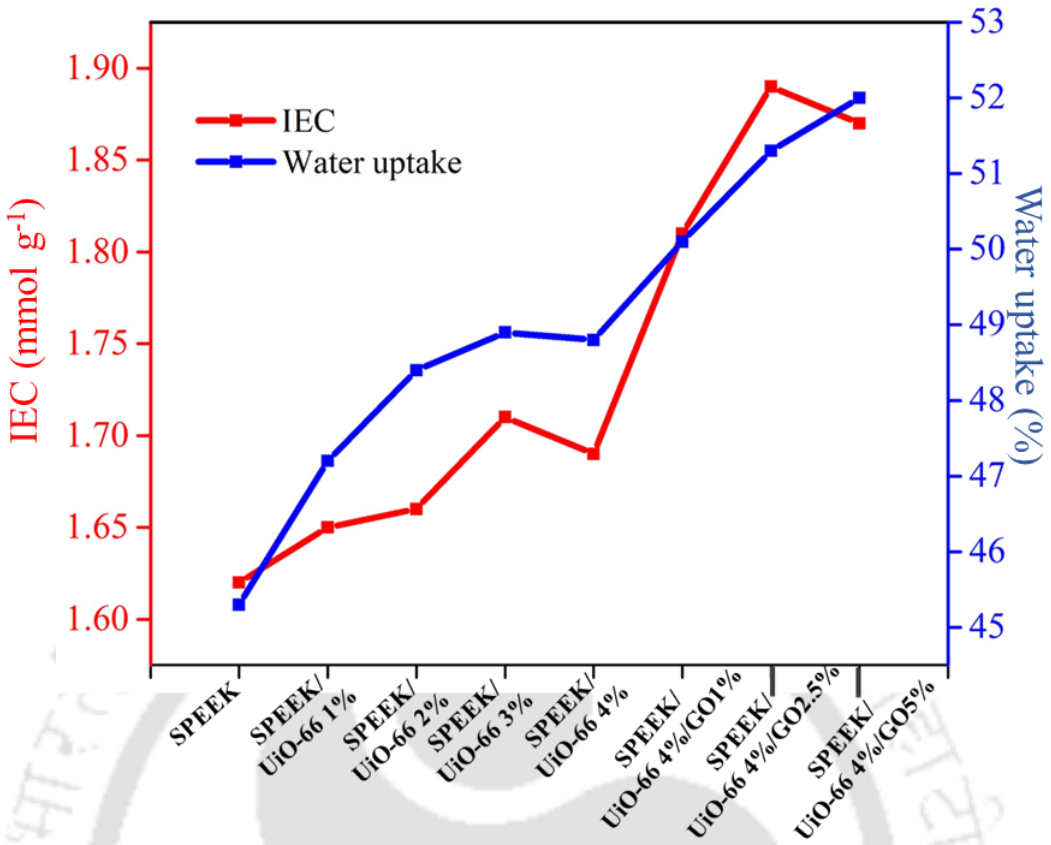

Figure 6.14 IEC and water uptake analysis of SPEEK and its composites membrane

6.3.2.5 Methanol permeability, conductivity and selectivity measurement

Pure SPEEK membrane shows methanol permeability around 2.18×10^{-6} cm^2 S^{-1}. After adding UiO-66 in the polymer matrix the methanol permeability reduced to 4.97×10^{-7} cm^2 S^{-1} where the amount of UiO-66 was 4 wt% (**Fig. 6.15**). From IEC experiment it has been found that after increasing the amount of UiO-66 above 3 wt% the IEC value of membrane is decreases, which is why 3 wt% of UiO-66 (where methanol permeability 5.08×10^{-7} cm^2 S^{-1}) has been chosen as the optimum amount for fabricating a composite membrane. 3 wt% UiO-66 has been further modified with a variation of GO (1-5 wt%). The SPEEK/UiO-66 composite membranes showed a higher methanol permeability than the SPEEK/UiO-66/GO membranes. Methanol permeability decreases with increasing amount of GO in UiO-66. The SPEEK/ UiO-66 (3wt%)/GO (5%) composite membrane

showed 4.65×10^{-7} cm^2 S^{-1}. The favorable low methanol permeability of the modified membranes is because of the methanol barrier that is formed by the connected UiO-66 and GO. An increased tortuosity in the methanol diffusion networks is indicated by the enhanced methanol rejection of the /SPEEKUiO-66-GO membranes. The UiO-66 and UiO-66/GO composite membranes were fully hydrated before the measurement of the conductivities and the conductivity was measured at room temperature. At first starting with the pure UiO-66 it has been found that with increasing the amount of UiO-66, the conductivities increased and reached a maximum of 1.26 mS/cm (3wt% UiO-66) from 1.04 mS/cm. Then further increase in amount from 3 wt% to 4 wt% the conductivity decreased 1.23 mS/cm. The 2.5 wt % GO doped UiO-66 (3wt%) nanocomposite membrane showed a better proton conductivity than the SPEEK/UiO-66 (3 wt%) membranes. They showed a peak at 1.88 mS/cm which significantly decreased with further increase in the amount GO in UiO-66 at 1.61 mS/cm.

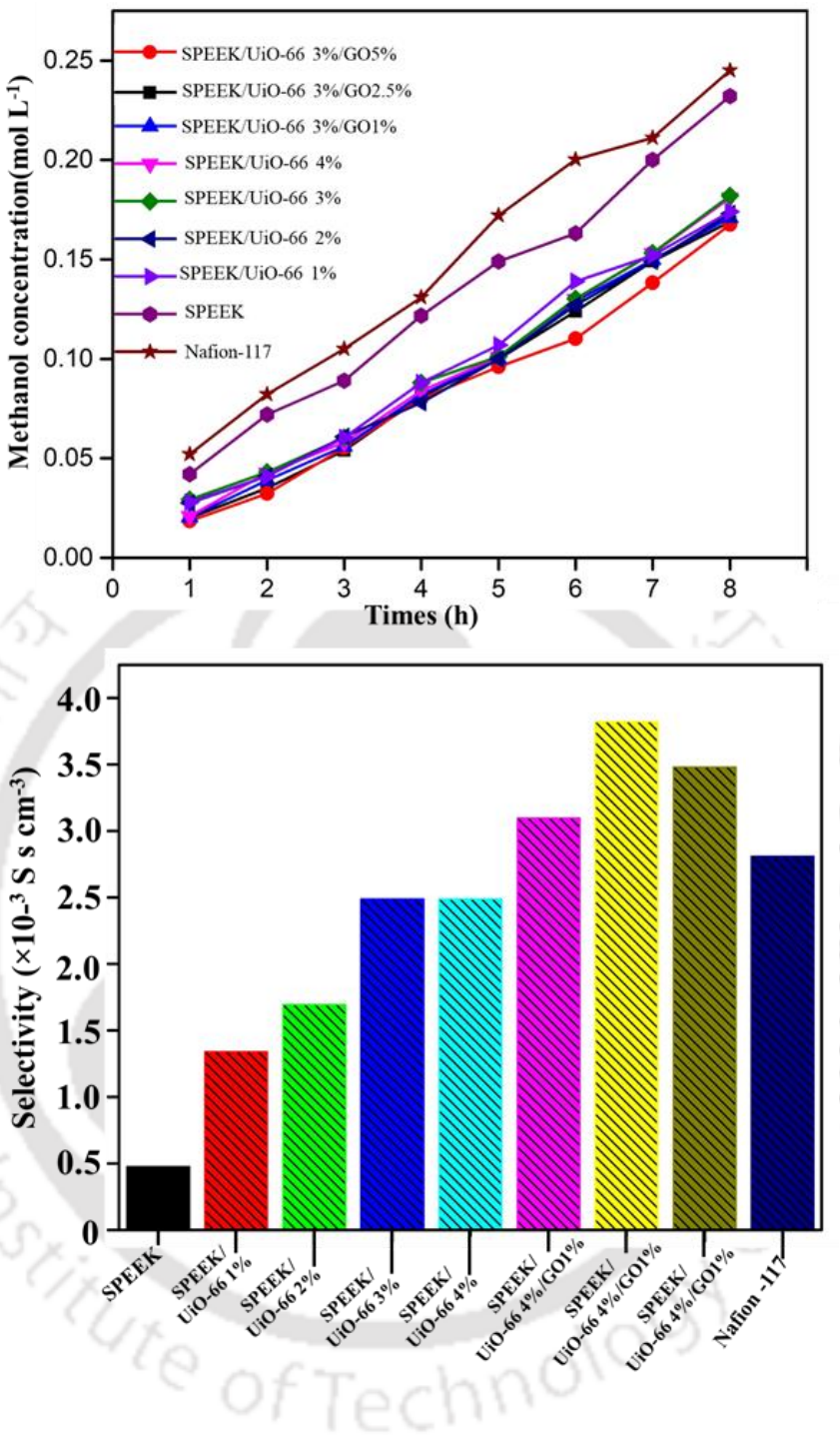

Figure 6.15 (a) Methanol permeability and (b) selectivity of SPEEK and of SPEEK/UiO-66/GO composites membrane

The covalent forces responsible for linkage of GO sheets with UiO-66 framework involves π-π interaction and hydrogen bonding (**Fig. 6.16**). π-π interaction occurs between the benzene rings of GO and organic linker of UiO-66 [23]. Presence of

hydroxyl groups on the surface of GO sheets results in hydrogen bonding with the carboxylic acid group present in the organic linker of UiO-66. However, both GO and UiO-66 are negatively charged, which rules out the possibility of electrostatic interection in the present scenario. The unsaturated metal sites in the UiO-66/GO help in trapping a lot of water molecules which significantly aids in the production of OH groups by hydrolysis [24]. The octahedral and tetrahedral sites of the framework absorb water molecules, which facilitates the formation of hydrogen-bonding networks which act as excellent pathways for proton conduction.

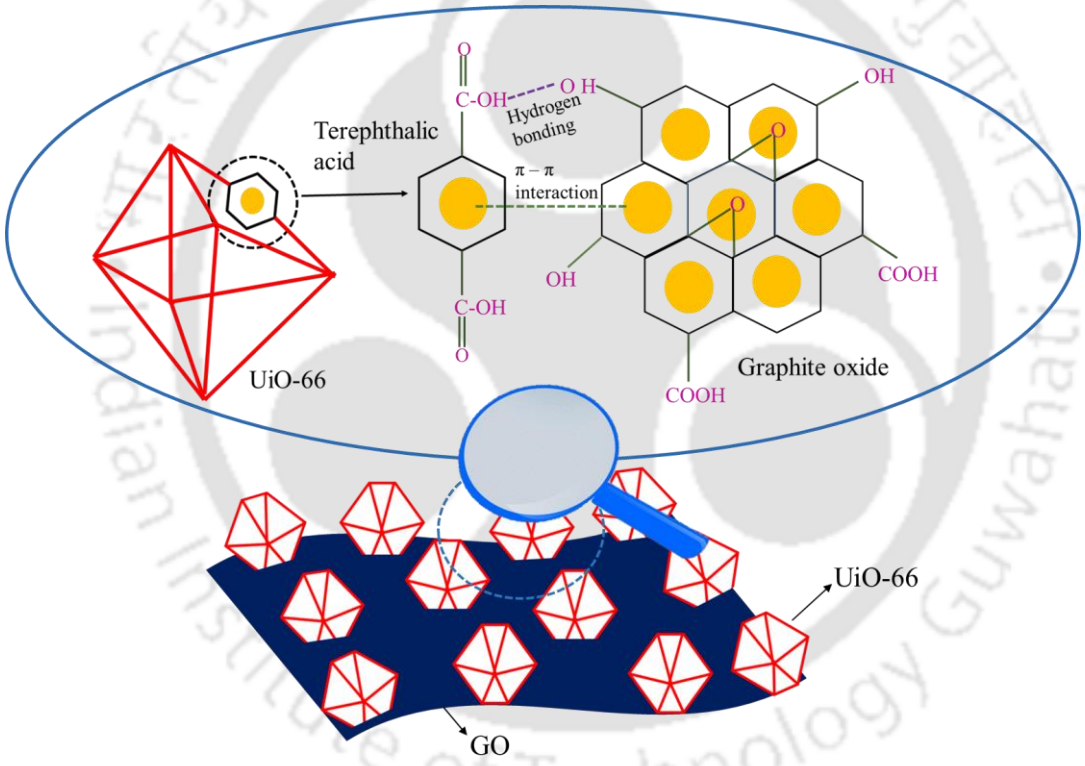

Figure 6.16 Possible interaction of GO with UiO-66

The proposed mechanism of the participation of water molecules is in agreement with the GrÖthous mechanism. Actually, the water is an important factor for GrÖthous and Vehicle mechanisms which are mechanisms of proton transport. The hydrophilic nature of GO enhanced the water absorbing property of the composite membrane which allow the membrane to absorb the water into its structure. On the other hand, the crystalline

tunnel-like architecture can be found from UiO-66 and their small porosity allow them to formation of orientated hydrogen bonded network of the guest water molecules as well as more hydrolytic stability to ensure a proper proton conduction performance. As the UiO-66/GO content increases, so does the number of metal sites which implies more number of hydrogen-bonding networks and hence, enhanced proton conductivity. The selectivity values of the SPEEK membranes increased from 4.77×10^2 S cm^{-3} s to 3.82×10^3 S cm^{-3} s (**Fig. 6.15b**). The selectivity of a membrane for DMFC application was calculated as the ratio of their ionic conductivity and methanol permeability and the selectivity of the SPEEK membrane has been increased range from 1.34×10^3 S cm^{-3} s to 3.85×10^3 S s cm^{-3} at room temperature.

6.4. Conclusions

The study had been formulated keeping in mind the objective of formulating UIO-66/GO composite for proton exchange membrane. The water uptake and ion exchange capacity was found to increase proportionally with the GO content in UiO-66 and the membranes were found to become more proton conductive. Selectivity values were found tobe increase up to 3.85×10^3 S s cm^{-3} at room temperature. However, the selectivity value for Nafion-117 membrane at the same experimental conditions was found to be 2.78×10^3 S cm^{-3} s and the proton conductivity of the composite membrane shows low value then Nafion-117, which concludes that further modification in the mixed matrix membrane is required to achieve the desired efficiency level. In order to fulfill this target, further study involves improvement in the properties of UiO-66/GO composite.

References

1. D.J. Kim, M.J. Jo, S.Y. Nam, A review of polymer–nanocomposite electrolyte membranes for fuel cell application, Journal of Industrial and Engineering Chemistry 21 (2015) 36-52.
2. C.R. Aguiar, É. Fontana, J.A. Valle, A.A. Souza, A.F. Morgado, S.M. Souza, Adsorption of Basic Yellow 28 onto chemically-modified activated carbon: Characterization and adsorption mechanisms, The Canadian Journal of Chemical Engineering 94(5) (2016) 947-955.
3. M. Arami, N.Y. Limaee, N.M. Mahmoodi, N.S. Tabrizi, Removal of dyes from colored textile wastewater by orange peel adsorbent: equilibrium and kinetic studies, Journal of Colloid and Interface Science 288(2) (2005) 371-376.
4. N. Niluroutu, K. Pichaimuthu, S. Sarmah, P. Dhanasekaran, A. Shukla, S.M. Unni, S.D. Bhat, A copper–trimesic acid metal–organic framework incorporated sulfonated poly (ether ether ketone) based polymer electrolyte membrane for direct methanol fuel cells, New Journal of Chemistry 42(20) (2018) 16758-16765.
5. F. Cui, W. Wang, C. Liu, X. Chen, N. Li, Carbon nanocomposites self-assembly UiO-66-doped chitosan proton exchange membrane with enhanced proton conductivity, International Journal of Energy Research 44(6) (2020) 4426-4437.
6. S. Edubilli, S. Gumma, A systematic evaluation of UiO-66 metal organic framework for CO_2/N_2 separation, Separation and Purification Technology 224 (2019) 85-94.
7. C. Petit, T.J. Bandosz, MOF–graphite oxide nanocomposites: surface characterization and evaluation as adsorbents of ammonia, Journal of Materials Chemistry 19(36) (2009) 6521-6528.

8. X. Sun, Q. Xia, Z. Zhao, Y. Li, Z. Li, Synthesis and adsorption performance of MIL-101 (Cr)/graphite oxide composites with high capacities of n-hexane, Chemical Engineering Journal 239 (2014) 226-232.
9. N. Shokouhfar, L. Aboutorabi, A. Morsali, Improving the capability of UiO-66 for Cr (VI) adsorption from aqueous solutions by introducing isonicotinate N-oxide as the functional group, Dalton Transactions 47(41) (2018) 14549-14555.
10. C. Petit, T.J. Bandosz, MOF–graphite oxide composites: combining the uniqueness of graphene layers and metal–organic frameworks, Advanced Materials 21(46) (2009) 4753-4757.
11. L. Li, X.L. Liu, H.Y. Geng, B. Hu, G.W. Song, Z.S. Xu, A MOF/graphite oxide hybrid (MOF: HKUST-1) material for the adsorption of methylene blue from aqueous solution, Journal of Materials Chemistry A 1(35) (2013) 10292-10299.
12. A.M. Ebrahim, T.J. Bandosz, Ce (III) doped Zr-based MOFs as excellent NO2 adsorbents at ambient conditions, ACS Applied Materials & Interfaces 5(21) (2013) 10565-10573.
13. A.M. Ebrahim, B. Levasseur, T.J. Bandosz, Interactions of NO_2 with Zr-based MOF: effects of the size of organic linkers on NO_2 adsorption at ambient conditions, Langmuir 29(1) (2013) 168-174.
14. L. Valenzano, B. Civalleri, S. Chavan, S. Bordiga, M.H. Nilsen, S. Jakobsen, K.P. Lillerud, C. Lamberti, Disclosing the complex structure of UiO-66 metal organic framework: a synergic combination of experiment and theory, Chemistry of Materials 23(7) (2011) 1700-1718.
15. C.A. Clark, K.N. Heck, C.D. Powell, M.S. Wong, Highly defective UiO-66 materials for the adsorptive removal of perfluorooctanesulfonate, ACS Sustainable Chemistry & Engineering 7(7) (2019) 6619-6628.

16. X. Mao, C. Wang, X. Ma, M. Zhang, L. Liu, L. Zhang, L. Niu, Q. Zeng, Y. Yang, C. Wang, Molecular level studies on binding modes of labeling molecules with polyalanine peptides, Nanoscale 3(4) (2011) 1592-1599.
17. W. Xu, M. Dong, L. Di, X. Zhang, A Facile Method for Preparing UiO-66 Encapsulated Ru Catalyst and its Application in Plasma-Assisted CO2 Methanation, Nanomaterials 9(10) (2019) 1432.
18. M.S. Denny Jr, L.R. Parent, J.P. Patterson, S.K. Meena, H. Pham, P. Abellan, Q.M. Ramasse, F. Paesani, N.C. Gianneschi, S.M. Cohen, Transmission electron microscopy reveals deposition of metal oxide coatings onto metal–organic frameworks, Journal of the American Chemical Society 140(4) (2018) 1348-1357.
19. H. Sun, B. Tang, P. Wu, Rational design of S-UiO-66@ GO hybrid nanosheets for proton exchange membranes with significantly enhanced transport performance, ACS Applied Materials & Interfaces 9(31) (2017) 26077-26087.
20. S. Castarlenas, C. Téllez, J. Coronas, Gas separation with mixed matrix membranes obtained from MOF UiO-66-graphite oxide hybrids, Journal of Membrane Science 526 (2017) 205-211.
21. N. Awang, J. Jaafar, A.F. Ismail, Thermal stability and water content study of void-free electrospun SPEEK/Cloisite membrane for direct methanol fuel cell application, Polymers 10(2) (2018) 194.
22. J. Jaafar, A.F. Ismail, T. Matsuura, Preparation and barrier properties of SPEEK/Cloisite 15A®/TAP nanocomposite membrane for DMFC application, Journal of Membrane Science 345(1-2) (2009) 119-127.
23. J. Li, Q. Wu, X. Wang, Z. Chai, W. Shi, J. Hou, T. Hayat, A. Alsaedi, X. Wang, Heteroaggregation behavior of graphene oxide on Zr-based metal–organic

frameworks in aqueous solutions: a combined experimental and theoretical study, Journal of Materials Chemistry A 5(38) (2017) 20398-20406.

24. L.G. da Trindade, K.M. Borba, L. Zanchet, D.W. Lima, A.B. Trench, F. Rey, U. Diaz, E. Longo, K. Bernardo-Gusmao, E.M. Martini, SPEEK-based proton exchange membranes modified with MOF-encapsulated ionic liquid, Materials Chemistry and Physics 236 (2019) 121792.

CHAPTER 7

Palladium decorated graphite oxide doped UiO-66 based composite membrane

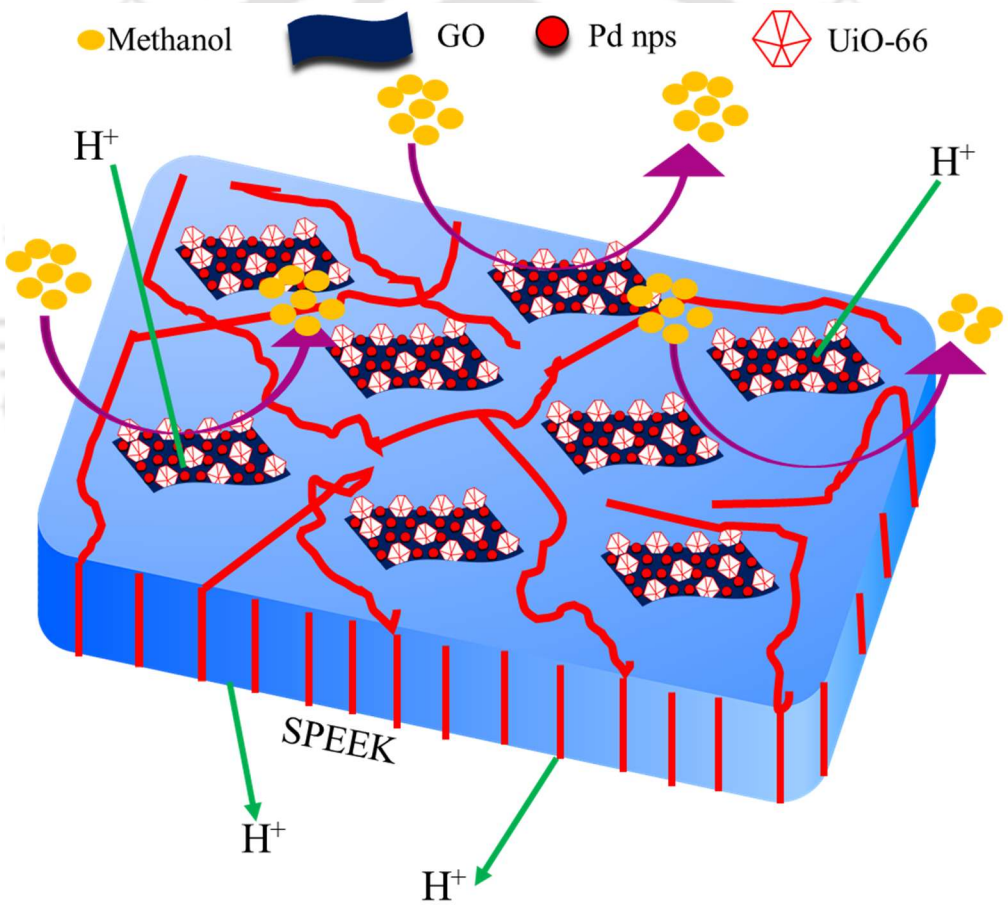

Graphical abstract of possible proton transport and methanol blocking effect in SPEEK/UiO-66/Pd-GO membrane.

CHAPTER 7

Palladium decorated graphite oxide doped UiO-66 based composite membrane

This chapter encompasses the fabrication of SPEEK membrane by incorporation of Palladium decorated graphite oxide doped UiO-66 composite. Palladium nanoclusters blocked the methanol permeability in the hydrophilic channel, thus significantly reducing the methanol crossover while the proton conductivity of the membrane stayed intact. This chapter shows the development of an efficient membrane that maintains the optimum methanol crossover.

7.1 Introduction

Palladium (Pd) is well known to be an effective medium for hydrogen and can easily form palladium hydride, and therefore widely used in the methanol-blocking PEM for its potential function of proton conduction [1,2]. The use of Palladium nanoparticle (Pd NPs) blocked the methanol permeability in the hydrophilic channel, thus significantly reducing the methanol crossover while the proton conductivity of the membrane stayed intact. The specific advantage of the positive charged nanoparticles is that they could be anchored to the sulfonic acid function group, $-SO_3$ on the membrane surface [3]. So, in this chapter palladium nanoparticle has been introduced in the UiO-66/GO composite. In this section, UiO-66 (3wt%)/GO (2.5 wt%) was chosen for the further modification.

7.2 Experimental

7.2.1 Synthesis of palladium grafted graphite oxide (Pd-GO)

Palladium grafted GO was synthesized by polyol process (glycol reduction method) [4]. In brief, 0.089 g of $PdCl_2$ was mixed with 50 mL HCl to make H_2PdCl_4 (0.01 M) solution and simultaneously 50 mg of synthesized GO was dispersed in 50 mL of DI water using a sonication bath for 60 minutes to form GO colloid (**Fig. 7.1**). Then 100 mL of ethylene glycol, 50 mL of GO colloid and 15 mL H_2PdCl_4 (0.01 M) were mixed in a beaker under magnetic stirring for 30 minutes. The reaction temperature was then raised to 373 K with continuous stirring for 6 h. The final resultant black precipitate was centrifuged and washed with DI water three times, and dried in a vacuum oven at 333 K for 12 h to obtain Pd-GO. The amount of Pd was varied in such a way that the expected amount of Pd introduced in the GO framework was 5 wt%, 10 wt%, 15 wt% of GO.

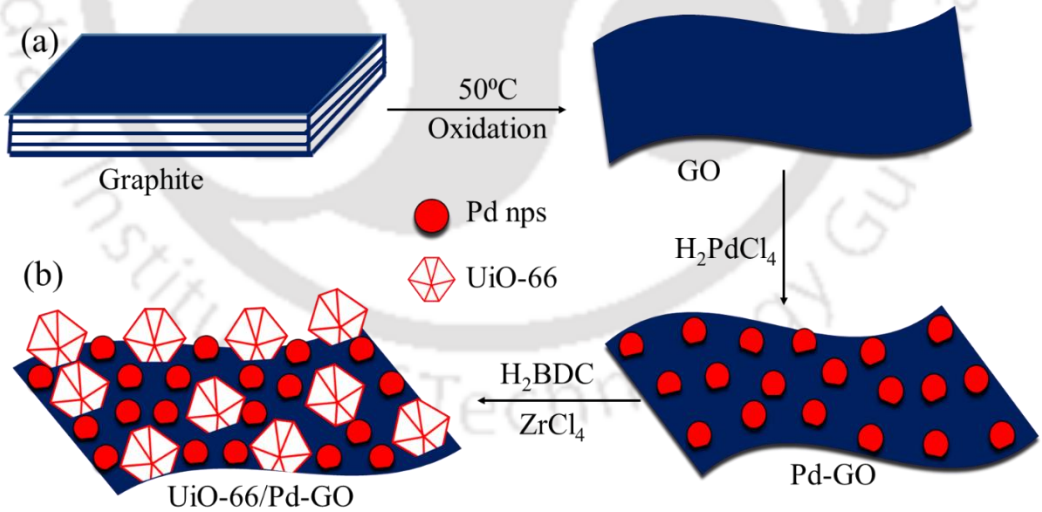

Figure 7.1 Synthesis of (a) Pd-GO and (b) UiO-66/Pd-GO

7.2.2 Synthesis of palladium decorated graphite oxide (Pd-GO) doped UiO-66

Synthesis procedure is same as discussed earlier in case of synthesis of UiO-66 and UiO-66/GO. For preparing the composites via in-situ solvothermal method, Pd-GO was dispersed in DMF by sonication to obtain a homogenous, stable slurry. 2.5wt% of both Pd-GO (5%) , Pd-GO (10wt%) and Pd-GO (15wt%) were used. After sonication for 2 h, it was then acidified by HCl followed by addition of BDC and similar protocol was followed as for UiO-66 synthesis. The as-synthesized powder was named as UiO-66-Pd-GO-n, where n=5, 10, 15 based on the amount of Pd-GO doped in the MOF.

7.2.3 Fabrication of composite membrane

To prepare the composite membrane, 1 g of SPEEK was dissolved in 5 g of DMAc solvent. On other side the 2.5 wt% of UiO-66/Pd-GO composites were added in 4 gm of DMAc and sonicated to get a homogeneous mixture. These two solutions were then mixed and kept in stirring overnight. The membrane was then cast onto a flat glass plate, dried at 333 K for 6 h, followed by annealing at 373 K for 4 h. It was cooled and immersed in deionized water for 24 h. Three membranes were fabricated varying the concentration of Pd from 5wt% to 15wt%.

7.2.4 Characterization

In this section X-ray diffractometer, field emission scanning electron microscope, X-ray photo electron spectroscopy, Fourier transform infrared spectra, Thermogravimetric analysis, Transmission Electron Microscope , BET surface area analyzer has been used for characterization of fabricated membrane and the weight differences between the full-hydrated membranes and the dried membranes along with their water uptake, methanol permeability and proton conductivity of the membranes (refer to Chapter 3).

7.3 Results and Discussion

7.3.1 Characterization of UiO-66/Pd-GO composite

7.3.1.1 FETEM analysis

Fig. 7.2 demonstrates the morphology of the composite nanosheets as obtained from the TEM. The GO is shown (**Fig. 7.2a**) to exhibit a characteristic transparent and laminar structure. Wrinkles could also be found on the GO as discussed earlier. The ultrasonic processing of a mixture of H_2PdCl4 indicated that the Pd nanoparticles were properly distributed on the GO surfaces [5]. The Pd nanoparticles were well-dispersed and were found to be highly densely clustered on the GO surfaces (**Fig. 7.2b**). **Fig. 7.2c** showed the spherical nature of the Pd nanoparticles. The particle size distribution of Pd on the GO surfaces was found to be narrow with a uniform size 5-10nm. The UiO-66 nanoparticles as such, without GO, showed an erratic particle size distribution, with many of the particles having a size smaller than 400nm. However, **Fig. 7.2d** showed the UiO-66 particles having a size around 200nm with the smaller particles of size 40-50nm in UiO-66/Pd-GO composite. These smaller particles were found to have a dense and uniform distribution on the Pd-GO layers. The HRTEM analysis done for UiO-66/Pd-GO composite showed two types of particle lattice as 0.221nm and 0.227nm which corresponds to the interplanar spacing of UiO-66 (**Fig. 7.2e**) and Pd NPs (**Fig. 7.2f**) [6,7]. The interplanar spacing of PdNps was found to be undeviating from the lattice spacing of a face-centered cubic Pd [5]. A strong coordination capability is exhibited by the phenolic and carboxylic groups on the GO sheets. This greatly favors the nucleation and growth of the MOF crystals. This excellent coordination capability between the metal ions from the oxygen-containing functional groups gives Zr^{4+}, the perfect anchoring sites to combine, which in turn promotes the nucleation and growth of UiO-66 crystals. Thus,

this in-situ growth technology is a feasible approach for homogeneous distribution of UiO-66 on the Pd-GO sheets surface.

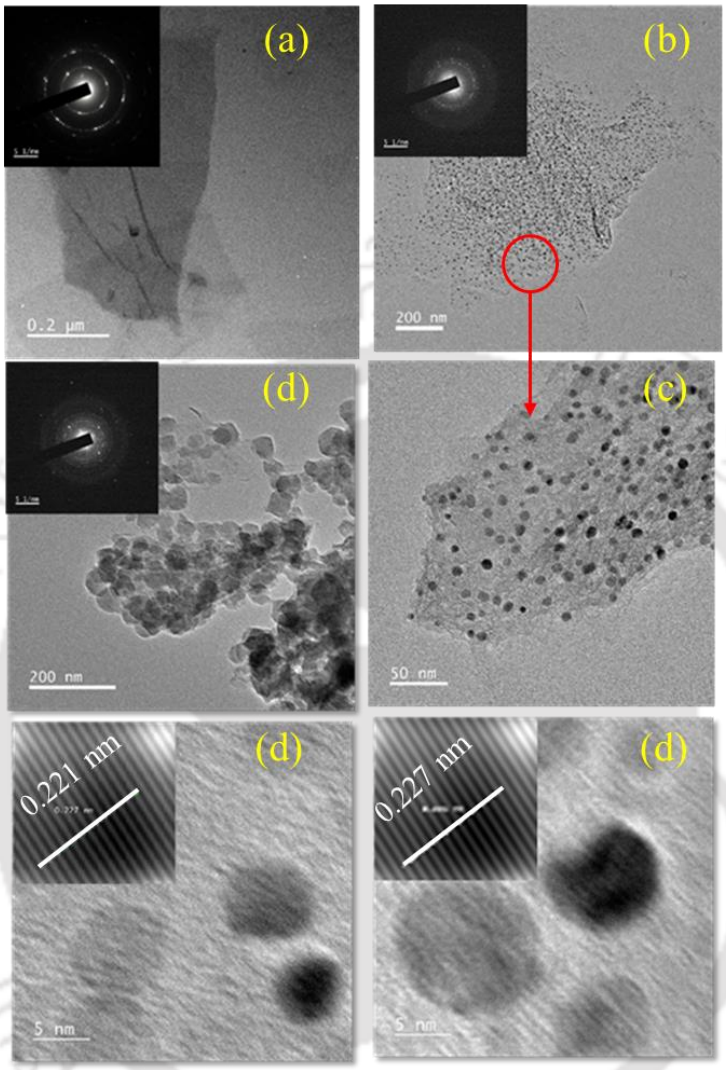

Figure 7.2 FETEM images for GO, Pd-GO and UiO-66-Pd-GO depicting their corresponding lattice spacing

7.3.1.2 FESEM analysis

The FESEM images of the UiO-66/Pd-GO along with graphite oxide and pure UiO-66 are shown in **Fig. 7.3**. The wrinkled structure was observed from the cross sectional view (**Fig. 7.3a**) and top surface view (**Fig. 7.3b**) of GO layers [8]. The size of UiO-66 used in this work was around 300nm (**Fig. 7.3c**), contrary to the 100nm reported in literature.

Fig. 7.3d-e shows the top surface and cross sectional view of UiO-66/Pd-GO composite. The irregularities of the composite particles also increased with addition of Pd-GO content, as opposed to the particle size of the composite particles. **Fig. 7.3f** shows the higher magnification view of UiO-66/Pd-GO composite.

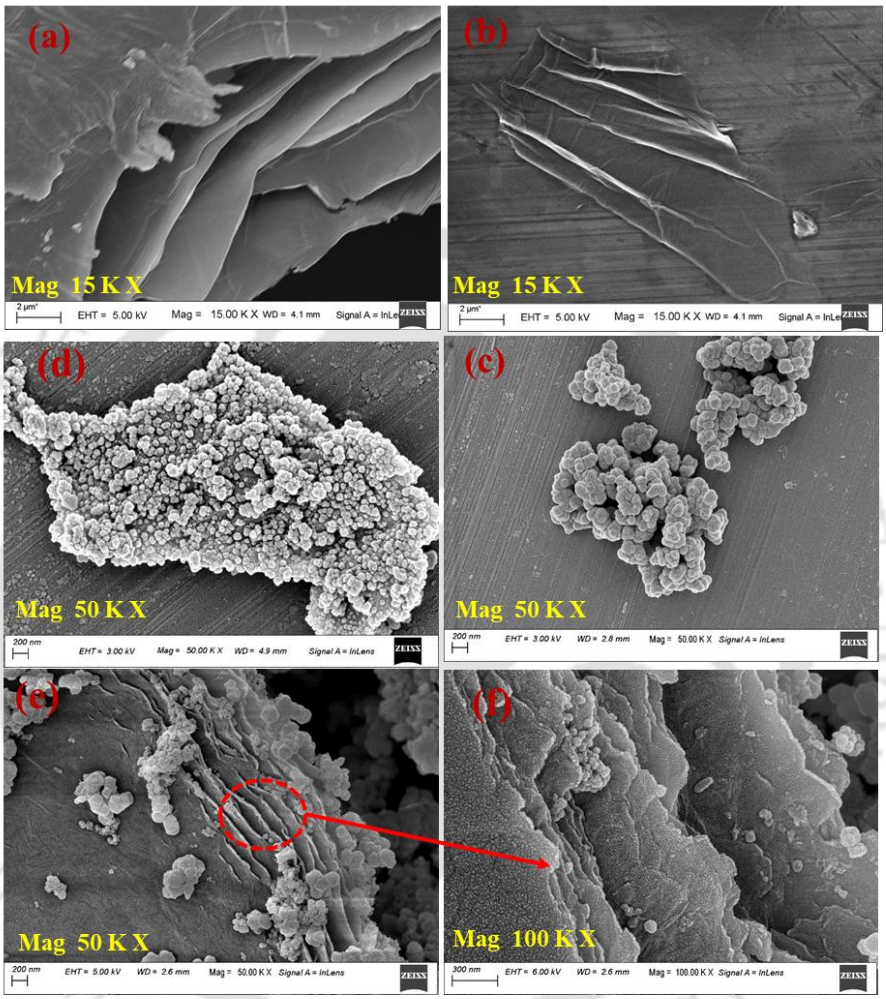

Figure 7.3 FESEM image of (a-b) cross section and top surface view of GO, (c) UiO-66, (d-f) cross section and top surface view of UiO-66/Pd- GO,

7.3.1.3 EDX analysis

The energy dispersive X-ray spectroscopy (EDS) mapping (**Fig. 7.4**) confirms the presence of palladium, zirconium, carbon and oxygen in UiO-Pd-GO composite. In addition, all elements seem to be well distributed on the surface thus confirming functionalization of UiO-66 in Pd-GO.

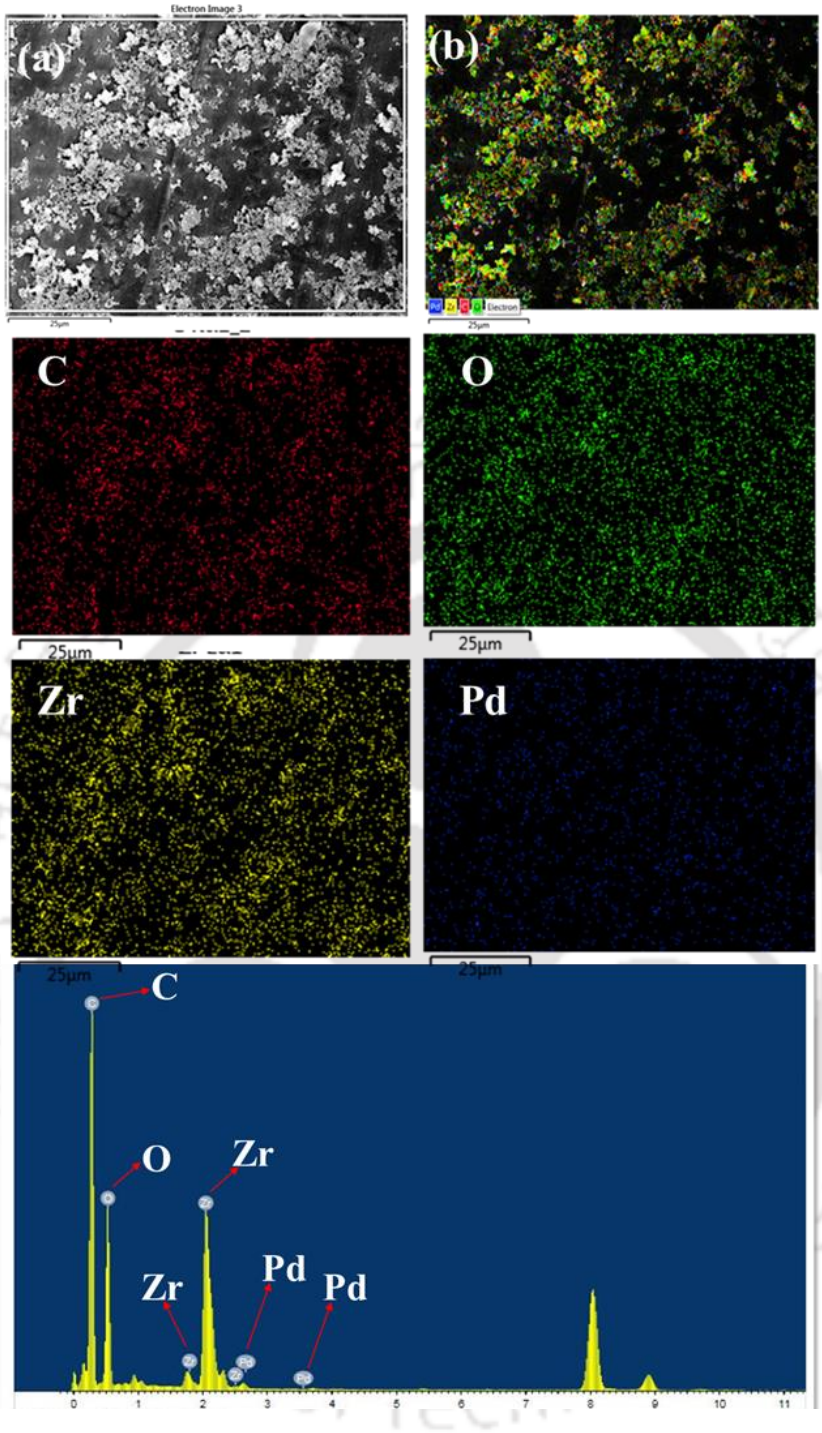

Figure 7.4 EDS mapping of UiO66-Pd-GO composite

7.3.1.4 XRD analysis

The XRD patterns of GO, Pd-GO, UiO-66 and UiO-66-Pd-GO composite are shown in **Fig. 7.5**. The characteristic diffraction peak of GO is shown at around 9.8. This diffraction peaks corresponded to the (002) plane. The graphitic planes were found to exhibit a

substantial amount of oxygenated functional groups. An inter-layer distance of 9.6Å was found. These results were found to be consistent with previous literature [9]. Addition of Pd NPs on the surface of GO shows a hump on 23.8º (002) which indicates the destruction of regular layer structure of GO by adding Pd NPs and also a little hump at 43.8º denotes the (200) planes which is formed due to the cubic (fcc) structure of PDNPs [10,11].

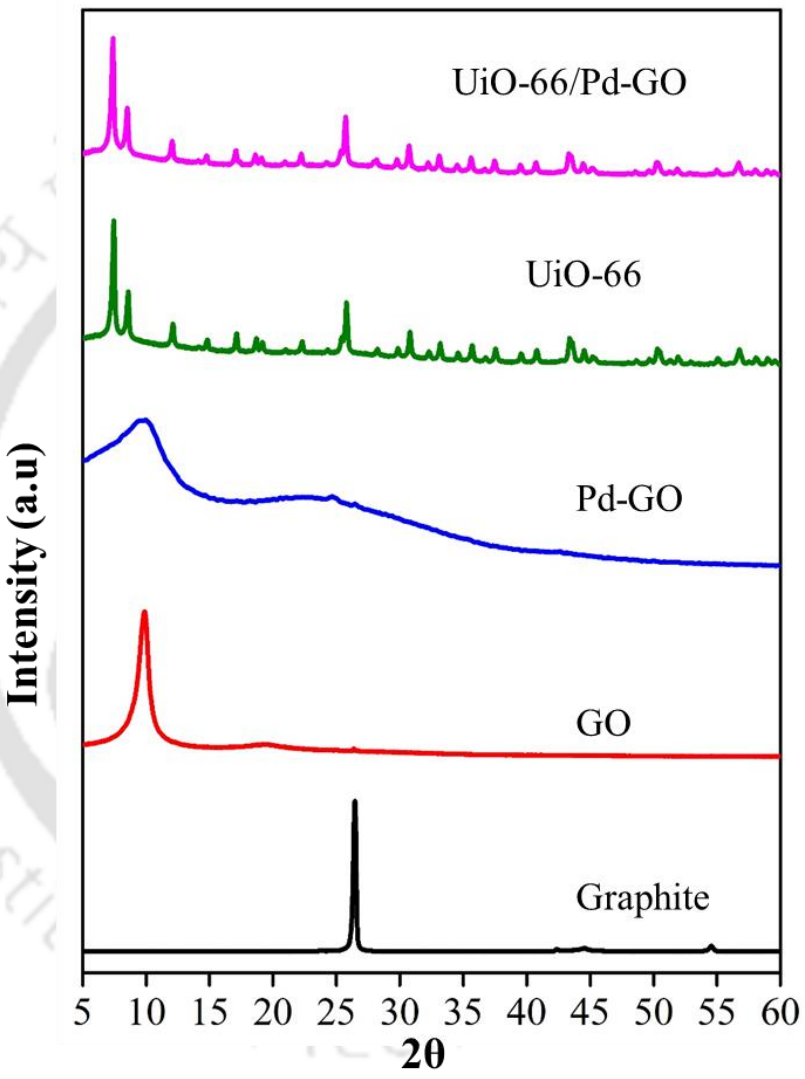

Figure 7.5 XRD patterns of Graphite, GO, Pd-GO, UiO-66 and UiO-66-Pd-GO

The UiO-66/Pd-GO and the UiO-66 showed an approximately identical peaks. These data indicated that no changes took place in the crystalline structures. However, a complete disappearance of the major diffraction peak of GO was observed. This could indicate

either a reduction in the GO content post the solvent-thermal process or a long range order dismissal in the GO sheets.

7.3.1.5 FTIR analysis

Fig. 7.6 shows the FTIR spectra of synthesized composites. The FTIR studies of GO showed peaks at 1393 cm^{-1} (stretching vibrations from C-O), at 1742 cm^{-1} (stretching vibrations from C=O), at 1632 cm^{-1} (stretching vibrations from C=C), 1046 cm^{-1} (stretching vibrations from C-O-C) and 3420 cm^{-1} (stretching vibrations from -OH). These peaks indicated the presence of functional groups which confirmed the successful oxidation of graphite [9]. In case Pd-GO, all the peak for GO has been found but the peak for C=O at 1742 cm^{-1} is shifted to the 1729 cm^{-1}. The H-bonding to the carbonyl may be observed by a shift of the C=O stretching mode (decrease of the wavenumber), but the change may be small depending of the interaction. [12,13]. The stretching and vibration of the functional groups present in the BDC generated the FTIR. The stretching vibration of C=O bond from the carboxylic acid group causes the weak peak at 1658 cm^{-1}, while the asymmetric stretching of the O-C-O group forms the strong band at 1581 cm^{-1}. The weak peak at 1505 cm^{-1} is attributed to the stretching vibrations of the unsaturated carbon (C=C) in the benzene rings of the BDC ligand, while the strong peak at 1398 cm^{-1} is formed by the symmetric stretching of C=O carboxylic acid [14, 15]. The C-H bond's vibrations cause the small peaks at 813 cm^{-1} and 753 cm^{-1}, whereas the peak at 664 cm^{-1} corresponds to the vibrations of the O-H bending. The FTIR spectra of the UiO-66 and the UiO-66-Pd-GO composites are similar, indicating no structural changes during the in-situ growth.

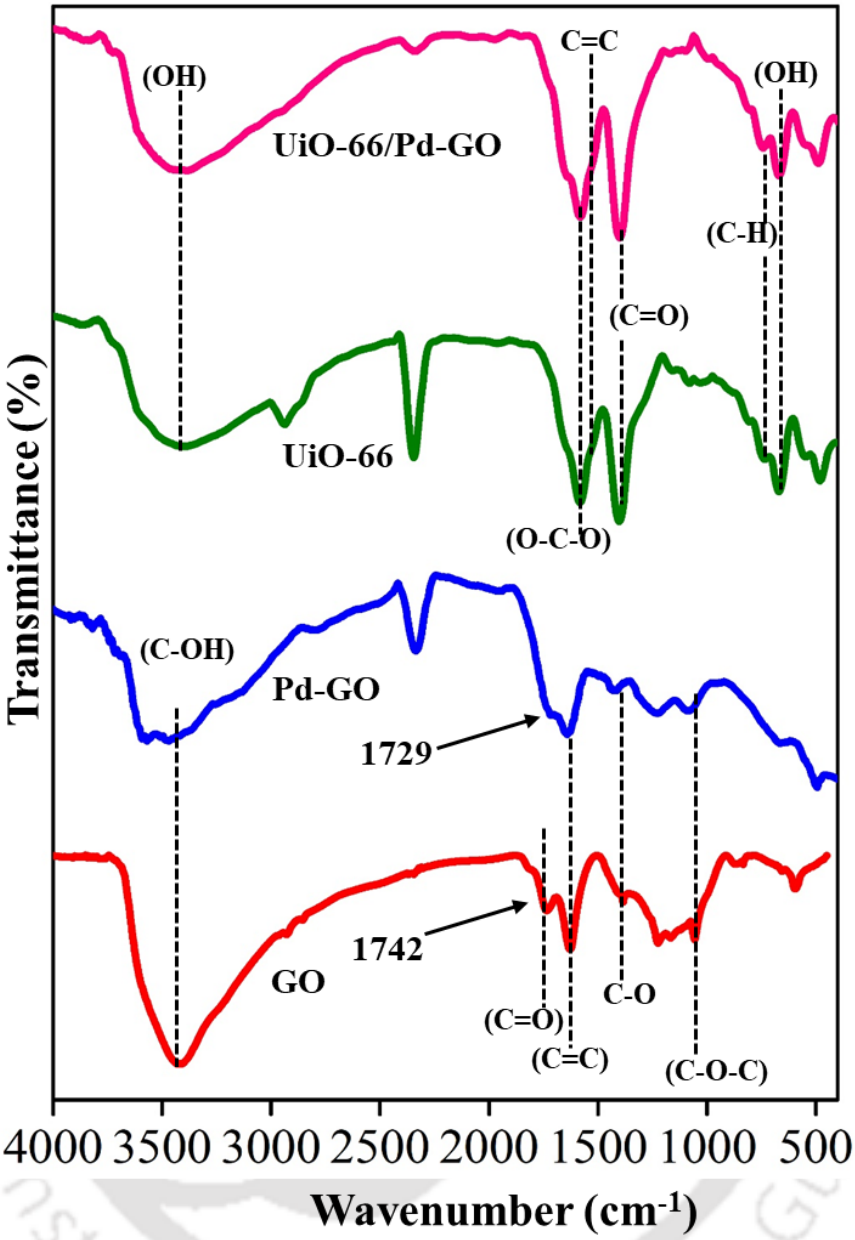

Figure 7.6 FTIR patterns of GO, Pd-GO, UiO-66 and UiO-66-Pd-GO

7.3.1.6 Raman spectroscopic analysis

The structural changes were also analyzed using Raman spectroscopy (**Fig. 7.7**). GO plays a crucial role in the preparation of Pd^{2+} which has been observed from the Raman Spectroscopy. Hence, it is important to study the structural changes in GO and Pd-GO before and after making a composite with UiO-66. Pure graphite shows a major peak at ~ 1600 cm^{-1} for in-planer starching of C-sp^2 bond which corresponds to G band

stretching. A D band at 1360 cm^{-1} was revealed by the spectrum in GO after oxidation. These results were in excellent agreement with the literature [9]. Disordered samples, edge defects and other defects such as sp^3 bonded carbon, bonds and valencies dangling, are implied by the D band while sp^2 carbon domains are associated with the G band. So, the number of structural defects is indicated by the intensity ratio of the D band and the G band (I_D/I_G). The average size of the sp^2 domains and the level of graphitization in the graphitic materials is generally quantified by this I_D/I_G ratio. Pd-GO shows slightly higher I_D/I_G ratio in comparison with GO (1.02 from 0.99). A higher I_D/I_G ratio was found in case of UiO-66/Pd-GO (1.05) as compared to pure UiO-66 (ID/IG = 0.88). These results indicated the reduction of the oxygen-containing groups. The carbon structure in the UiO-66/Pd-GO was found to be more disordered. This may be because of the decrease in the average size of the in-plane sp^2 domains [16].

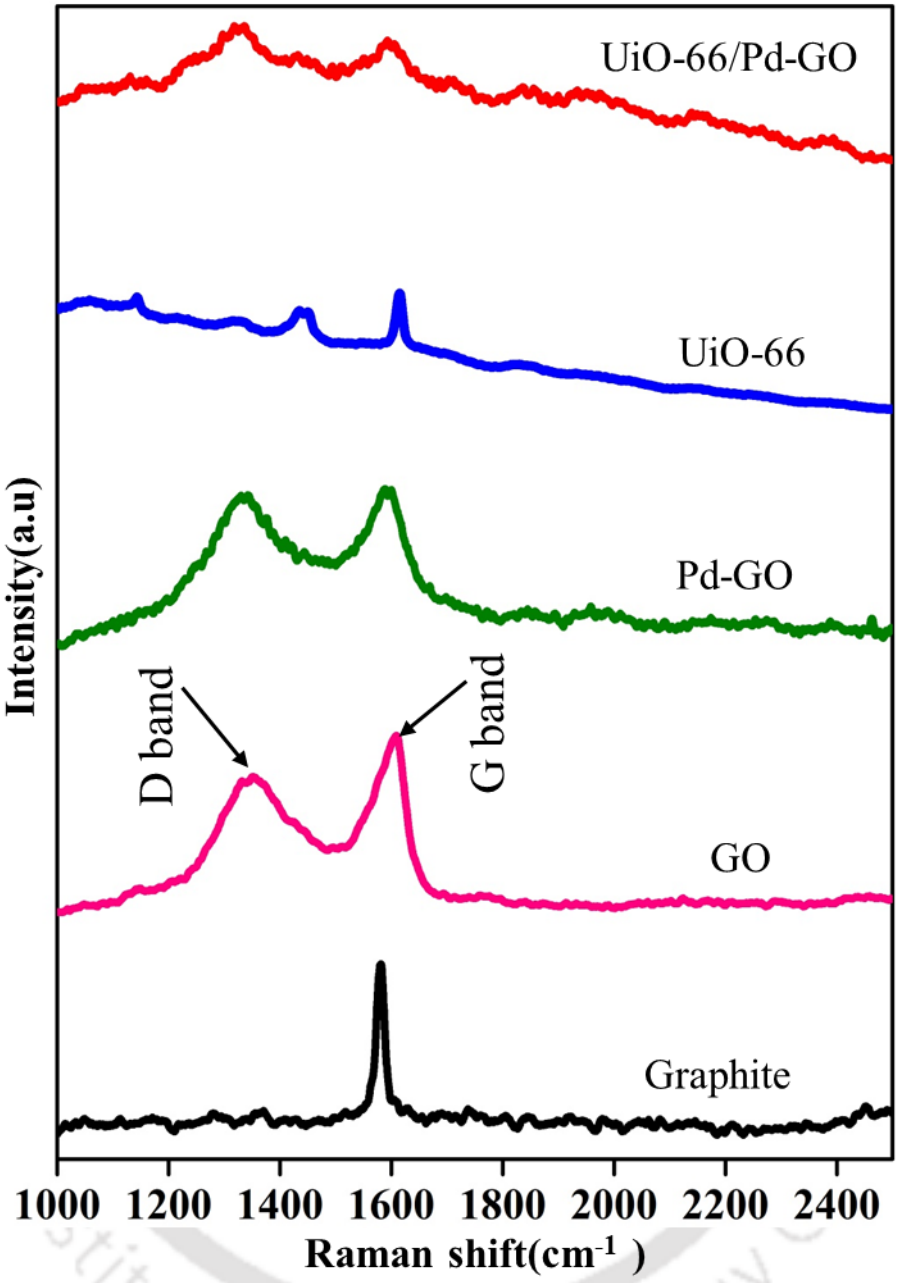

Figure 7.7 Raman spectra of GO, Pd-GO, UiO-66 and UiO-66/Pd-GO

7.3.1.7 XPS analysis

Fig. 7.8 shows the XPS spectra of the elements in focus, namely C, O, Zr 3d, Pd from UiO-66 and Uio-66/Pd-GO nanocomposites. The peaks at 330, 350 and 440 eV, as seen in **Fig 7.8a** can be attributed to Zirconium's 3p, 3p 3/2 and 3s orbital electrons [17,18]. After deconvolution of C1s region, the XPS spectra indicate mainly the presence of C=C

sp^2 bond (at 284.7 eV), with minor contributions from the C–C sp^3 (at 285.5 eV), C–O (at 286.7 eV), C=O (at 287.8 eV), and COOH (at 289.0 eV) bonds. O1s shows three major peak at 533.6 eV, 532.4 eV and 530.5 eV which is correspond to O-C=O, Zr-O-C and Zr-O-Zr. The XPS spectrum of the UiO-66/Pd-GO nanocomposites showed new peaks associated with Pd3d. Double peaks with binding energies at 334.6 eV and 340.2 eV were found in the XPS spectrum of Pd, as seen in **Fig. 7.8b**, which corresponded to Pd3d5/2 and Pd2d3/2, respectively [19].

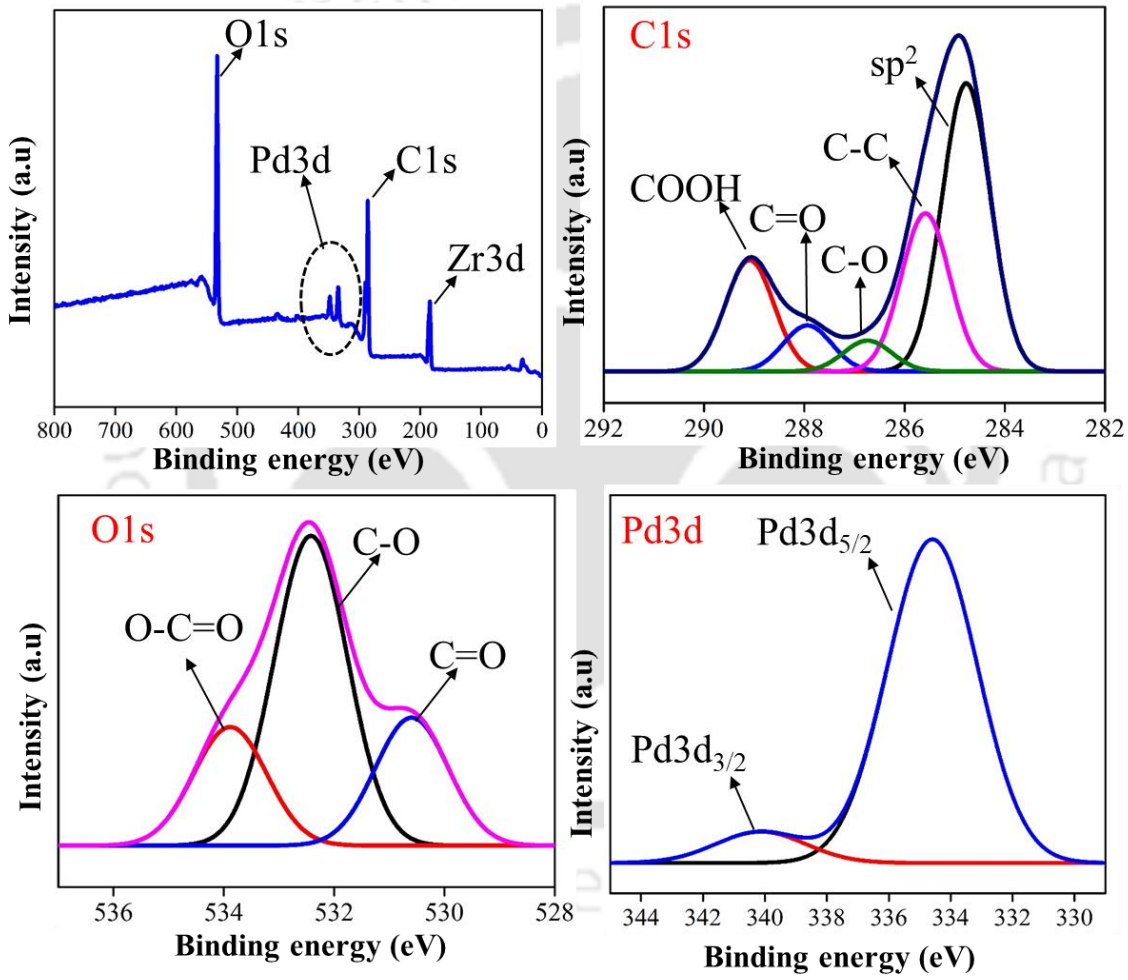

Figure 7.8 XPS spectra of UiO-66 and UiO-66/Pd-GO.

7.3.1.8 TGA analysis

The thermogravimetric curves of UiO-66, UiO-66/GO and UiO-66-Pd-GO are shown in **Fig. 7.9**. All the three samples exhibited similar turning points. The decrease in weight due to the loss of physically adsorbed water and solvent molecules was found to be exhibited till 100℃, following which a stability was exhibited by all of the molecules until 480℃. This could be inferred from the fact that no significant weight loss was observed till this point. However, structural degradation was found beyond 520℃ based on the significant weight loss and degradation post this period [20]. The introduction of GO and Pd-GO introduced chemical changes in the UiO-66 which can be deduced from the reduced weight loss [16]. The TGA showed that inducing Pd-GO into the UiO-66 improved the thermal stability of UiO-66 materials.

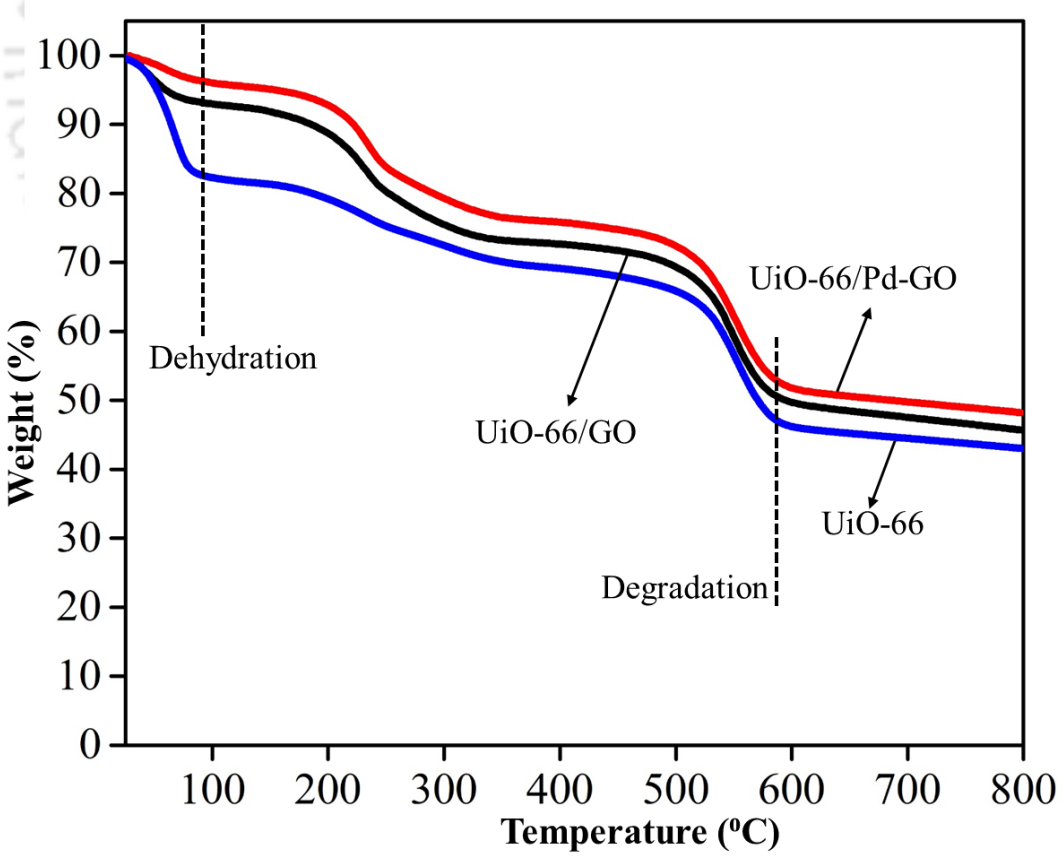

Figure 7.9 TGA patterns of UiO-66, UiO-66/GO and UiO-66-Pd-GO

7.3.2 Characterization of UiO-66/Pd-GO composite membrane

7.3.2.1 FESEM analysis

The surface of the SPEEK/UiO-66-Pd-GO was found to be rougher (**Fig. 7.10**). The mutual interactions between the SPEEK and UiO-66/Pd-GO nanosheets may be a possible reason for this roughness. The hydrophobic nature and the strong interparticle interactions of the MOF particles makes it particularly difficult to achieve a uniform dispersion [21], which is why large clusters of UiO-66/Pd-GO were found on the SPEEK/UiO-66-Pd-GO composite membranes. However, a uniform dispersion was seen in the case of UiO-66/Pd-GO particles induced in SPEEK membranes because of the unique hybrid structure of the sheets. The FESEM images were found to be in agreement with the morphology as mentioned above. There is a good affinity between the SPEEK membranes and the UiO-66/Pd-GO, owing to the mutual interactions between them. There might be a strong hydrogen bonding between the -SO_3H groups of the SPEEK and the UiO-66/Pd-GO which can be attributed to these mutual interactions. This might also be a probable effect of the π-π interactions between the unsaturated C-C bonds in graphene oxide and benzene rings in SPEEK as discussed earlier [22].

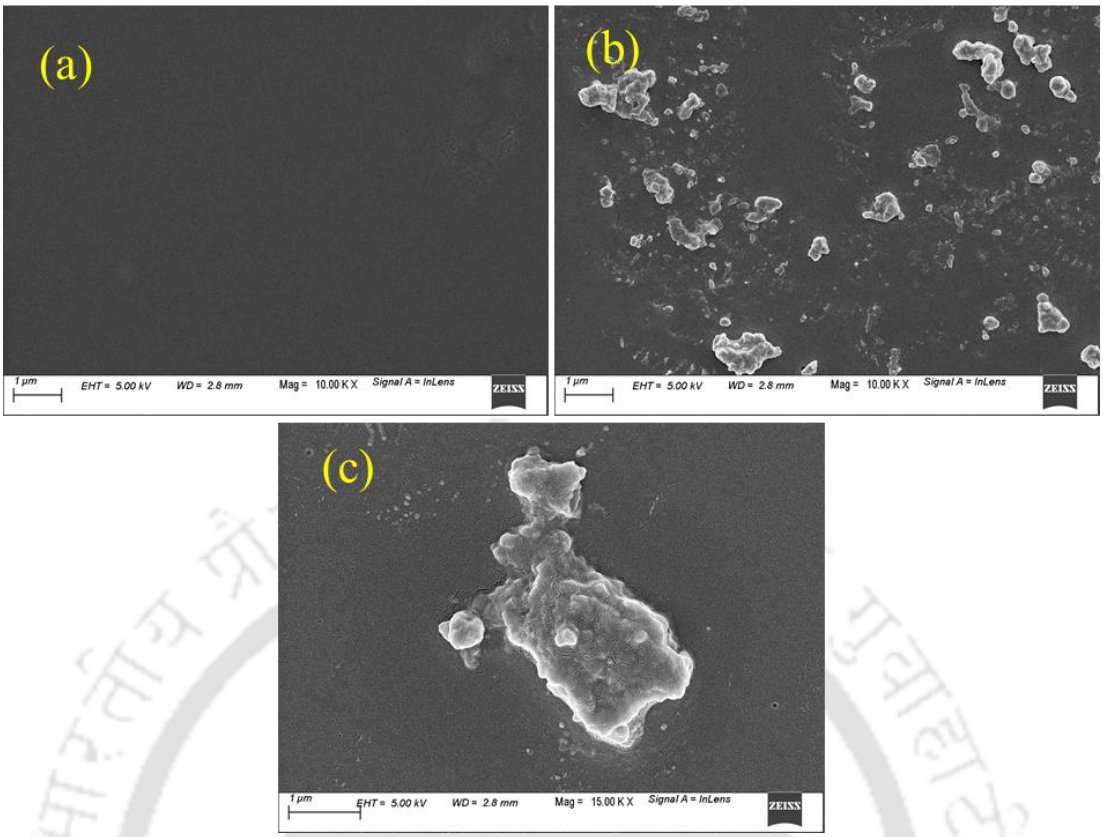

Figure 7.10 FESEM images of (a) SPEEK and (b-c) SPEEK/UiO-Pd-GO

7.3.2.2 XPS analysis

Further, XPS analysis was performed to determine the inducement effect of UiO-66/Pd-GO composite in SPEEK membrane (**Fig. 7.11**). As discussed earlier, SPEEK membrane shows a peak around 168 eV due the presence of sulfur group from $–SO_3H$ groups [24] but in this case two new small humps arise at 184 eV and 334 ev, which correspond to Zr 3d and Pd 2d, respectively. The presence of Zr and Pd demonstrated that the UiO-66/Pd-GO composite was successfully doped into the SPEEK membrane.

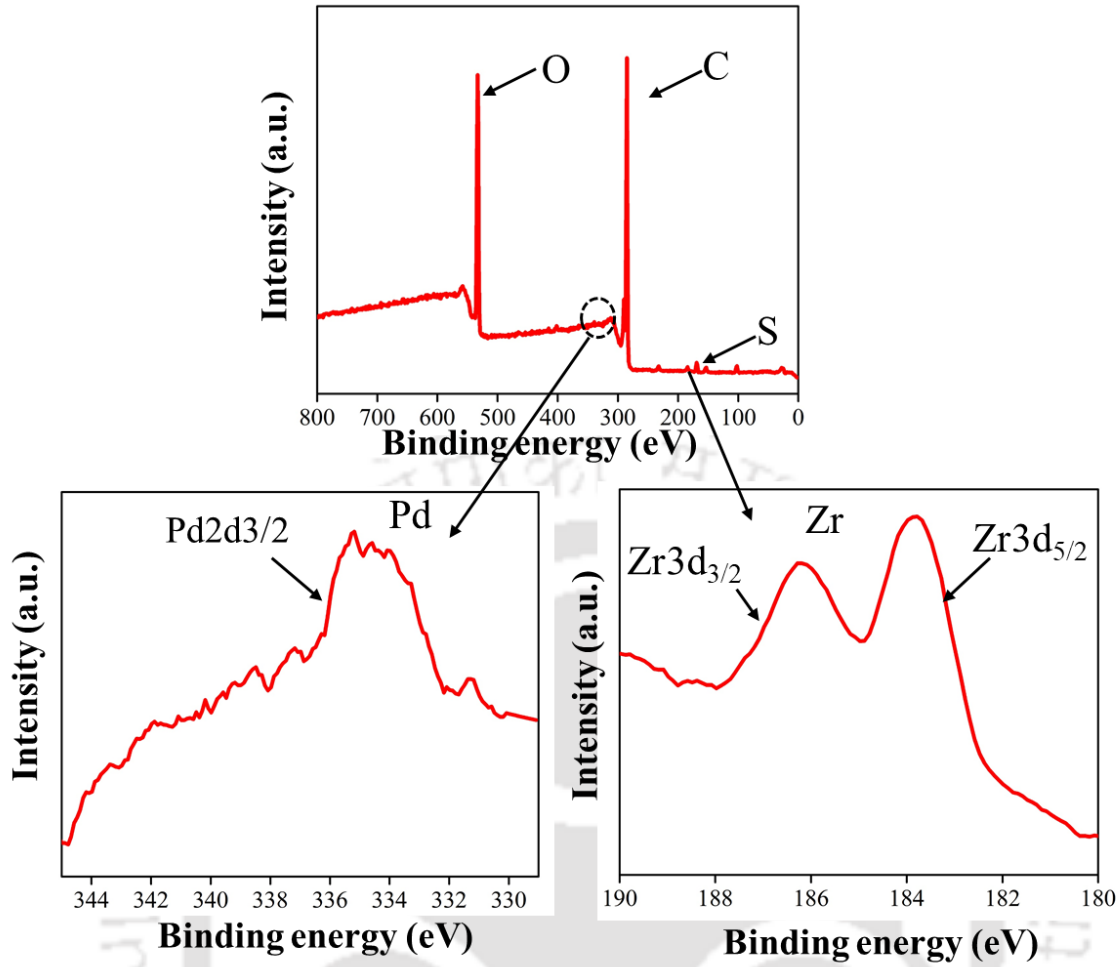

Figure 7.11 XPS analysis of SPEEK/UiO-66/Pd-GO membrane

7.3.2.3 TGA analysis

Fig. 7.12 represents the TGA plots of the SPEEK, SPEEK/UiO-66, SPEEK/UiO-66/GO and SPEEK/UiO-66/Pd-GO membranes. The thermal stability of the membranes is an important parameter for SPEEK/UiO-66/Pd-GO membranes. It is important for estimating the viability of the membrane for DMFC application. All the samples showed almost similar trend in the thermal degradation plots. The evaporation of water absorbed by hydrophilic UiO-66/Pd-GO fillers and SO3H groups present in the membrane leads to initial weight loss till 100 °C. [25]. Desulfonation of SPEEK also contributes to weight loss in this regime. The decomposition of sulfonic acid group in the temperature

up to 380°C is improved in the composite membrane compared to pure SPEEK. This might be due to the interaction between the hydroxyl groups of the UiO-66/Pd-GO composite and sulfonic acid groups on the polymeric membrane surface, which results in enhancement of the thermal resistance of the membrane. This is followed by a final stage decomposition (>450 °C) where degradation of the polymeric backbone occurs [26,27]. The composite membrane shows an improved stability. Moreover, the residual mass of the composite membrane was found to be greater than pure SPEEK membrane, indicating their improved stability.

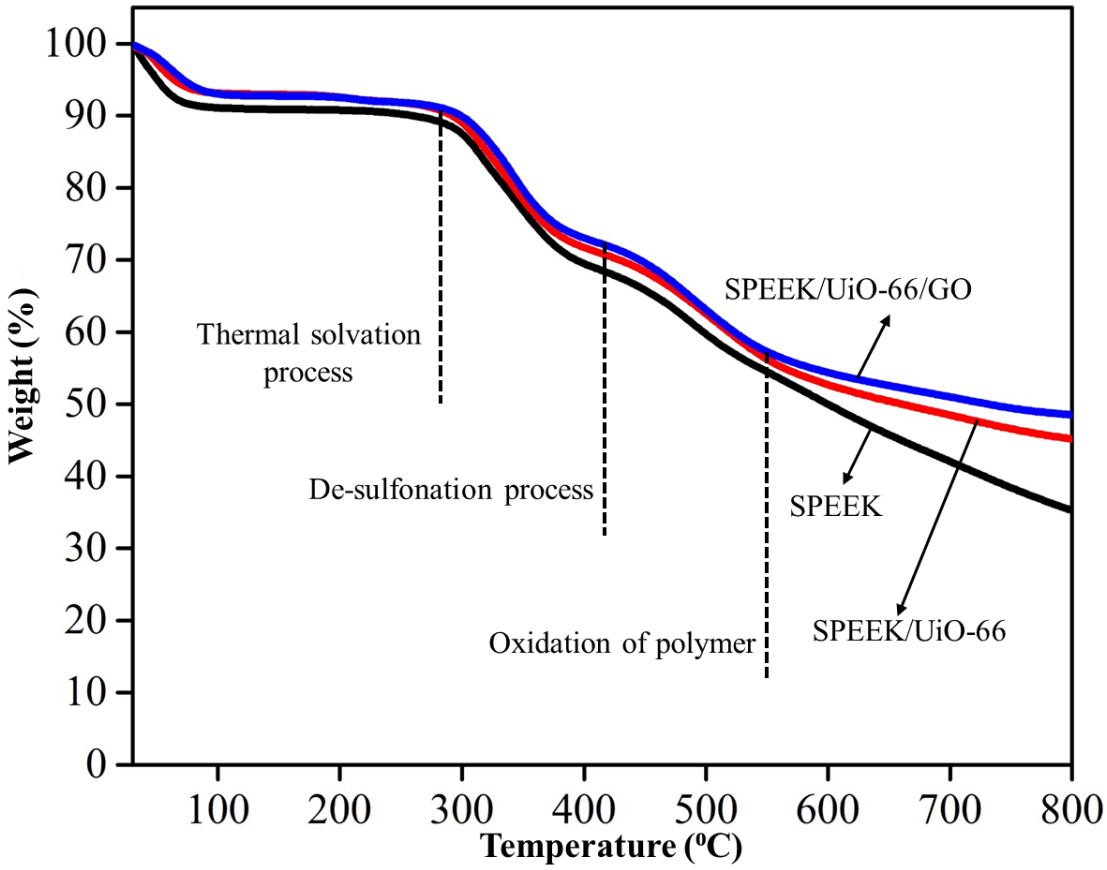

Figure 7.12 TGA analysis of SPEEK, SPEEK/UiO-66, SPEEK/UiO-66/GO, SPEEK/UiO-66/GO composites membrane.

7.3.2.4 Water uptake and IEC measurement

The proton conductivity and mechanical stability of membranes largely depends on the water uptake and ion exchange capacity. The relationship between the IEC and the water uptake of pristine SPEEK membranes and the modified nanocomposite SPEEK membranes infused with UiO-66-Pd-GO is shown in **Fig. 7.13**. The water uptake and IEC was found to increase with an increase in the UiO-66-GO content but after adding Pd NPs from 5 wt% to 10 wt% these values significantly decreased. This phenomenon is happening probably because the Pd composite has the most compact structure with less swelling effect as compared to UiO-66/GO. On other hand, it also probably has a strong interaction with the functional groups from UiO-66 and GO as well as with the sulfonic group from SPEEK membrane which reduces the free void spaces in the membrane [2]. The affinity of the membranes towards moisture is affected by the nature of the Pd NPs, which explains the obtained trends.

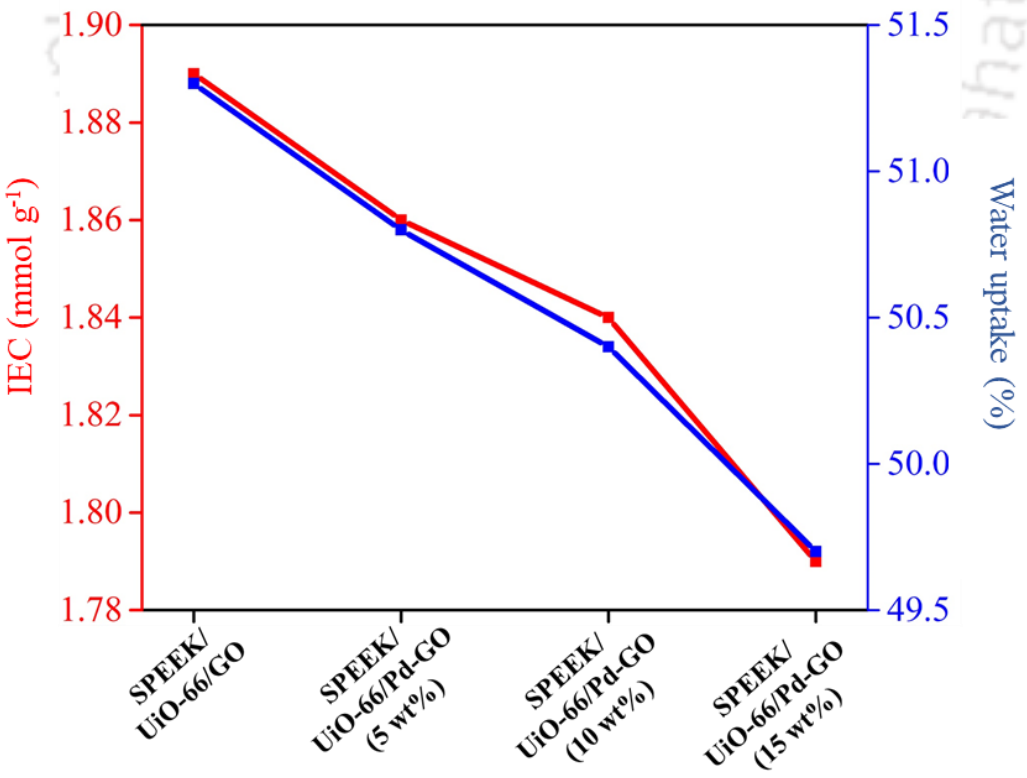

Figure 7.13 IEC and water uptake capacity of fabricated membranes

7.3.2.5 Methanol permeability, conductivity and selectivity measurement

The measurement of methanol permeability along with the selectivity of SPEEK/UiO-66/GO and SPEEK/UiO-66/Pd-GO composite membranes are summarized in **Fig. 7.14**. In Chapter 6, SPEEK/UiO-66(3%)/ GO (2.5%) membrane showed methanol permeability 4.94×10^{-7} cm^2 S^{-1} which gradually decreased with the increasing percentage of Pd NPS 3.75×10^{-7} cm^2 S^{-1} to 3.58×10^{-7} cm^2 S^{-1}. The proton conductivity of the SPEEK/UiO-66(3%)/ GO (2.5%) membranes was about 1.88 mS/cm and after adding Pd NPs into the composites, it increased to 2.11 mS/cm. This clearly demonstrates the effectiveness of the self-assembled Pd nanoparticles in the blocking of the methanol crossover. The drastic reduction in the methanol permeability demonstrates the effective blocking of the sites for the methanol crossover through the self-assembly of the Pd nanoparticles at the SPEEK membrane surface.

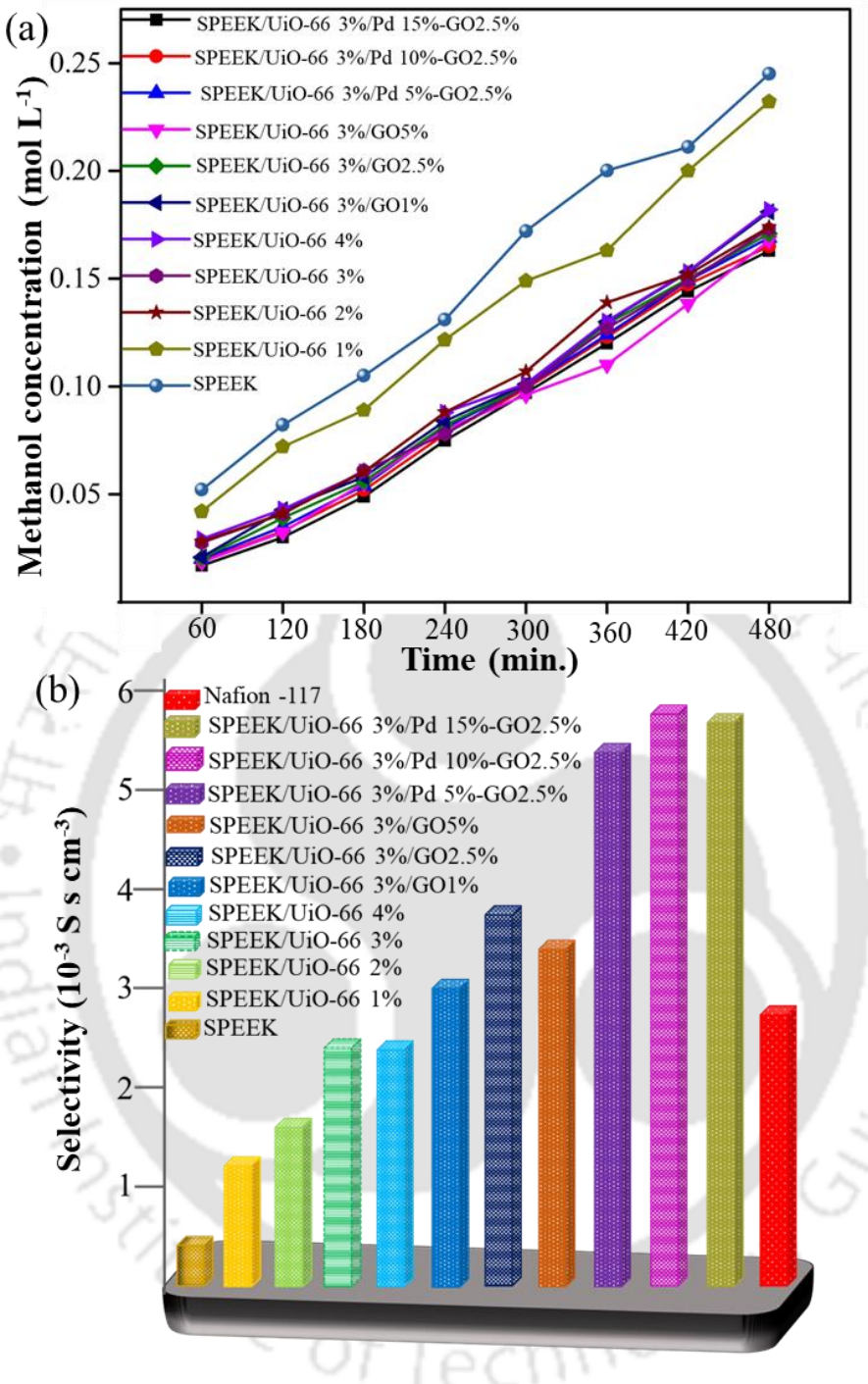

Figure 7.14 (a) Methanol permeability and (b) selectivity of SPEEK/UiO-66/GO and of SPEEK/UiO-66/Pd-GO composites membranes

The use of this strategy proved to be very promising, and Pd NPs with 10 wt% in GO shows selectivity up to 5.85 $\times 10^{-3}$ S s cm^{-3} where the pure SPEEK has a selectivity of 0.47 $\times 10^{-3}$ S s cm^{-3}. Pd is well known to be an effective medium for hydrogen passage and can easily form palladium hydride, and therefore widely used in the methanol-

blocking PEM for its potential function of proton conduction. The specific advantage of the positively charged nanoparticles is that they could be anchored to the sulfonic acid function group, $–SO_3$, on the membrane surface. Especially, the Pd particles of 1.8 nm are smaller than SO_3cluster (about 4 nm) but larger than SO_3cluster-bridge channels (about 1nm) [28,29]. This makes these particles anchor to SO_3 clusters without entering into the SPEEK membrane (**Fig. 7.15**). On other hand, the electrostatic interaction between the positively charged Pd nanoparticles and the negatively charged SO_3H groups results in attachment of Pd nanoparticles on the SPEEK membrane surface. This restricts the methanol permeation sites in Pd doped composite in SPEEK membrane. However, smaller size of protons allows their unrestricted passage through the membrane. Thus the advantage of doping Pd NPs doped GO in UiO-66 for modifying SPEEK membrane is reduction of methanol permeability without affecting the high proton conductivity of the membranes. The hydrophilicity/hydrophobicity and water uptake of the SPEEK membrane, which are the key criteria for high proton conductivity, remain unchanged. However, further research regarding the mechanism of reduction of methanol crossover and enhanced performance of SPEEK/ UiO-66/Pd-GO membrane for application in direct methanol fuel cells needs to be performed.

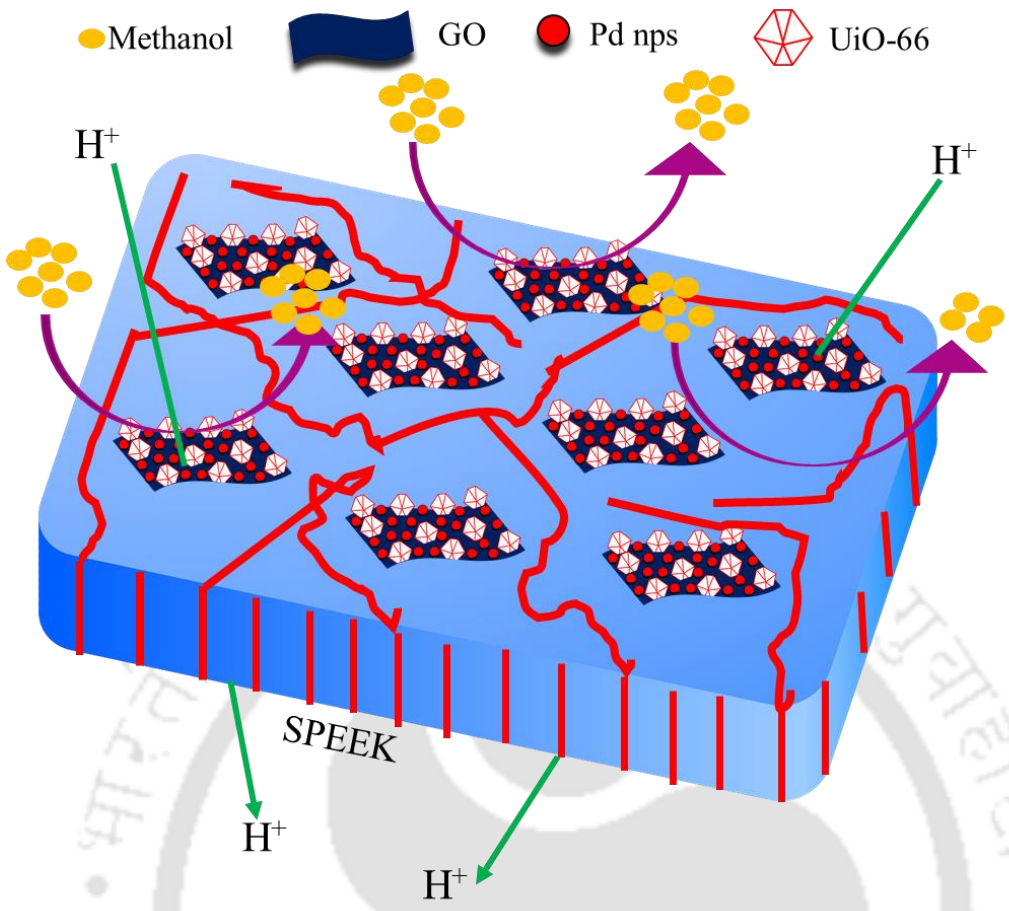

Figure 7.15 Proposed proton and methanol transport mechanism in SPEEK/ UiO-66/Pd-GO membrane.

7.4. Conclusions

Composite membranes of varying composition were fabricated to minimize the methanol permeability without affecting the proton conductivity of the membranes, for making them suitable for DMFC applications. Analysis of the membrane morphology indicated formation of a uniform, defect-free membrane with homogeneous distribution of the composites on the SPEEK membrane matrix. Increasing Pd content above 10 wt% resulted in reduction in methanol crossover as well as proton conductivity. Thus the composite consisting of 10 wt% Pd was considered as the optimized concentration which results in desirable methanol crossover and proton conductivity. The selectivity of the aforementioned membrane was found to be 5.86×10^3 S cm^{-3} s which is almost double

compared to benchmark Nafion- 117 (refer to section 6.4). This concludes that the fabricated membrane can be used as potential candidate for DMFC application. However, the fabricated membrane showed lower conductivity than the Nafion-117. Hence, the further study was undertaken to improve the proton conductivity of the membrane.

References

1. T. Fujigaya, C. Kim, K. Matsumoto, N. Nakashima, Palladium-based anion-exchange membrane fuel cell using KOH-doped polybenzimidazole as the electrolyte, ChemPlusChem 79(3) (2014) 400-405.
2. H. Thiam, W. Daud, S. Kamarudin, A. Mohamad, A. Kadhum, K. Loh, E. Majlan, Nafion/Pd–SiO2 nanofiber composite membranes for direct methanol fuel cell applications, International Journal of Hydrogen Energy 38(22) (2013) 9474-9483.
3. L. Brandão, J. Rodrigues, L. Madeira, A. Mendes, Methanol crossover reduction by Nafion modification with palladium composite nanoparticles: application to direct methanol fuel cells, International Journal of Hydrogen Energy 35(20) (2010) 11561-11567.
4. C. Xu, X. Wang, J. Zhu, Graphene metal particle nanocomposites, The Journal of Physical Chemistry C 112(50) (2008) 19841-19845.
5. S. Hemmati, L. Mehrazin, M. Pirhayati, H. Veisi, Immobilization of palladium nanoparticles on Metformin-functionalized graphene oxide as a heterogeneous and recyclable nanocatalyst for Suzuki coupling reactions and reduction of 4-nitrophenol, Polyhedron 158 (2019) 414-422.
6. B. Kılıç, S. Şencanlı, Ö. Metin, Hydrolytic dehydrogenation of ammonia borane catalyzed by reduced graphene oxide supported monodisperse palladium nanoparticles: high activity and detailed reaction kinetics, Journal of Molecular Catalysis A: Chemical 361 (2012) 104-110.
7. Z. Xu, L. Yang, C. Xu, Pt@ UiO-66 heterostructures for highly selective detection of hydrogen peroxide with an extended linear range, Analytical Chemistry 87(6) (2015) 3438-3444.

8. F. Ban, S. Majid, N. Huang, H. Lim, Graphene oxide and its electrochemical performance, Int. J. Electrochem. Sci 7(5) (2012) 4345-4351.
9. P. Das, B. Mandal, S. Gumma, Engineering of structural and surface functional characteristics of graphite oxide nanosheets by controlling oxidation temperature, Applied Surface Science 504 (2020) 144444.
10. J. Liu, H. Zhou, Q. Wang, F. Zeng, Y. Kuang, Reduced graphene oxide supported palladium–silver bimetallic nanoparticles for ethanol electro-oxidation in alkaline media, Journal of Materials Science 47(5) (2012) 2188-2194.
11. S. Yang, C. Shen, Y. Tian, X. Zhang, H.-J. Gao, Synthesis of cubic and spherical Pd nanoparticles on graphene and their electrocatalytic performance in the oxidation of formic acid, Nanoscale 6(21) (2014) 13154-13162.
12. A. Viswadevarayalu, P.V. Ramana, J. Sumalatha, S.A. Reddy, Biocompatible synthesis of palladium nanoparticles and their impact on fungal species, Journal of Nanoscience and Technology (2016) 169-172.
13. A. Omidvar, M. RashidianVaziri, B. Jaleh, N.P. Shabestari, M. Noroozi, Metal-enhanced fluorescence of graphene oxide by palladium nanoparticles in the blue–green part of the spectrum, Chinese Physics B 25(11) (2016) 118102.
14. A.M. Ebrahim, T.J. Bandosz, Ce (III) doped Zr-based MOFs as excellent NO_2 adsorbents at ambient conditions, ACS Applied Materials & Interfaces 5(21) (2013) 10565-10573.
15. A.M. Ebrahim, B. Levasseur, T.J. Bandosz, Interactions of NO_2 with Zr-based MOF: effects of the size of organic linkers on NO_2 adsorption at ambient conditions, Langmuir 29(1) (2013) 168-174.
16. X. Liu, X. Zhao, M. Zhou, Y. Cao, H. Wu, J. Zhu, Highly stable and active palladium nanoparticles supported on a mesoporous UiO66@ reduced graphene oxide complex

for practical catalytic applications, European Journal of Inorganic Chemistry 2016(20) (2016) 3338-3343.

17. Li, B.; Wu, W.; Zhang, T.; Jiang, S.; Chen, X.; Zhang, G.; Zhang, X. Ferrocene Particles Incorporated into Zr-Based Metal–Organic Frameworks for Selective Phenol Hydroxylation to Dihydroxybenzenes. RSC Adv.2017, 7, 38691.
18. Y. Luan, Y. Qi, H. Gao, N. Zheng, G. Wang, Synthesis of an amino-functionalized metal–organic framework at a nanoscale level for gold nanoparticle deposition and catalysis, Journal of Materials Chemistry A 2(48) (2014) 20588-20596.
19. S. Yang, J. Dong, Z. Yao, C. Shen, X. Shi, Y. Tian, S. Lin, X. Zhang, One-pot synthesis of graphene-supported monodisperse Pd nanoparticles as catalyst for formic acid electro-oxidation, Scientific Reports 4 (2014) 4501.
20. M.S. Denny Jr, L.R. Parent, J.P. Patterson, S.K. Meena, H. Pham, P. Abellan, Q.M. Ramasse, F. Paesani, N.C. Gianneschi, S.M. Cohen, Transmission electron microscopy reveals deposition of metal oxide coatings onto metal–organic frameworks, Journal of the American Chemical Society 140(4) (2018) 1348-1357.
21. H. Wu, B. Tang, P. Wu, Development of novel SiO2–GO nanohybrid/polysulfone membrane with enhanced performance, Journal of Membrane Science 451 (2014) 94-102.
22. J. Wang, Y. Wang, Y. Zhang, A. Uliana, J. Zhu, J. Liu, B. Van der Bruggen, Zeolitic imidazolate framework/graphene oxide hybrid nanosheets functionalized thin film nanocomposite membrane for enhanced antimicrobial performance, ACS applied Materials & Interfaces 8(38) (2016) 25508-25519.
23. H. Sun, B. Tang, P. Wu, Rational design of S-UiO-66@ GO hybrid nanosheets for proton exchange membranes with significantly enhanced transport performance, ACS Applied Materials & Interfaces 9(31) (2017) 26077-26087.

24. Y. Quan, G. Wang, A. Li, X. Wei, F. Li, J. Zhang, J. Chen, R. Wang, Novel sulfonated poly (ether ether ketone)/triphenylamine hybrid membrane for vanadium redox flow battery applications, RSC Advances 9(7) (2019) 3838-3846.
25. D. Aili, M.K. Hansen, C. Pan, Q. Li, E. Christensen, J.O. Jensen, N.J. Bjerrum, Phosphoric acid doped membranes based on Nafion®, PBI and their blends–Membrane preparation, characterization and steam electrolysis testing, International Journal of Hydrogen Energy 36(12) (2011) 6985-6993.
26. L. Lou, H. Pu, Preparation and properties of proton exchange membranes based-on Nafion® and phosphonic acid-functionalized hollow silica spheres, International Journal of Hydrogen Energy 36(4) (2011) 3123-3130.
27. Z. Zhang, F. Désilets, V. Felice, B. Mecheri, S. Licoccia, A.C. Tavares, On the proton conductivity of Nafion–Faujasite composite membranes for low temperature direct methanol fuel cells, Journal of Power Sources 196(22) (2011) 9176-9187.
28. B. Smitha, S. Sridhar, A. Khan, Solid polymer electrolyte membranes for fuel cell applications—a review, Journal of Membrane Science 259(1-2) (2005) 10-26.
29. K.A. Mauritz, R.B. Moore, State of understanding of Nafion, Chemical Reviews 104(10) (2004) 4535-4586.

CHAPTER 8

Amino acid grafted palladium decorated graphite oxide based composite membrane

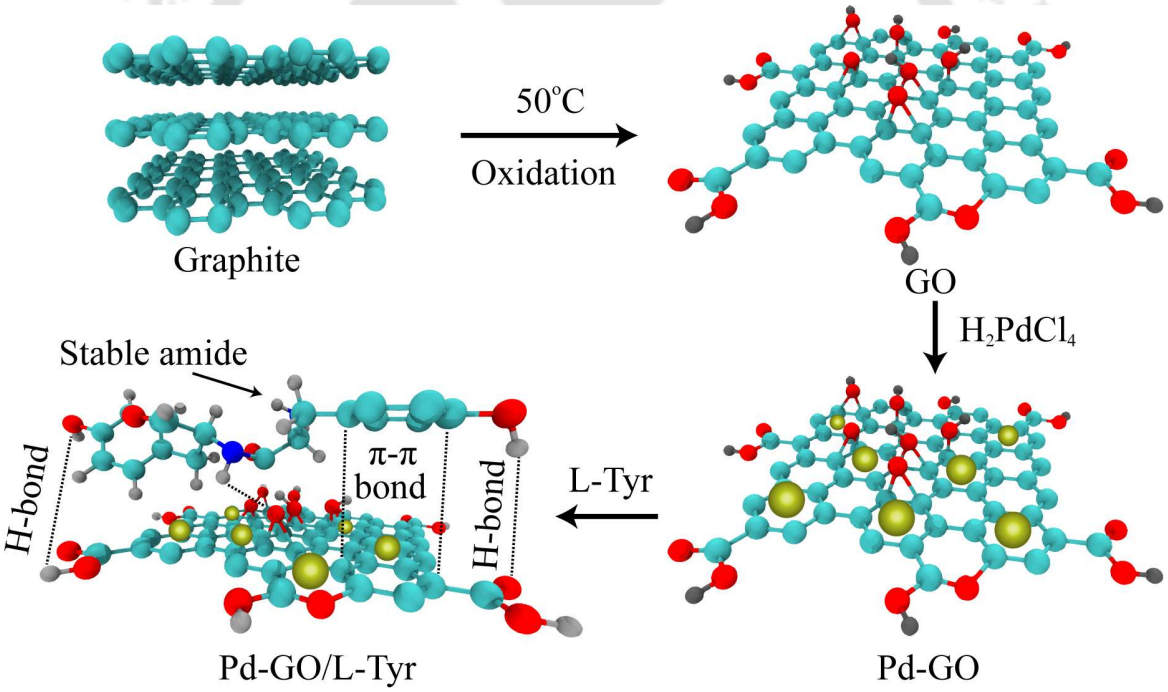

Graphical abstract of Probable mechanism for intercalation of L-Tyr and Pd decorated GO

CHAPTER 8

Amino acid grafted palladium decorated graphite oxide based composite membrane

This chapter encompasses preparation of amino acid functionalized palladium grafted graphite oxide based nanocomposite membranes and determination of their selectivity as a proton exchange membrane. Membrane synthesis involved homogenous, uniform dispersion of L-Tyrosine (L Tyr) functionalized palladium (Pd) grafted graphite oxide (Pd-GO-L Tyr). The physicochemical properties of the SPEEK/Pd-GO-L Tyr membranes were analyzed in terms of their ion exchange capacity (IEC), water uptake, methanol permeability, proton conductivity.

8.1 Introduction

An amino acid is a type of the organic molecule with amino and carboxyl groups [1]. It has been demonstrated that these groups facilitate transport of protons [2]; after losing a proton the carboxyl group forms a carboxylate ion, while the amino group is protonated to an ammonium ion (**Fig. 8.1**). The intramolecular proton exchange mediates zwitterion formation in amino acids; thus, they act both as a proton donor and a proton acceptor simultaneously facilitating proton transport [2]. To leverage this property of amino acids, L-Tyrosine (L-Tyr) was chosen for the present study due to the presence of aromatic hydroxyl group [3,4]. We hypothesize that the lower energy barrier in this system with aromatic hydroxyl group [4] might be favourable for proton transport.

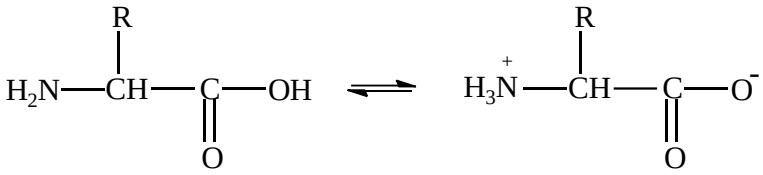

Figure 8.1 Dipolar nature of amino acid

In this work, we report the synthesis and performance of amino acid (L-Tyr) grafted palladium graphite oxide and SPEEK composite membranes for DMFC applications. As discussed earlier, SPEEK was chosen as the base polymer for fabrication of the hydrophilic membrane due to its superior properties for DFMC application. We chose to introduce palladium nanoparticles on the surface of graphite oxide sheets. Pd was chosen due to its catalytic activity and stability towards methanol oxidation. The smaller nanoparticles of Pd allow for better dispersion in the GO matrix. The Pd-GO was then functionalized using L-Tyrosine amino acid. Subsequently composite of this modified Pd-GO with SPEEK was used to make the final membrane. We hypothesized that the Pd-GO particles might act as an obstruction and block the methanol from freely migrating through the membrane, thereby reducing methanol crossover; on the other hand addition of L-Tyr would enhance its proton conductivity. The results indicate that selectivity of these composite membranes is better than that of Nafion. This work provides a potential approach for synthesis of high performance DFMC membranes.

8.2. Experimental

8.2.1 Materials and chemicals

For this study all materials were purchased from commercial sources. For synthesis of graphite oxide graphite powder (Sigma-Aldrich), analytical grade sulphuric acid (H_2SO_4,

98 wt% Merck), orthophosphoric acid (H_3PO_4, 88 wt% Merck), hydrochloric acid (HCl, 37 wt%, Merck), hydrogen peroxide (H_2O_2, 30 wt%, Merck), potassium permanganate ($KMnO_4$, Merck), ethyl glycol (Merck) were used. N-hydroxysuccinimide (NHS) was purchased from Alfa Aesar. L-Tyrosine and 1-ethyl-3-(3-dimethylaminopropyl) carbodiimide (EDC), dimethyl sulfoxide (DMSO), dimethylacetamide (DMAc) and palladium chloride ($PdCl_2$) were obtained from Spectrochem Private Limited. Poly(ether ether ketone) (PEEK) was supplied by Polyscience Lab. All chemicals were used as obtained with no additional purification. Milipore® water was used throughout.

8.2.2 Synthesis of palladium grafted graphite oxide (Pd-GO)

Palladium decorated GO has been synthesized by polyol process (glycol reduction method) as discussed earlier in chapter 8. 10wt% palladium was chosen in this section for further modification (**Fig. 8.2a**).

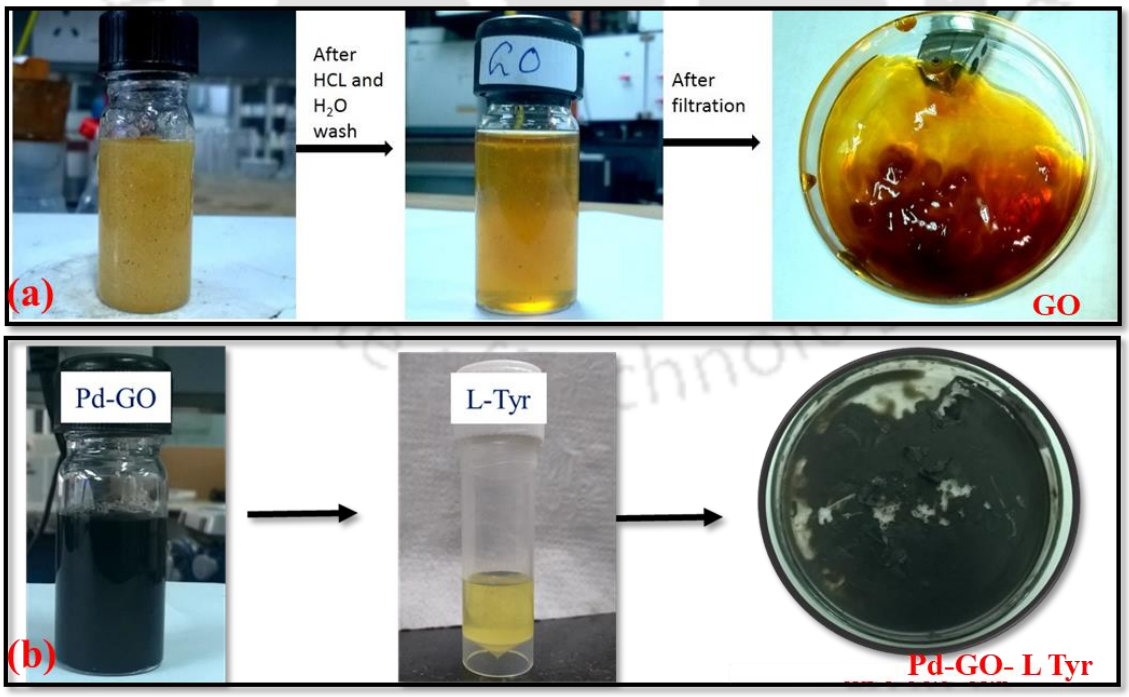

Figure 8.2 Synthesized GO, Pd-GO and Pd-GO-Ltyr

8.2.3 Synthesis of L-tyrosine conjugated palladium grafted graphite oxide (Pd-GO-Tyr)

L-Tyr (0.750 g), EDC (0.867 g, 1.1 eq.) and NHS (0.522g, 1.1 eq.) were dissolved in DMSO (5 mL) and allowed to react for 1 h by mechanical stirring to activate the carboxyl group of L-tyrosine [5]. Then the mixture was added into the aqueous solution of Pd-GO (0.717 g) and was allowed to react for 12 h at room temperature. Final product was collected via centrifugation (**Fig. 8.2b**).

8.2.4 Fabrication of composite membrane

To prepare the membrane, 1g of SPEEK was dissolved in 9g of dimethylacetamide (DMAc) in order to make a 10wt % solution. Fabrication procedure of membrane is the same as discussed in Chapter 5. For preparation of the composite membrane, 1 wt% (based on the mass of the PEEK) of the composites (GO, Pd-GO and Pd-GO-Tyr) were added and the composite membrane fabrication procedure is the same as discussed earlier.

8.2.5 Characterization

In this section X-ray diffractometer, field emission scanning electron microscope, X-ray photo electron spectroscopy, Fourier transform infrared spectra, Thermogravimetric analysis, Transmission Electron Microscope , BET surface area analyzer has been used for characterization of fabricated membrane and the weight differences between the full-hydrated membranes and the dried membranes along with their water uptake, methanol permeability and proton conductivity of the membranes (refer to Chapter 3).

8.3 Results and Discussion

The activation of L-Tyr occurs when the EDC reacts with the carboxylic group and forms an unstable reactive ester (**Fig. 8.3**). EDC is a zero-length crosslinking agent which is used for activation of carboxylic acid groups in presence of NHS [6], wherein the reactive ester converts into semi-stable amine intermediate which may react with an amine on L-Tyr and adjoining molecules via a stable amide bond [7].

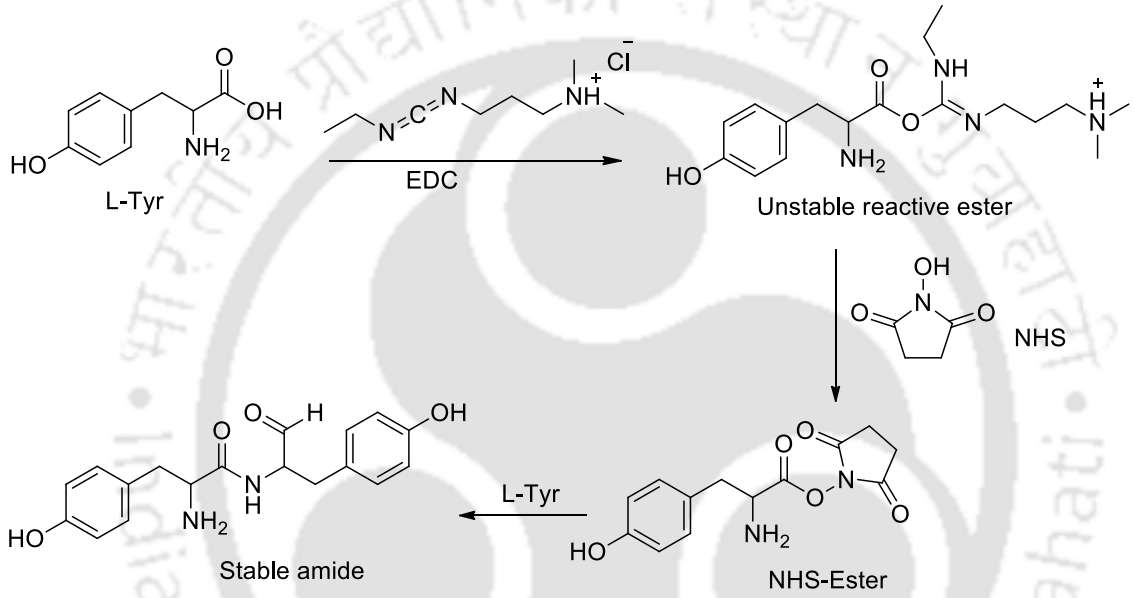

Figure 8.3 Probable reactions for activation of L-Tyrosine

The formation of graphite oxide from graphite occurs due to the introduction of oxygen containing functional group into the carbon lattice [8]. The formation of hydroxyl, carboxyl, carbonyl and epoxy groups in GO helps to increase the interlayer spacing and makes it hydrophilic (**Fig. 8.4b**). The Pd nanoparticles were found to be well-dispersed on the surface of GO (**Fig. 8.4c**).

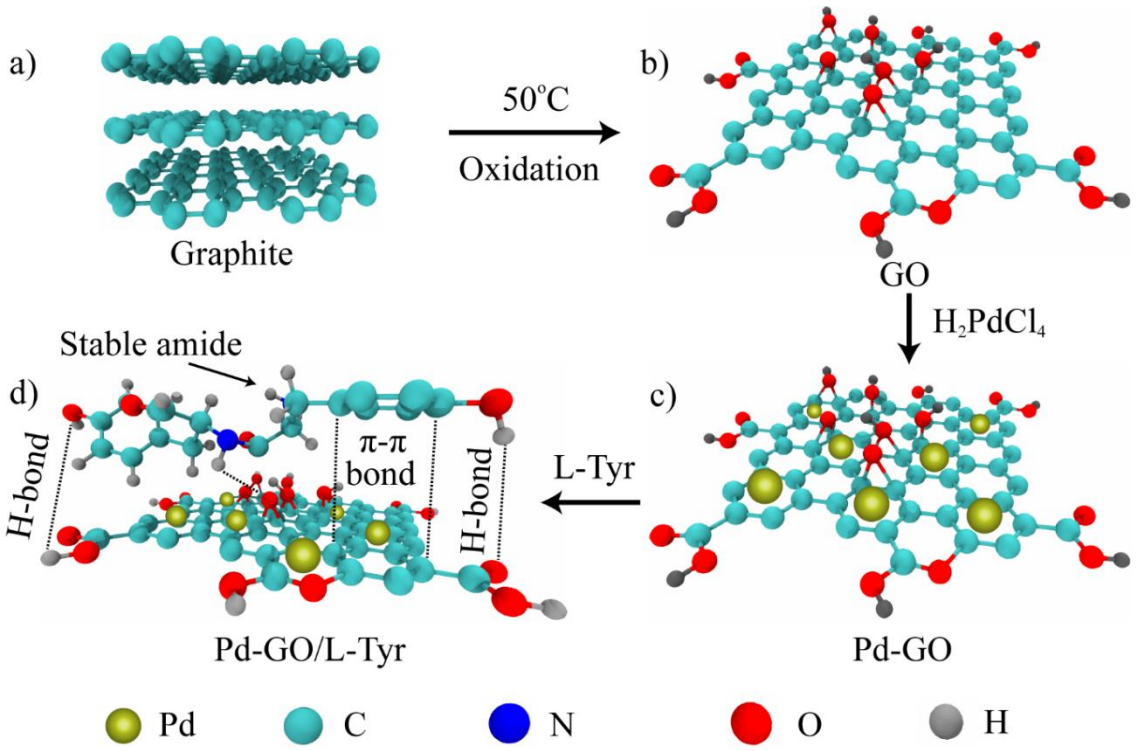

Figure 8.4 Probable mechanism for intercalation of L-Tyr and Pd decorated GO

After adding Pd-GO solution to the activated L-Tyr, it interacts with the oxygen-containing functional groups of GO via hydrogen bonding to form Pd-GO-L-Tyr composite (**Fig. 8.4d**). The formation of this composite primarily occurs via intercalated L-Tyr into the interlayer zone of GO [9]. According to the atomic orbital-molecular orbital approach, π-π stacking interaction occurs between the aromatic rings of L-Tyr and GO where they orient parallel to each other resulting in high binding energy [10].

8.3.1 FETEM analysis

The transmission electron microscopy (TEM) analysis of the nanocomposites is shown in **Fig. 5**. Thin graphene oxide sheets (**Fig. 5a**) are uniformly decorated with Pd nanoparticles in the Pd-GO composite (**Fig. 5b**). Modification of Pd nanoparticles of diameters 5-10 nm can be seen in the high resolution transmission electron microscopy (HRTEM) images (**Fig. 5c**). From HRTEM pattern, the lattice spacing of Pd

nanoparticles was calculated to be 0.227 nm which corresponds to (111) plane of the face centered cubic (fcc) crystal structure of Pd [11]. TEM

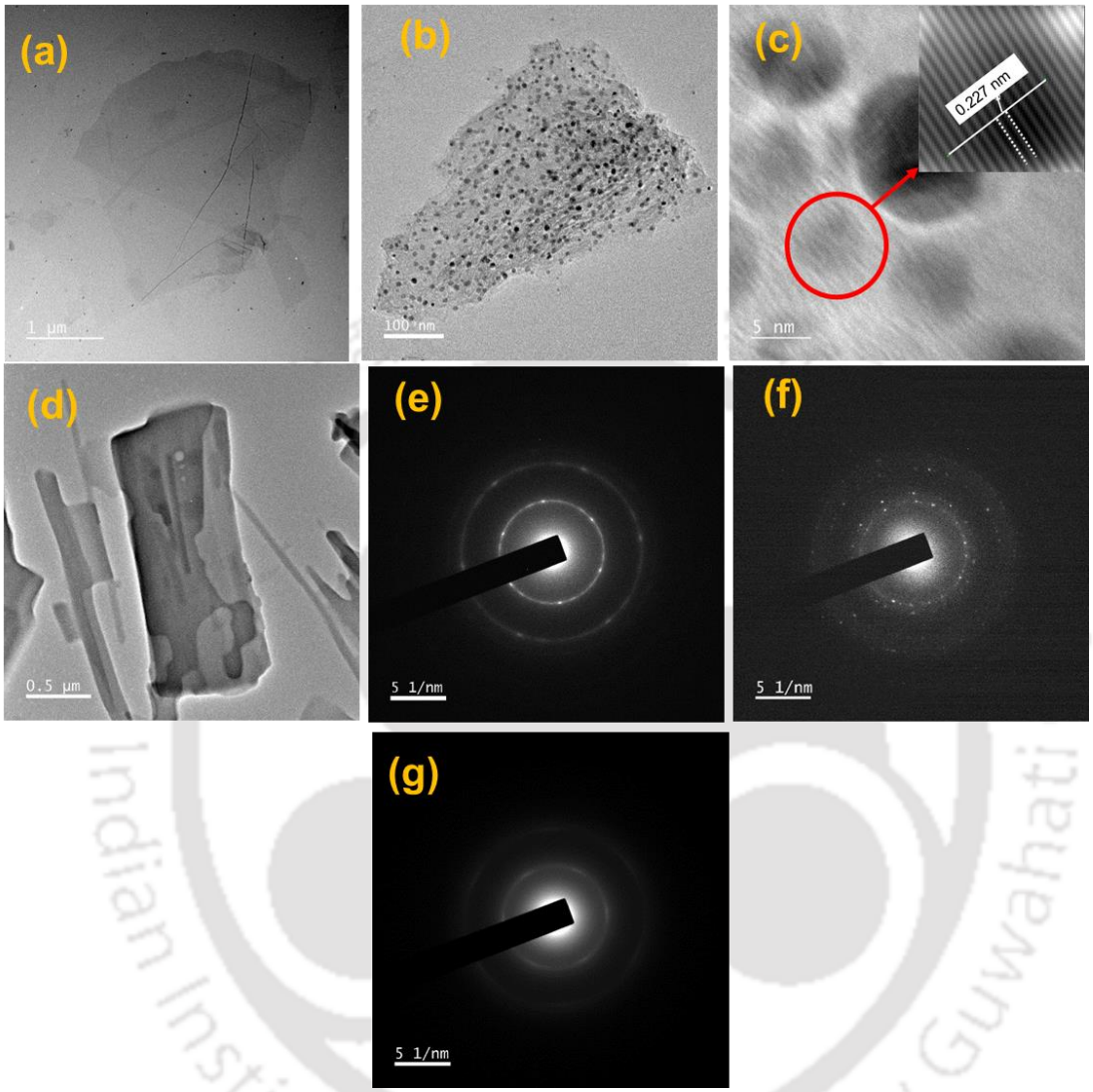

Figure 8.5 (a) – (d) TEM images for GO, Pd-GO, Pd-GO depicting lattice spacing and Pd-GO-L-Tyr respectively (e) – (g) SAED patterns for GO, Pd-GO and Pd-GO-L-Tyr

micrograph of L-Tyr functionalized palladium graphite sheet shows a scroll type nature as shown in **Fig. 8.5d**. This is possibly a result of parallel orientation of aromatic ring in amino acid with the benzene ring from the graphite surface [12]. Selected area electron diffraction (SAED) for GO and Pd-GO (**Fig. 8.5e and 8.5f**) indicates crystalline nature of these materials, although somewhat diffused patterns in Pd-GO indicates that it is more

amorphous compared to GO. In case of Pd-GO-L-Tyr, the two aforementioned interactions lead to reduction in crystalline nature (**Fig. 8.5g**).

8.3.2 EDS analysis

The energy dispersive X-ray spectroscopy (EDS) mapping (**Fig. 8.6**) confirms the presence of palladium, nitrogen, carbon and oxygen in Pd-GO-L-Tyr composite. In addition, all elements seem to be well distributed on the surface thus confirming functionalization of L-Tyr in Pd-GO.

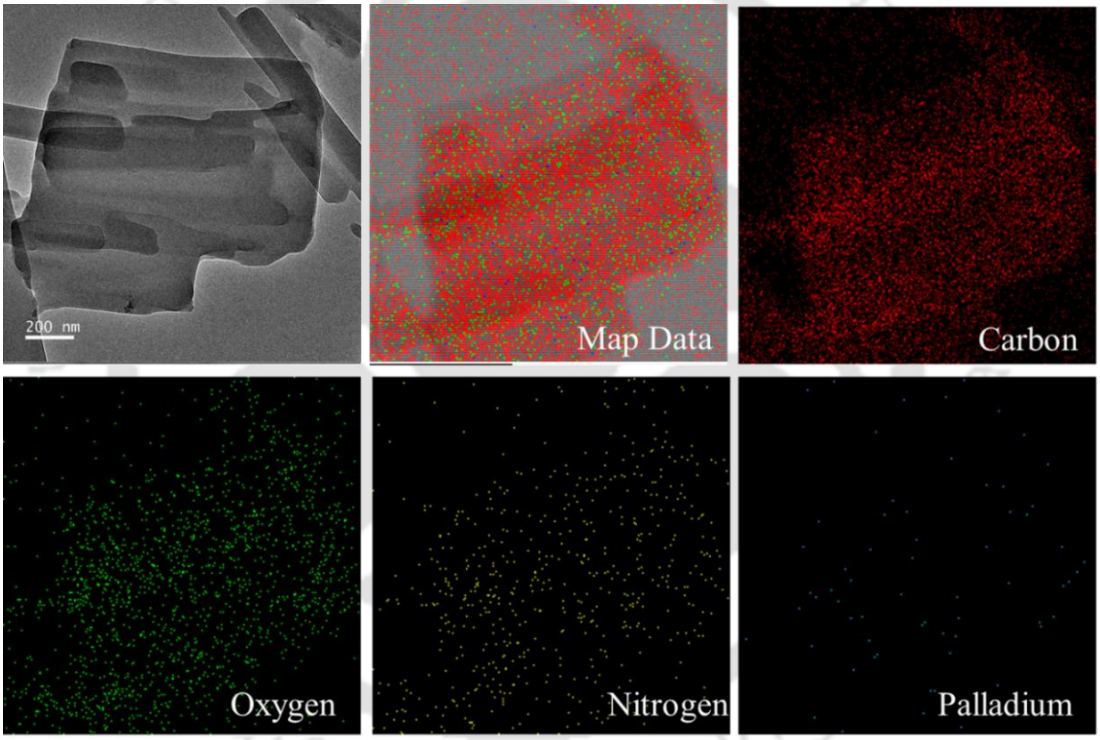

Figure 8.6 EDS mapping of Pd-GO-L-Tyr composite

8.3.3 XRD analysis

XRD image (**Fig. 8.7**) shows a distinct difference between the patterns of nascent GO, Pd-GO and amino acid functionalized GO. From XRD analysis, a typical peak for GO at a 2θ of 10° in (001) plane with a 8.33 Å spacing was observed. Graphite shows very sharp

peak at 26.5° with a d-spacing of 3.36 Å, which moves to lower Bragg's angle after formation of GO, due to the addition of oxygen functional groups to each layer [13]. A broad peak appears at a 22.5°, after the addition of Pd nanoparticles conforming the destruction of layered structure of GO [14]. Pd-GO shows a small hump at 38.2° which corresponds to (111) plane [14]. Doping of L-Tyr in Pd-GO results in shift of peak position to 24.4° with increasing interlayer distance. The π-π stacking between aromatic rings and H-bonding between oxygen of hydroxyl, carboxyl groups of GO and hydrogen of phenolic OH of amino acid, may lead to shift in layer-to-layer spacing and even restacking back to graphite. In case of SPEEK, SPEEK-GO, SPEEK-Pd-GO-L-Tyr, the broad peaks at 2θ values between 18° and 20° appear, indicating low crystallinity, due to the presence of $-SO_3H$ groups that prevent polymer chain packing [15]. For DMFC a low crystalline membrane is preferable, because low crystallinity preferred the local chain segment and high ionic conductivity [16]. It is also noteworthy that the peak position of composite membrane shifted from 18.28° to 19.94° indicating dilation in the structure, that may possibly increase its water retention and hence proton conductivity.

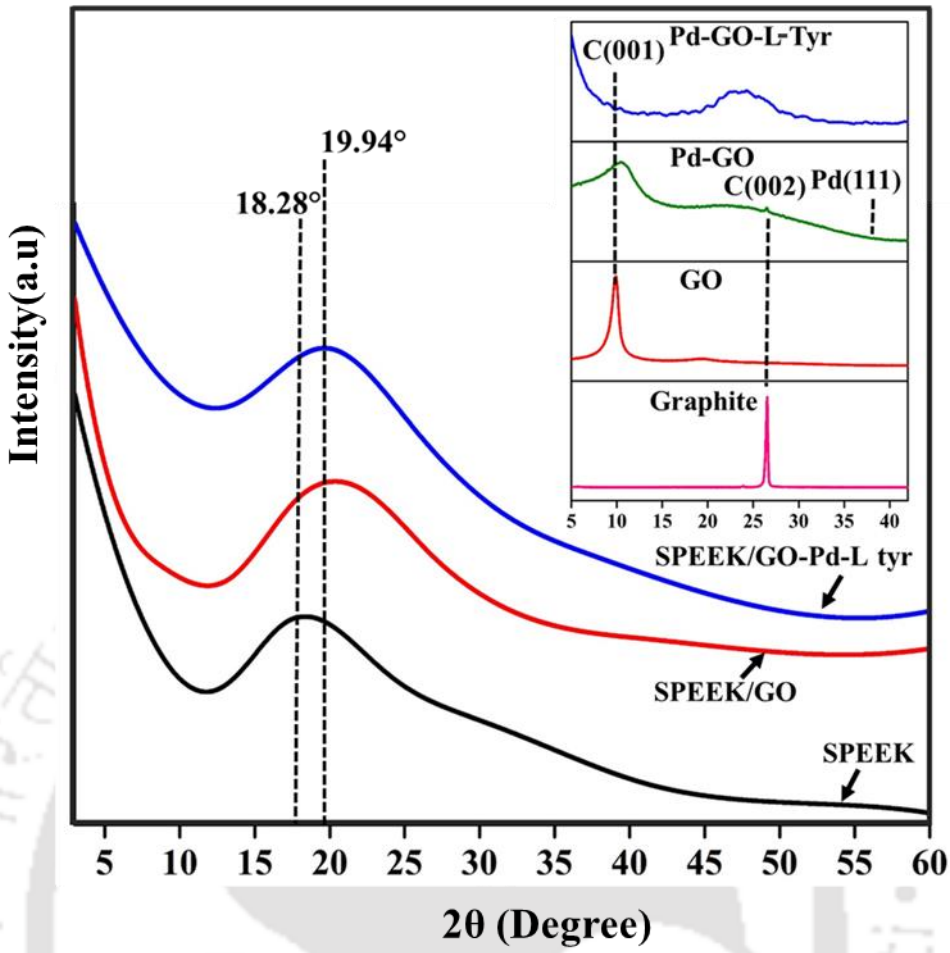

Figure 8.7 XRD patterns of Graphite, GO, Pd-GO, Pd-GO-L-Tyr, SPEEK, SPEEK/GO and SPEEK/Pd-GO-L-Tyr

8.3.4 FESEM analysis

Field emission scanning electron microscope (FESEM) images are shown in **Fig. 8.8**. GO has well defined porous network, with interlinked layers resembling a loose sponge like structure as shown in the cross-section (**Fig. 8.8a**). The texture of GO sheets shows wrinkled, fluffy morphology (**Fig. 8.8b**) [17]. Uniform and homogenous dispersion of Pd nanoparticles on GO surface results in enhancement of their active sites and hence the specific surface area [18]. Upon incorporation of amino acid L-Tyr the composite shows a cage-like arrangement (**Fig. 8.8c**) where the composites are entrapped by rod shaped L-Tyr.

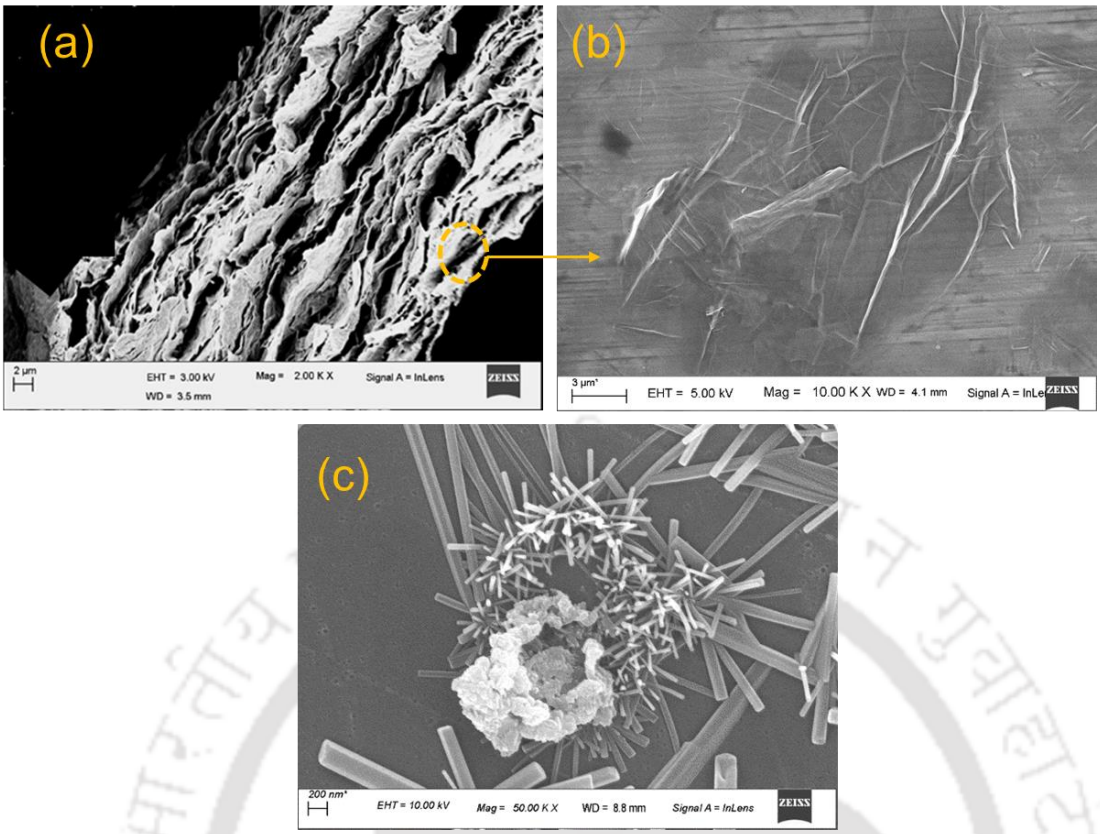

Figure 8.8 FESEM images of (a) cross section view of GO, (b) top surface view of and (c) Pd-GO-L-Tyr

8.3.5 AFM analysis

The dense and smooth surface of the pristine SPEEK membrane in **Fig. 8.9a** becomes comparatively rough due to the embedded GO-Pd-L-Tyr composite (**Fig. 8.9b**). The interfacial interactions between SPEEK and polar groups in GO composite leads to good compatibility, which makes a uniform distribution of the composite in SPEEK. The roughness was also confirmed by AFM analysis. The addition of Pd-GO-L-Tyr to the smooth SPEEK structure results in membrane roughness (**Fig. 8.9c** and **8.9d**), due to the formation of hydrophilic interconnected channels [19]. Presence of hydrophobic and hydrophilic domains in matrix is illustrated by dark (hydrophilic) and yellow (hydrophobic) regions. Due to enhanced membrane surface roughness, free volume and water accommodation increase, thereby allowing for enhanced passage of protons [20].

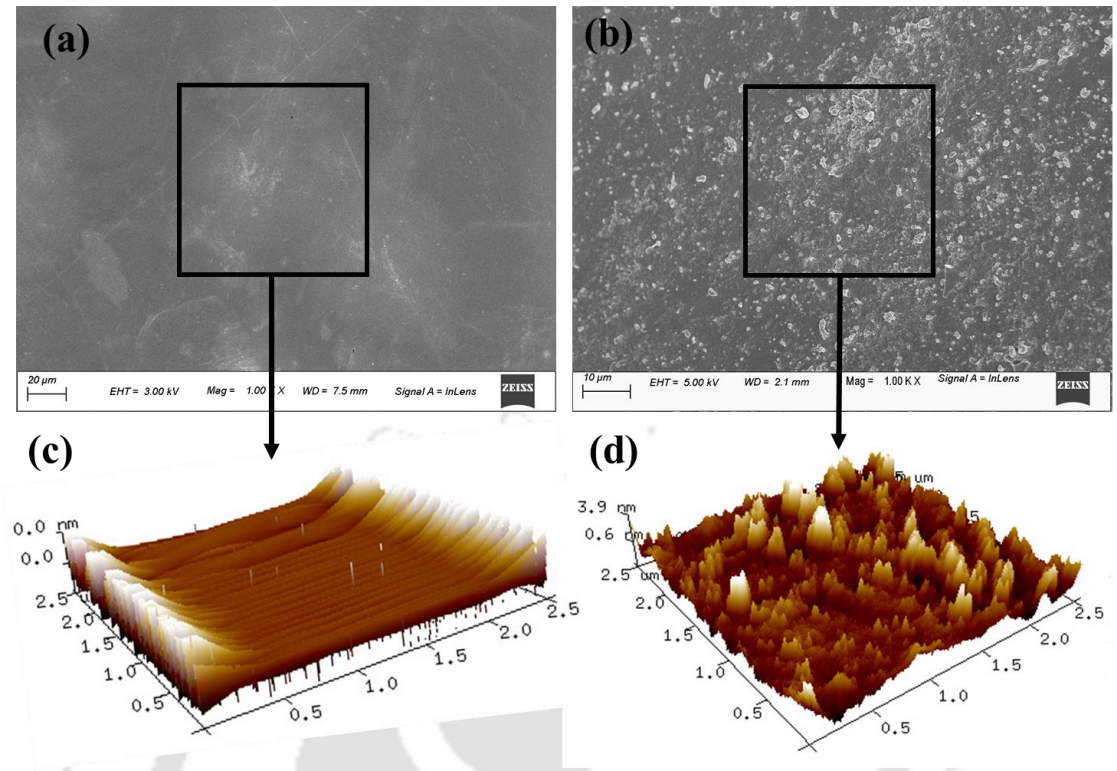

Figure 8.9 FESEM and AFM images of (a, c) SPEEK and (b, d) SPEEK/Pd-GO-L-Tyr membrane

8.3.6 TGA analysis

The thermal stability of graphite, GO, Pd-GO, Pd-GO-L-Tyr was examined by TGA analysis. Pure graphite shows a one step of weight loss (**Fig. 8.10a**). The weight loss below 140 °C is due to removal of adsorbed moisture and other volatiles from the stacked GO layers (**Fig. 8.10b**). In contrast, Pd-GO shows a good thermal stability up to 300 ºC. A gradual weight loss occurs in the range of 140 to 280 °C which can be attributed to deformation of CO and CO_2 from the oxygen functional groups of the composite Pd-GO-L-Tyr [21]. At 290 °C, weight loss of 46% occurs for GO which decreases to 27% in Pd-GO-L-Tyr because of partial re-stacking of GO sheets due to functionalization of Pd and amino acid. **Fig. 8.10e** and 8.**10f** show TGA analysis for pristine SPEEK and SPEEK/Pd-GO-L-Tyr composite membranes. The thermal degradation for both membranes occurs

in three stages and is almost similar, as the amount in Pd-GO-L-Tyr is only ~ 1wt%. The first weight loss step is the loss of absorbed moisture; the next step occurs between 290 and 380 °C due to desulfonation resulting in release of SO_2 and loss of amino acids; the last weight loss step is due to thermal degradation of aromatic polymeric framework between 480 to 600 °C [21].

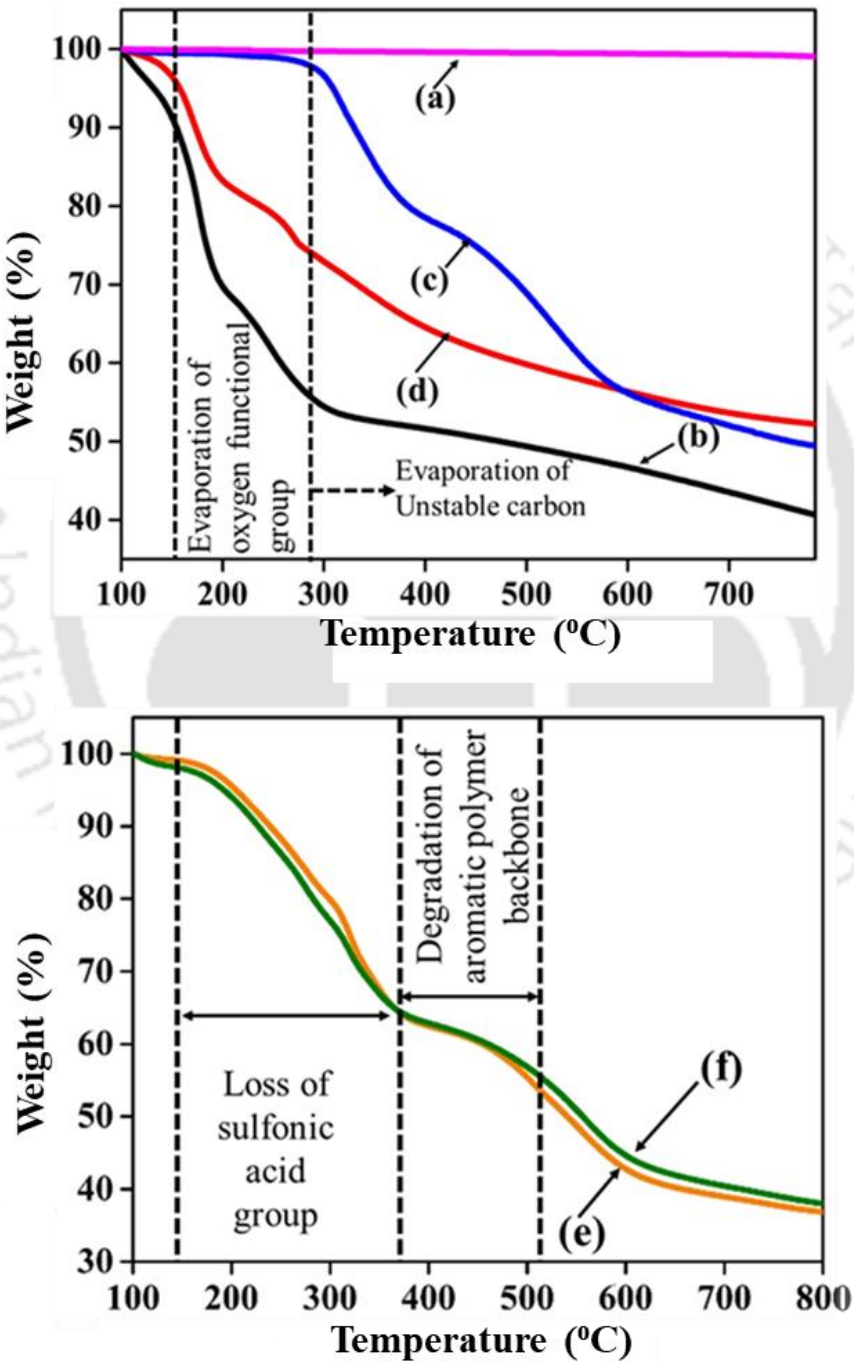

Figure 8.10 TGA of (a) Graphite, (b) GO, (c) Pd-GO, (d) Pd-GO-L-Tyr, (e) SPEEK and (f) SPEEK/Pd-GO-L-Tyr.

8.3.7 FTIR analysis

FTIR was done to analyze the interfacial interaction and chemical structure of synthesized materials and membranes. **Figure 8.11** shows the FTIR spectra of GO and Pd-GO-L-Tyr. In both the cases, the bands at 3425 cm^{-1} and 1727 cm^{-1} are due the presence of carboxylic -OH and C=O, respectively. The peaks at 1628 cm^{-1}, 1221 cm^{-1} and 1054 cm^{-1} are assigned to the C=C, C-O-C (epoxy) and C-O (alkoxy) groups, respectively [8]. As opposed to GO, Pd-GO- L-Tyr composite shows new bands at 1366 cm^{-1}, 1546 cm^{-1} and 1582 cm^{-1} which confirm the presence of C-N stretching and N-H bending due to the incorporation of the L-Tyr group [23].

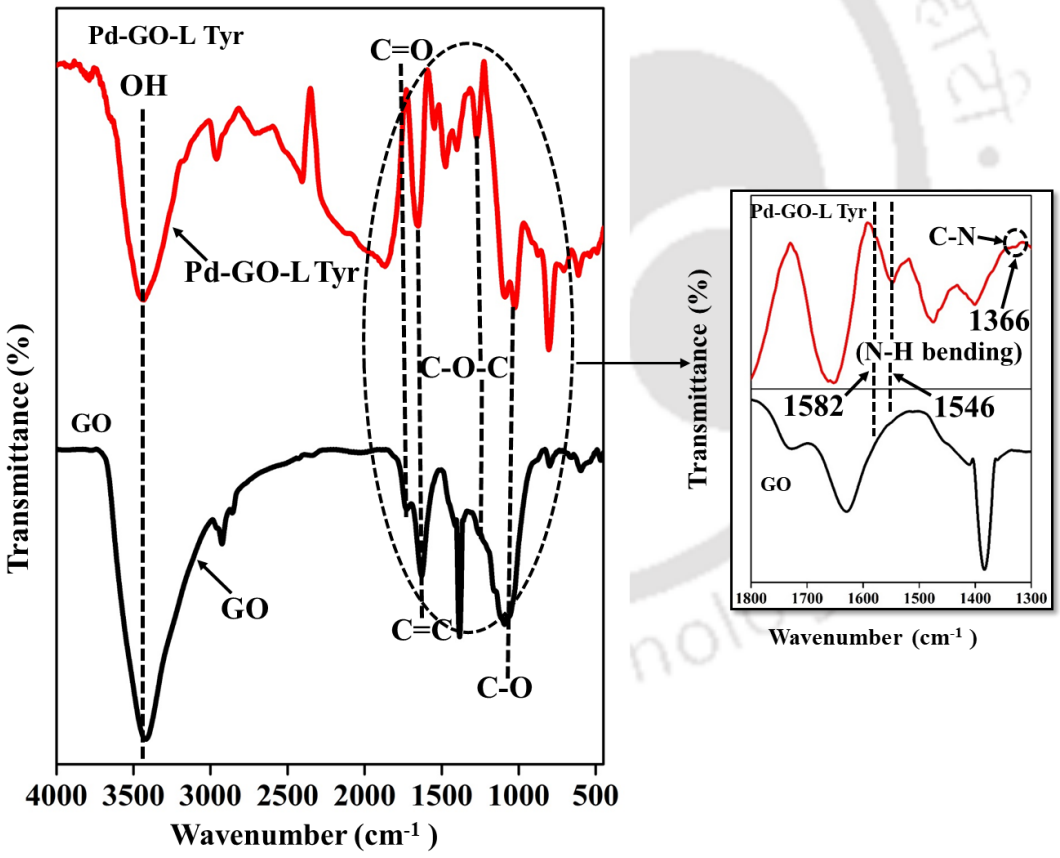

Figure 8.11 FT-IR spectra for GO and Pd-GO-L-Tyr composite

8.3.8 XPS analysis

XPS analysis was done to analyse the chemical states of C, N, O, Pd and S in synthesized composite materials and membranes. **Table 8.1** shows the individual contributions of various elements.

Table 8.1 Contributions of individual chemical moieties in atomic %:

Sample	C1 s	O1 s	N1 s	Pd 3d	S 2p
GO	63.5	36.6	NA	NA	NA
Pd-GO-L-Tyr	65.5	28.9	4.8	0.8	NA
SPEEK	75.4	18.6	1.0	NA	1.8
SPEEK/Pd-GO-L-Tyr	75.2	19.4	2.1	0.4	2.9

Fig. 8.12a shows surface survey analysis of GO and Pd-GO- L-Tyr in the region of 0-800 eV and **Fig. 8.12b-e** shows the deconvoluted C1s and O1s spectra. The spectrum of GO shows two major peaks at 285.4 and 533.3 eV, assigned to C1s and O1s. In the case of Pd-GO- L-Tyr, two new peaks at 402.0 and 338.1 eV were observed indicating the presence of N1s and Pd3d. Deconvolution of C1s of GO (**Fig. 8.12c**) show four major peaks at 284.7 eV, 286.6 eV, 287.6 eV and 288.9 eV arising from C=C (from sp^2 bond), C-O (from hydroxyl or epoxy group), C=O (from carbonyl group) and O-C=O (from carboxyl group), respectively.[8] Here, after amino acid modification, a new peak at 286.0 eV (**Fig. 8.12b**) is observed. This indicates the formation of C-N bands [24] due to the interaction between epoxy group of GO and NH_2 group from amino acid [12]. Furthermore, deconvolution of O1s in GO shows two major peak at 531.1 and 532.5 eV (**Fig. 8.12c**) which are assigned to COOH and C-OH groups, respectively. In case of Pd-

GO- L-Tyr, the intensity of COOH band from O1s become stronger (**Fig. 8.12d**) possibly due to the additional contribution of the COOH groups from the amino acid [12].

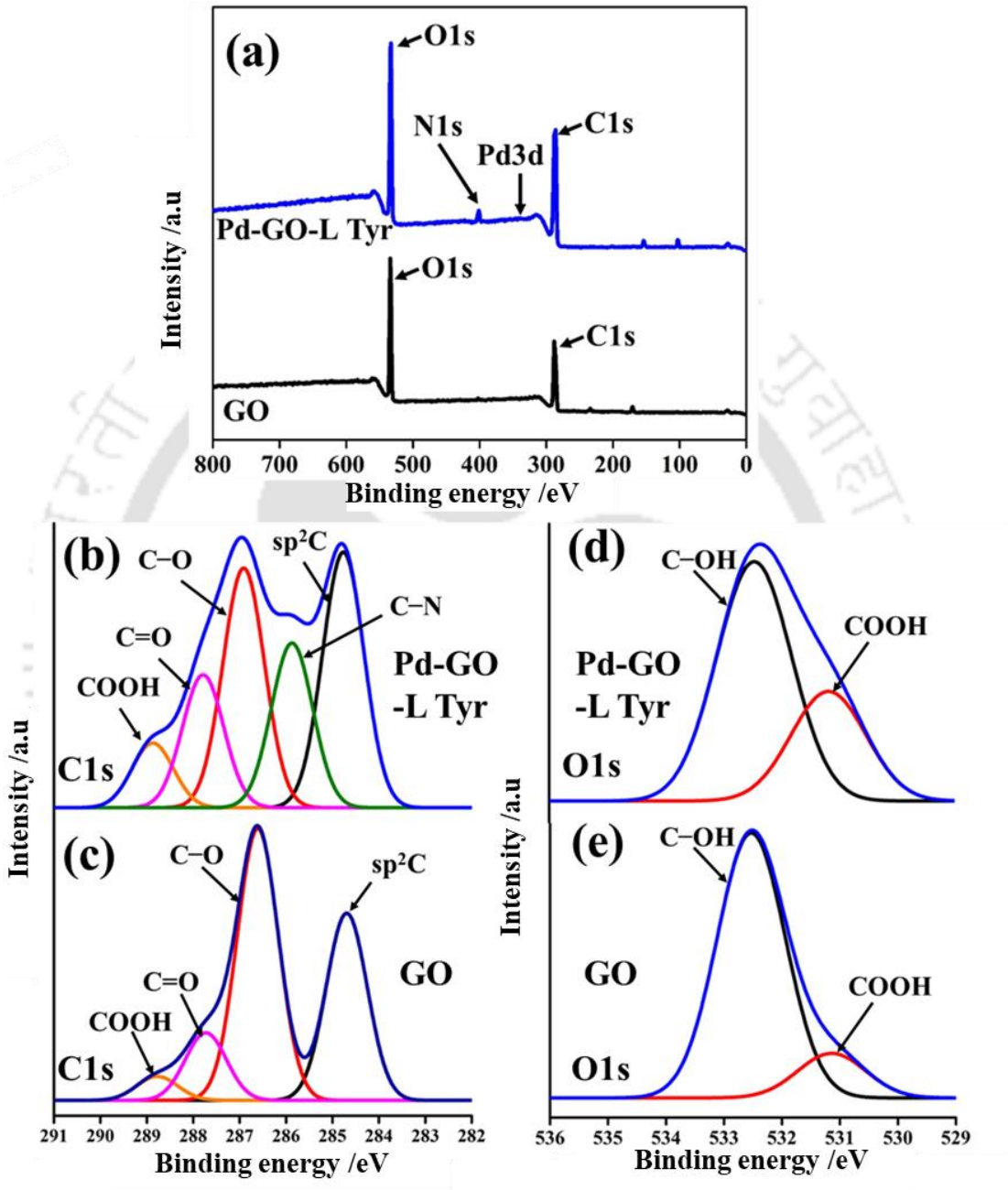

Figure 8.12 XPS spectra of GO and Pd-GO-L-Tyr: (a) survey spectrum of GO and Pd-GO-L-Tyr; (b-c) deconvolution of C1s spectrum; (d-e) deconvolution of O1s spectrum

A typical XPS spectrum of SPEEK and modified SPEEK is shown in **Fig. 8.13**. After sulfonation of SPEEK, three main peaks were observed at 28.7 eV 531.3 eV and 167.4 eV as depicted in the figure and they are attributed due to the presence of carbon, oxygen and sulfur, respectively. After modification of SPEEK, trace of two new peaks at 338.4 eV and 400.4 eV was found, which is an indication of presence of palladium and nitrogen (**Fig. 8.13b-c**).

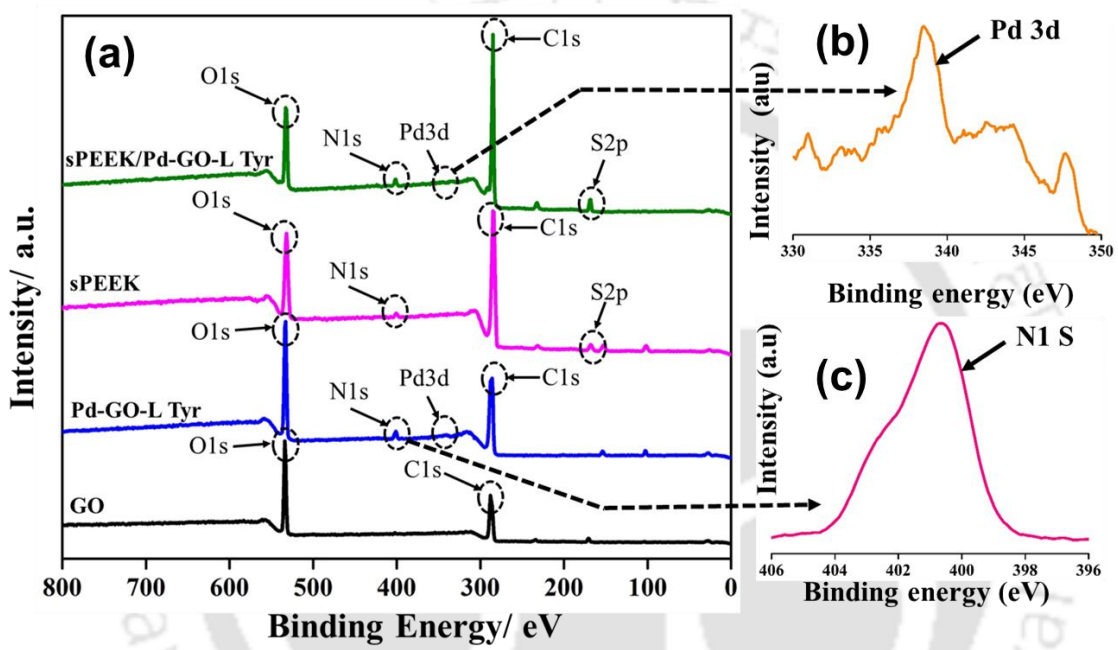

Figure 8.13. XPS spectra polymer and composites: (a) survey spectrum of SPEEK and SPEEK/ Pd-GO-L-Tyr; (b) Pd 3d spectrum of SPEEK/ Pd-GO-L-Tyr; (c) N1s spectrum of SPEEK/ Pd-GO-L-Tyr.

8.3.9 Contact angle, water uptake and IEC measurement

The controlling factors for judging the suitability of a membrane for proton exchange applications include its contact angle, water uptake, and IEC. The proton transport by the membrane is directly proportional to its water uptake which proceeds via vehicular mechanism thus enhancing the proton conductivity. Water uptake of 45.3% by the nascent SPEEK membrane increases to 50.6% for the composite SPEEK/Pd-GO-L-Tyr

membrane, as it is more porous, leading to increased accumulation of water in the pores (**Fig. 8.14a**). Moreover, sulfonation generates more hydrophilic channels in a membrane which further improves its water absorption [25]. The surface wettability of the membranes was found from their contact angle measurements (**Fig. 8.14b-c**). The SPEEK membrane shows contact angle of 84° due to the presence of $-SO_3H$ groups which decreases to 66.2° for the composite membrane indicating its higher surface hydrophilicity and wettability [26]. The ion-exchange capacity of the SPEEK membrane was 1.32 meq/g; it increases to 2.05 meq/g for SPEEK/Pd-GO-L-Tyr (**Fig. 8.14a**) due to the presence of more amount of carboxylic and hydroxyl groups in Pd-GO-L-Tyr [2].

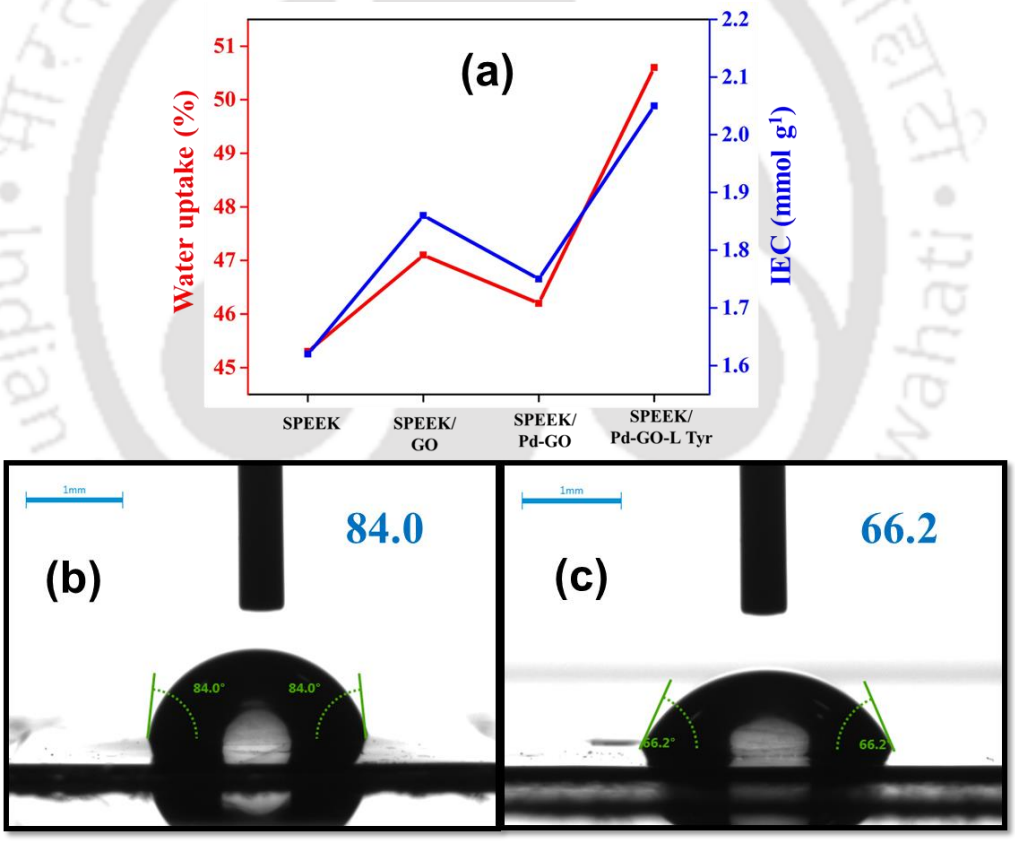

Figure 8.14 (a) IEC and water uptake, water contact angle images: (b) SPEEK (c) SPEEK/ Pd-GO-L-Tyr

8.3.10 Methanol permeability, conductivity and selectivity measurement

An important parameter related to performance of a proton exchange membrane in DMFC is methanol permeability. The fuel utilization efficiency of the DMFC increases with decreasing methanol permeability. Thus, membranes with low methanol permeability with a moderate proton conductivity are highly desirable. **Table 8.2** lists the methanol permeability of various membranes synthesized in this work along with the benchmark Nafion membrane.

Table 8.2 Ionic conductivity, methanol permeability and selectivity of the SPEEK, SPEEK/GO, SPEEK/Pd-GO, SPEEK/Pd-GO-L-Tyr and Nafion-117 membranes.

Sample	Conductivity ($S\ cm^{-1} \times 10^{3}$)	Permeability ($cm^{2}\ s^{-1} \times 10^{6}$)	Selectivity ($S\ s\ cm^{-3} \times 10^{-3}$)
SPEEK	1.04	2.18	0.48
SPEEK/GO	1.41	0.79	1.78
SPEEK/Pd-GO	1.7	0.65	2.62
SPEEK/Pd-GO-L-Tyr	2.56	0.46	5.57
Nafion -117	6.4	2.3	2.78

In a sulfonated membrane, the ionic channels formed upon aggregation of sulfonic acid groups result in good proton and methanol transport. Larger ionic clusters in commercial Nafion membranes leads to their higher methanol permeability compared to narrow channels in SPEEK [27]. Moreover, hydrogen bonding interactions between amino acid modified Pd-GO and SPEEK inhibit formation of wide ionic channels, thus limiting the methanol permeability [22]. Thus methanol permeability reduced from 2.18×10^{-6} cm^{2} s^{-1} to 0.46×10^{-6} cm^{2} s^{-1} after incorporation of Pd-GO-L-Tyr composite in the membrane,

possibly due to the additional blocking effect of Pd as well as GO (**Fig. 8.15**). This little drop in methanol permeability of SPEEK for the latter is insignificant to retard it as applicable as proton exchange membrane in accordance with existing works literature which varies in the range of 0.5×10^{-6}-1.95×10^{-6} $cm^2\ s^1$ [28,29].

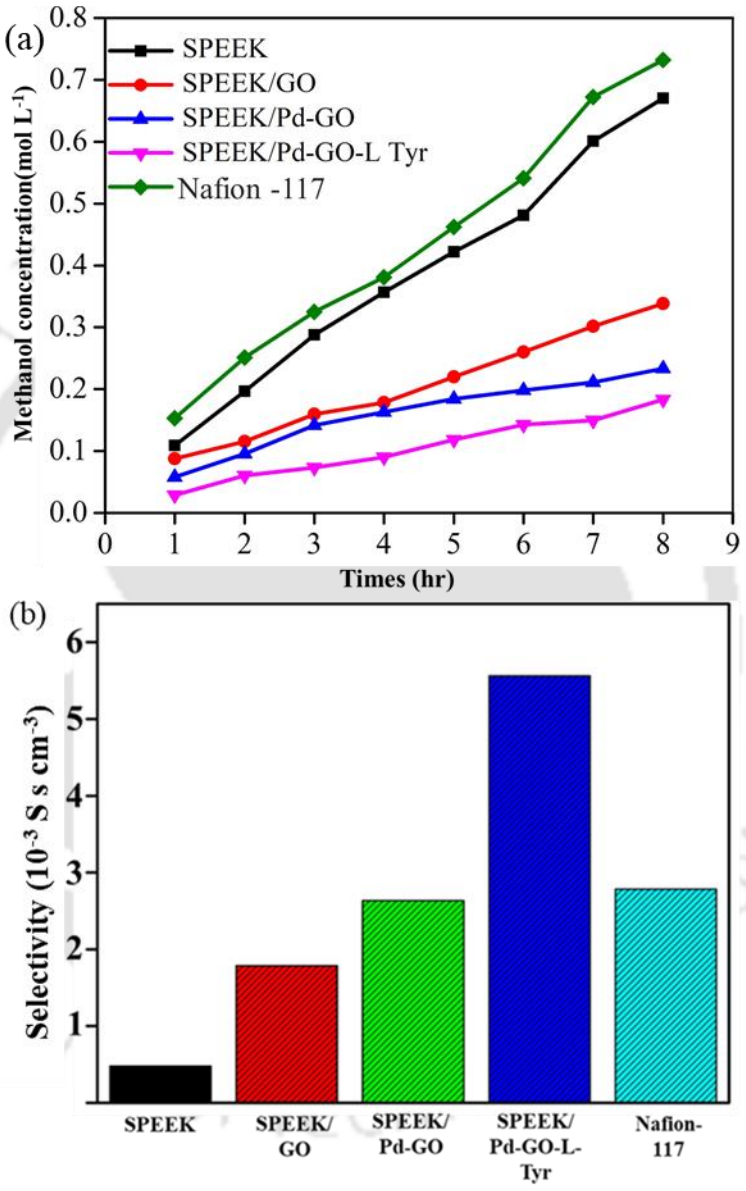

Figure 8.15. (a) Methanol permeation with time and (b) selectivity.

An important factor determining the membrane conductivity is their water uptake capacity. The proton conductivity in composite membrane is governed by the synergistic effect of proton hopping through ion conducting groups (i.e. GrÖthous mechanism) and

protons transfer as hydronium ions (i.e. vehicular mechanism) [4]. The measured proton conductivity of all membranes were summarized in **Table 8.2**. The conductivity value for Nafion-117 at room temperature was found to be 6.4 mS/cm which is quite comparable to the earlier reported literature [30,31]. This implies the efficiency of the lab made cell set up along with the single cell assembly. In case of SPEEK proton conductivity value was measured to be 1.04 mS/cm and an improvement of 2.4 fold for proton conductivity was noticed for Pd-GO-L-Tyr. Impregnation of Pd gives a pathway for selective transportation of hydrogen ion or water molecules, which in turn inhibits the passage of methanol molecules (**Fig. 8.16a**). On other hand, the GO surface holds different functional groups such as hydroxyl, carboxyl, carbonyl and epoxy groups (**Fig. 8.16b**) that become negatively charged upon deprotonation in water molecule. Subsequent hydration results in a nano-capillary network that creates pathways and for conduction of proton [28]. Among the various membranes, SPEEK/Pd-GO-L-Tyr was found to have higher conductivity compared to pristine SPEEK, SPEEK/GO and SPEEK/Pd-GO (**Table 8.2**). The amino acid doped composite membrane in this study forms zwitterion (NH_3^+-R-COO^-) by proton transfer from carboxylic acid group to the amine group (**Fig. 8.16c)**. This zwitterion leads to dissociation of carboxylic acid and sulfonic acid groups of the composite membrane, resulting in formation of negatively charged carboxylate and sulfonate moieties, thereby favoring proton hopping mechanism. In addition, hydration layer generated due to the electrostatic interaction of carboxylic acid group of L-Tyr and GO with water molecules is responsible for vehicular mechanism for proton transport.

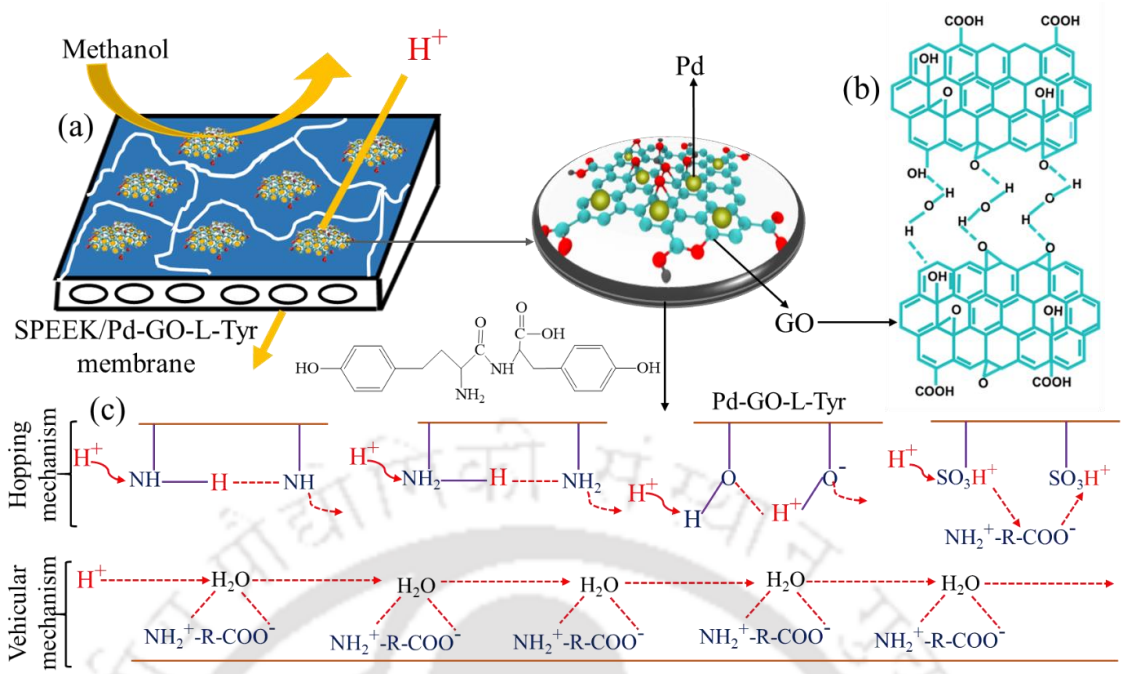

Figure 8.16 Proposed proton transport mechanism in SPEEK/ Pd-GO-L-Tyr membrane.

Although the conductivity of Nafion membrane is superior to any of the samples prepared in this work, the permeabilities are lower (by about a factor of 5). This difference in permeabilities is significant, as it results in better methanol selectivity for our membranes compared to that of Nafion-117.

8.4 Conclusions

Pd-GO was successfully functionalized by L-Tyr to yield Pd-GO-L-Tyr. AFM analysis showed that SPEEK membrane had a smooth surface morphology, whereas the composite membrane indicated surface roughness. The increase in hydrophilicity, surface wettability and ion exchange capacity (due to the increased presence of hydroxy and carboxyl groups) in the composite membrane enhance its proton conductivity as compared to that of pristine SPEEK membrane. The presence of various functional groups within the composite membrane framework, allow it to transfer protons via both

GrÖthous and vehicular mechanisms. The incorporation of Pd-GO-L-Tyr into the SPEEK membrane matrix act as a physical barrier to prevent the methanol crossover. The high proton conductivity and low methanol crossover of SPEEK/Pd-GO-L-Tyr membrane resulted in its significantly high selectivity (5.57×10^3 S cm^{-3} s) as compared to the SPEEK membrane (4.8×10^2 S s cm^{-3}) and Nafion 117 (2.78×10^3 S s cm^{-3}) membranes. The conductivity of the Pd-GO-L –Tyr mixed composite membrane was enhanced compared to other membranes (refer to sections 6.4 and 7.4). This opens up the scope of application of this fabricated membrane as a promising PEM for DMFC application.

References

1. S. Damodaran, Amino acids, peptides and proteins, CRC Press: Boca Raton, FL2008.
2. G. Rambabu, S.D. Bhat, Amino acid functionalized graphene oxide based nanocomposite membrane electrolytes for direct methanol fuel cells, Journal of Membrane Science 551 (2018) 1-11.
3. S.L. Bourke, J. Kohn, Polymers derived from the amino acid L-tyrosine: polycarbonates, polyarylates and copolymers with poly (ethylene glycol), Advanced Drug delivery Reviews 55(4) (2003) 447-466.
4. C. Nagamani, U. Viswanathan, C. Versek, M.T. Tuominen, S.M. Auerbach, S. Thayumanavan, Importance of dynamic hydrogen bonds and reorientation barriers in proton transport, Chemical Communications 47(23) (2011) 6638-6640.
5. R. Jin, C. Lin, A. Cao, Enzyme-mediated fast injectable hydrogels based on chitosan–glycolic acid/tyrosine: preparation, characterization, and chondrocyte culture, Polymer Chemistry 5(2) (2014) 391-398.
6. Z. Guler, A. Sarac, Electrochemical impedance and spectroscopy study of the EDC/NHS activation of the carboxyl groups on poly (ε-caprolactone)/poly (m-anthranilic acid) nanofibers, Express Polymer Letters 10(2) (2016).
7. J. Bart, R. Tiggelaar, M. Yang, S. Schlautmann, H. Zuilhof, H. Gardeniers, Room-temperature intermediate layer bonding for microfluidic devices, Lab on a Chip 9(24) (2009) 3481-3488.
8. P. Das, B. Mandal, S. Gumma, Engineering of structural and surface functional characteristics of graphite oxide nanosheets by controlling oxidation temperature, Applied Surface Science 504 (2020) 144444.

9. A.B. Bourlinos, D. Gournis, D. Petridis, T. Szabó, A. Szeri, I. Dékány, Graphite oxide: chemical reduction to graphite and surface modification with primary aliphatic amines and amino acids, Langmuir 19(15) (2003) 6050-6055.
10. C. Rajesh, C. Majumder, H. Mizuseki, Y. Kawazoe, A theoretical study on the interaction of aromatic amino acids with graphene and single walled carbon nanotube, The Journal of Chemical Physics 130(12) (2009) 124911.
11. M. Celebi, K. Karakas, I.E. Ertas, M. Kaya, M. Zahmakiran, Palladium nanoparticles decorated graphene oxide: active and reusable nanocatalyst for the catalytic reduction of hexavalent chromium (VI), ChemistrySelect 2(27) (2017) 8312-8319.
12. S. Mallakpour, A. Abdolmaleki, S. Borandeh, Covalently functionalized graphene sheets with biocompatible natural amino acids, Applied Surface Science 307 (2014) 533-542.
13. F.T. Johra, J.-W. Lee, W.-G. Jung, Facile and safe graphene preparation on solution based platform, Journal of Industrial and Engineering Chemistry 20(5) (2014) 2883-2887.
14. R.C. Fierascu, A. Ortan, S.M. Avramescu, I. Fierascu, Phyto-nanocatalysts: Green synthesis, characterization, and applications, Molecules 24(19) (2019) 3418.
15. P. Hosseinabadi, K. Hooshyari, M. Javanbakht, M. Enhessari, Synthesis and optimization of nanocomposite membranes based on SPEEK and perovskite nanoparticles for polymer electrolyte membrane fuel cells, New Journal of Chemistry 43(41) (2019) 16232-16245.
16. Q. Che, H. Fan, X. Duan, F. Feng, W. Mao, X. Han, Layer by layer self-assembly fabrication of high temperature proton exchange membrane based on ionic liquids and polymers, Journal of Molecular Liquids 269 (2018) 666-674.

17. D.K. Gupta, R.S. Rajaura, K. Sharma, Synthesis and Characterization of Graphene Oxide Nanoparticles and their Antibacterial Activity, Int. J. Environ. Sci. Technol 1(1) (2015) 16-24.
18. H. Veisi, T. Tamoradi, B. Karmakar, P. Mohammadi, S. Hemmati, In situ biogenic synthesis of Pd nanoparticles over reduced graphene oxide by using a plant extract (Thymbra spicata) and its catalytic evaluation towards cyanation of aryl halides, Materials Science and Engineering: C 104 (2019) 109919.
19. S. Gahlot, V. Kulshrestha, Dramatic improvement in water retention and proton conductivity in electrically aligned functionalized CNT/SPEEK nanohybrid PEM, ACS Applied Materials & Interfaces 7(1) (2015) 264-272.
20. R.P. Mariappan, C. Liu, G. Cao, R.P. Manimuthu, Tailoring SPEEK/SPVdF-co-HFP/La2Zr2O7 Ternary Composite Membrane for Cation Exchange Membrane Fuel Cells, Industrial & Engineering Chemistry Research 59(11) (2020) 4881-4894.
21. T. Kuilla, S. Bhadra, D. Yao, N.H. Kim, S. Bose, J.H. Lee, Recent advances in graphene based polymer composites, Progress in Polymer Science 35(11) (2010) 1350-1375.
22. Y. Heo, H. Im, J. Kim, The effect of sulfonated graphene oxide on sulfonated poly (ether ether ketone) membrane for direct methanol fuel cells, Journal of Membrane Science 425 (2013) 11-22.
23. A. Kumar, M. Khandelwal, Amino acid mediated functionalization and reduction of graphene oxide–synthesis and the formation mechanism of nitrogen-doped graphene, New Journal of Chemistry 38(8) (2014) 3457-3467.
24. J. Ederer, P. Janoš, P. Ecorchard, J. Tolasz, V. Štengl, H. Beneš, M. Perchacz, O. Pop-Georgievski, Determination of amino groups on functionalized graphene oxide

for polyurethane nanomaterials: XPS quantitation vs. functional speciation, RSC Advances 7(21) (2017) 12464-12473.

25. A.R. Kim, D.J. Yoo, A comparative study on physiochemical, thermomechanical, and electrochemical properties of sulfonated poly (ether ether ketone) block copolymer membranes with and without Fe3O4 nanoparticles, Polymers 11(3) (2019) 536.
26. D.B. Babu, K. Giribabu, K. Ramesha, Permselective SPEEK/nafion composite-coated separator as a potential polysulfide crossover barrier layer for Li–S batteries, ACS applied Materials & Interfaces 10(23) (2018) 19721-19729.
27. L. Li, J. Zhang, Y. Wang, Sulfonated poly (ether ether ketone) membranes for direct methanol fuel cell, Journal of Membrane Science 226(1-2) (2003) 159-167.
28. Y. Heo, H. Im, J. Kim, The effect of sulfonated graphene oxide on sulfonated poly (ether ether ketone) membrane for direct methanol fuel cells, Journal of Membrane Science 425 (2013) 11-22.
29. N. Zhang, G. Zhang, D. Xu, C. Zhao, W. Ma, H. Li, Y. Zhang, S. Xu, H. Jiang, H. Sun, Cross-linked membranes based on sulfonated poly (ether ether ketone)(SPEEK)/Nafion for direct methanol fuel cells (DMFCs), International Journal of Hydrogen Energy 36(17) (2011) 11025-11033.
30. A.U. Devi, K. Divya, D. Rana, M.S.A. Saraswathi, A. Nagendran, Highly selective and methanol resistant polypyrrole laminated SPVdF-co-HFP/PWA proton exchange membranes for DMFC applications, Materials Chemistry and Physics 212 (2018) 533-542.
31. P. Umsarika, S. Changkhamchom, N. Paradee, A. Sirivat, P. Supaphol, P. Hormnirun, Proton exchange membrane based on sulfonated poly (aromatic imide-co-aliphatic imide) for direct methanol fuel cell, Materials Research 21(1) (2018).

CHAPTER 9

Overall Conclusions and Recommendation for Future Work

CHAPTER 9

Overall conclusions and recommendation for future work

This chapter summarizes appropriate conclusions of the present work based on the characterization and investigations. This chapter also provides some useful recommendations for future research in the relevant field.

This study has been formulated keeping in mind the need for a viable proton exchange membrane (PEM) for applications in Direct Methanol Fuel Cells (DMFCs). A novel PEM has been synthesized and studied for the same. Inorganic advancements were made in a pristine SPEEK membrane with UiO-66, Pd, GO and L-Tyr. The commercial Nafion 117 membrane was used as standard. This research work expands on the synthesis of the membrane, characterization and application. It also mentions the research tactics to be implemented for an improved DMFC performance.

9.1 Major Conclusions

The major conclusions of the thesis are summarized below:

- The sulfonation process of Polyether ether ketone (PEEK) and fabrication of a sulfonated poly (ether ether ketone) (SPEEK) membrane was done. Successfully fabricated membrane shows a conductivity value 1.04 mS/cm at room temperature which was 8.3 fold lesser than Nafion 117 (6.46mS/cm). However, sulfonation resulted in an increase in the water uptake and conductivity in the SPEEK membranes. The methanol permeability value of SPEEK found to be 2.17×10^{-6} S s cm^{-3}.

- GO has been synthesized in the control over the oxidation temperature in the range of 30-110 ºC using modified Hummer's method to modulate the structural and surface functional properties. Analytical investigations suggested that the concentration of functional groups on the surface of GO nanosheets increases with increase in oxidation temperature up to 50 ºC and decreases with further increase in temperature as the condensation reaction between epoxy and hydroxyl groups proceed. The temperature dependent structural as well as surface functional properties changes of GO are explained based on the chemical condensation and modulation of the functional groups present on their surface. This study is vital for tailoring the properties of GO nanosheets and thus towards the progress of sustainable carbon materials as well as designing the charged based electronic materials. GO-50 has been chosen for further study and synthesis of composite for SPEEK membrane.

- A facile synthesis of GO doped UiO-66 nanocomposite was done and used for efficient composite for DMFC membrane. The incorporation of UiO-GO composite in the SPEEK polymer resulted in the formation of the splendid SPEEK/UiO-66/GO composite proton exchange membrane that showed an excellent promising nature for applications in DMFCs. Hydrothermal method was used for the preparation of UiO-66/GO composite. An increase in the proton conductivity was observed in the UiO-66/GO infused SPEEK membranes. The SPEEK membrane with UIO-66 (3wt%) /GO (2.5wt%) composite was found to have both high conductivity of 1.88 mS/cm without compromising the thermal and chemical stability. The commercial Nafion 117 membrane, used as a reference in this study, also exhibited comparable values of proton conductivity. This composite membrane showed a methanol permeability 4.5 times lower than that of Nafion 117.

- A novel palladium (Pd) decorated GO doped UiO-66 composite was developed for selective DMFC membrane. The use of Palladium nanoclusters blocked the methanol permeability in the hydrophilic channel, thus significantly reducing the methanol crossover while the proton conductivity of the membrane stayed intact. Although UiO-66/Pd-GO composite based membrane shows an increasing proton conductivity comparison to pure UiO-66 mixed membrane at room temperatures. The maximum proton conductivity was exhibited by the UiO-66 (3wt %) /Pd (10wt%)-GO (2.5%) mixed membranes which is 2.11 mS/cm. A lower methanol permeability was found in the composite membranes (3.6×10^{-7} S s cm^{-3}) content as compared to the Nafion 117 membrane. This optimized concentration of UiO-66/Pd-GO composite membrane shows selectivity 5.85×10^{3} S s cm^{-3} which is approximately two times higher than Nafion-117.

- Pd-GO nanocomposite was further used to functionalize L-Tyrosine (amino acid) for making another novel composite for PEM. These Pd-GO-L-Tyr membranes showed an increased proton conductivity. This can be attributed to the interactions of the zwitterions induced because of the functionalization of Pd-GO with L-Tyr. The IEC and water uptake were also found to be higher as compared to the pure SPEEK membranes. A better compatibility and reduced methanol permeability were found in the composite membranes due to the improved interactions caused by the induction of functional groups by L-Tyr and Pd. The highest proton conductivity was exhibited by the 1 wt% Pd-GO-L-Tyr sample which is 2.56 mS/cm. The results implied that these nanocomposite membranes can be used for DMFC applications by fine tuning the morphology and optimising the nano additive concentration. The high proton conductivity and low methanol crossover of SPEEK/Pd-GO-L-Tyr membrane resulted in its significantly high selectivity (5.57×10^{3} S cm^{-3} s) as

compared to the SPEEK membrane (4.8×10^2 S s cm^{-3}) and Nafion 117 (2.78×10^3 S s cm^{-3}) membranes.

- *Comparative study:* This study was undertaken to improve the selectivity of a proton exchange membrane for use in DMFC application. To achieve this, two approaches has been undertaken. The first approach was blocking the methanol so that permeability can be reduced and the second one was improving the conductivity. By adding UiO-66 and GO composite in the membrane matrix, a reasonable performance was obtained. However, the selectivity value was found to be low as compared to Nafion-117. Incorporation of palladium nanoparticles enabled the newly fabricated composite membrane to curtail the support pore blocking phenomenon during methanol permeability experiment. Additionally, we embarked on to explore L-Tyrosine (amino acid) for proton exchange membrane. The performance was quite encouraging. Presence of zwitterion in the amino acid demonstrated facilitated transport of protons because they can act both as a proton donor and a proton acceptor simultaneously. Successful modification of the composites resulted in accomplishment of the target of increasing proton conductivity and reducing methanol permeability (**Table 9.1**). This led to enhanced membranes selectivity compared to Nafion -117.
- Overall, it can be concluded that the work undertaken here forwards an innovative route for utilization of novel composites in the fabrication of proton exchange membrane with an effort to convert waste to wealth along with positive impact on energy and environment.

Table 9.1 Ionic conductivity, methanol permeability and selectivity exhibited by membranes studied in this dissertation.

Membrane	Conductivity ($S\ cm^{-1} \times 10^{3}$)	Permeability ($cm^{2}\ s^{-1} \times 10^{6}$)	Selectivity ($S\ s\ cm^{-3} \times 10^{-3}$)
SPEEK	1.04	2.18	0.48
SPEEK/UiO-66(3%)/ GO(2.5%)	1.89	0.49	2.62
SPEEK/UiO-66(3%)/ Pd(10%)-GO(2.5%)	2.11	0.36	5.86
SPEEK/L-Tyr(1%)/ Pd(10%)-GO(2.5%)	2.56	0.46	5.57
Nafion -117	6.4	2.3	2.78

9.2 Recommendations for Future Research

The DMFCs have established themselves as the flag bearers for the future generation in the field of green and sustainable energy. This has the potential to act as the most ideal power source for portable equipment in the long run. SPEEK has time and again been considered for DMFCs and has been an active research topic. The current study has obtained several promising results from the matrix SPEEK polymer. This study created a novel SPEEK membrane infused with UiO-66/Pd-GO and Pd-GO-L-Tyr composite. The membranes showed remarkable results in the domains of chemical and thermal stability as well as barrier properties. Hence, it is worthwhile to further probe these characteristics so as to create successful, commercial alternatives to Nafion membrane. This work shows favorable outcomes by incorporating inorganic materials. Thus, further research should be done on finding and optimizing that right inorganic materials other

than the ones that have already been experimented upon with long term performing stability tests and optimizing the membrane inorganic composition.

Furthermore, the fundamental research methods for the characterization need to be expanded. The current study expands on the morphology, proton conductivity, methanol permeability, selectivity and water uptake, which form the fundamental elements of characterization. Future work can include several other characterization elements in the likes of mechanical stability, longevity, repeatability with a proper cost estimation which can help in establishing a conditional prediction of the DMFCs. Experiments should be conducted varying at a significant range of temperature to analyze the working conditions of a real fuel cell. Future work may involve the development of a new experimental setup better suited for the validation of the characterization methods. However, in such a case, maintenance of the basic nature of the DMFC setup should be carefully taken into account as the simple structural design of the DMFCs are one of their coveted strengths that makes them promising for consideration as an energy alternative. Economic evaluation of the prepared membranes also can be appraised to endorse their applications for commercial usages in industries.

Front Page of the Paper Published in Reputed International Journal

Research Output

Journal publications

1. Das, P. Mandal, B. and Gumma, S. Engineering of structural and surface functional characteristics of graphite oxide nanosheets by controlling oxidation temperature; ***Applied Surface Science,*** **(Elsevier)** (**Impact Factor: 6.128**).

2. Das, P. Mandal, B. and Gumma, S. L-Tyrosine grafted palladium graphite oxide and SPEEK composite as novel membrane for direct methanol fuel cell **(To be communicated).**

3. Das, P. Mandal, B. and Gumma, S. Interfacial growth of MOF UiO-66 on palladium grafted graphene sheet as a composite for proton exchange membrane **(To be communicated)**.

4. Das, P. Mandal, B. and Gumma, S. A review on performance analysis of sulphonated polymer electrolyte membranes for fuel cells **(To be communicated)**.

5. Das, P. Mukherjee, D. Mandal, B. and Gumma, S. and Mandal, B. Role of graphite oxide decorated metal oganic framework (UiO-66) for enhanced congo red dye removal from aqueous solution with synergistic effect of adsorption and ultra-sonication **(To be communicated).**

Research Output

International Conference:

1. Das, P. Gumma, S. and Mandal, B; Effect of temperature on the structural parameter of graphene oxide; AIChE Annual Meeting; November, 2019; Orlando, Florida, United States of America.

2. Das, P. Mukherjee, D, Gumma, S. and Mandal, B.; Fabrication of palladium grafted graphene oxide based sulfonated poly(ether ether ketone) proton exchange membrane for direct methanol fuel cell applications ; ASP; October, 2019; Japan.

3. Das, P. Gumma, S. and Mandal, B; Sulfonated poly(ether ether ketone) membranes with modified graphene oxide for direct methanol fuel cell ; SFCHT; April, 2019; Kuala Lumpur ; Malaysia

4. Das, P. Gumma, S. and Mandal, B; Novel mixed matrix membrane using metal organic framework and graphene oxide for CO_2 separation; AIChE Annual Meeting; October, 2019; Minneapolis, United States of America.

National Conference:

1. Das, P. Mukherjee, D, Gumma, S. and Mandal, B.; Graphite Oxide decorated Uio-66 MOF for CR dye adsorption using ultra sonication; Bio-inspired Nanomaterials for Environmental Applications; February, 2020; IIT Guwahati, Assam, India.

2. Das, P. Gumma, S. and Mandal, B; Graphene oxide modified cellulose acetate membrane for direct methanol fuel cell; Research Conclave; March, 2020; IIT Guwahati, Assam, India.

3. Das, P. Gumma, S. and Mandal, B; GO based polymeric membrane for CO_2 separation; ASP; January, 2018; IIT Guwahati, Assam, India.

4. Das, P. Prasad, B. Kalita, H. Mandal, B.; Synthesis of chitosan/GO mixed-matrix membrane for CO_2 separation, CHEMCON; December, 2017; HIT WestBengal, India.